

Stereochemistry Reveals the Mechanism of Bacterial Alkane Activation without Oxygen

A Thesis Submitted to the

UNIVERSITY OF NEWCASTLE UPON TYNE



For the degree of DOCTOR OF PHILOSOPHY

MASIH SADEGHI

MAY 2013

Declaration

The work described in this thesis was carried out between March 2009 and April 2013 in the School of Chemistry, Bedson Building, Newcastle University, Newcastle upon Tyne, NE1 7RU. Projects were performed in collaboration with Dr H. Wilkes (Organische Geochemie, Helmholtz-Zentrum Potsdam Deutsches GeoForschungsZentrum GFZ Haus B228, Telegrafenberg, 14473 Potsdam, Germany), Prof. Dr W. Buckel (Max-Planck-Institut für Terrestrische Mikrobiologie, Karl-von-Frisch-Strasse 10, 35043 Marburg, Germany), Prof. Dr R. Rabus and Prof. Dr F. Widdel (Max-Planck-Institut für Marine Mikrobiologie, Celsiusstrasse 1, 28359 Bremen, Germany).

The biological part of this work, which was undertaken by the collaborators listed above, is being, or has been submitted for a degree, diploma, or other qualification at German universities.

This work contains no material that has been accepted for the award of any other degree, diploma or any other qualification in any other Institution or University, and, to the best of knowledge and belief, contains no material previously published or written by any other person, except where due reference has been made in the text.

I give consent for this copy of my thesis, when deposited in the University Library, to be available for loan or photocopying.

Acknowledgements

I would like to gratefully acknowledge the following people:

Firstly, my sincere appreciation for the support and guidance of my supervisor, Professor Bernard Golding, who has helped me to gain the knowledge and experience necessary for a future career in science.

My wonderful father, Prof Majid Sadeghi, who shared with me, his vast knowledge of science, supported me through all these years and came to be an incredible role model in every possible way.

Past and present members of NewChem Technologies, especially Dr Manuel Monerris Mascaro, Dr Alistair Henderson and Dr Phil Butler for help and chemistry advice.

Dr Peter Friedrich, our postdoc and my friend, for chemistry advice, support and encouragement.

Dr. Ross W. Harrington for performing X-ray Crystallography.

Prof. William McFarlane and Dr Corinne Wills for maintaining NMR facilities in the School of Chemistry at Newcastle University.

Our collaborators, Prof Wolfgang Buckel, Prof. Dr. Ralf Rabus, Dr Heinz Wilkes, Prof Friedrich Widdel and their teams for an extraordinary team work.

Marta Drozdowska, Robin Ingleton, Dr Zuleykha McMillan, Dr Julian Knight, Andrew Crawford, Isobel Lamb, Claire Nicoll, Susan Reay, Janny Rolfe, David Dunbar, James Dyson, for their friendship and help.

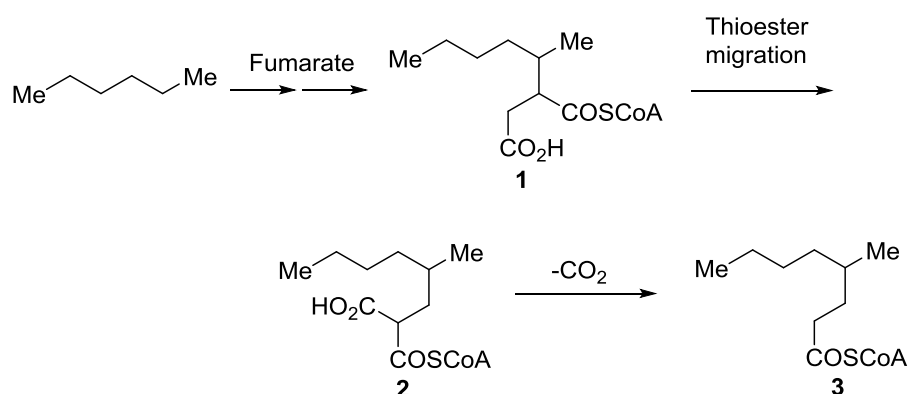
My mother Molouk, brother Mehrdad and sister Mitra for their constant support and motivation.

Finally, I would like to thank Deutsche Forschungsgemeinschaft (DFG, German Research Foundation) for providing the generous funding that enabled all the research, described in this thesis.

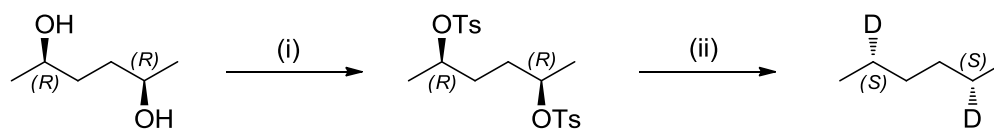


Abstract

The denitrifying bacterium strain HxN1 converts hexane and fumarate to 4-methyloctanyl-CoA. It was proposed that an initial adduct derived from fumarate and the hex-2-yl radical is converted to a CoA-thioester, (1'-methylpentyl)-succinyl-CoA **1**, which rearranges to (2-methylhexyl)malonyl-CoA **2** by a mechanism similar to that of coenzyme B₁₂-dependent radical enzyme methylmalonyl-CoA mutase. Decarboxylation of (2-methylhexyl)malonyl-CoA affords 4-methyloctanyl-CoA **3**:

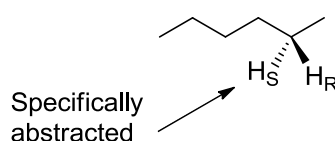


To explore the stereochemistry of the mechanism of hexane degradation we have synthesised hexanes specifically labelled with deuterium: (2*R*,5*R*)-2,5-dideuteriohexane, (2*S*,5*S*)-2,5-dideuteriohexane, (2*R*,5*S*)-2,5-dideuteriohexane, 2,2,5,5-tetradeuteriohexane and 2,2-dideuteriohexane. This was achieved by tosylation of the relevant diol followed by reduction using LiAl²H₄ as shown in example below:

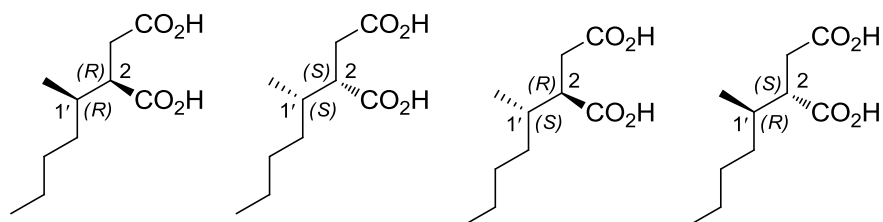


(i) *p*-toluenesulfonyl chloride, pyridine in dichloromethane, 0 °C, 72 h; (Ts = *p*-toluenesulfonyl); (ii) LiAl²H₄, tetraglyme, 120 °C, 2 h.

Analysis of products from the action of HxN1 on these labelled hexanes showed that the *pro-S* hydrogen is abstracted from C-2 of hexane with a primary kinetic isotope effect of ca. 3:

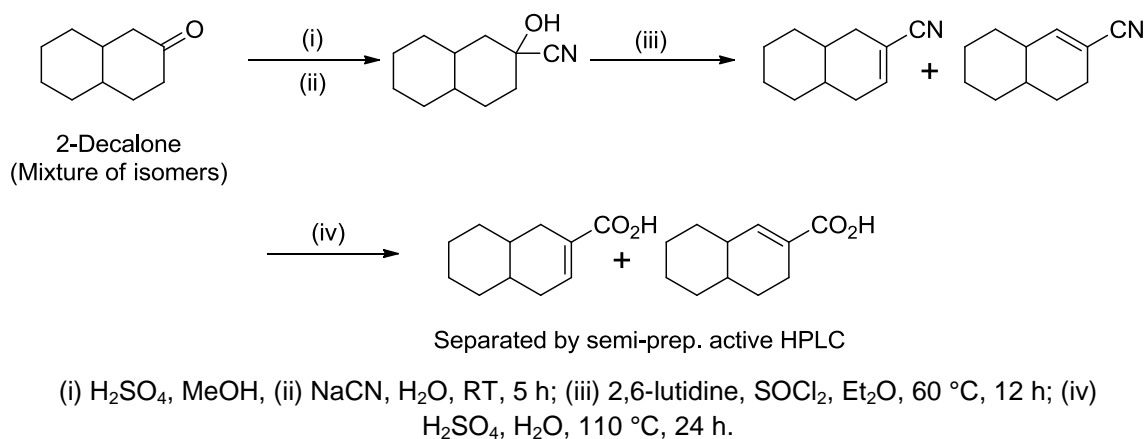


To elucidate the configuration at the newly formed stereocenters, all four stereoisomers of (1-methylpentyl)succinate were synthesised as shown below, in order to use them as standards for comparison with metabolites from strain HxN1.



Comparison using gas chromatography (GC) showed that, anaerobic growth of the bacterium strain HxN1 with *n*-hexane gives nearly equal amounts of (2*R*,1'*R*)- and (2*S*,1'*R*)-(1-methylpentyl)succinate, which are formed by the radical addition of the hydrocarbon to fumarate. As a result of these stereochemical studies, a new concerted mechanism has been postulated for the enzymatic reaction combining hexane with fumarate.

The anaerobic degradation pathways of the environmentally relevant polycyclic aromatic hydrocarbons are largely unknown and therefore the final part of this thesis describes a study of the enzymatic de-aromatisation reactions involved in the degradation of naphthalene by the sulfate-reducing enrichment culture N47. This study required the synthesis of 1,4,4a,5,6,7,8,8a-octahydronaphthalene-2-carboxylic acid and 3,4,4a,5,6,7,8,8a-octahydronaphthalene-2-carboxylic acid, in order to check whether these compounds are intermediates in the degradation of naphthalene. Synthesis of these compounds was achieved using the method shown below:



HPLC, GCMS, NMR and UV/vis spectrum analysis suggested that 5,6,7,8-tetrahydro-2-NCoA (THNCoA) is reduced by two electrons rather than by four electrons as suggested, therefore affording one of the possible hexahydro-2-naphthoyl-CoA (HHNCoA) isomers:



Possible HHNCoA conjugated isomers

List of abbreviations

Ado	deoxyadenosyl
Ado [•]	5'-deoxyadenosyl radical
AdOH	5'-deoxyadenosine
AdoCbl	adenosylcobalamin
Ar	aromatic (ring)
Asp	asparagine
ATP	adenosine-5'-triphosphate
BDE	bond dissociation energy
br	broad
Bss	benzylsuccinate synthase
BssAE	benzylsuccinate synthase activating enzyme
Cbl	cobalamin
CNCb	cyanocobalamin
CoA, CoASH	coenzyme A
CYP 450	cytochrome P450
Cys	cysteine
DCM	dichloromethane
DME	1,2-dimethoxyethane
DMF	<i>N,N</i> -dimethyl formamide
DMSO	dimethyl sulfoxide
DNA	deoxyribonucleic acid
eq	equivalent
FAD	flavin adenine dinucleotide
FMN	flavin monooxygenases
GCMS	gas chromatography-mass spectrometry
Glu	glutamic acid
h	hour
His	histidine
HPLC	high performance liquid chromatography
Hz	Hertz
IR	Infra-Red
<i>J</i>	coupling constants
<i>K</i>	reaction rate constant

LCMS	liquid chromatography mass spectrometry
LDA	lithium diisopropylamide
M	molar
Mas	(1-methylalkyl)succinate synthase
Mp	melting point
MPS	(1-methylpentyl)succinate
<i>m/z</i>	mass/ charge ratio
NAD(P)H	nicotinamide adenine dinucleotide phosphate oxidase
NBS	<i>N</i> -bromosuccinimide
NCS	<i>N</i> -chlorosuccinimide
NDO	naphthalene 1,2-dioxygenase
NHPI	<i>N</i> -hydroxyphthalimide
NMR	nuclear magnetic resonance
Nrd	ribonucleotide reductase
PAH	polycyclic aromatic hydrocarbon
Pd/C	palladium on carbon
Pfl	pyruvate formate-lyase
PH	phenol hydroxylase
pMMO	particulate methane monooxygenase
ppm	parts per million
py	pyridine
ROS	reactive oxygen species
rt	room temperature
SAM	S-adenosylmethionine
sMMO	soluble methane monooxygenases
SRB	sulfate reducing proteobacteria
TFA	trifluoroacetic acid
TFE	trifluoroethanol
THF	tetrahydrofuran
Ts	4-methylbenzenesulfonyl, tosyl
UV/VIS	ultraviolet-visible

CONTENTS

Declaration	iii
Acknowledgements	iv
List of abbreviations	v
Abstract	ix
Chapter 1: Biological Oxidation of Alkanes	
1.1 Introduction to alkane oxidation	2
1.2 Aerobic degradation of alkanes	3
1.2.1 <i>Pathways for aerobic degradation of n-alkanes</i>	3
1.2.2 <i>Alkane hydroxylases related to methane monooxygenase</i>	6
1.2.3 <i>The AlkB family of alkane hydroxylases</i>	7
1.2.4 <i>Cytochrome P450 alkane hydroxylases</i>	8
1.2.5 <i>Alkane hydroxylases for long chain n-alkanes</i>	8
1.2.6 <i>Metabolism of the alcohols and aldehydes derived from the oxidation of alkanes</i>	9
1.3 Anaerobic degradation of alkanes	10
1.3.1 <i>Methanogenesis</i>	12
1.3.2 <i>Nitrate-reducers</i>	15
1.3.2.1 <i>General growth conditions</i>	16
1.3.2.2 <i>Quantification of alkane consumption and nitrate reduction</i>	17
1.3.2.3 <i>Anaerobic growth tests with alkanes and alkanoates</i>	23
1.3.2.4 <i>Growth tests with different electron acceptors</i>	24
1.3.2.5 <i>Search for metabolites and genes involved in alkane degradation</i>	26
1.3.2.6 <i>Linkage of alkane activation in strain HdN1 to the nitrate reduction pathway?</i>	31
1.3.2.7 <i>Summary</i>	33
1.3.3 <i>Sulfate reducers</i>	36
1.3.4 <i>Comparison of aerobic and anaerobic degradation pathways of n-alkanes</i>	46
1.3.5 <i>Environmental and other aspects of anaerobic alkane degradation</i>	46
1.4 Radical enzymes in anaerobes	50
1.4.1 <i>Generation of radicals</i>	51
1.4.2 <i>Coenzyme B₁₂-dependent enzymes</i>	51
1.4.3 <i>S-Adenosylmethionine radical enzymes</i>	53
1.4.3.1 <i>Common features</i>	54
1.4.3.2 <i>Proposed mechanism of SAM</i>	54
1.4.4 <i>Glycyl radical enzymes</i>	56
1.5 Anaerobic degradation of n-hexane	59
1.5.1 <i>Possible presence of a glycyl radical</i>	64
Chapter 2 – Introduction to Enzyme Stereospecificity	

2.1.	Enzyme stereospecificity	68
2.2.	Isotopic labelling	72
2.2.1	<i>Applications of double ¹³C labelling</i>	73
2.3	Conclusion	84
Chapter 3 – Synthesis of Deuterated Substrates for Anaerobic Cultivation with Strain HxN1		
3.1	Deuterated hexane	86
3.1.1	<i>Confirmation of deuteration</i>	95
3.1.2	<i>Inversion of configuration (S_N2) following by LiAlH₄</i>	100
3.1.3	<i>Analysis of the metabolites</i>	102
3.1.4	<i>Proposed mechanism</i>	104
3.1.5	<i>Summary</i>	105
3.1.6	<i>Comparison of the known transformation of succinyl-CoA to propionyl-CoA via methylmalonyl-CoA with the present pathway</i>	106
3.2	Deuterated decanes	108
3.2.1	<i>Synthesis of decane-2,9-diol di-p-toluenesulfonates</i>	108
3.2.2	<i>(2S,9S)-2,9-dideuteriodecane</i>	110
Chapter 4 – Synthesis of Succinic Acid Metabolites Produced by Strain HxN1 During Anaerobic Growth with Hexane		
4.1	Assignment of configuration of stereocenters in (1-methylpentyl)succinic acid isomers produced by strain HxN1 during anaerobic growth with <i>n</i> -hexane	114
4.2	Assignment of configuration of 4-methyl octanoic acid produced by strain HxN1 during anaerobic growth with <i>n</i> -hexane	119
4.3	Proposed stereochemistry of the reactions involved in the initial steps of the anaerobic oxidation of <i>n</i> -hexane in the denitrifying strain HxN1	119
4.4	Labelling patterns of other metabolites detected upon anaerobic growth of strain HxN1 with various deuterium-labelled substrates	108
Chapter 5 – Anaerobic Degradation of Naphtalene		
5.1	Introduction to polycyclic aromatic hydrocarbons	110
5.1.1	<i>Synthesis of intermediates</i>	130
5.2	In vitro assay and conclusion	135
Chapter 6 – Experimental		
6.1	General Experimental Details	141
6.2	Details of microbiological experiments	142
References		154

Chapter 1

Biological Oxidation of Alkanes

1.1 INTRODUCTION TO ALKANE OXIDATION

Alkanes are major constituents of crude oil but can also be produced by many living organisms where they can serve as chemo-attractants or protecting agents against water loss, insects and pathogens. They are present in most soils and waters, but maintain a relatively constant concentration as a result of ongoing biodegradation processes.

Alkanes are reduced molecules with a high energy and carbon content and therefore can be very good carbon and energy sources for microorganisms which can metabolise them. However, the metabolism of these compounds poses two problems:

- 1) They are very hydrophobic and their water solubility is extremely low which creates a problem for their uptake.
- 2) They are chemically inert compounds and must be activated before they can be metabolised, which requires a lot of energy.

Despite these problems, many microorganisms (bacteria, fungi and yeast) have acquired the ability to metabolise alkanes and use them as a carbon source.¹⁶ A typical soil, sand or ocean sediment contains 10^4 - 10^6 hydrocarbon degrading microorganisms per gram,¹⁷ but this number can increase significantly in oil-polluted sites.¹⁸

Many of the alkane degraders are bacteria with a very adaptable mechanism and therefore alkanes are among many other substrates which can be metabolised and can serve as carbon sources.¹⁹ However, in the past few years some bacterial species have been characterised which can specifically degrade alkanes. They are called hydrocarbonoclastic bacteria and play a key role in the removal of hydrocarbons from polluted environments.²⁰ One example is *Alcanivorax borkumensis*, a marine bacterium that can metabolise linear and branched alkanes, but is unable to use aromatic hydrocarbons, sugars, amino acids, fatty acids and most other common substrates as their carbon source.²¹ They are present in non-polluted sea water in low numbers, probably using the alkanes produced by algae and other sea organisms as substrates but become predominant after a spill of crude oil. Therefore they are believed to play a key

role in the bioremediation of oil spills worldwide.²² Hydrocarbonoclastic alkane-degrading bacteria of the genera *Thalassolituus*²³, *Oleiphilus*²⁴ and *Oleispira*²⁵ also play an important role in the biodegradation of oil spills in several environments.^{7d, 11} Alkanes can be metabolised aerobically or anaerobically. The pathways and the enzymology for both types of degradation are described below.

1.2 AEROBIC DEGRADATION OF ALKANES

The water solubility of *n*-alkanes decreases exponentially as their molecular weight increases (Table 1).²⁶ The exact way in which alkanes enter a cell is unclear, but the mechanism differs depending on the microorganism considered, the molecular weight of the alkane and the characteristics of the environment.^{16b} The direct uptake of alkane molecules from water can only be considered for lower molecular weight alkanes which are sufficiently soluble in water to assure a mass transfer. For longer chain *n*-alkanes, microorganisms may uptake these compounds either via a hydrophobic cell surface or by a surfactant-facilitated access.

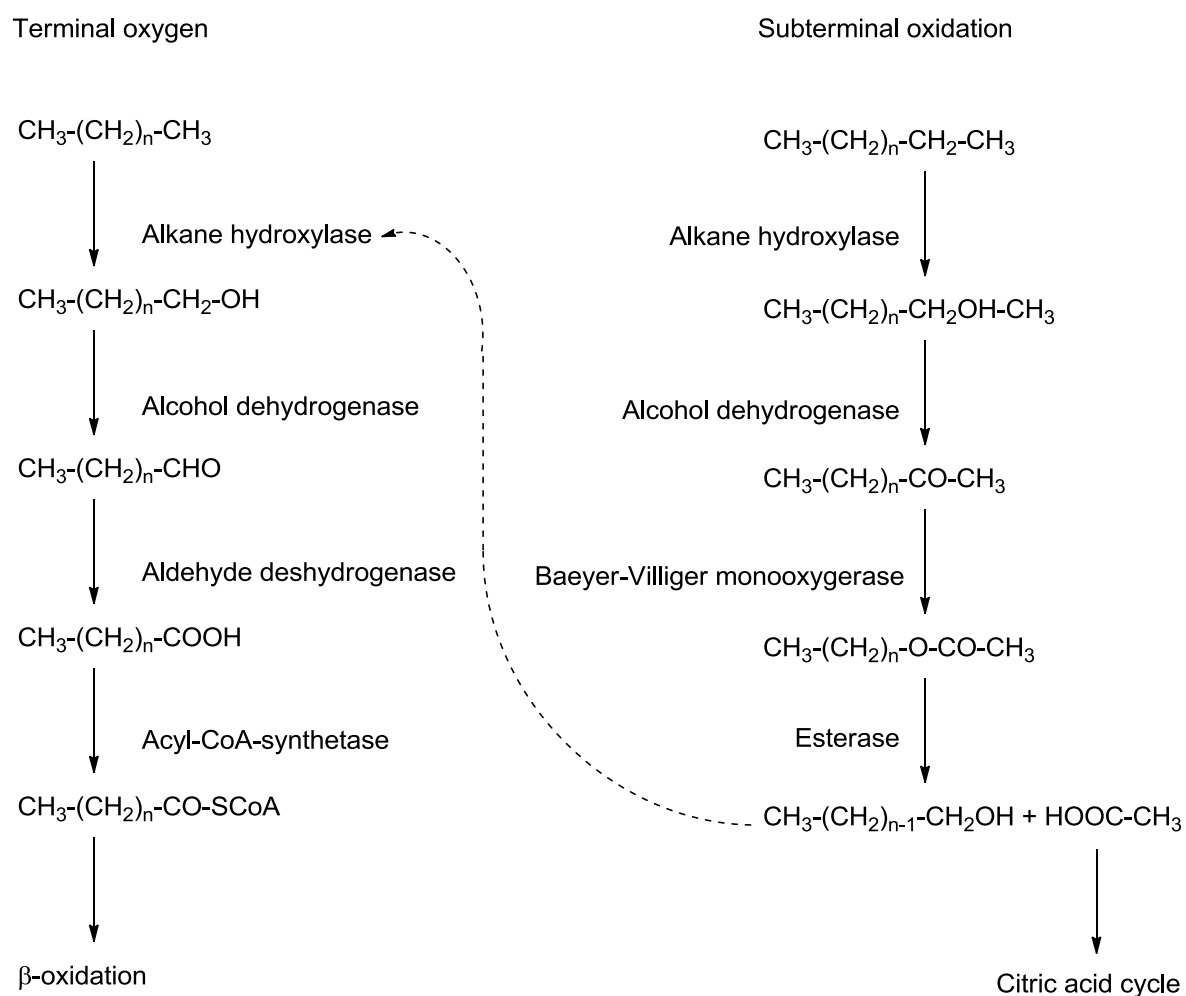
❖ Table 1 - Water solubility of <i>n</i> -alkanes (at 25 °C)			
<i>n</i> -Alkane	Carbon atoms	Molecular weight (g/mol)	Solubility (mol/dm ³)
Propane	3	44.1	5×10^{-3}
Hexane	6	86.2	1.4×10^{-4}
Nonane	9	128.3	10^{-6}
Dodecane	12	170.3	2×10^{-8}
Hexadecane	16	226.4	2×10^{-10}
Eicosane	20	282.6	10^{-12}
Hexacosane	26	366.7	4×10^{-16}

Most of the bacteria which are able to degrade *n*-alkanes produce surfactants. Biosurfactants are produced by a variety of oil-degrading microorganisms. These biosurfactants can be of low molecular weight, acting by decreasing the oil–water interfacial tension, or high molecular weight acting as biodispersants by preventing coalescence of oil drops in water. For example, alasan, produced by a strain of *Acinetobacter radioresistens*, is a complex of an anionic polysaccharide and protein with a molecular weight of approximately 106 Da.

The polysaccharide component of alasin is unusual in that it contains covalently bound alanine. The protein is highly effective in stabilising oil-in-water emulsions and in solubilising hydrocarbons, including polycyclic aromatic hydrocarbons.²⁷

1.2.1 Pathways for aerobic degradation of *n*-alkanes

Aerobic degradation of *n*-alkanes in most cases starts by the oxidation of a terminal methyl group to a primary alcohol, which is further oxidised to the corresponding aldehyde, and finally converted into a fatty acid. Fatty acids are conjugated to coenzyme A and further processed by β -oxidation to generate acetyl-CoA. Subterminal oxidation also occurs, but is less common with microorganisms (Scheme 1).^{16b}



Scheme 1 – Pathways for aerobic degradation of *n*-alkanes.

While oxidation of fatty alcohols and fatty acids is common among microorganisms, activation of alkanes requires specific enzymes which are much less common. The initial terminal hydroxylation of *n*-alkanes can be carried out by enzymes belonging to different families (Table 2).^{16a}

❖ Table 2 – Alkane oxidising enzyme classes			
Enzyme class	Characteristics	Substrate length	Host
MMO, methane monooxygenase	$\alpha_2 \beta_2 \gamma_2$ hydroxylase; dinuclear iron reductase, [2Fe–2S], FAD, NADH regulatory subunit	C ₁	Bacteria
PRM, propane monooxygenase	Non-heme iron monooxygenase similar to sMMO	C ₃	Bacteria
sBMO, butane monooxygenase	Non-heme iron monooxygenase similar to sMMO	C ₂ - C ₉	Bacteria
pBMO, butane monooxygenase	Copper-containing monooxygenase similar to pMMO	C ₂ - C ₉	Bacteria
CYP153	Soluble cytochrome P450 monooxygenase	C ₅ - C ₁₂	Bacteria
CYP52	Membrane-bound cytochrome P450 monooxygenase	C ₁₀ - C ₁₆	Yeasts
AlkB-related	Non-heme iron monooxygenase	C ₃ - C ₁₃ or C ₁₀ - C ₂₀	Bacteria
AlmA	Flavin-binding monooxygenase	C ₂₀ - C ₃₆	Bacteria
LadA	Thermophilic flavin-dependent monooxygenase	C ₁₀ - C ₃₀	Bacteria
Dioxygenase	Copper flavin-dependent dioxygenase	C ₁₀ - C ₃₀	Bacteria
The substrate range is approximate.			

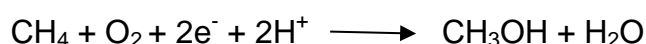
Microorganisms degrading short-chain-length alkanes (C₂ - C₄) have enzymes associated with methane monooxygenases. Strains degrading medium-chain-length alkanes (C₅ - C₁₁), or long-chain-length alkanes (>C₁₂), commonly contain integral membrane non-heme iron monooxygenases related to the *Pseudomonas putida* GPo1 AlkB alkane hydroxylase. However, some strains

contain alkane hydroxylating enzymes that belong to a family of soluble cytochrome P450s (CYP450s) and that are active against C₅ – C₁₁ alkanes. Finally, several strains which are able to oxidise alkanes of more than 18 carbon atoms contain alkane hydroxylases that seem to be unrelated to the former ones and that only recently have started to be characterised. Several yeasts can also oxidise alkanes as well with enzymes belonging to the family of microsomal CYP450 monooxygenases. Therefore, the role of yeasts in the biodegradation of alkanes may be more significant than previously thought.²⁸

1.2.2 Alkane hydroxylases related to methane monooxygenase

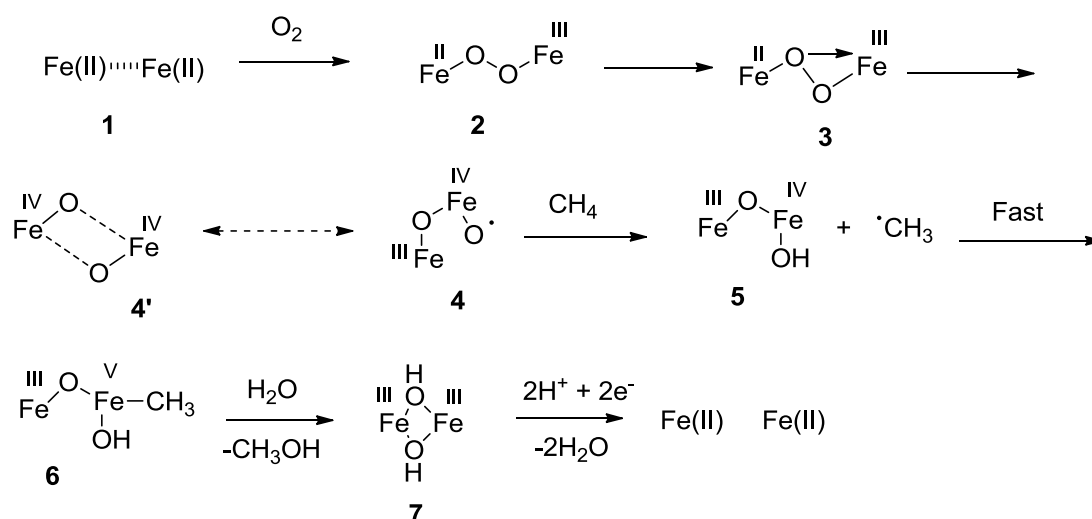
The enzymes that initially oxidise short chain alkanes are related to methane monooxygenases. There are two different forms of methane monooxygenase. All methanotrophs produce a membrane-bound form of methane monooxygenase (pMMO) which oxidises a narrow range of alkanes, while some others additionally produce a soluble form of methane monooxygenase (sMMO) that is active on a broader range of substrates and oxidises C₁ – C₇ alkanes to the corresponding alcohols.²⁹

The catalytic iron core of the soluble methane monooxygenase (MMO) has the unique ability to hydroxylate methane:



Quantum chemical calculations and crystallographic studies have provided the mechanism for the reaction sequence for the activation of methane by MMO leading to formation of methanol (Scheme 2).³⁰ As shown in Fig. 2 the starting cluster **1** binds and activates dioxygen to form the superoxo species **2**. As the O-O bond dissociates, one of the oxygens is bridge bonded but the other oxygen is only bound to the iron (**3**). Once the O-O bond is broken, it gives the key radical species (**4**) which is in equilibrium with **4'**. The oxy radical **4** abstracts a hydrogen atom from methane to form Fe(IV)-OH group (**5**) and a methyl radical. The methyl radical recombines with the Fe(IV) centre to give intermediate **6**, which has a weak Fe-C bond. The alkyl complex formed can

now lose methanol to form intermediate **7**. This latter species is then reduced to regenerate intermediate **1**, which reacts with dioxygen.



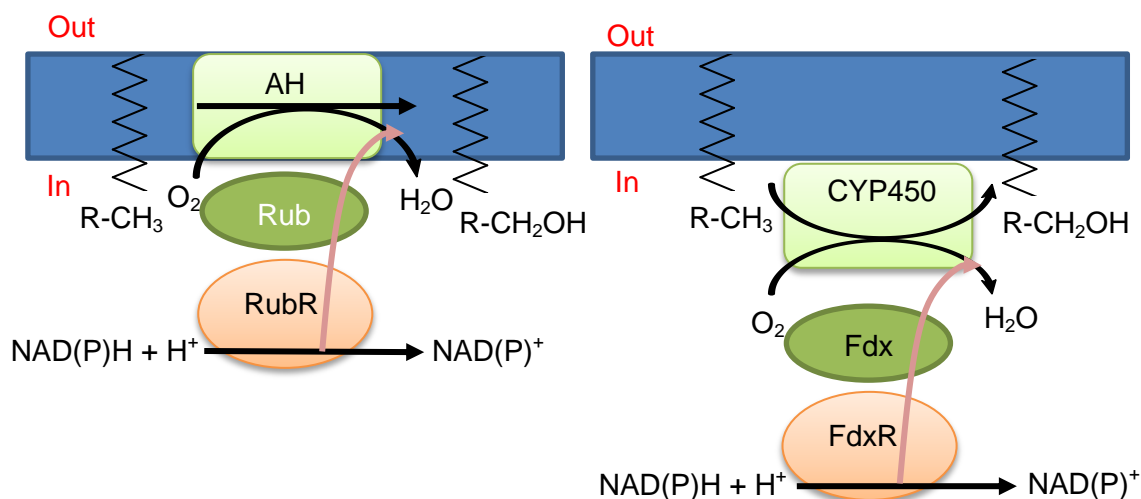
Scheme 2 – Mechanism of activation of methane by MMO.

1.2.3 The AlkB family of alkane hydroxylases

The most extensively characterised alkane degradation pathway is from the AlkB family, which have a non-heme diiron monooxygenase membrane. AlkB requires two soluble electron transfer proteins named rubredoxin and rubredoxin reductase. Rubredoxin reductase, via its cofactor FAD, transfers electrons from NADH to the rubredoxin, which in turn transfers electrons to AlkB (Fig. 1).³¹

The diiron cluster allows the oxygen-dependent activation of the alkane molecule through a substrate radical intermediate. One of the oxygen atoms of dioxygen is transferred to the terminal methyl group of alkane, while the other oxygen atom is reduced to H₂O by electrons transferred by the rubredoxin. Oxidation is both regio- and stereo-specific.

More than sixty AlkB homologs are known to date in both gram-positive and gram-negative microorganisms. Only a few of these enzymes oxidise C₃ - C₁₃ alkanes, whereas most members of this family prefer alkanes larger than C₁₀.³²



✚ **Figure 1** – Oxidation of *n*-alkane hydroxylases belonging to the AlkB family (left) or to the bacterial cytochrome P450 family (right). AH, membrane bound alkane hydroxylase; Rub, rubredoxin; RubR, rubredoxin reductase; CYP450, soluble cytochrome P450; Fdx, ferredoxin; FdxR, ferredoxin reductase. The blue bar represents the cytoplasmic membrane; the phospholipid layer facing the cytoplasm is marked as “In”.

1.2.4 Cytochrome P450 alkane hydroxylases

CYP450s are heme-thiolate proteins that catalyse the oxygenation of a large number of compounds. They are ubiquitous among all kingdoms of life and can be grouped in more than 100 families. Almost all eukaryotic P450s are membrane-bound (CYP52) enzymes, while most prokaryotic P450s are soluble (CYP153) and require the presence of a ferredoxin and ferredoxin reductase that transfers electrons from NAD(P)H to the cytochrome (Fig. 1).³³ CYP450s from *Mycobacterium sp.* have been purified and shown to hydroxylate C₆-C₁₁ alkanes to 1-alkanols with high affinity and regioselectivity.³⁴

As mentioned, several yeasts can assimilate alkanes as well. The enzymes involved are membrane bound cytochrome P450s of the CYP52 family and receive electrons from NADPH via flavin adenine dinucleotide (FAD)- and flavin mononucleotide (FMN)-containing reductases.³⁵

1.2.5 Alkane hydroxylases for long chain *n*-alkanes

Several bacterial strains have been reported to oxidise alkanes larger than C₂₀. The enzymes responsible for the oxidation of such alkanes, which are solid at room temperature, are still poorly characterised.^{16b} In *Acinetobacter sp.* M1, which can grow on C₁₃ – C₄₄ alkanes, several alkane oxidising enzymes have

been detected. Two of them, named AlkMa and AlkMb, are related to the AlkB family and are membrane bound.³⁶ A third enzyme has been reported that is soluble, requires Cu^{2+} , does not receive electrons from NADH and is therefore clearly unrelated to the AlkB family of hydroxylases (Maeng et al., 1996). This enzyme has been proposed to be a dioxygenase which oxidises $\text{C}_{10} - \text{C}_{30}$ alkanes and generates *n*-alkyl hydroperoxides that are converted to the corresponding aldehyde.

A different *Acinetobacter* strain, named DSM 17874, also contains at least three alkane oxidizing enzymes. Two of them are AlkB paralogs similar to the AlkMa and AlkMb enzymes described above, and oxidise alkanes in the range of $\text{C}_{10} - \text{C}_{20}$ (Throne-Holst et al., 2006). A third enzyme has been reported that oxidises alkanes in the range of C_{20} to $> \text{C}_{32}$. Its gene, designated *almA*, has been identified and codes for a flavin-binding monooxygenase.³⁷ Genes homologous to *almA* were identified in several long-chain *n*-alkane degrading strains.

A different long-chain alkane hydroxylase has been characterized in the thermophilic bacterium *Geobacillus thermodenitrificans* NG80-2. This enzyme is known as LadA and oxidises $\text{C}_{15} - \text{C}_{36}$ alkanes, generating the corresponding primary alcohols. Its crystal structure has been solved, revealing that it belongs to the bacterial luciferase family of proteins, which are two-component flavin-dependent oxygenases. LadA is believed to oxidise alkanes by a mechanism similar to that of other flavoprotein monooxygenases.³⁸

Several bacterial strains can degrade $> \text{C}_{20}$ alkanes using enzyme systems that have still not been characterised. It is likely that new enzyme classes will be found in the near future responsible for the oxidation of these high molecular weight alkanes.

Some bacterial strains contain only one alkane hydroxylase. However, it is more common for these strains to contain more than one alkane oxidation system and in most cases they have different substrate ranges.

1.2.6 Metabolism of the alcohols and aldehydes derived from the oxidation of alkanes

The primary fatty alcohols generated by terminal oxidation of alkanes are further oxidised to aldehydes by an alcohol dehydrogenase (ADH). Subterminal

alcohols are respectively converted to ketones by alcohol dehydrogenases. There are several types of ADHs. Some use NAD(P)^+ as electron acceptor, while others do not depend on NAD(P)^+ and use electron acceptors such as cytochromes or ubiquinone. Most NAD(P)^+ -independent ADHs contain pyrroloquinoline quinone and are commonly named quinoprotein ADHs.

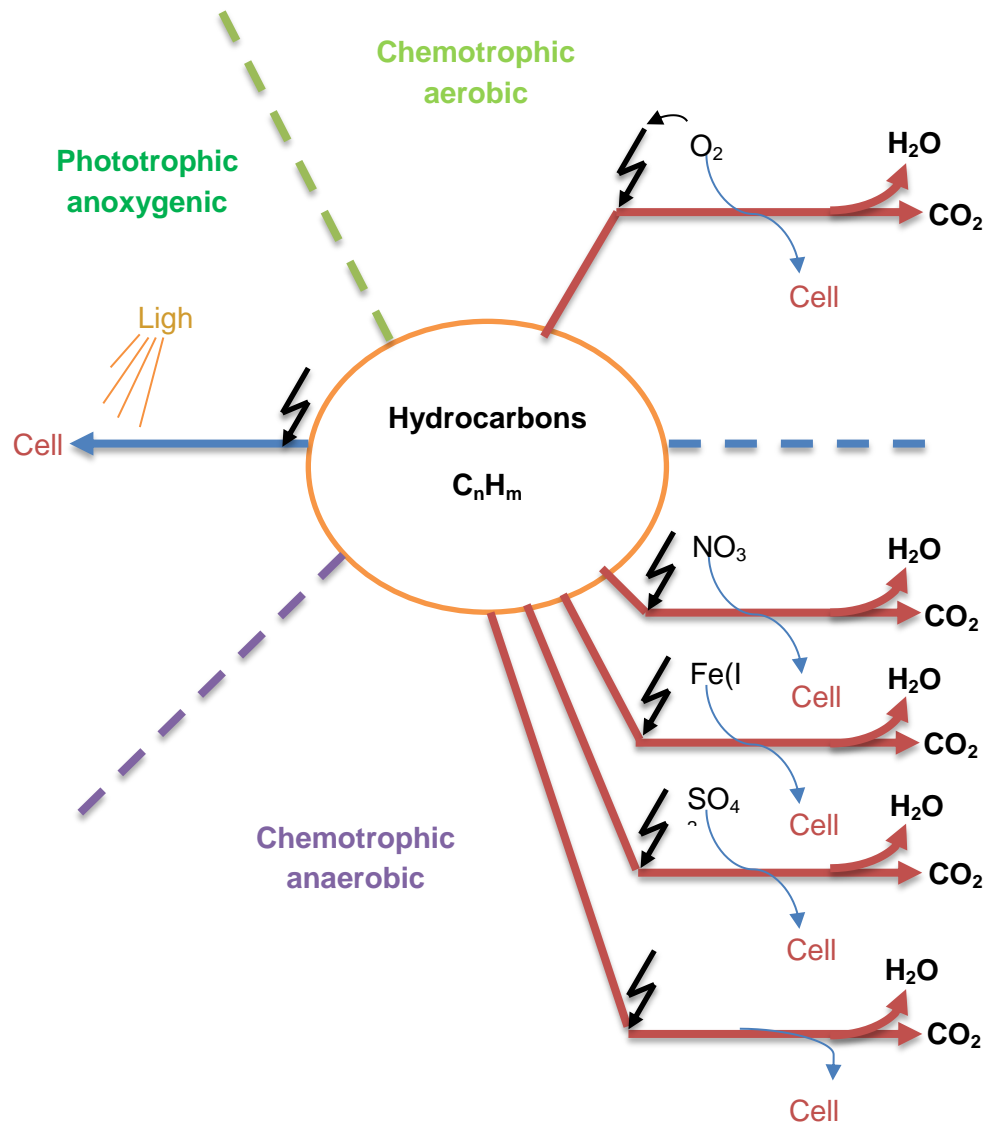
The fatty acids generated by oxidation of the aldehydes are further metabolised by β -oxidation, generating an acyl-CoA that enters the tricarboxylic acid cycle. However, when the carbon source is in excess relative to nitrogen, many bacteria use part of the carbon to generate storage materials such as triacylglycerols, wax esters, poly(hydroxybutyrate) or poly(3-hydroxyalkanoates), which accumulate as lipid bodies.³⁹ These compounds can serve as carbon and energy sources later during starvation periods.

1.3 ANAEROBIC DEGRADATION OF ALKANES

Bacteria and fungi that utilise hydrocarbons in the presence of dioxygen have been known since the beginning of the 20th century. The fact that dioxygen is not available in all the environments where hydrocarbons occur (e.g. in deep sediments and in oil reservoirs) has repeatedly evoked the question as to whether or not the biodegradation of hydrocarbons is possible under anoxic conditions and if so to what extent. It was not until the late 1980s that novel types of microorganisms were definitively shown to degrade hydrocarbons under strictly anoxic conditions (Fig. 2).⁴⁰ Phototrophy is the process by which organisms trap light energy (photons) and store it as chemical energy in the form of ATP and/or reducing power in NADPH. Phototrophic anoxygenic is the photosynthetic process where light energy is captured and converted to ATP, without the production of dioxygen. Water is therefore not used as an electron donor. There are several groups of bacteria that undergo anoxygenic photosynthesis: green sulfur bacteria, green and red filamentous anoxygenic phototrophs (FAPs), phototrophic purple bacteria, phototrophic acidobacteria, and phototrophic heliobacteria.⁴¹

Chemotrophs are organisms that obtain energy by the oxidation of electron donors in their environments. These electron donors can be organic

(chemoorganotrophs) or inorganic (chemolithotrophs). The chemotroph designation is in contrast to phototrophs, which utilise solar energy.⁴²



✚ **Figure 2** – Experimentally verified possibilities for the microbial utilisation of hydrocarbons. In all chemotrophic reactions, a part of the hydrocarbon is oxidised for energy conservation (catabolism) and another part is assimilated into cell mass. In aerobic oxidation of hydrocarbons dioxygen is not only the terminal electron acceptor, but is also needed for substrate

From a thermodynamic point of view, anaerobic biodegradation of alkanes under nitrate, sulfidogenic, and methanogenic conditions is possible⁴³ (see Table 3 with hexadecane as a model substrate). As of yet no studies of degradation of alkanes under iron-reducing conditions has been reported.

❖ Table 3 - Gibbs free energies for hexadecane (C ₁₆ H ₃₄) degradation coupled to selected redox reactions at standard conditions (298 K) at pH=7.			
Electron acceptor (ox/red)	Overall energetic equation	ΔG° (KJ/mol) ^a	$\Delta G^\circ'$ (KJ/mol) ^b
O ₂ /H ₂ O ^c	C ₁₆ H ₃₄ + 24.5O ₂ → 16HCO ₃ ⁻ + H ₂ O + 16H ⁺	-9677	-10316
NO ₃ ⁻ /N ₂	C ₁₆ H ₃₄ + 19.6NO ₃ ⁻ + 3.6H ⁺ → 16HCO ₃ ⁻ + 9.8N ₂ + 10.8H ₂ O	-9819	-9676
Fe ³⁺ /Fe ²⁺	C ₁₆ H ₃₄ + 98Fe ³⁺ + 48H ₂ O → 16HCO ₃ ⁻ + 98Fe ²⁺ + 114H ⁺	-5336	-9891
SO ₄ ²⁻ /H ₂ S	C ₁₆ H ₃₄ + 12.25SO ₄ ²⁻ + 8.5H ⁺ → 16HCO ₃ ⁻ + 12.25H ₂ S + H ₂ O	-897	-557
CO ₃ ⁻ /CH ₄	C ₁₆ H ₃₄ + 11.25H ₂ O → 3.75HCO ₃ ⁻ + 12.25CH ₄ + 3.75H ⁺	-204	-353

a) ΔG° : standard Gibbs free energy: reactants and products at 1 M concentration and gases at a partial pressure of 1 atm. Hexadecane (C₁₆H₃₄) was chosen as the model substrate for free energy calculations. Gibbs free energy of formation for *n*-hexadecane in the liquid state was taken from Helgeson et al. (1998).^{43a} For all other compounds the data were taken from Thauer et al. (1977)^{43b} and Hanselmann (1991).^{43c} Methane, hydrogen, nitrogen and oxygen are in the gaseous phase at partial pressures of 1 atm. All other compounds are in the aqueous phase.

b) $\Delta G^\circ' = \Delta G^\circ + m \times 2.303RT \log 10^{-7}$ (*m* is the net number of protons formed in the equation).

c) The reaction with dioxygen is shown for comparison.

1.3.1 Methanogenesis

This is referred to as the biological formation of methane that is carried out by strictly anaerobic microorganisms, Methanogenic degradation is the least energetically favourable process when compared to the other anaerobic respirations (Table 3). The main route whereby alkanes are converted to methane is assumed to involve syntrophic alkane conversion to acetate and hydrogen linked to syntrophic acetate oxidation to H₂ and CO₂ and coupled with methanogenesis from CO₂ reduction (Fig. 3), which is known as the MADCOR process.⁴⁴ So far no methanogenic isolates have been obtained and only a few studies have provided the phylogeny of microorganisms potentially involved in this syntrophic association. In the ditch mud methanogenic enrichment, it is assumed that the community is essentially composed of: (i) syntrophic proton reducing acetogenic bacteria (*Syntrophus spp.*) which decompose the alkane to

acetate and H₂; (ii) a group of archaea (*Methanosaeta*) which form methane and CO₂ from acetate; and (iii) another group of archaea (*Metanospirillum* and *Methanoculleus*) converting CO₂ and H₂ to methane.⁴⁵

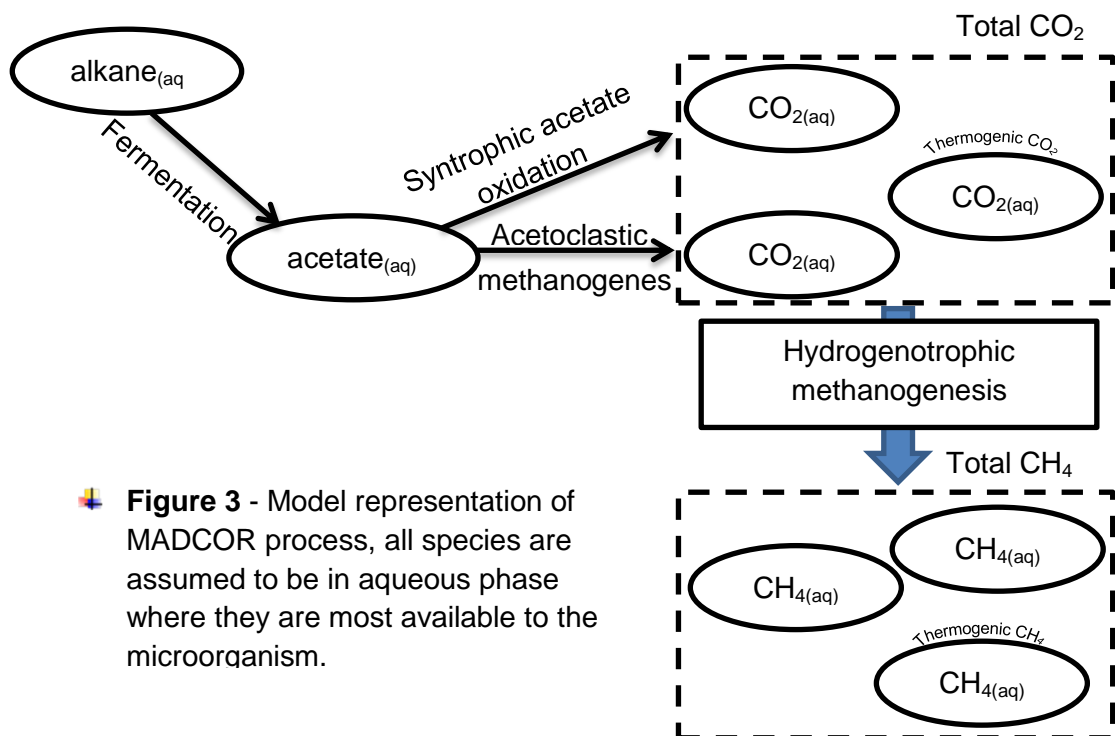
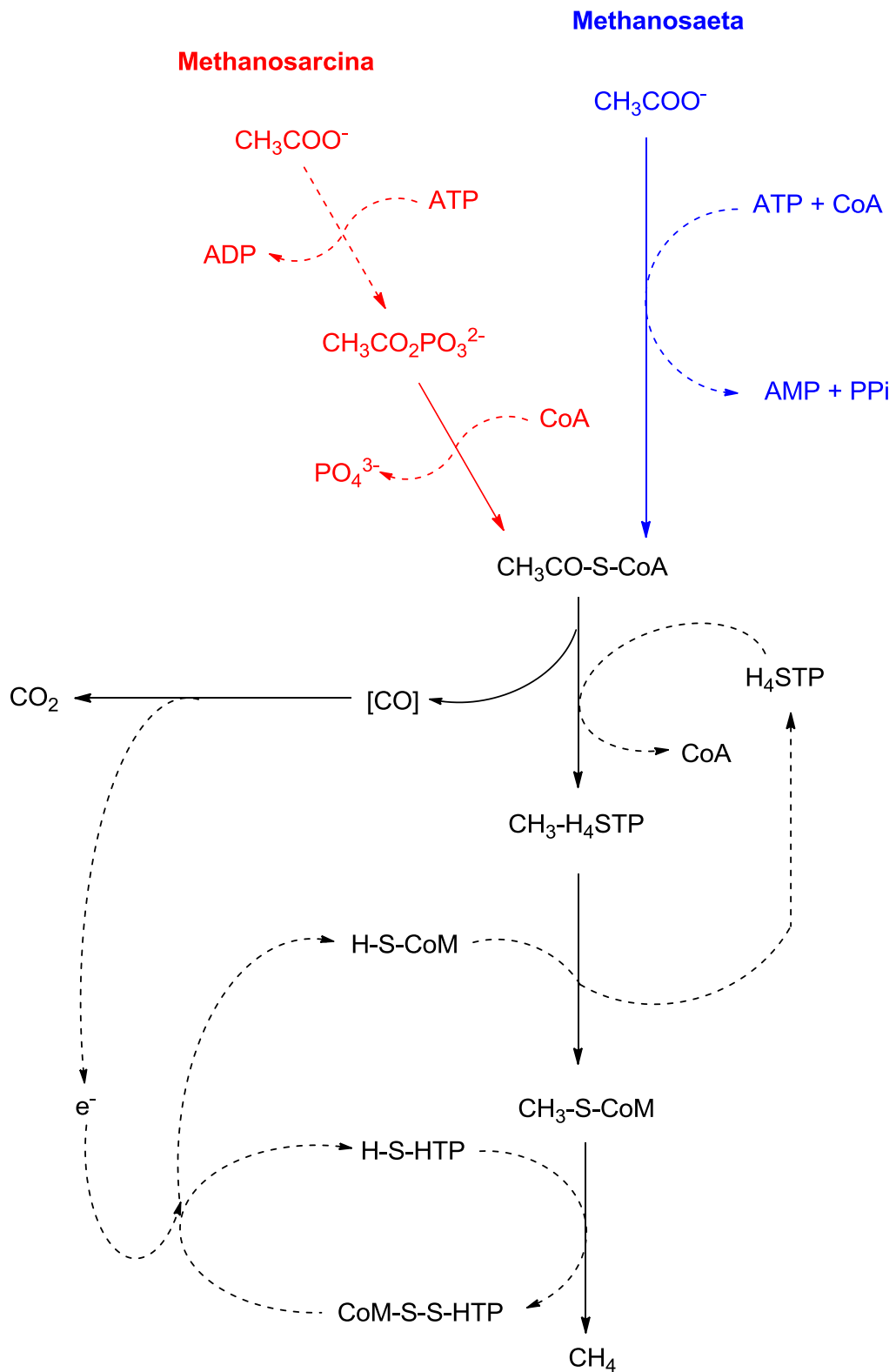


Figure 3 - Model representation of MADCOR process, all species are assumed to be in aqueous phase where they are most available to the microorganism.

The majority of biological methanogenesis (about 70%) originates from conversion of the methyl group of acetate to methane; However, only two genera are known, *Methanosarcina* and *Methanosaeta*, which utilise acetate as an energy source (Fig. 3).⁴⁶

As described in Scheme 3 the *Methanosarcina* utilise a two step pathway to fix acetate to acetyl-CoA, while the *Methanosaeta* utilise only one step. The pathways converge at acetyl-CoA. The solid lines represent steps where bonds to acetate carbon (carbon originating at either position) are formed or broken, while the dashed lines indicate steps which do not directly involve these carbon atoms. Both carbon atoms of acetate are generally conserved; the carboxyl position goes to CO₂ while the methyl position goes to CH₄.



Scheme 3 - Catabolic pathways of aceticlastic methanogens. ATP (adenosine triphosphate), PPi (inorganic diphosphate), CoA (coenzyme A), H_4STP (tetrahydrosarcinapterin), CoM (coenzyme M), and H-S-HTP (*N*-7-mercaptoheptanoyl-*O*-phospho-L-threonine).

1.3.2 Nitrate-reducers

These microorganisms are able to grow under anoxic conditions by coupling alkane oxidation to CO₂ with NO₃⁻ reduction to N₂. Anaerobic degradation of alkanes under nitrate-reducing conditions has been regarded as an effective method in the bioremediation of crude oil.⁴⁷

Three of the identified denitrifying isolates which are able to grow under anoxic conditions by coupling alkane oxidation to CO₂ with NO₃⁻ reduction to N₂ are strains HxN1, OcN1 and HdN1 (Fig. 4).⁹

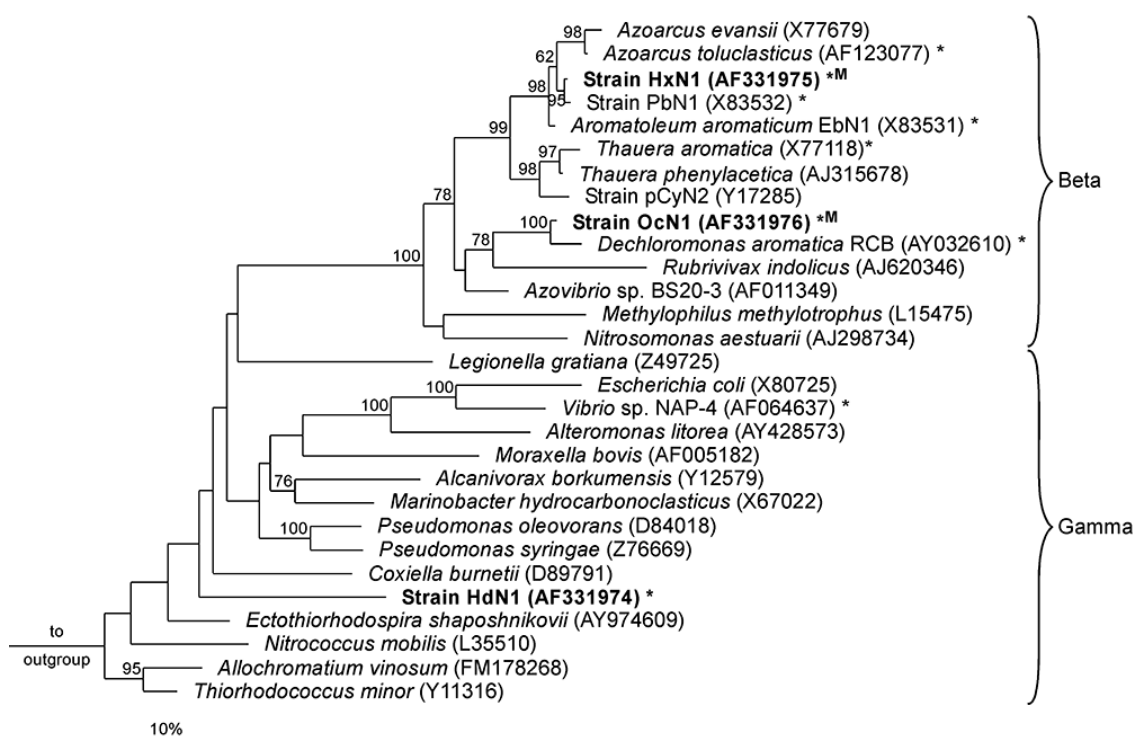


Figure 4 - Phylogenetic (16S rRNA-based) affiliation of strain HdN1 with selected *Beta*- and *Gamma*-proteobacteria including other strains able to degrade aromatic or saturated petroleum hydrocarbons with nitrate (*). Strains able to degrade *n*-alkanes anaerobically are highlighted in bold; occurrence of (1-methylalkyl)succinate formation for alkane activation is also indicated (^M). Bootstrap values (%; only > 60% shown) were obtained after 1000 resamplings. Scale bar, 10% estimated sequence divergence.

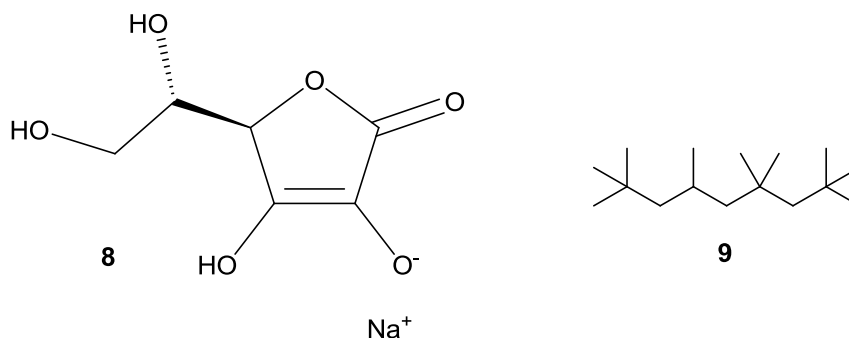
Oxidation of alkanes with nitrate as electron acceptor under strict exclusion of air have been demonstrated in quantitative growth experiments with pure cultures. Published enrichment studies, isolation and the comparison of the

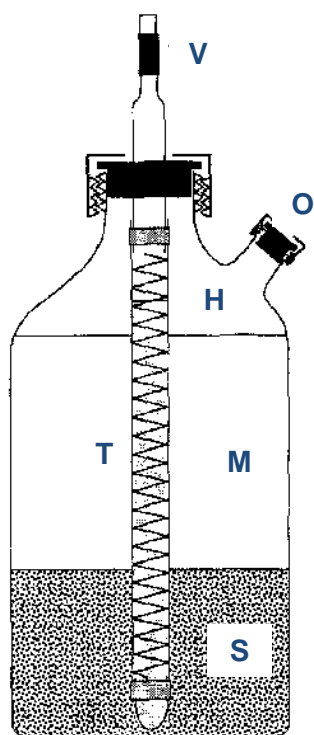
three mentioned *n*-alkane-degrading denitrifying bacteria are described and summarised below.

1.3.2.1 General growth conditions

According to published results by Ehrenreich et al.⁹, enrichment cultures (Fig. 6) with individual alkanes and crude oil were inoculated with a homogenised mixture of sediment samples from ditches in Bremen, Germany (source of strains HxN1 and OcN1). The inoculum for the enrichment culture with aliphatic mineral oil was activated sludge from the sewage plant in Lintel/Osterholz-Scharmbeck, Germany (source of strain HdN1).⁹

Bacteria were grown under strict anoxic conditions in defined bicarbonate/CO₂-buffered media (Fig. 5).⁴⁸ Traces of dioxygen from air could lead to hydroxyl compounds through monooxygenases (which can be further degraded anaerobically). Hence, in addition to physical exclusion of air, a reductant ('redox buffer') was also used. Unlike sulfate-reducing bacteria that form a chemical reducing agent, sulfide, nitrate-reducing bacteria do not produce a reductant. Addition of sulfide (or other reducing sulfur compounds) is inappropriate because it could easily oxidise in by-reactions of the 'high-potential' nitrate reduction pathway or it may inhibit denitrifiers. Hence fresh sodium ascorbate⁴⁹ **8** was used in addition to establish reducing conditions (ascorbate does not serve as a growth substrate for the presently studied pure cultures). The initial pH of the medium was adjusted to 7.1 and 5 mM NaNO₃ was added. Anoxic conditions in enrichment cultures were achieved solely by deaeration and flushing with N₂/CO₂ (90/10, v/v). Alkanes were added to the cultures as diluted solutions (0.5–10%, v/v) in 2,2,4,4,6,8,8-heptamethylnonane (HMN) **9** as inert carrier phase to avoid toxic effects.





✚ **Figure 5** - Special glass bottle used for anoxic enrichment of alkane degrading denitrifying bacteria. Bottles were filled with approx. 400 mL freshwater sediment (S) and 600 mL mineral medium (M). The headspace (H) contained an anoxic atmosphere of N_2/CO_2 (90/10, v/v). Stoppers were of butyl rubber. Alkanes were added to the cultures as diluted solutions (0.5–10%, v/v) in 2,2,4,4,6,8,8-heptamethylnonane inside a large (inner diameter, 18mm) thin-walled (1 mm) silicon tubing (T) sealed at the bottom with a glass cap. Collapse of the silicon tubing was prevented by an inserted spiral of stainless steel. The top of the silicon tubing was connected to a glass orifice sealed with a short piece of Viton tubing (V) and a glass rod. Withdrawal of samples for analyses and release of formed N_2 was achieved via the stopper of the side opening (O) using a syringe.

1.3.2.2 Quantification of alkane consumption and nitrate reduction

The batches were prepared by autoclaving a defined volume of deaerated HMN in a serum-stoppered, crimped vial under nitrogen and subsequently the required amount of the filter-sterilised alkane that serves as substrate is injected. Aliquots were withdrawn and injected into culture tubes by using nitrogen-flushed syringes with plastic piston (without rubber).⁹

The time course of nitrate consumption during growth of strains HxN1, OcN1 and HdN1 on alkanes has been measured with hexane, octane and hexadecane, respectively, where aliquots were withdrawn during growth from the aqueous phase by means of nitrogen-flushed syringes and used for subsequent determination of nitrate and nitrite. Separate cultures have also used to determine the balance of alkane degradation by strains HxN1 and HdN1, each incubated with a low and high amount of the organic substrate (Table 4).⁹

❖ **Table 4 - Quantification of alkane consumption and nitrate reduction by strains HxN1 and HdN1.**

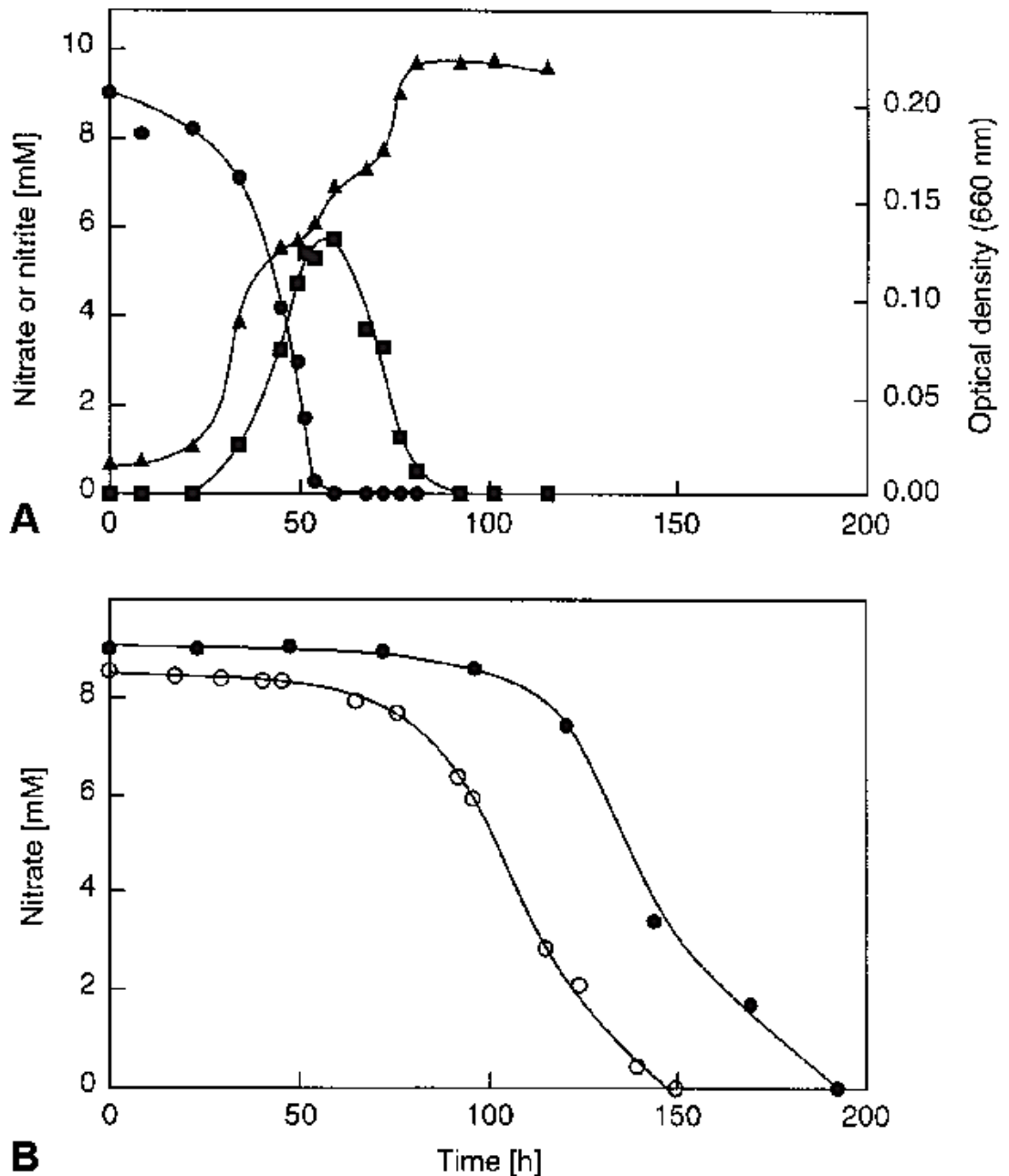
Exp.	Alkane added (mmol)	Alkane used (mmol) ^a	Nitrate added (mmol)	Nitrate used (mmol)	Nitrite formed (mmol)	Cell dry mass (mg)	Alkane dissimilated (mmol) ^b	Electrons from alkane dissimilated (mmol) ^{c, d}	Electrons used by NO ₃ ⁻ reduction (mmol) ^e
Strain HxN1									
Cells with small amount of hexane	0.10	0.09	1.0	0.56	0.07	4.16	0.07	2.66	2.59
Cells with large amount of hexane	0.27	0.18	1.0	1.0	0	9.85	0.14	5.32	5.00
Cells without hexane	0	0	1.0	0.02	0.01	0			0.07
Cells without nitrate	0.27	0.02	0	0	0	0			
Strain HdN1									
Cells with small amount of hexadecane	0.10	0.098	3.4	1.0	0	13.0	0.076	7.45	5.00
Cells with large amount of hexadecane	0.20	0.174	1.6	1.6	0	21.0	0.139	13.62	8.00
Cells without hexadecane	0	0	1.6	0	0	0			0
Cells without nitrate	0.20	0.003	0	0	0	0			0



+ **Figure 6** - Phase-contrast photomicrographs of isolated denitrifying bacteria that can grow anaerobically on alkanes.⁹ **A)** Strain HxN1 grown on hexane (oval-shaped, non-motile cells). **B)** Strain OcN1 grown on octane (rod-shaped, motile cells). **C)** Strain HdN1 grown on valerate. **D)** Strain HdN1 grown on hexadecane (Oval, pleomorphic, partly motile cells). with cells accumulated around a droplet of the alkane. *Bar* =10 mm. Cells for micrographs **A–C** were concentrated by centrifugation.

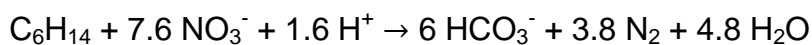
For strain HxN1 the isolation of pure cultures is carried out via anoxic, liquid dilution series with hexane, cells showed to be $1 - 1.5 \times 1.8 - 2 \mu\text{m}$ in size (Fig. 6.A) and non motile. Strain OcN1 is isolated via anoxic agar dilutions with caproate (hexanoate), cells showed to be $0.5 \times 1 - 2 \mu\text{m}$ in size (Fig. 6.B) and highly motile. In contrast to strain HxN1, cells of strain OcN1 show a strong tendency to adhere to the hydrocarbon phase. Isolation of strain HdN1 is carried out via streaking on Gelrite (brand of gelling agent different to agar) medium with emulsified hexadecane and later restreaking with valerate (pentanoate) in anoxic bottles, which develops colonies of oval cells varying in size between 0.5×1.5 and $2 \times 2.5 \mu\text{m}$ (Fig. 6.C & D). Subsequent studies and results suggest that this variation is not due to different types of bacteria, but rather that only one type of denitrifying bacterium was isolated that exhibited a certain pleomorphism (bacteria that can to alter their shape or size in response to environmental conditions). Small cells were often motile and cells grown on hexadecane were partly associated with the hydrocarbon phase and often contained droplet-like inclusions.

A semilogarithmic plot of growth experiment with strain HxN1, OcN1 and HdN1 provided an estimate of the shortest initial doubling time. Unlike OcN1 and HdN1, strain HxN1 excreted nitrite during growth which was further consumed after depletion of nitrate (Fig. 7.A & B). Using these plots anaerobic alkane consumption during nitrate reduction and formation of cell mass are measured (Table 4). In all cultures, the volume of gas produced per mol of nitrate reduced was in good agreement with nitrate reduction to dinitrogen.

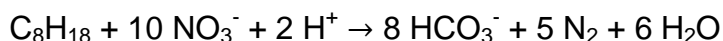


✚ **Figure 7** - Time courses of anaerobic growth of alkane-utilising denitrifying bacteria. **A**) Consumption of nitrate (●), formation of nitrite (■) and cell growth (▲) of strain HxN1 in a culture with hexane. **B**) Consumption of nitrate by strain OcN1 (○) and HdN1 (●) growing anaerobically with octane and hexadecane, respectively; nitrite was not detectable. Reliable monitoring of cell growth of strains OcN1 and HdN1 is not possible because cells grew partly in association with the alkane phase.

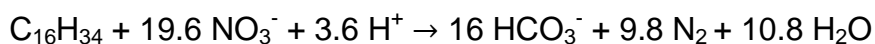
Using quantitative growth experiments equations for complete oxidation of hexane, octane and hexadecane have been determined:



$$\Delta G^\circ = -492.8 \text{ kJ per mol nitrate}$$



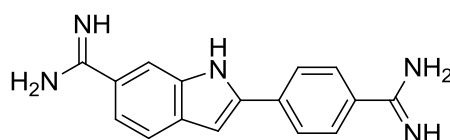
$$\Delta G^\circ = -493.1 \text{ kJ per mol nitrate}$$



$$\Delta G^\circ = -493.7 \text{ kJ per mol nitrate}$$

Further tests have been carried out with strain HdN1⁴⁹ to get a better understanding of this isolate. The strain was grown with *n*-tetradecane and NO_3^- or NO_2^- .⁴⁹ The cell shape of strain HdN1 has shown to be unusually variable and significantly influenced by the organic growth substrate.⁹ In particular long-chain alkanes cause swelling of a large fraction of the cells. In such cells, spacious inclusions resembling storage compounds could be seen at high magnification (Fig 8.A). Cells in alkane cultures tended to grow in close contact with the overlying insoluble hydrocarbon phase. The bulk of alkane-grown cells was buoyant, possibly due to association with or storage of alkane droplets. Alkane storage and buoyancy are features known from aerobic alkane degraders.⁵⁰

Growth experiments have been carried out separately with *n*-tetradecane or *n*-valerate (*n*-pentanoate) for strain HdN1. The isolated strain HdN1 was also mixed with strain OcN1, and a specific 16S rRNA-targeting fluorescent oligonucleotide probe DAPI **10** was applied. Whereas in the pure culture all cells exhibited the specific hybridisation signal (Fig 8.B), the mixed culture contained in addition the expected non-hybridising cells that exhibited only the general fluorescent stain (Fig 8.C). Hence, strain HdN1 is in principle distinguishable from contaminants by specific probing.



10

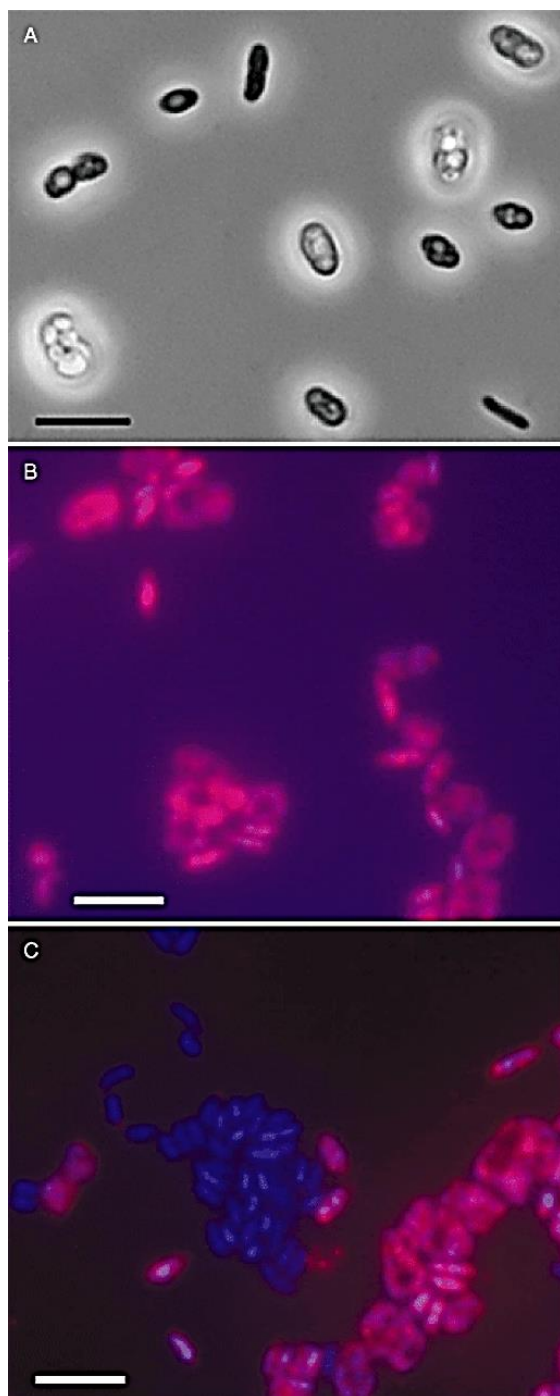


Figure 8 - Microscopic images of strain HdN1. **A)** Highly variable cell forms of strain HdN1 grown anaerobically with hexadecane and nitrate. Phase-contrast micrographs of viable cells. Bar, 5 mm. **B)** Cells from a pure culture of strain HdN1 hybridised with a specific 16S rRNA-targeted oligonucleotide probe and stained with 4',6-diamidino-2-phenylindole (DAPI*). The image represents an overlay of the probe and the DAPI signal. Bar, 5 mm. **C)** Mixed cells of strains HdN1 and OcN1 hybridised, stained and visualised as in (B). Bar, 5 mm.

*(DAPI is a fluorescent stain that binds strongly to A-T rich regions in DNA. It is used extensively in fluorescence microscopy. DAPI can pass through an intact cell membrane therefore it can be used to stain both live and fixed cells, though it passes through the membrane less efficiently in live cells and therefore the effectiveness of the stain is lower).¹⁴

1.3.2.3 Anaerobic growth tests with alkanes and alkanoates

The capability of strain HdN1 for complete hexadecane oxidation with nitrate according to $5 \text{ C}_{16}\text{H}_{34} + 98 \text{ NO}_3^- + 18 \text{ H}^+ \rightarrow 80 \text{ HCO}_3^- + 49 \text{ N}_2 + 54 \text{ H}_2\text{O}$ has been verified formally with small, precisely quantifiable amounts of alkane.⁹ In all subsequent experiments, significantly higher amounts of alkanes were added

than could be oxidised by the electron acceptor (10 mM NO₃⁻). In this way, a large contact area between the insoluble hydrocarbon and the aqueous phase was provided which favoured growth, tests have revealed that strain HdN1 utilised *n*-alkanes from C₆ (*n*-hexane) to C₃₀ (*n*-triacontane) as carbon sources and electron donors (C₆ to C₂₀, C₂₄, C₂₆, C₂₈, C₃₀, C₃₆ and C₄₀ tested). The other strains, HxN1 and OcN1, utilise a significantly narrower range of alkanes, which was from C₆ to C₈ (*n*-octane) and C₈ to C₁₂ (*n*-dodecane) respectively.

1.3.2.4 Growth tests with different electron acceptors

All three strains can also grow aerobically with alkanes. Examination of strain HdN1 in more detail has revealed that almost the same range of *n*-alkanes (and fatty acids) was oxidised with dioxygen as in anaerobic cultures with NO₃⁻. Only *n*-hexane has not so far been utilised with dioxygen. To further examine the capability for efficient use of NO₂⁻ and N₂O, these electron acceptors have been tested individually in the absence of NO₃⁻.

Growth with alkanes can also occur with added NO₂⁻ (instead of NO₃⁻), but takes a longer time. Surprisingly, strain HdN1 did not grow with alkanes in the growth tests with N₂O. In accordance with the lack of growth, N₂O was not consumed (Fig. 9.A, upper curve), and N₂ (Fig. 9.C) or CO₂ (Fig. 9.E) were not formed. In contrast, growth with 1-tetradecanol, 1-hexadecanol or fatty acids was possible with added N₂O, and consumption of N₂O (Fig. 9.B) as well as formation of N₂ (Fig. 9.D) and CO₂ (Fig. 9.F) was obvious. A minor formation of N₂ from N₂O during incubation with hexadecane can be explained by reduction with an endogenous electron source in the inoculum. The formation of N₂ from N₂O requires only 2 e⁻, whereas formation of N₂ from NO₃⁻ requires 10 e⁻ from an electron donor:



For physiological comparison, strains HxN1 and OcN1 were also incubated with N₂O as the only electron acceptor and utilisable alkanes (*n*-hexane and *n*-octane, respectively). These strains were able to grow with N₂O and alkanes. Results are summarised in Fig. 10. The inability for coupling alkane utilisation to N₂O reduction is apparently unique for strain HdN1.

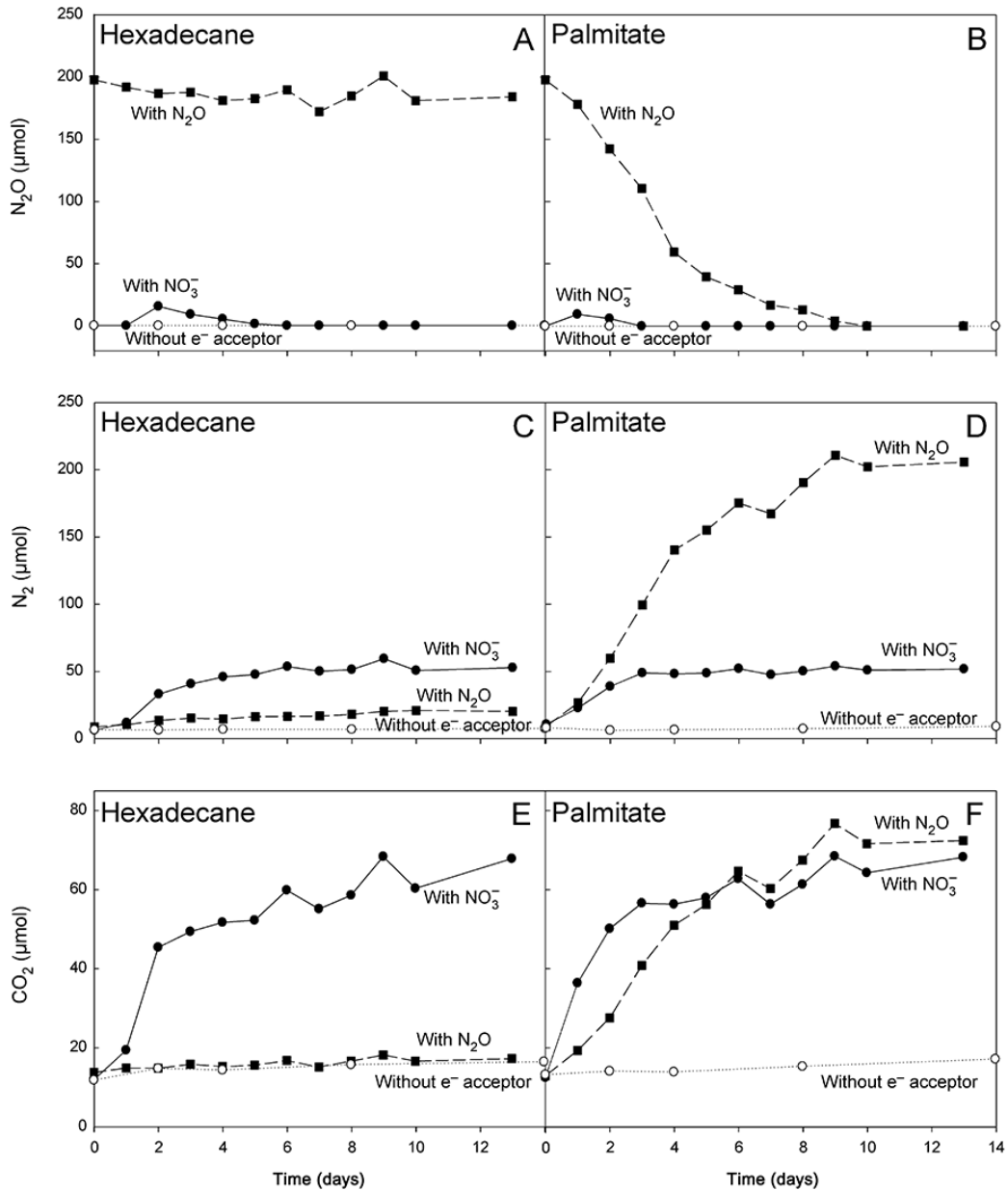
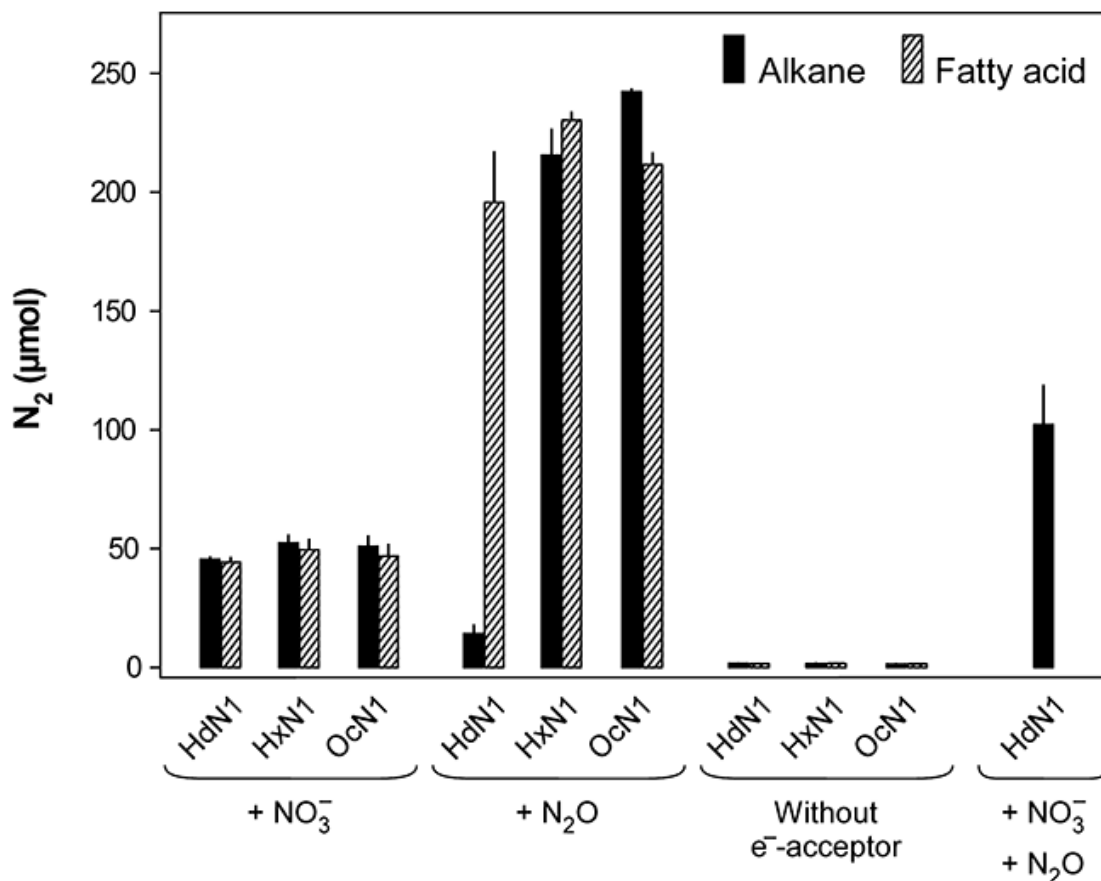


Figure 9 - Time-courses of the formation of N_2O (A and B), N_2 (C and D) and CO_2 (E and F) in anaerobic cultures of strain HdN1 with *n*-hexadecane (A, C and E) or palmitate (B, D and F).



✚ **Figure 10** - N₂ formed in anaerobic cultures of strains HdN1, HxN1 and OcN1 with alkanes (black bars) or fatty acids (striated bars) and either NO₃⁻ (100 µmol) or N₂O (250 µmol). A control experiment with strain HdN1 for excluding N₂O toxicity received both NO₃⁻ and N₂O. Here, more N₂ was formed than with NO₃⁻ alone. This indicated that not only NO₃⁻ but also N₂O was used in the anaerobic respiratory chain if alkane degradation was enabled by NO₃⁻.

1.3.2.5 Search for metabolites and genes involved in alkane degradation

Further research regarding difference in characteristics between HxN1, OcN1 and HdN1 can be achieved by identification and analysis of the genes involved in the anaerobic degradation of *n*-alkanes in each culture.

Metabolite analyses in a denitrifying isolate strain HxN1 proposed an anaerobic activation of the *n*-alkanes at a secondary carbon atom, followed by the addition of fumarate, resulting in a substituted succinate. In denitrifying strain HxN1 diastereomers of (1-methylpentyl)succinate as *n*-hexane derivatives (Fig. 11) have been identified. The reaction resembles anaerobic toluene activation, which leads to benzylsuccinate via a glycol radical enzyme (Scheme 19). Strain

HxN1 a useful organism for detailed investigation into the anaerobic degradation of alkanes. This section gives an insight into the strain HxN1 by analysing proteins specifically formed with *n*-hexane, identifying the encoding genes and comparing the derived amino acid sequences with those of benzylsuccinate synthase that catalyses an analogous reaction in the anaerobic metabolism of toluene.⁵¹

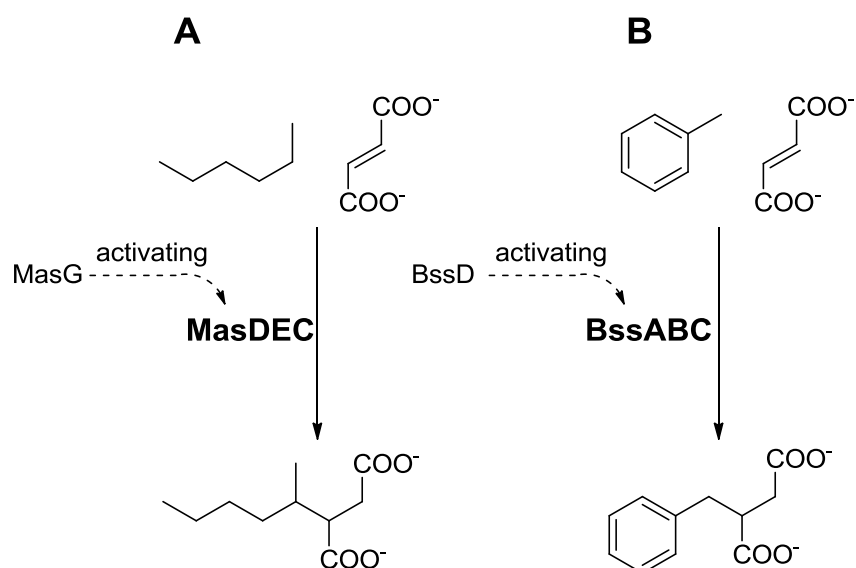
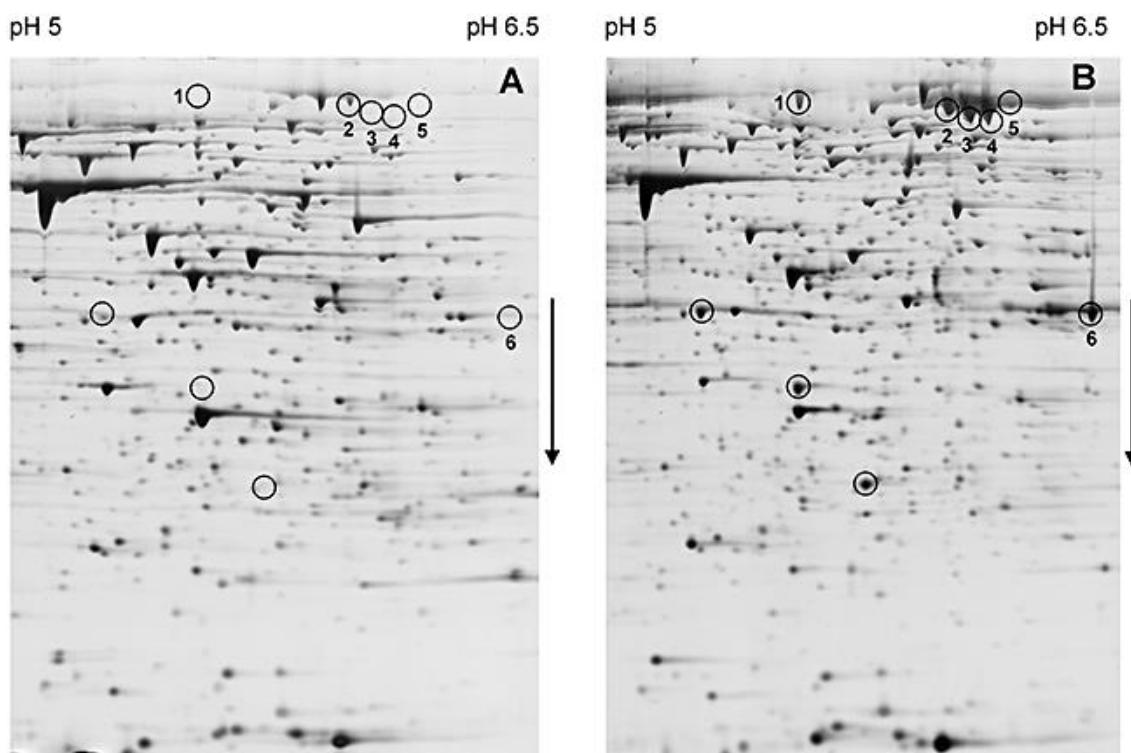


Figure 11 - Anaerobic activation of saturated hydrocarbons and toluene.
A. Anaerobic activation of *n*-hexane according to metabolite analyses (Rabus *et al.*, 2001)²; the indicated gene indicate the presence of enzyme (1-methylalkyl)succinate synthase. MasG is the tentative activase that introduces the radical into the large subunit, MasD.
B. Analogous reaction principle in the well-studied anaerobic activation of toluene by benzylsuccinate synthase (Heider, 2007).¹³

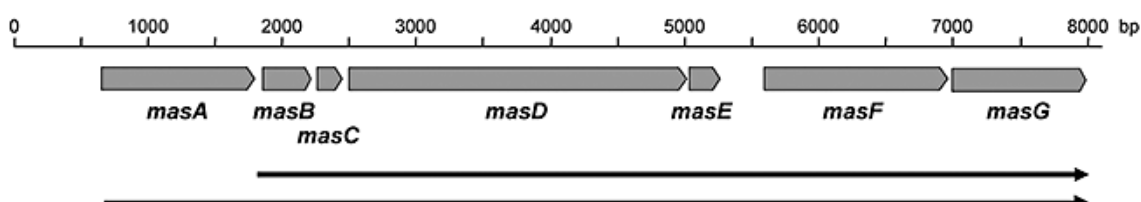
Extract from HxN1 cells upon growth can be used for identification of the underlying genes from amino acid sequences of proteins. Extraction of cells from anaerobic growth by caproate (hexanoate) and nitrate and also *n*-hexane and nitrate, and subsequent two-dimensional gel electrophoresis of cell lysates grown with *n*-hexane versus cells grown with caproate, can be used to identify the proteins formed with the alkane as a substrate (Fig. 12). The latter was identified by partial amino acid sequencing, which showed similarity to the subsequences of BssA and BssC, the α - and γ -subunit of benzylsuccinate synthase. Alignment of sequences of positive clones revealed a putative operon structure with seven open reading frames (ORFs), as shown in Fig. 13. The deduced

amino acid sequences of four of the ORFs contained partial amino acid sequences of the four *n*-hexane initially analysed proteins. The seven ORFs identified most likely contain the genes encoding the *n*-alkane activating enzyme (1-methylalkyl)succinate synthase and are referred to as genes *masA* to *masG*.



✚ **Figure 12** - Two-dimensional gel electrophoresis of cell-free extract from strain HxN1 upon growth with (A) caproate and (B) *n*-hexane. Major *n*-hexane-specific proteins (and corresponding positions on the gel from caproate-grown cells) have been circled. Assignment due to partial amino acid sequencing and identified genes: 1 - 5, putative large subunit of *n*-alkane-activating enzyme (MasD); 6, putative acyl-CoA dehydrogenase (MasA).

Gene products, MasC, MasD and MasE, have been shown to be structural homologues of the three subunits of benzylsuccinate synthase (BssABC).



✚ **Figure 13** - Map of the chromosomal region of strain HxN1 with identified open reading frames including the tentative structural genes of the *n*-hexane-activating enzyme, *masC*, *masD* and *masE*. The gene products of *masA*, *masB*, *masC* and *masD* were detected as *n*-hexane-specific proteins via two-dimensional gel electrophoresis.

As shown in Fig. 14.A a large degree of identity exists between the large protein MasD and the large (α) subunit of benzylsuccinate synthase, BssA. Every glycy radical enzyme requires activation by an activating protein that abstracts a hydrogen atom from the reactive glycine. All activases of this type belong to the enzyme family of S-adenosylmethionine-dependent radical generators (SAM-radical enzymes).⁵²

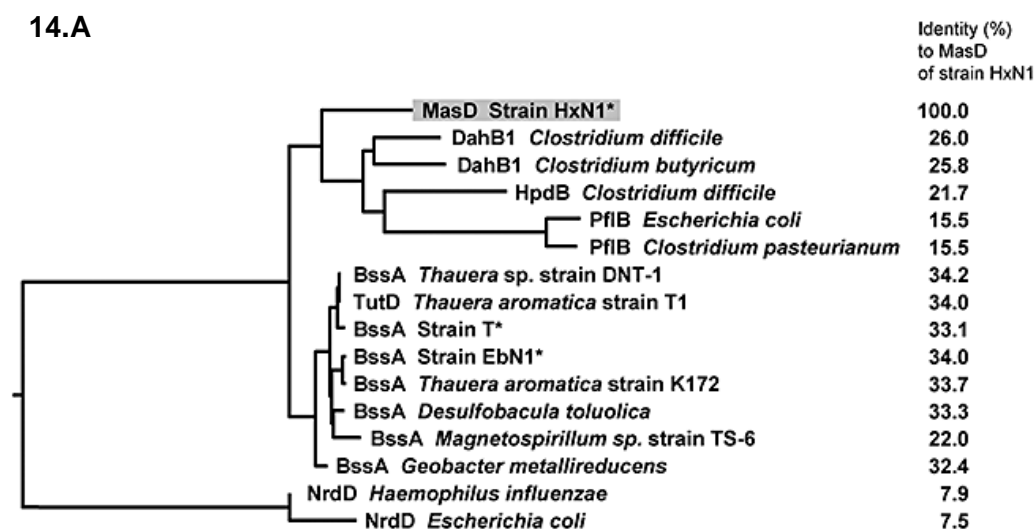


Figure 14.A - Relationships between the large subunit, MasD, of the assumed *n*-alkane activating enzyme from strain HxN1 and radical-bearing subunits of other glycy radical enzymes. Bss, benzylsuccinate synthase; Tut, synonym of BSS; Dah, glycerol dehydratase; Hpd, hydroxyphenylacetate decarboxylase; Pfl, pyruvate formate lyase; Nrd, ribonucleotide reductase.

MasG contains sequences which represent typical [Fe₄S₄] ferredoxin motifs; similar sequences are also present in activases of benzylsuccinate synthases and other glycy radical enzymes (Fig. 14.B).⁵³

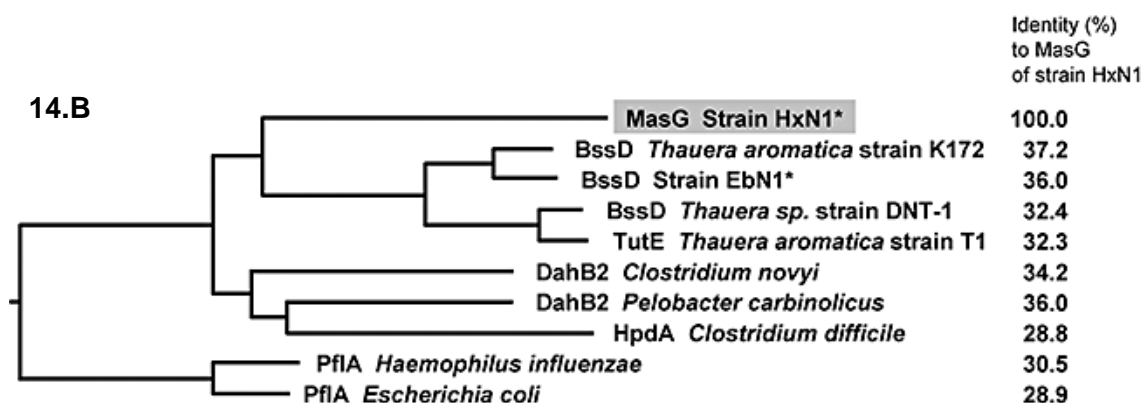


Figure 14.B - Relationships between MasG, the assumed activase of the *n*-alkane-activating enzyme of strain HxN1, and activases of other glycy radical enzymes.

In summary following studies based on the induction effect of *n*-hexane on strain HxN1, analogies in the mechanisms of anaerobic activation of *n*-hexane² and toluene¹³ and the similarity relationship in sequence between three *mas* gene products and the three subunits of the toluene activating enzyme benzylsuccinate synthase, it is possible to conclude that genes MasC, MasD and MasE are the subunits of the *n*-alkane activating enzyme (1-methylalkyl)succinate synthase in strain HxN1.

Investigation of metabolites and genes involved in alkane degradation via addition to fumarate have been reported for strain HxN1.^{2, 8} Metabolite analysis of strain OcN1 upon growth with *n*-octane and NO₃⁻ reveals (1-methylheptyl)succinate⁵⁴, again indicating an activation via addition to fumarate. In contrast, alkyl-substituted succinates were never detectable in cultures and cells of strain HdN1. Another product searched for in anaerobic *n*-hexadecane cultures of strain HdN1 was 1-hexadecanol. If air was strictly excluded and if the culture was inactivated by heat² before extraction, 1-hexadecanol was not detectable. In contrast, 1-hexadecanol was detected if the anaerobically grown culture was exposed to air for 20 - 30 min. Such 1-alkanol formation is a long-known indicator of alkane monooxygenase activity. Metabolite analysis in anaerobic alkane degraders with facultative aerobic metabolism thus requires careful avoidance of artefacts due to reaction with O₂ from air.

The gene possibly encoding the alkane-activating enzyme in strain OcN1 was retrieved via polymerase chain reaction with degenerate primers for *mas* and *ass* genes, generation of a probe and screening of a genomic library, similar as described for strain HxN1. The derived amino acid sequence reveals a close relationships (Fig. 15) to the orthologue from strain HxN1 and a sulfate-reducing bacterium.^{51, 55} Attempts to amplify in an analogous manner *mas*- or *ass*-like genes from strain HdN1 failed. Therefore, a shotgun genomic library of strain HdN1 was established. This allowed assemblage of the complete genome sequence but neither this revealed *mas*- or *ass*-like genes.⁴⁹

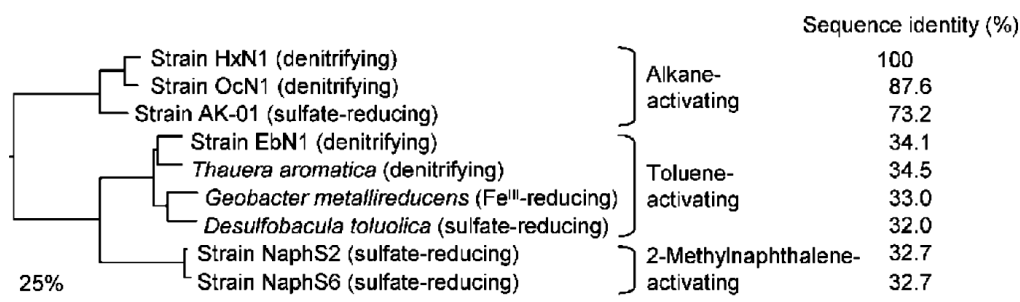


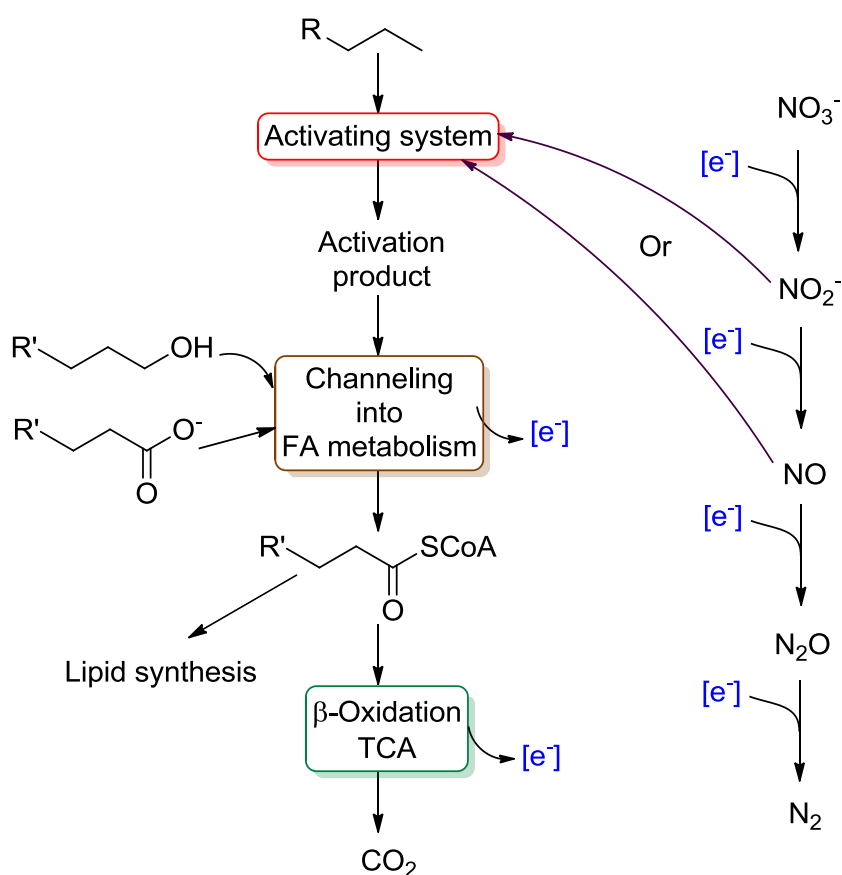
Figure 15 - Relationship of the assumed catalytic (large) subunit (MasD) of the *n*-alkane activating enzyme in strain OcN1 to other enzymes activating hydrocarbons via addition to fumarate. Bar, 25% amino acid exchange.

These findings suggested that the mechanism for alkane activation in strain HdN1, which has to involve the cleavage of a strong, apolar C–H bond, differs basically from the mechanism with fumarate as co-substrate in the two other strains.

1.3.2.6 Linkage of alkane activation in strain HdN1 to the nitrate reduction pathway?

The distinctive results of the incubation experiments with either alkanes or functionalised (O-group-containing) substrates and N₂O may offer a clue as to how strain HdN1 could initiate alkane degradation under anoxic conditions. The electron acceptor tests with functionalised electron donors as well as identified genes indicate that strain HdN1 employs the common reduction sequence (NO₃⁻ → NO₂⁻ → NO → N₂O → N₂), which is in principle able to readily reduce N₂O. Also during growth with alkanes as organic substrates and NO₃⁻ or NO₂⁻ as electron acceptors, N₂O must have been a regular intermediate because N₂ rather than N₂O was the end-product. However, N₂O added alone did not allow growth with alkanes. An early reaction during alkane utilisation must thus depend on a nitrogen–oxygen (N–O) species other than N₂O. The early reaction could be the biochemically crucial activation of the alkane. The required N–O species cannot be NO₃⁻, because growth with alkanes was also possible if NO₂⁻ was added instead of NO₃⁻. Hence, NO₂⁻ or NO (or a so far unknown product from NO₂⁻ reduction) may be essential for alkane activation. The basic hypothesis is depicted in Scheme 4. From a thermodynamic point of view, an involvement of N–O species in alkane activation under anoxic conditions is an

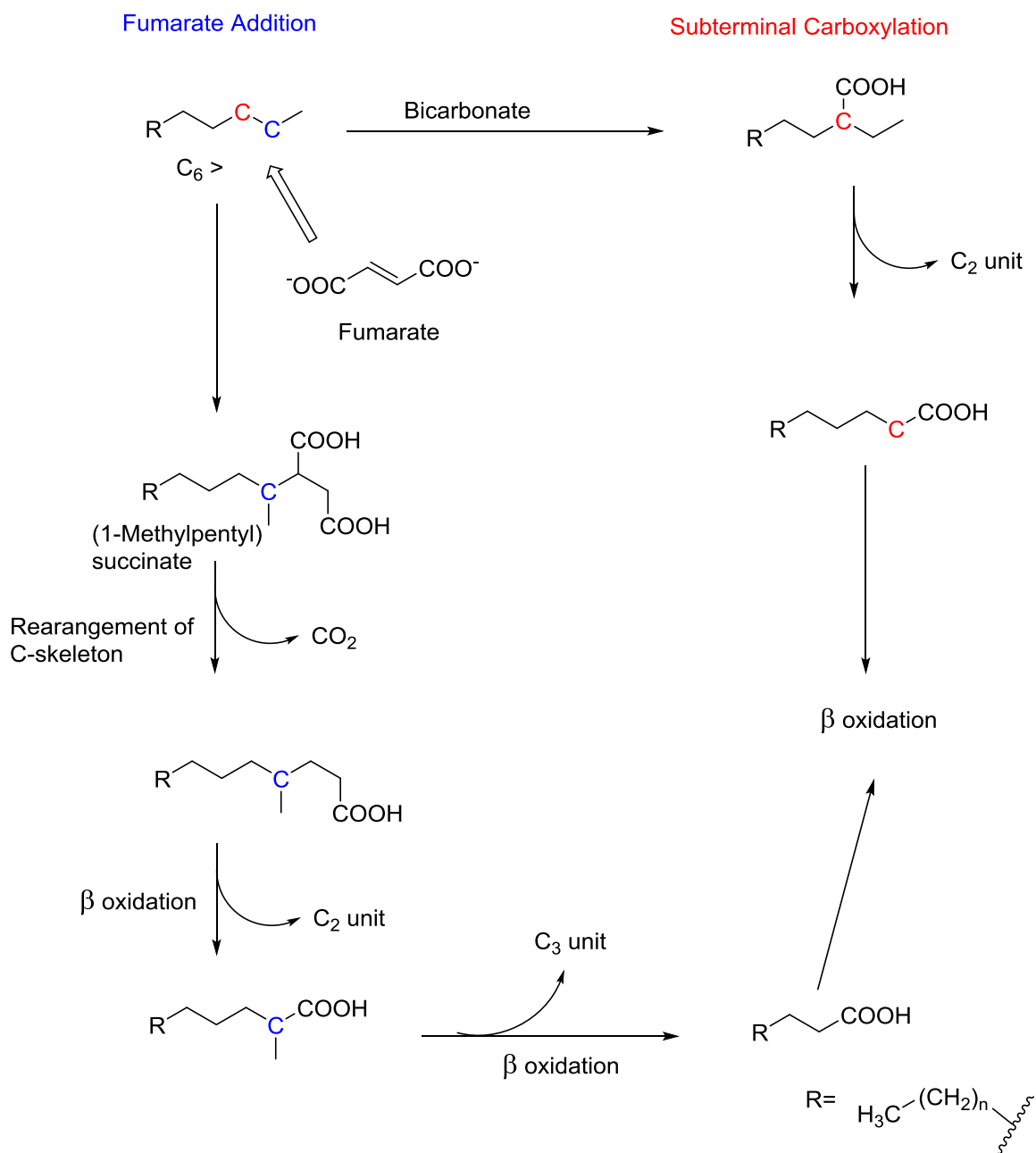
appealing hypothesis. N–O species other than NO_3^- are all metastable^{43b} and represent or can provide strong potential oxidants; this property may be enzymatically exploited to achieve alkane activation. An indirect use to form another reactive compound as well as a direct use of an N–O species can be envisaged.



Scheme 4 - Hypothetical involvement of denitrification intermediates in alkane activation. It is assumed that a small proportion of NO_2^- or NO is deviated from the respiratory chain for alkane activation. FA, fatty acid; TCA, tricarboxylic acid cycle.

1.3.2.7 Summary

Strains HxN1 and OcN1, which are both **Betaproteobacteria**, as suggested by metabolite and gene analyses, utilise *n*-alkanes from C₆ to C₈ and C₈ to C₁₂ respectively and both activate alkanes anaerobically in a fumarate-dependent reaction yielding alkylsuccinates,. However, strain HdN1 is unique in several respects. It belongs to the **Gammaproteobacteria** and is more versatile towards alkanes, utilising the range from C₆ to C₃₀ and neither analysis of metabolites nor analysis of genes in the complete genome sequence of strain HdN1 have hinted at fumarate-dependent alkane activation. Moreover, whereas strains HxN1 and OcN1 grew with alkanes and NO₃⁻, NO₂⁻ or N₂O added to the medium, strain HdN1 oxidized alkanes only with NO₃⁻ or NO₂⁻ but not with added N₂O. However N₂O is still readily used for growth with long-chain alcohols or fatty acids. Results suggest that NO₂⁻ or a subsequently formed nitrogen compound other than N₂O is needed for alkane activation in strain HdN1. From an energetic point of view, nitrogen–oxygen species are generally rather strong oxidants and may enable enzymatic mechanisms that are not possible under conditions of sulfate reduction or methanogenesis and thus allow a special mode of alkane activation. The most established mechanism for anaerobic activation of alkanes to date is the radical-catalysed addition to fumarate yielding alkylsuccinates.² Genes encoding the putative enzyme have been detected in a nitrate-reducing⁵¹ and a sulfate-reducing strain⁵⁵, However, an alternative pathway (sub-terminal carboxylation)¹² for the anaerobic alkane oxidation has also been observed in the sulfate-reducing bacterium strain Hxd3 (Scheme 5). A comparative study has revealed that strains HxN1 and OcN1 form alkylsuccinates during growth with alkanes and contain a gene which encodes the responsible enzyme. In contrast, alkylsuccinates are not detectable in strain HdN1, and its complete genome sequence has not revealed any gene likely to encode (1-methylalkyl)succinate or alkylsuccinate synthase. A unique physiological characteristic of strain HdN1 was that it did not grow with alkanes if N₂O was added instead of NO₃⁻, whereas growth with alcohols and fatty acids readily occurred with N₂O. In contrast, strains HxN1 and OcN1 grew well with N₂O and alkanes. These findings suggest that alkane activation in strain HdN1 differs principally from alkane activation in strains HxN1 and OcN1 and requires an NO₃⁻-derived compound other than N₂O.



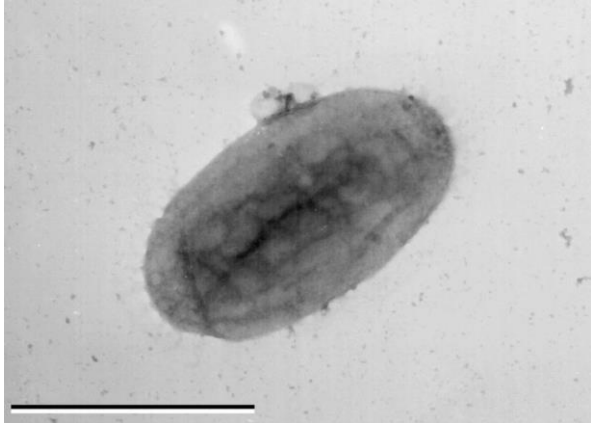
Scheme 5 - The anaerobic degradation pathway of alkanes showing the two types of anaerobic degradation pathway that have currently been identified. To date, subterminal carboxylation has only been found in the sulfate-reducing bacterium strain Hxd3.¹² For short-chain *n*-alkanes, such as propane, refer to Kniemeyer et al (2007).¹⁵

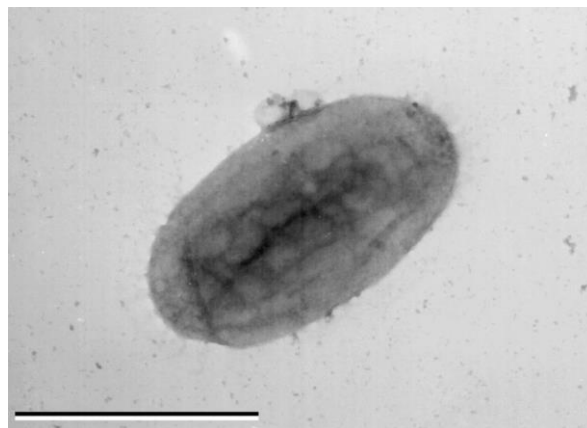
❖ **Table 5** – Properties of nitrate and sulfate reducing, alkane degrading bacteria under anoxic conditions.

Organism	Affiliation	Source	Substrate range	Mechanism involved	Alternative electron acceptors	D.T.	Ref.
Nitrate reducing							
Strain HxN1	β- Prot.	Ditch sediments	C ₆ -C ₈	Fumarate	NO ₂ ⁻ , N ₂ O	11 h	2, 9
Strain HdN1	γ- Prot.	Activated sludge	C ₆ -C ₃₀	Unknown		11-13 h	9, 56
Strain OcN1	β- Prot.	Ditch sediments	C ₈ -C ₁₂	Fumarate	N ₂ O	nd	9
<i>Marinobacter</i> sp. BC36	γ- Prot.	Lagoon mats	C ₁₈	nd		nd	57
<i>Marinobacter</i> sp. BP42	γ- Prot.	Lagoon mats	C ₁₈	nd		nd	57
<i>Pseudomonas balearica</i> strain BerOc6	γ- Prot.	Brakish lagoon	C ₁₅ -C ₁₈	nd		nd	58
Sulfate reducing							
Strain Hxd3	δ-Prot.	Oil-water separator	C ₁₂ -C ₂₀	Carboxylation		9 d	12
Strain AK-01	δ-Prot.	Petroleum-contaminated estuarine sediments	C ₁₃ -C ₁₈	Fumarate	Thiosulfate and sulfite	3 d	1
<i>Desulfatibacillum aliphaticivorans</i> CV2803 ^T	δ-Prot.	Hydrocarbon-polluted marine sediments	C ₁₃ -C ₁₈	Fumarate	Thiosulfate and sulfite	nd	59
<i>Desulfoglaeba alkanexedens</i> strain ALDCT	δ-Prot.	Oily sludge	C ₆ -C ₁₂	Fumarate	Thiosulfate	5.3 d	60
Strain BuS5	δ-Prot.	Marine hydrocarbon seeps	C ₃ -C ₄	Fumarate		4-5 d	15
Strain PL12	δ-Prot.	Petroleum contaminated sediments	C ₆ , C ₁₀	nd			61
Clone Butane12-GMe	δ-Prot.	Gulf of Mexico sediments	C ₄	nd			15
<i>Desulfothermus naphthae</i> TD3 ^T	δ-Prot.	Guaymas Basin sediments	C ₆ -C ₁₆	nd	Thiosulfate	9 d	62
nd: not documented; DT: doubling time; β-, γ-, δ- Prot.: β-, γ-, δ-Protobacteria							

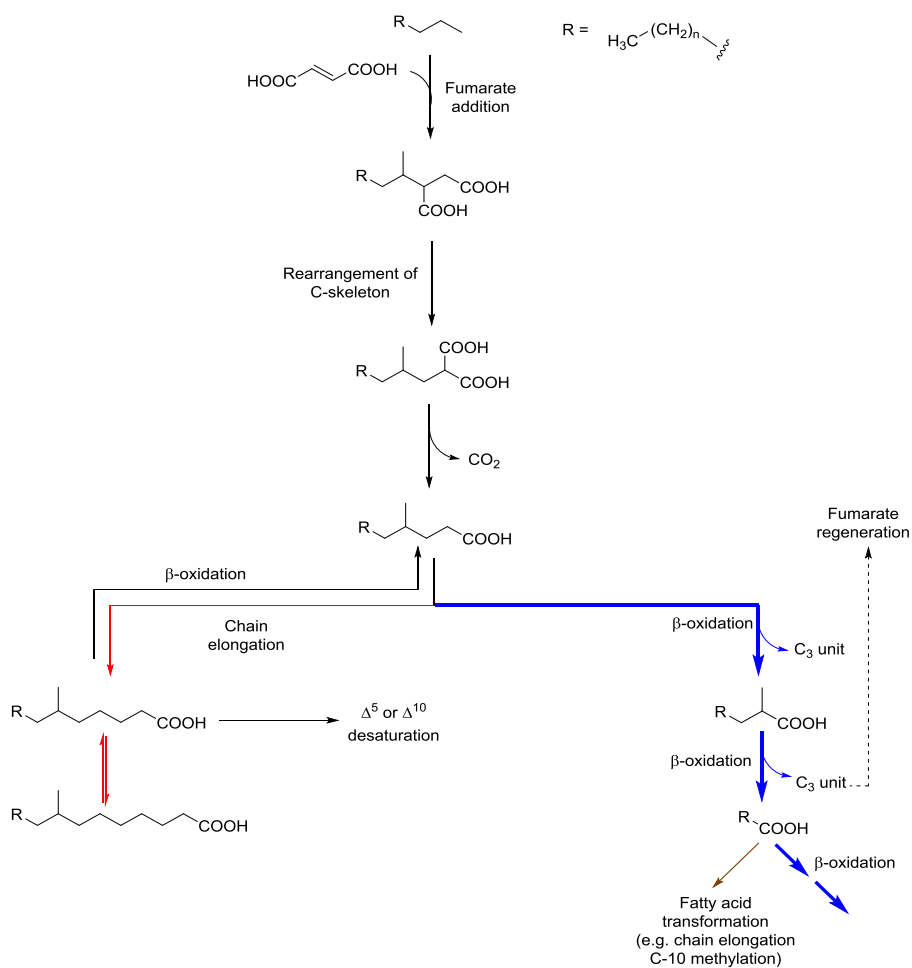
1.3.3 Sulfate reducers

Sulfate-reducing bacterial can obtain energy by oxidising organic compounds while reducing sulfate (SO_2^{-4}) to hydrogen sulfide (H_2S).

 **Figure 16** - Transmission electron photomicrograph of strain AK-01 grown on hexadecane (negatively stained with uranyl acetate). Bar, 1 μm .¹

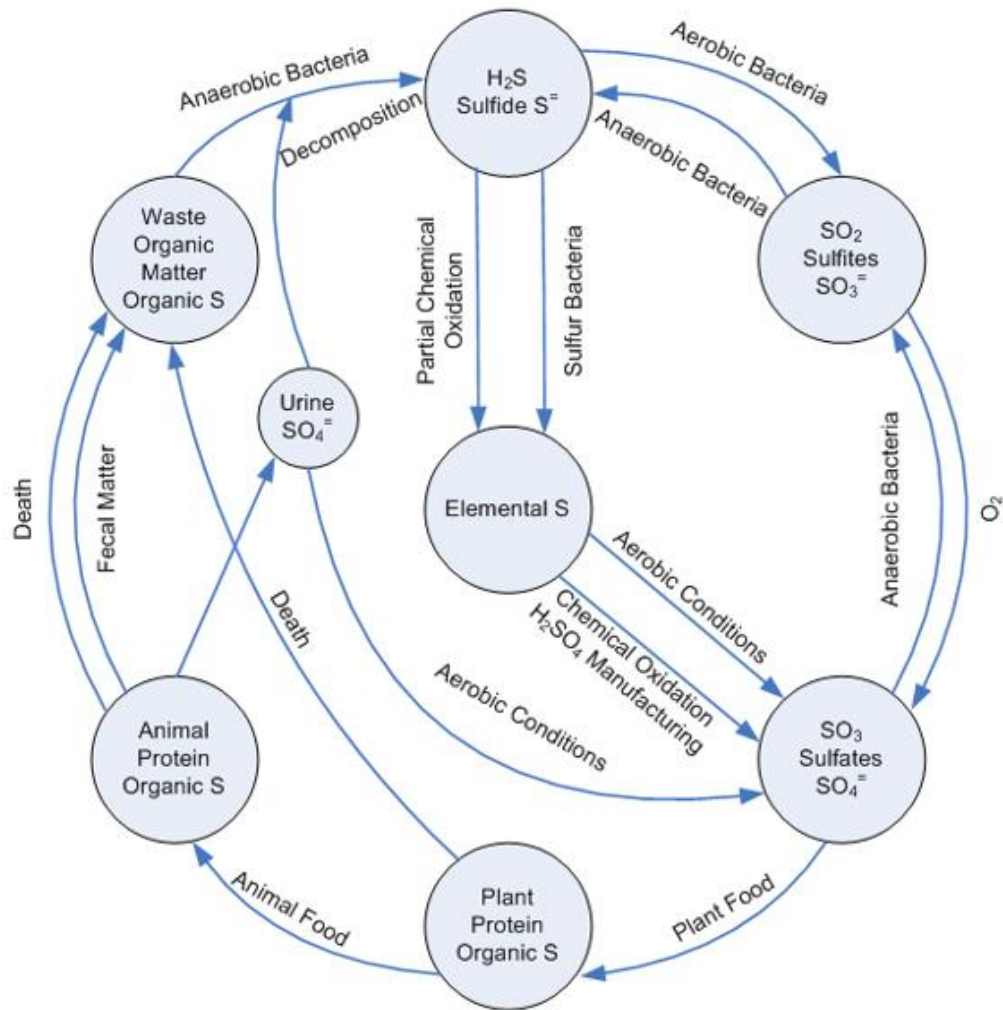


The interest in these microorganisms stems from observations of sulfide formation in oil reservoirs. Phylogenetic analysis and functional genes suggest that sulfate-reducing bacterial (SRB) communities are affiliated with the family *Desulfobacteraceae* within the δ -*Proteobacteria*. Most members of this family are strict anaerobes that perform complete oxidation of organic compounds. In contrast to nitrate-reducers, sulfate-reducers that anaerobically oxidise saturated hydrocarbons are from hydrocarbon rich environments. So far eight alkane degrading sulfate-reducers have been isolated and reported in literature (Table 5). E.g. The alkane-degrading, sulfate-reducing bacterium *Desulfatibacillum aliphaticivorans* strain CV2803^T, which was recently isolated from marine sediments, is able to grow by oxidising *n*-alkanes ranging from C_{12} – C_{20} (Scheme 6).⁶³



Scheme 6 - Proposed pathway for anaerobic *n*-alkane metabolism by the sulfate-reducing bacterium *D. aliphaticivorans* strain CV2803^T (bold arrows indicate the major pathway).

These microorganisms play an important part in sulfur cycle (Fig. 17).¹⁰ Sulfur which is a necessary element for life, is taken up as sulfate by SRB and subsequently plants and animals. Decomposition of dead organisms in the absence of dioxygen releases the sulfur again as hydrogen sulfide.



✚ **Figure 17** – Sulfur cycle¹⁰

SRB can cause a serious problem for industries, such as the offshore oil industry, because of the production of sulfide, which is highly reactive, corrosive and toxic. However, these organisms can also be beneficial by removing sulfate and heavy metals from waste streams.

The most recent reported alkane degrading sulfate reducers, which have been isolated, are strains AK-01, Hxd3 and TD3. All three strains have been isolated from environments which are anoxic and chronically exposed to hydrocarbons. However, there are some major differences between these strains. While both strains AK-01 and Hxd3 are mesophiles (grow best in moderate temperature, typically between 20 and 45 °C), TD3 is a thermophile (thrives at relatively high temperatures, between 45 and 122 °C) that originated from the hydrothermally

active Guaymas Basin. A phylogenetic tree displaying the relationship between these strains and other selected bacteria is shown in Fig. 18.¹

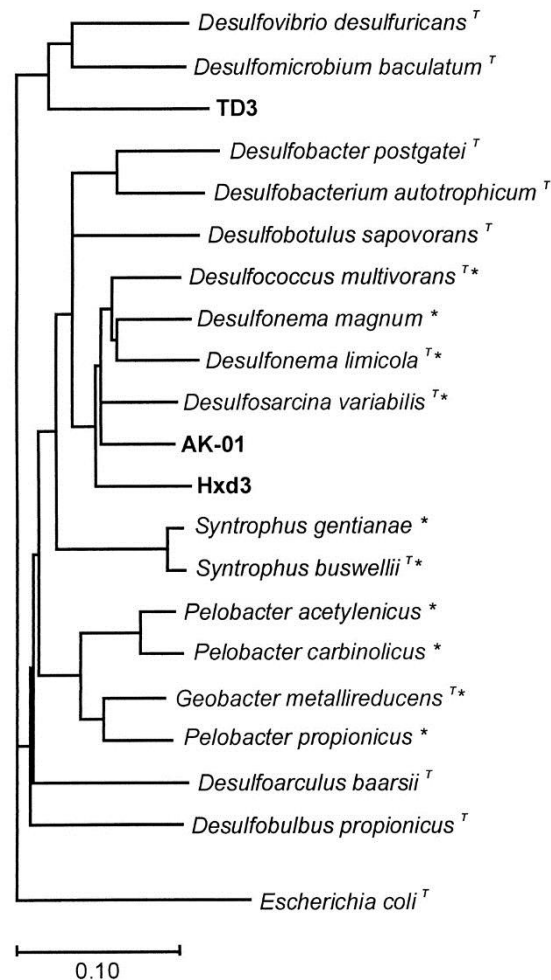


Figure 18 - Phylogenetic relationship between the three alkane-degrading strains AK-01, Hxd3, and TD3 and other bacteria in the class Proteobacteria based on 16S rRNA sequence. The tree was constructed from approximately 1,300 aligned bases; *T*, type species in the genus; *, the 10 bacteria with their 16S rRNA sequences most similar to that of strain AK-01.¹

Research conducted within the last decade has shown that activation of hydrocarbons occurs under anoxic conditions, where two proposed mechanisms appear to be important among several bacterial genera capable of anaerobic *n*-alkane utilisation. In the case of *n*-alkanes, the subterminal carbon can be added to the double bond of fumarate to produce methyl-branched alkylsuccinates. This is the more common mechanism observed within bacteria capable of anaerobic hydrocarbon utilisation.⁶⁴

To date, the only other mechanism elucidated for *n*-alkane activation is that of strain Hxd3, a sulfate reducer closely related to the genus ***Desulfococcus***.

Strain Hxd3 utilises C₁₂ - C₂₀ alkanes and carboxylates hexadecane at the C-3 carbon, with subsequent elimination of the terminal and subterminal carbons.¹² As a result, Hxd3 produces C-odd and C-even fatty acids when grown on C-even and C-odd alkanes, respectively. Therefore this mechanism of *n*-alkane degradation appears to be unique among strains studied thus far.¹²

In contrast to strain Hxd3, studies have shown that sulfate-reducing strains AK-01, Pnd3, and *Desulfatibacillum aliphaticivorans* strain CV2803 produce C-even and C-odd fatty acids when grown on C-even and C-odd *n*-alkanes, respectively.^{55, 63}

In the recent years these mechanism have been under study to determine the initial step in the biodegradation of alkane and also to find more evidence for both fumarate addition and carboxylation. Enrichment studies and the isolation of alkane-degrading denitrifying bacteria are described and summarised here.

According to the results published by Callaghan et al,⁶⁴ Ak-01 cultures were incubated with either H₃₄-hexadecane or d₃₄-hexadecane and the metabolites were derivatized with N,O-bis(trimethylsilyl)trifluoroacetamide (BSTFA) **11**, which replaces the hydroxyl group with the more stable O-trimethylsilyl group, this protects the labile group and allows the compound to be used for analytical purposes.

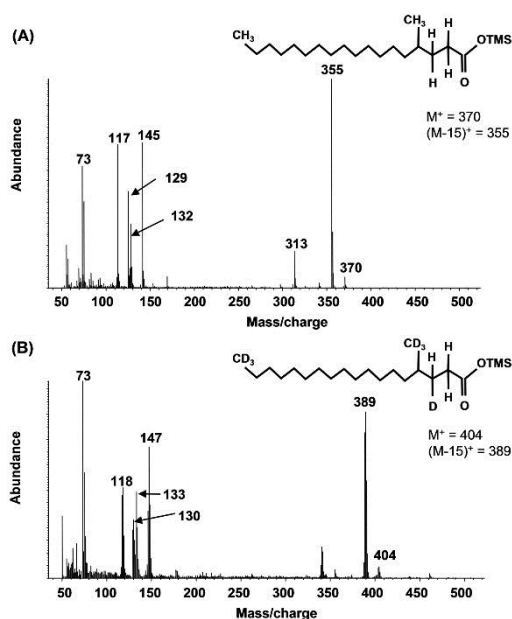


Figure 19(i) - Mass spectra of silylated protonated 4-methyloctadecanoic acid **(A)** and deuterated 4-methyloctadecanoic acid **(B)** identified in AK-01 incubations. Fragment m/z 133 in **B** indicates that 4-methyloctadecanoic acid undergoes a McLafferty rearrangement during the GC-MS analysis (Scheme 7).

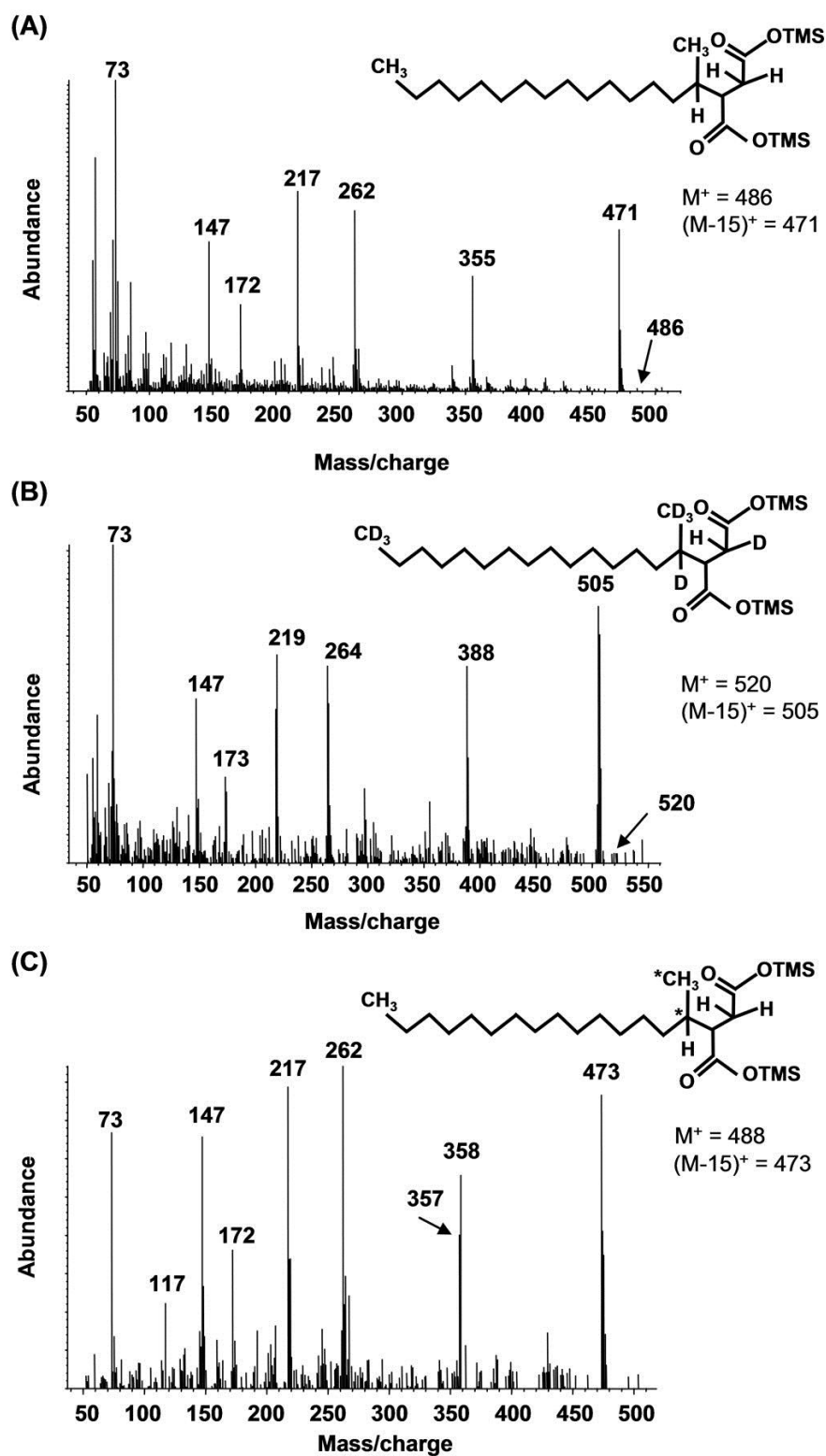
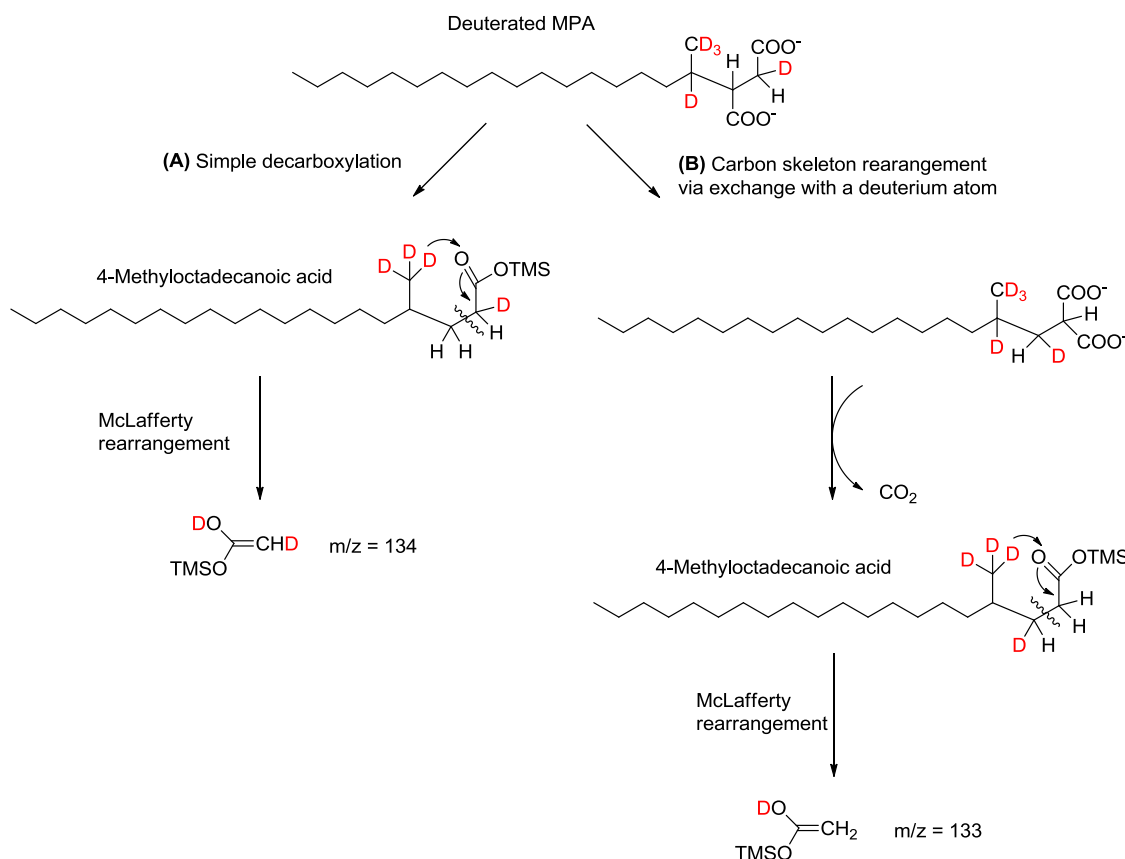
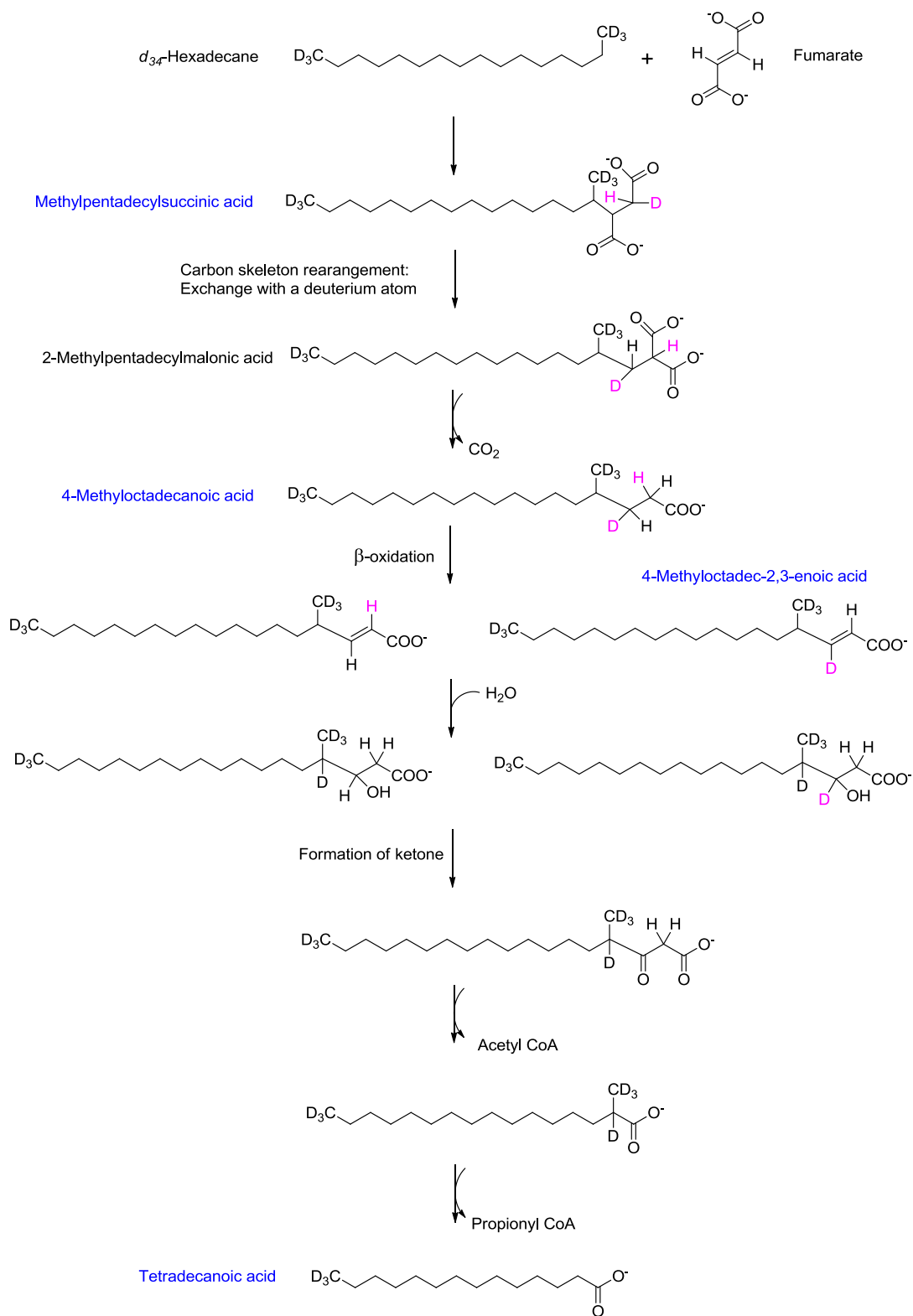


Figure 19(ii) - Mass spectra of the putative silylated metabolite methylpentadecylsuccinic acid from AK-01 cultures incubated with protonated hexadecane (A), AK-01 cultures incubated with d_{34} -hexadecane (B), and the sulfate-reducing consortium incubated with $[1,2-^{13}\text{C}_2]$ hexadecane (C).



Scheme 7 - McLafferty ions that result from decarboxylation of deuterated MPA that has not undergone carbon skeleton rearrangement (m/z 134) (A) and carbon skeleton rearrangement of MPA followed by decarboxylation (m/z 133) (B). The latter ion was experimentally observed in the mass spectrum of d_{34} -4-methyloctadecanoic acid (Fig. 4B).

In addition to the identified metabolites which support a mechanism of hexadecane adding to the double bond of fumarate, no evidence suggesting carboxylation of hexadecane, such as deuterated pentadecanoic and tridecanoic acids, was detected in strain AK-01 extracts. The observed results demonstrated that the succinyl moiety in the metabolites is not attached to the terminal carbon atom in the hexadecyl moiety but is, rather, in a subterminal position yielding chromatographically distinct stereoisomers (diastereomers). Based on these observations, a pathway for carbon skeleton rearrangement and subsequent degradation of d_{34} -hexadecane by the sulfate reducer AK-01 was proposed, which is analogous to that for hexane degradation under denitrifying conditions by strain HxN1 (Scheme 8).²



Scheme 8 - Proposed mechanism of deuterated hexadecane degradation by strain AK-01. Putative deuterated metabolites are highlighted in blue.

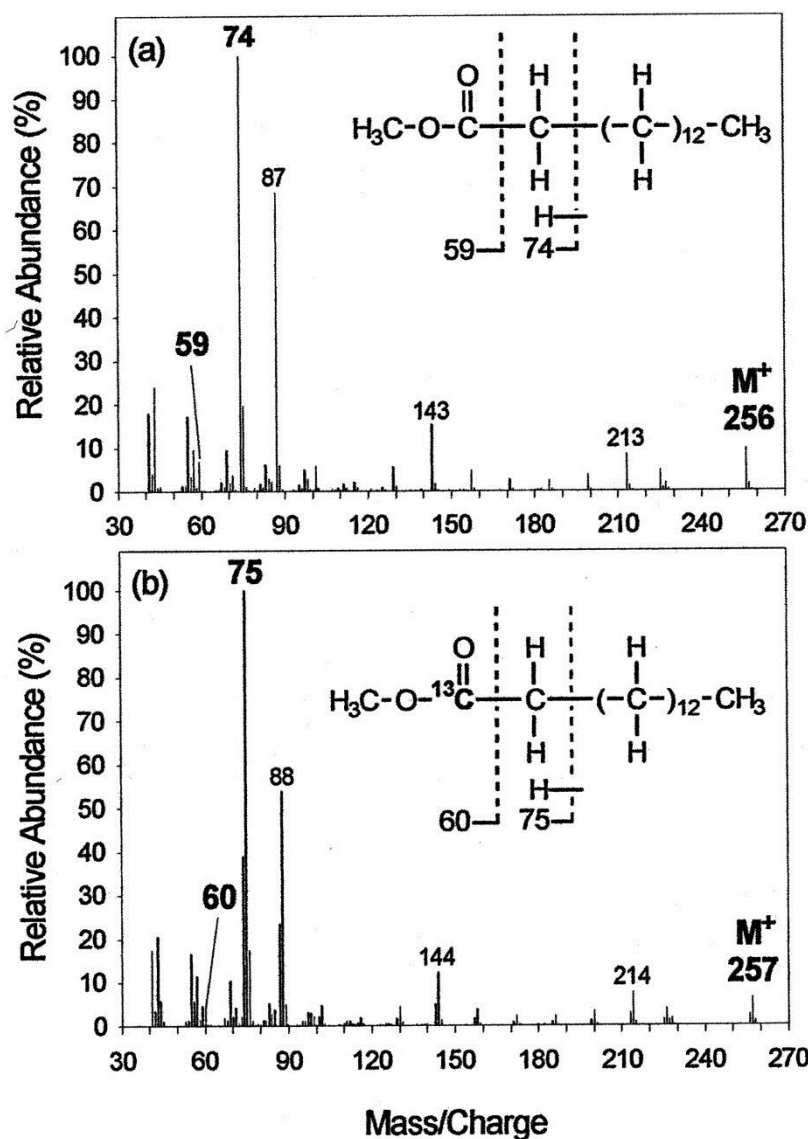
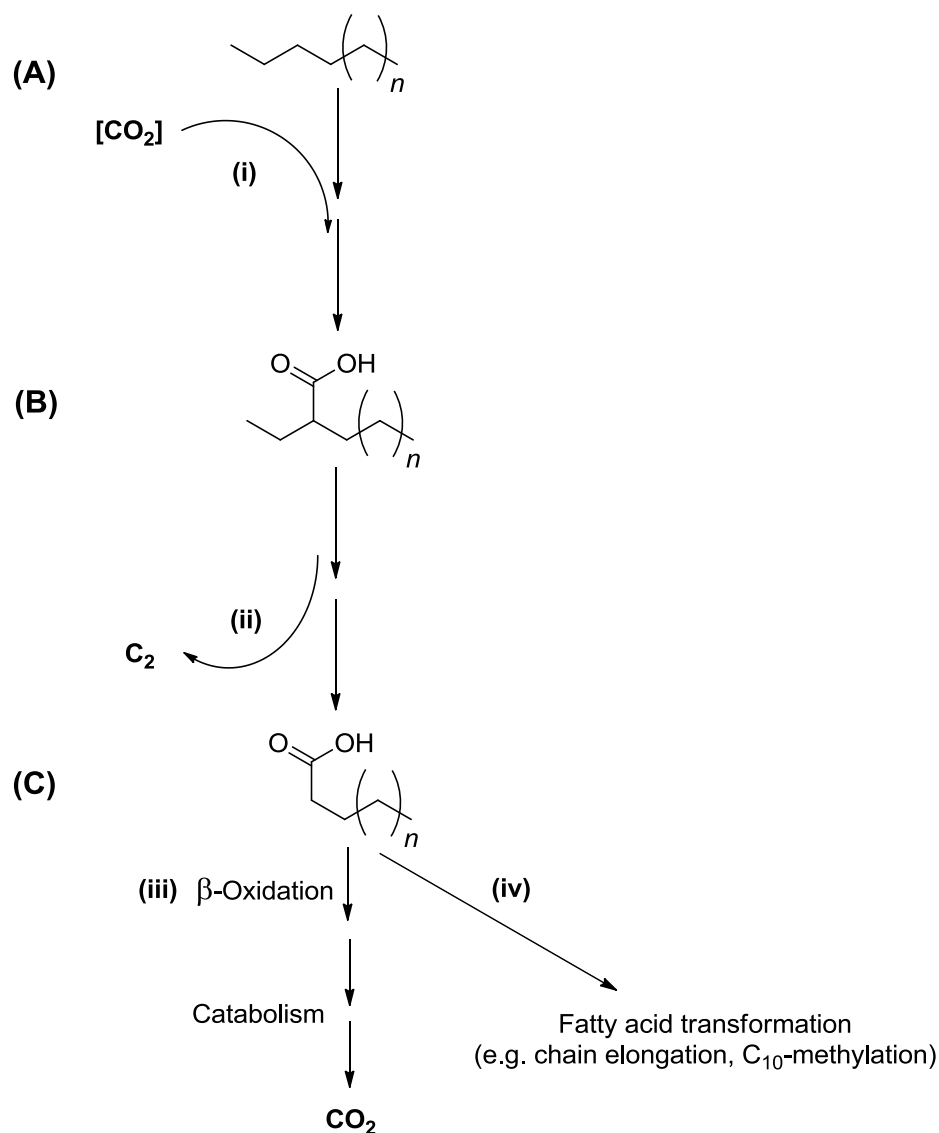


Figure 20 - Mass spectra of the methyl esters of the 15:0 fatty acid recovered from cultures of strain Hxd3 grown on hexadecane with unlabeled bicarbonate (a) or ^{13}C bicarbonate (b). Chemical structures represented by the mass spectra are shown as insets. Key diagnostic ion peaks are annotated in bold type with their m/z values, and the structural compositions of the represented ion fragments are delineated. Intersection with a dotted line indicates a point of bond cleavage, and the ion fragment formed subsequently contains only the part of the molecule to the left of the dotted line.



Scheme 9 - Proposed pathway for the oxidation of alkane to fatty acid by strain Hxd3. An alkane (A) is subterminally carboxylated at C-3 (step I) to form an intermediate (B). Two adjacent terminal carbon atoms are then eliminated (step II) to form a fatty acid one carbon shorter than the original alkane (C). This fatty acid can be beta oxidized (step III) and subsequently mineralized to CO_2 or undergo transformation, such as chain elongation and C-10 methylation (step IV). Compound B (in brackets) is only a hypothetical intermediate and has not been observed. Atoms originating from the alkane are shown in bold type.

1.3.4 Comparison of aerobic and anaerobic degradation pathways of *n*-alkanes

To summarise, activation of alkanes by microbes can be carried out under both aerobic and anaerobic conditions with different enzyme systems. Under aerobic conditions, dioxygen serves as the electron acceptor, while under anaerobic conditions, compounds like sulfate and nitrate accept electrons in order to complete the process (Fig. 21).^{16b}

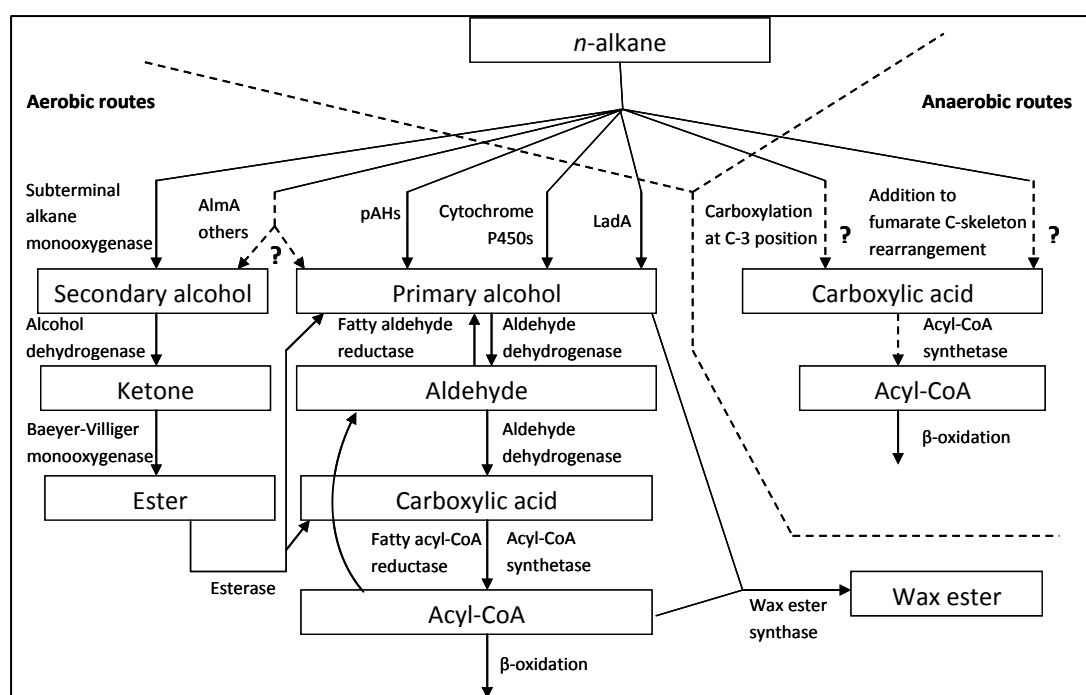


Figure 21 – Aerobic and anaerobic alkane oxidation

1.3.5 Environmental and other aspects of anaerobic alkane degradation

Many studies of the anaerobic biodegradation of the hydrocarbons in natural habitats were initiated to determine whether or not bioremediation processes are possible in deep, anoxic petroleum-contaminated or fuel-contaminated sediments and aquifers.⁶⁵ A basic idea for the study of anaerobic bioremediation is to make electron acceptors in injected water available at concentrations higher than that of dissolved dioxygen from air.⁶⁶ The concentration of dioxygen in air-saturated water (8.6 mg/dm³ at 25 °C) has the capacity to oxidise, for instance, no more than 2.8 mg toluene/L. Nitrate and sulfate are much more soluble, for example, even gypsum (CaSO₄), a form of

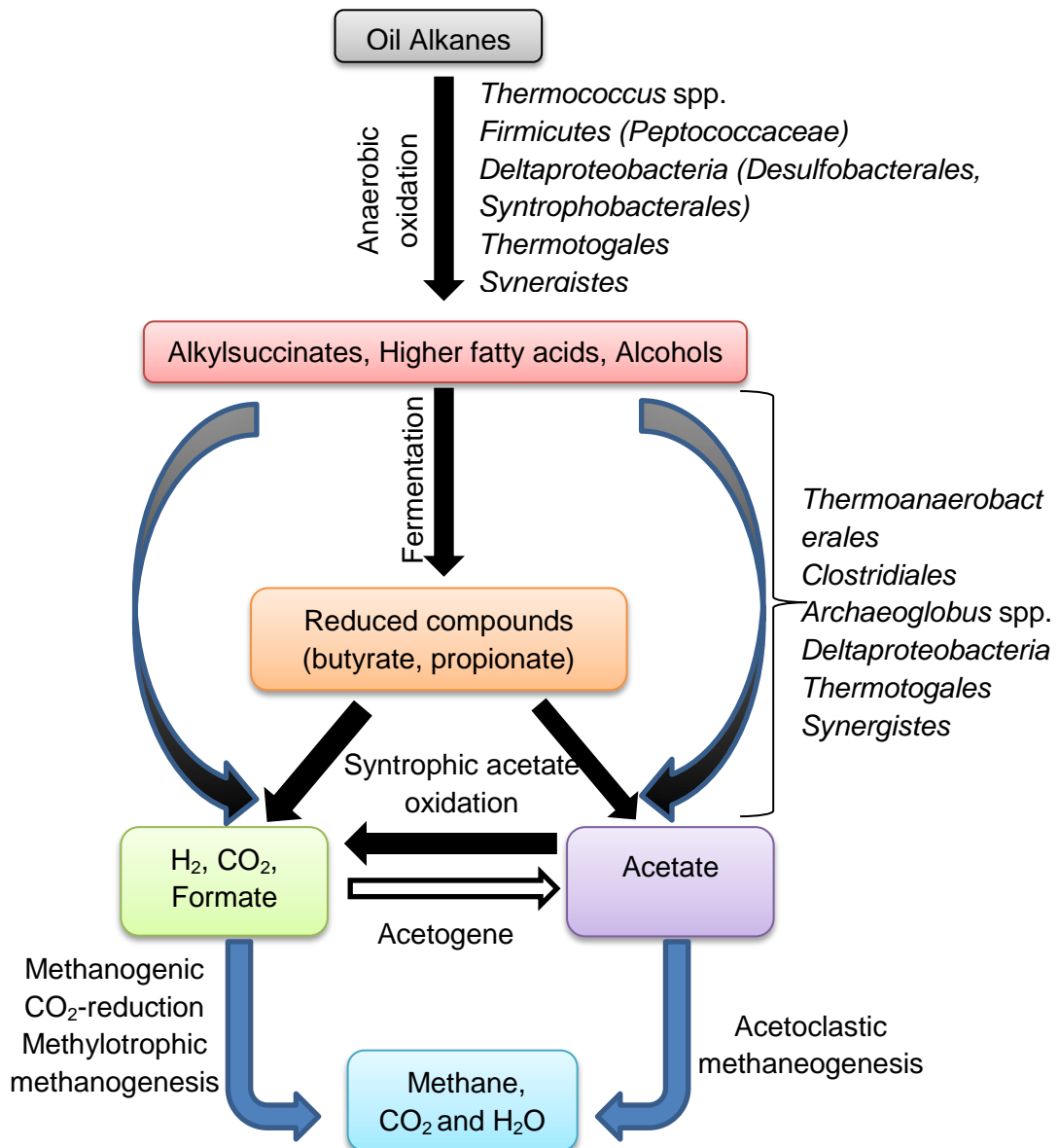
sulfate with low solubility and a saturation concentration of $2 \text{ g CaSO}_4/\text{dm}^3$ would allow the anaerobic oxidation of $300 \text{ mg toluene}/\text{dm}^3$. There is no doubt that the degradation of petroleum and refined products is much faster under oxic than anoxic conditions. Furthermore, aerobic microorganisms seem to degrade a much wider range of hydrocarbon compounds than anaerobic microorganisms.

The extent of the degradation of hydrocarbons from oil and the groups of microorganisms involved have been studied in enrichment cultures with sulfate⁶⁷ or nitrate⁵⁶ as electron acceptors. If crude oil is present in growth-limiting amounts, the portion that can be oxidised under anoxic conditions can be estimated from the amount of reduced electron acceptor (e.g., sulfate or nitrate).

Alkanes are quantitatively the most important fraction in crude oil. The biodegradation of alkanes which occurs in anoxic habitats is of great importance to the oil industry. Today, this process remains an exciting area of investigation to understand the factors that govern the biodegradation of oil in deep-subsurface reservoirs. It is now well known that microbial activities associated with petroleum reservoirs have led to the decrease of oil quality, making refining more costly and recovery more difficult. For example the utilisation of hydrocarbons by SRB has been regarded as a source of hydrogen sulfide. Hydrogen sulfide is toxic, stimulates corrosion of steel and diminishes the value of oil and gas by increasing the sulfur and forms FeS precipitates that delay the separation of oil and water. Therefore, a better understanding of these microorganisms could have a huge influence on the efficiency and quality of the extracted oil.⁶⁶

Petroleum reserves have been depleted to certain levels, and anaerobic degradation is considered to be one of the major processes responsible for this phenomenon. Furthermore, bioorganic methane associated with biodegraded oil reservoirs is believed to be the result of microbial decomposition of oil alkanes.⁴⁴ Therefore, *in situ* methanogenic biodegradation activities may offer a route for potential alternative and innovative energy recovery from existing oil

reservoirs after extraction. Following extensive water flooding, a large amount of the crude oil still remains trapped in the reservoir.



✚ **Figure 22** – Presumptive methanogenic degradation of oil

Hence the recovery of energy from conventional reserves via *in situ* conversion of even a small amount residual oil to methane could provide a considerable supply of energy. This is of great interest because the world requirements for methane is constantly increasing and methanogenic conversion of oil alkanes could be seen as a future solution for world energy needs (Fig. 22).⁴⁵ Understanding the alkane degrading communities and their biochemical function will significantly advance the knowledge about the organisms mediating the specialised biochemical reaction steps. This will allow us to understand better the biological processes responsible for oil biodegradation in natural

environments and in petroleum reservoirs for possible biotechnological innovation and applications in utilisation of the residual oils. The anaerobic degradability of several hydrocarbons from crude oil does not necessarily contradict their obvious preservation in reservoirs (Fig. 23). First, oil in reservoirs is trapped in the pores of rocks, such that molecular diffusion into aqueous surroundings where bacteria can, in principle develop, is very limited. Second, many anaerobic bacteria formerly buried with sediments may have died due to substrate limitations or high temperature during catagenesis. Also extremely high salt concentrations may limit the diversity of bacteria that can develop in stratal waters. On the other hand, there are assumptions that anaerobic bacteria deposited with the original sediments have survived millions of years.

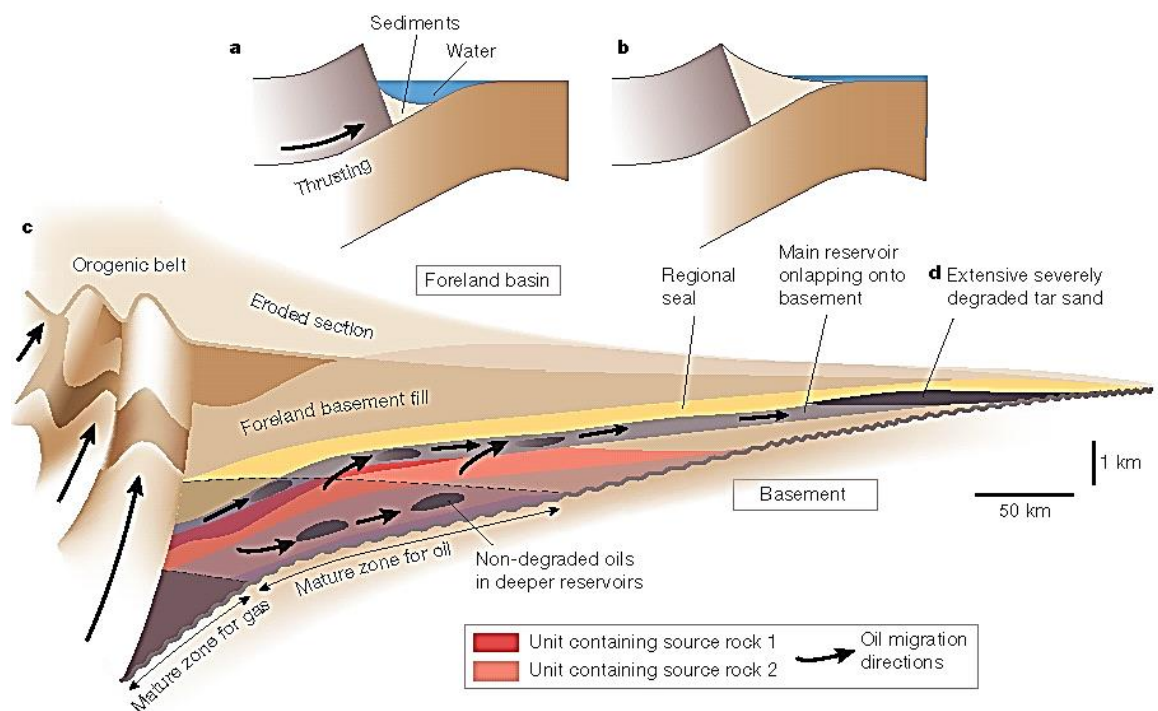
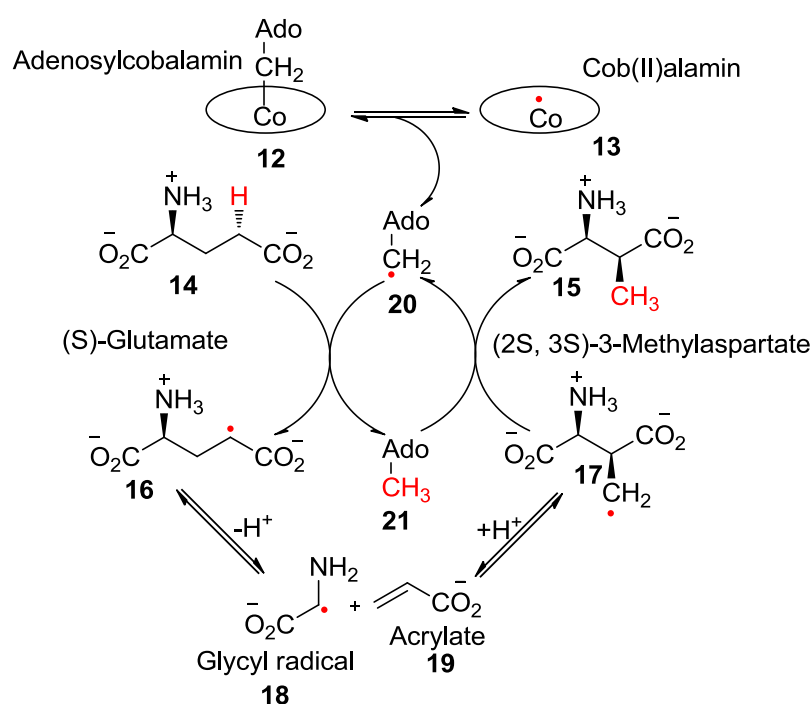


Figure 23 –At the flanks of the basins, reservoir sediments lie on top of older basement rocks and produce reservoirs that are shallow, cool and may have local active meteoric water circulation, conditions ideal for biological activity. ⁵

1.4 RADICAL ENZYMES IN ANAEROBES

These are enzymes that contain radicals and/or catalyse reaction with radical intermediates. Since radicals irreversibly react with dioxygen, most of these

enzymes occur in anaerobic bacteria and archaea, apart from the families of coenzyme B₁₂ and S-adenosylmethionine (SAM)-dependent radical enzymes (Fig. 24), of which some members also occur in aerobes. Radical enzymes catalyse many of the key metabolic steps in anaerobes. Nature only relies on higher energy pathways via radicals when there is no low energy pathway alternative. This can be illustrated in the reduction of (S)-glutamate to butyrate. The most simplified and elegant proposed mechanism for the action of glutamate mutase is described in Scheme 10 in which carbon skeleton rearrangement of (S)-glutamate to (2S,3S)-3-methylaspartate occurs via intermediate radicals, in a reaction that is coenzyme B₁₂-dependent.⁵²



 **Scheme 10** – Proposed mechanism of action for glutamate mutase.

In 3-methylaspartate the hydrogen atom β to the ammonium group is much more acidic than the corresponding protons in glutamate due to the adjacent carboxylate, and therefore ammonia can be eliminated.

Coenzyme B₁₂ (adenosylcobalamin) (Fig. 11(a)) is a derivative of vitamin B₁₂ and generates a 5'-deoxyadenosyl radical (Fig. 11(b)) by homolysis of the Co-C bond.

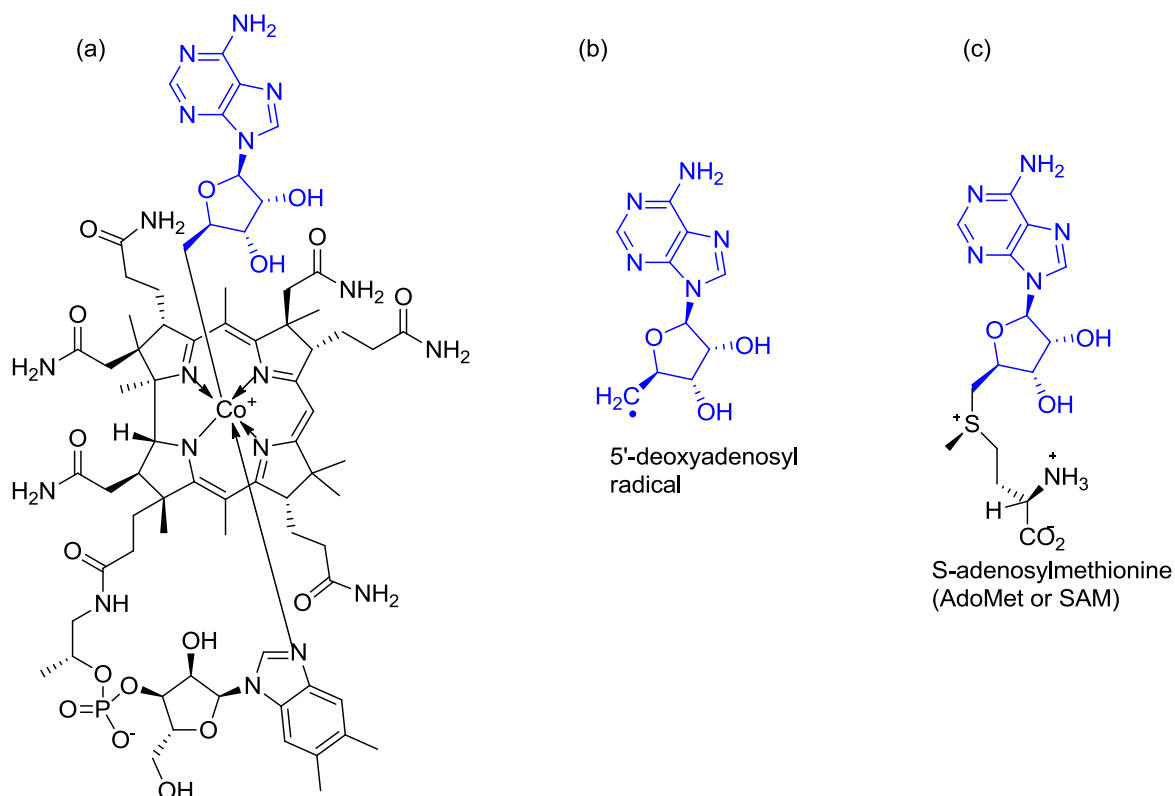


Figure 24 – Molecular structures of (a) AdoCbl, (b) Ado•, and (c) AdoMet.

1.4.1 Generation of radicals

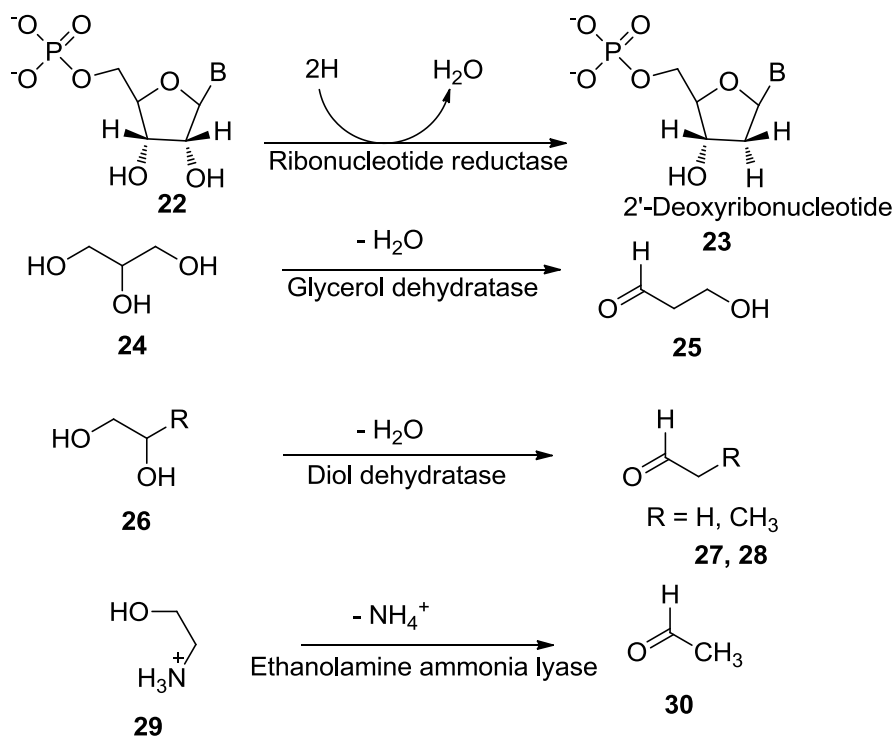
Enzymatic radical reactions progress by at least four steps:⁵²

- 1) Generation and storage of an initiating radical.
- 2) Reaction of the initiating radical with a substrate to give a substrate-derived radical.
- 3) Conversion of the substrate-derived radical into the product-related radical
- 4) Conversion of the product-related radical into product which may result in recycling of the initiating radical.

1.4.2 Coenzyme B₁₂-dependent enzymes

There are two different groups of coenzyme B₁₂-dependent enzymes:⁶⁸


- 1) The eliminase family which comprises of ribonucleotide reductase, ethanolamine ammonia lyase and diol and glycerol dehydratases (Fig. 25).



✚ **Figure 25** – The family of coenzyme B₁₂ dependent eliminases. B = nucleobase. The coenzyme B₁₂ dependent ribonucleotide reductase takes ribonucleoside triphosphates as substrates.

- 2) The mutase family which comprises of carbon skeleton mutase and aminomutase sub-families. The carbon skeleton mutase sub-family consists of glutamate mutase, methylmalonyl-CoA mutase, 2-methyleneglutarate mutase and isobutyryl-CoA mutase. The aminomutase sub-family consists of β-lysine-5,6-aminomutase and D-ornithine-4,5-aminomutase (Fig. 26).

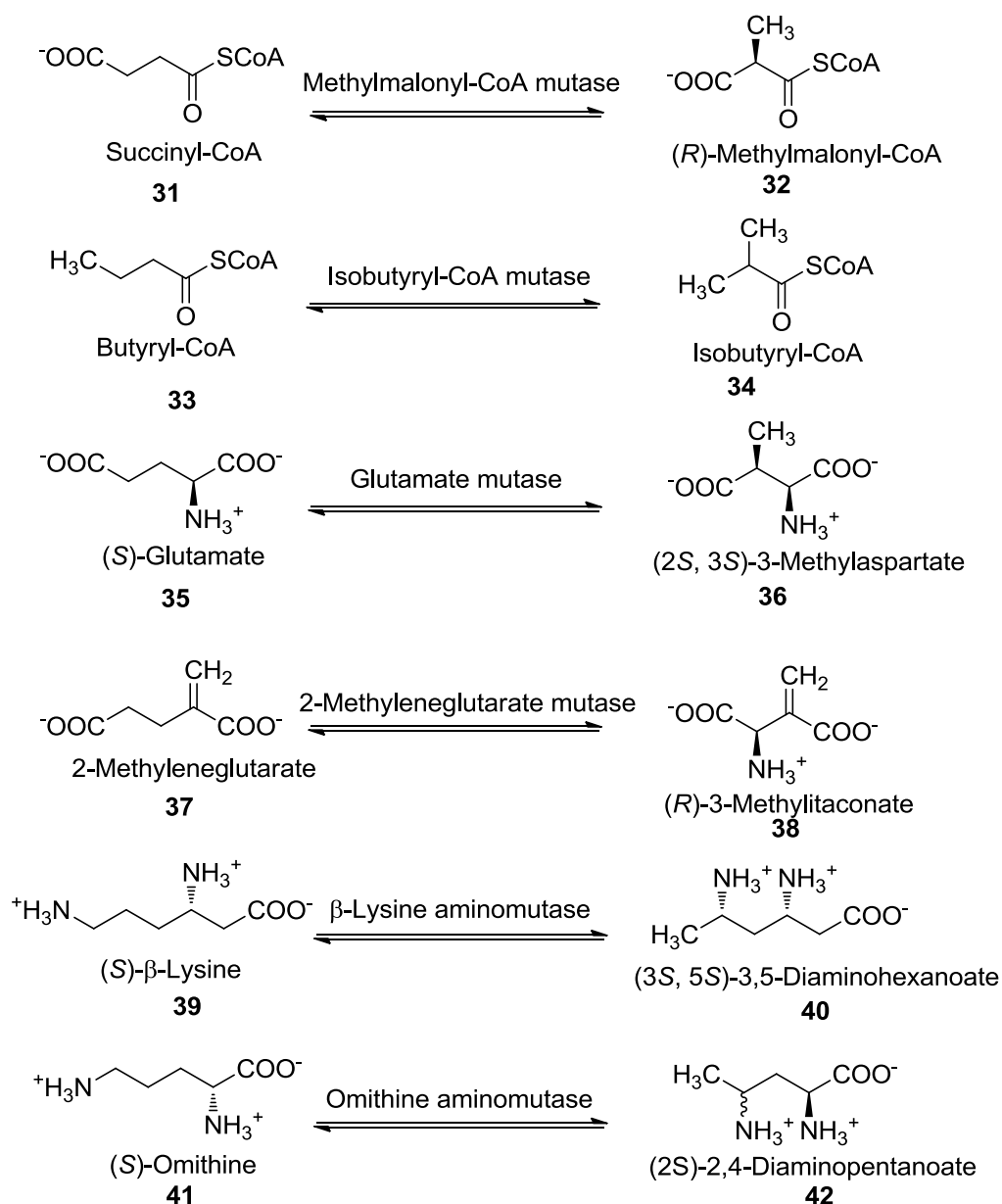


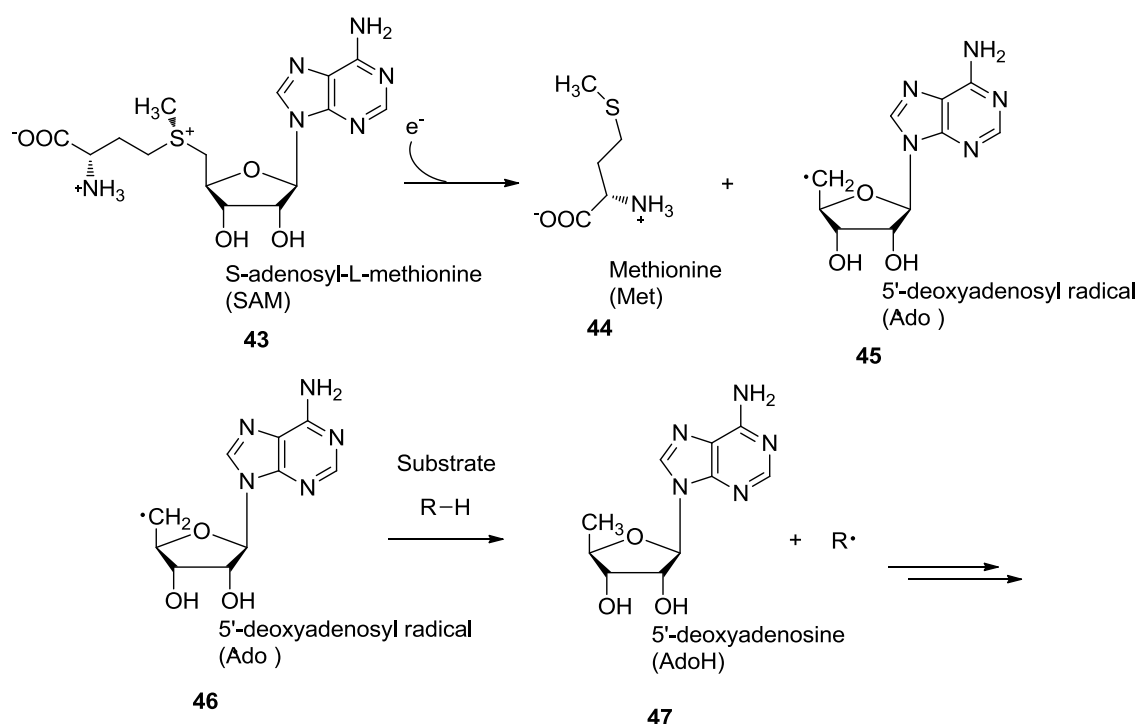
 **Figure 26** – The family of coenzyme B₁₂ dependent mutases. The methylene group in each reaction is reversibly converted into a methyl group via a methylene radical which may be stabilised by cob(II)alamin.

Both eliminases and mutases have similar pathways (Fig. 17) which involves the exchange between two adjacent carbon atoms of a group X (OH, NH₃⁺, or a carbon containing residue).

1.4.3 S-Adenosylmethionine radical enzymes

SAM is an alternative to coenzyme B₁₂ as a generator of the 5'-deoxyadenosyl radical.

All SAM-dependent radical enzymes reduce SAM to methionine and 5'-deoxyadenosyl radical, which initiates catalysis, generally by hydrogen atom abstraction from the substrate (Scheme 11).⁶⁹



Scheme 11 – SAM in Radical Enzymes.

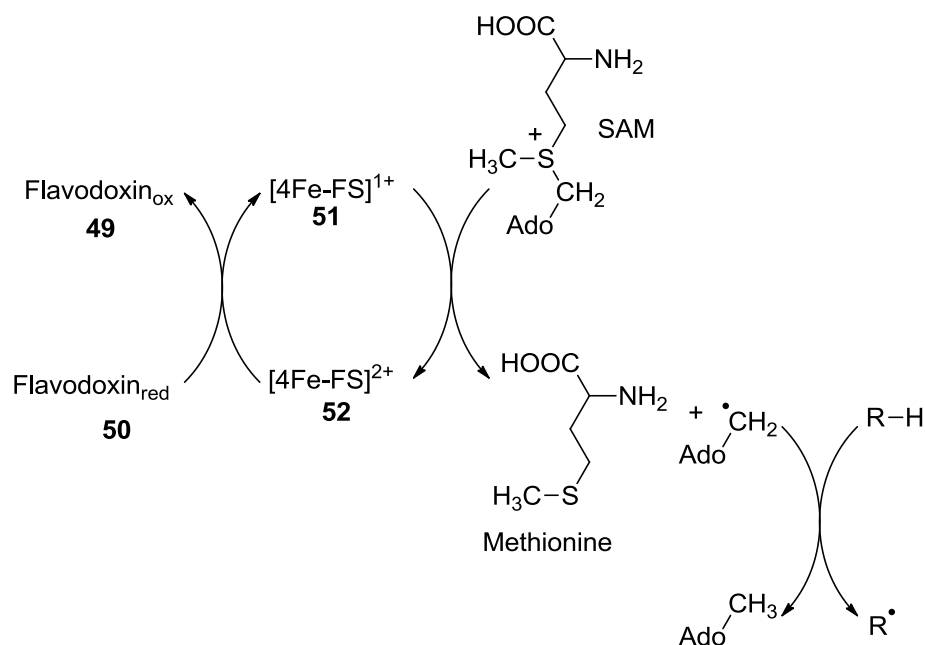
1.4.3.1 Common features


Despite their surprisingly diverse functions, all radical SAM enzymes contain an unconventional [4Fe-4S] cluster coordinated by three rather than four closely-spaced cysteine residues site. Also they all need a low-potential one-electron donor, ferredoxin or flavodoxin, in order to reduce SAM. The 5'-deoxyadenosine formed is either irreversibly released as product or recycled to regenerate SAM, The majority of the SAM-dependent radical enzymes belong to the irreversible type.

1.4.3.2 Proposed mechanism of SAM

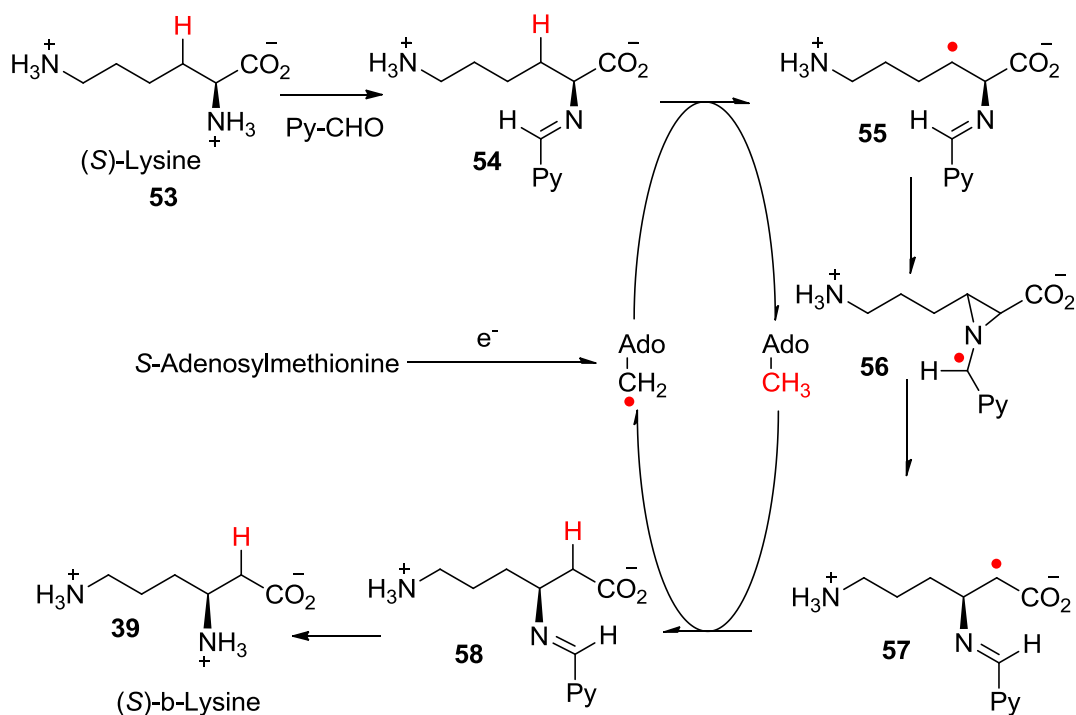
The first common step in all radical SAM enzyme reactions is the reduction of the [4Fe-4S] centres from the resting +2 to the active +1 state, The reduced [4Fe-4S] centre ([4Fe-4S]⁺) is believed to transfer an electron to the sulfonium

of SAM, resulting in its homolytic cleavage to methionine and the highly reactive 5'-deoxyadenosyl radical (Scheme 12).



 **Scheme 12** – Proposed mechanism of SAM.

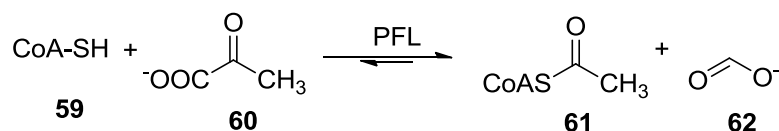
The first SAM-dependent enzyme to be described that catalysed a rearrangement similar to a coenzyme B₁₂-dependent reaction was lysine-2,3-aminomutase.⁷⁰ In the initial catalytic step a hydrogen atom is removed from C-3 of lysine bound via the amino group to pyridoxal-5'-phosphate. The resulting 5'-deoxyadenosine acts as a spectator during the consecutive rearrangement of the α-lysine-3-yl radical to the β-lysine-2-yl radical, probably via an azacyclopropylcarbonyl radical. Finally, 5'-deoxyadenosine donates one methyl hydrogen atom back to the β-lysine-2-yl radical (as its pyridoxal imine) and the pyridoxal-5'-phosphate imine of β-lysine is formed (Scheme 13).⁵²



✚ **Scheme 13** – Proposed mechanism of action of lysine-2,3-aminomutase. Py-CHO, pyridoxal-5'-phosphate.

1.4.4 Glycyl radical enzymes⁷¹

A glycyl radical is formed by the removal of a hydrogen from a glycine and the resulting radical is located on the protein main chain. The first member of this class to be characterised as a radical enzyme was pyruvate:formate lyase, which is produced in *Escherichia coli* only under anoxic conditions, where it catalyses the reversible cleavage of pyruvate by CoASH to acetyl-CoA and formate (Scheme 14).⁷²

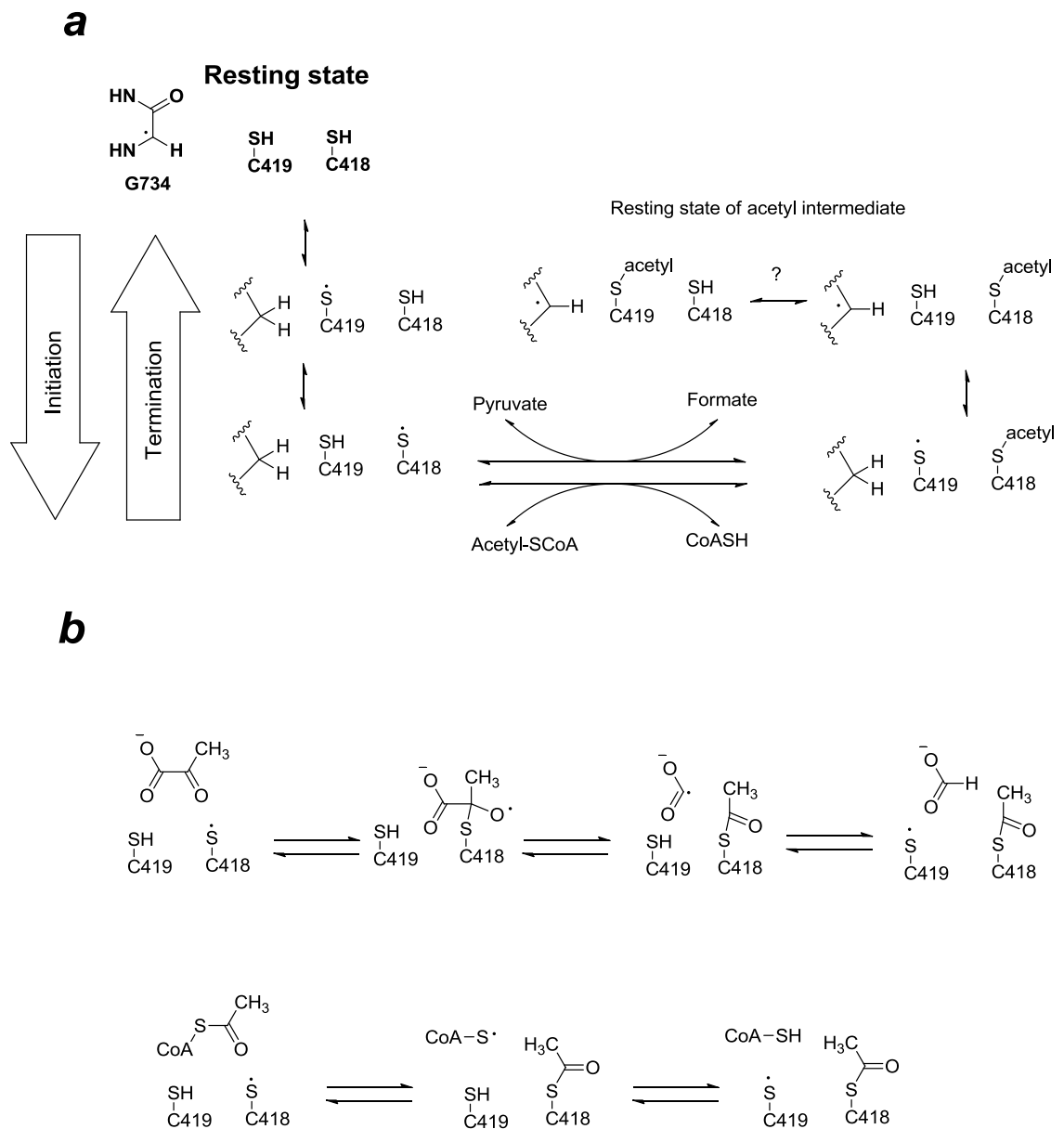


✚ **Scheme 14** – The conversion of pyruvate to formate as catalysed by PFL.

In pyruvate:formate lyase the fairly stable glycyl radical exhibits a characteristic electron paramagnetic resonance (EPR) signal, resulting from the coupling of the hydrogen that remained on the amino acid. The reaction of the radical with dioxygen inactivates the enzyme by cleavage of the polypeptide chain at the

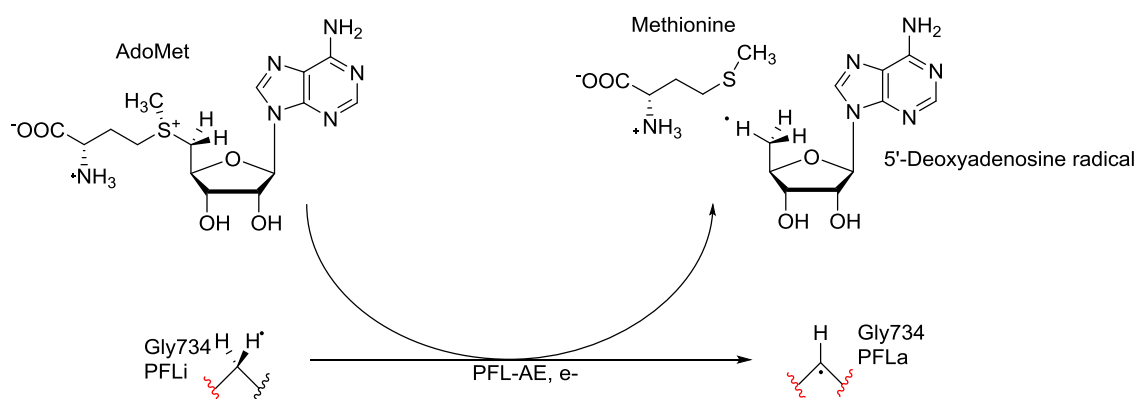
glycine residue. Therefore these enzymes can only occur in anaerobic microorganisms. The 5'-deoxyadenosyl radical is generated by the action of a SAM-dependent activating enzyme, which contains at least one [4Fe-4S] cluster.

The proposed mechanism of pyruvate:formate lyase⁷³ suggests that the Gly734 radical abstracts a hydrogen from Cys419 and causes radical formation at Cys418. This radical interacts with pyruvate to facilitate C–C bond homolysis yielding formate (Scheme 15).



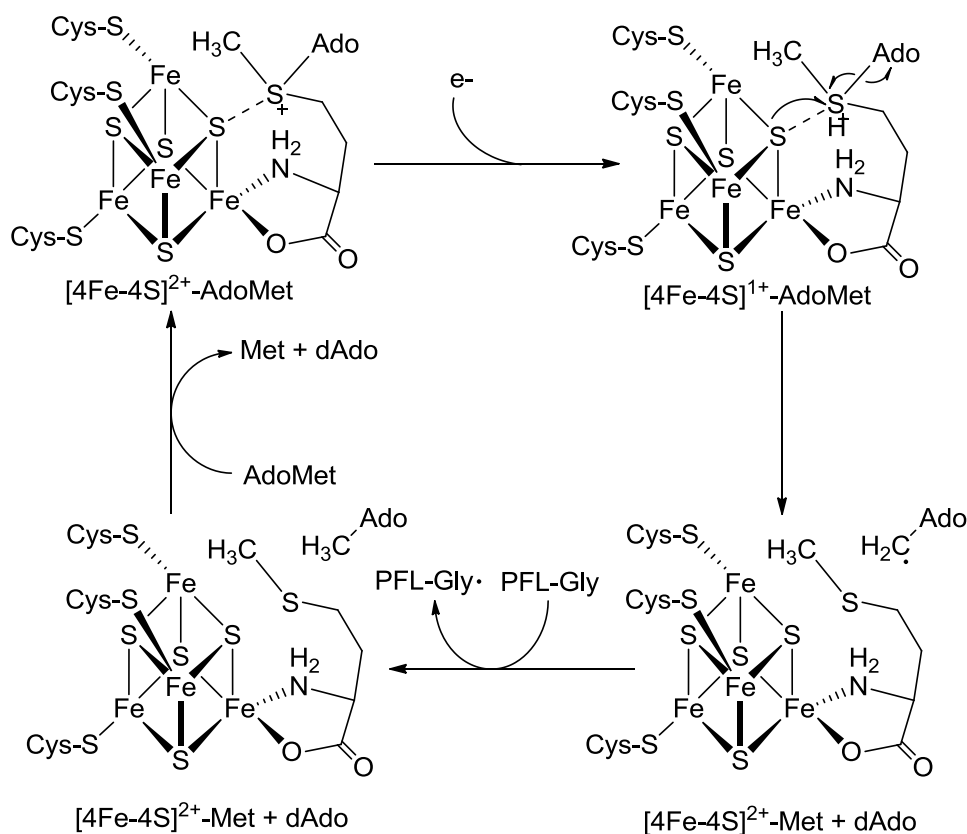
 **Scheme 15** – Proposed mechanism of pyruvate:formate lyase.

Pyruvate formate lyase-activating enzyme (PFL-AE) catalyses the formation of the Gly734 radical of PFL. It has been proposed that PFL-AE uses a Fe-S cluster to cleave AdoMet to form a 5'-deoxyadenosyl radical and that this radical goes on to abstract the pro-S hydrogen of the Gly734 residue of PFL, thus activating the enzyme (Scheme 16).



Scheme 16 – From *Archives of Biochemistry and Biophysics* **2005**, 433 (1), 290
The reaction catalysed by pyruvate formate lyase activating enzyme. PFL-AE facilitates AdoMet cleavage to methionine and the 5'-deoxyadenosyl radical, producing a glycy radical at Gly734 and activating PFL.

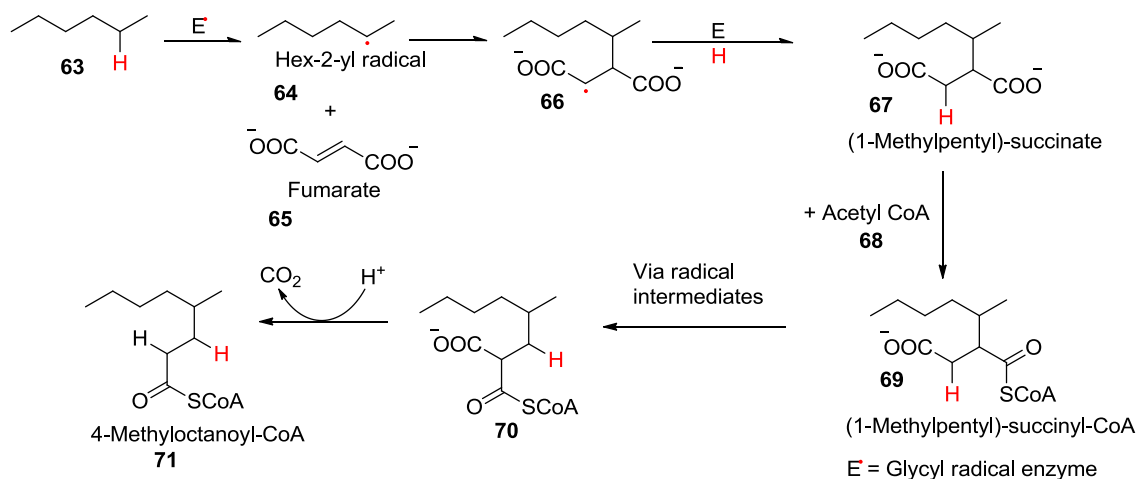
The PFL-AE employs a radical cluster that utilises an Fe-S cluster for catalysis. This mechanism has common initiation steps in the SAM super-family (Scheme 17).



58

Scheme 17 – Proposed mechanism for the activation of PFL by PFL-AE and AdoMet.

Anaerobic hexane oxidation in a denitrifying bacterium HxN1 starts with an addition of the hex-2-yl radical to fumarate leading to (1-methylpentyl)succinate.⁷⁴ Although the enzyme has not been purified, a strong EPR signal indicative of a glycyl radical enzyme became visible in whole cells grown on hexane but not in cells grown on hexanoate (Fig. 21). This system is a major component of this thesis.



Scheme 18 – Anaerobic hexane oxidation in denitrifying bacterium.

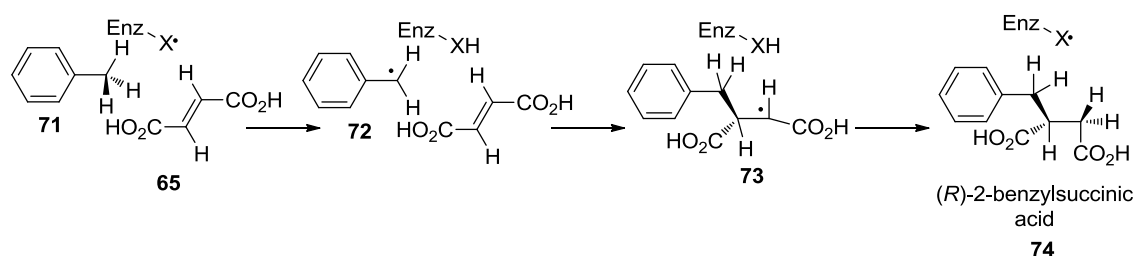
1.5 ANAEROBIC DEGRADATION OF *n*-HEXANE

First investigations into the anaerobic metabolism of *n*-alkanes were conducted with two phylogenetically related sulfate-reducing bacteria, strains Hxd3 and Pnd3.⁷⁵ Studies suggested that anaerobic degradation of alkanes does not occur via desaturation to 1-alkenes. These findings also suggested different modes of initial reactions in the two *n*-alkane-degrading sulfate-reducing strains. However, by labelling studies, the methyl branch of the fatty acids was shown to be the original terminal carbon of the *n*-alkane, suggesting addition of a carbon compound to the subterminal position (C-2) of the *n*-alkanes. This showed a common principle in the mechanism of initial reactions of *n*-alkanes in both strains.

The recently isolated denitrifying strain HxN1² was chosen for experiment. In contrast to other *n*-alkane degrading anaerobic bacteria, strain HxN1 grows relatively rapidly and does not adhere to the insoluble alkane phase, so that cells can be harvested easily. Strain HxN1 utilises *n*-alkanes with relatively short chains of C₆ - C₈ that are ultimately oxidised to CO₂; other anaerobic *n*-

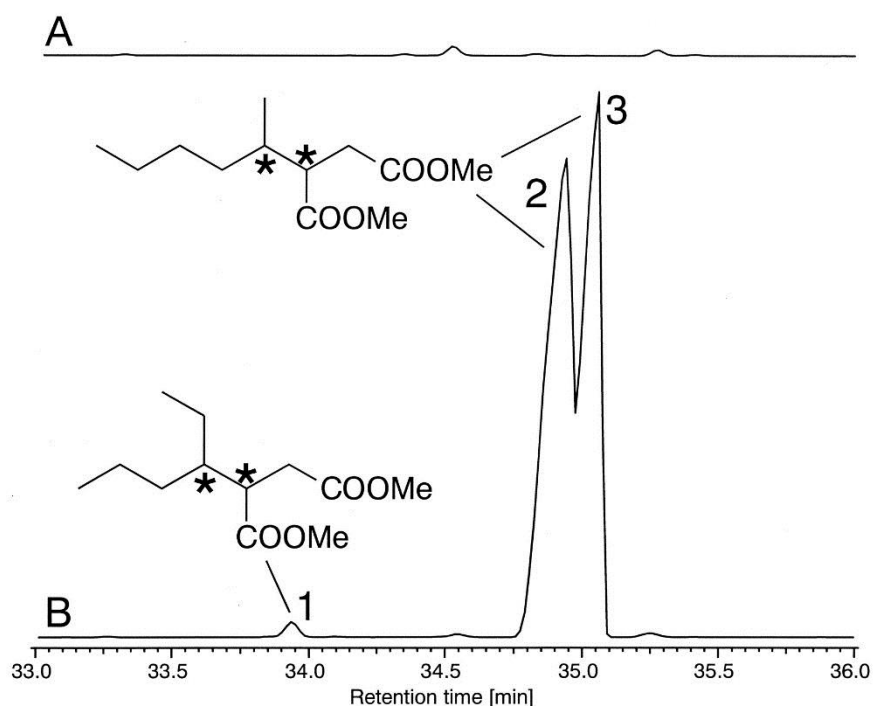
alkane-degrading strains grow preferentially with chain lengths between C₈ and C₁₈ (See Table 4). Recently, two-dimensional gel electrophoresis of cell extracts of strain HxN1 revealed specific formation of proteins during growth on *n*-hexane that were not formed with growth on *n*-hexanoate. These proteins were therefore supposed to be specifically involved in initial reaction steps of *n*-alkanes.

The mode of anaerobic hexane activation can be elucidated by chemical analysis of metabolites. The denitrifying *Azoarcus*-like isolate (strain HxN1) growing on *n*-hexane forms alkyl-substituted succinates. This suggests an initial reaction similar to that in the anaerobic degradation of toluene because in the N terminus, one of these proteins exhibited a similarity to the small subunit (BssC) of benzylsuccinate synthase in denitrifying bacteria. The glycyl radical enzyme 'benzylsuccinate synthase' (BSS) from *Thauera aromatica* (β -proteobacteria) converts toluene to a benzyl radical, which stereospecifically attacks the second substrate fumarate leading to 2-benzylsuccinate-3-yl radical and finally, the hydrogen is re-added, also in a stereospecific manner (Scheme 19).⁷⁶



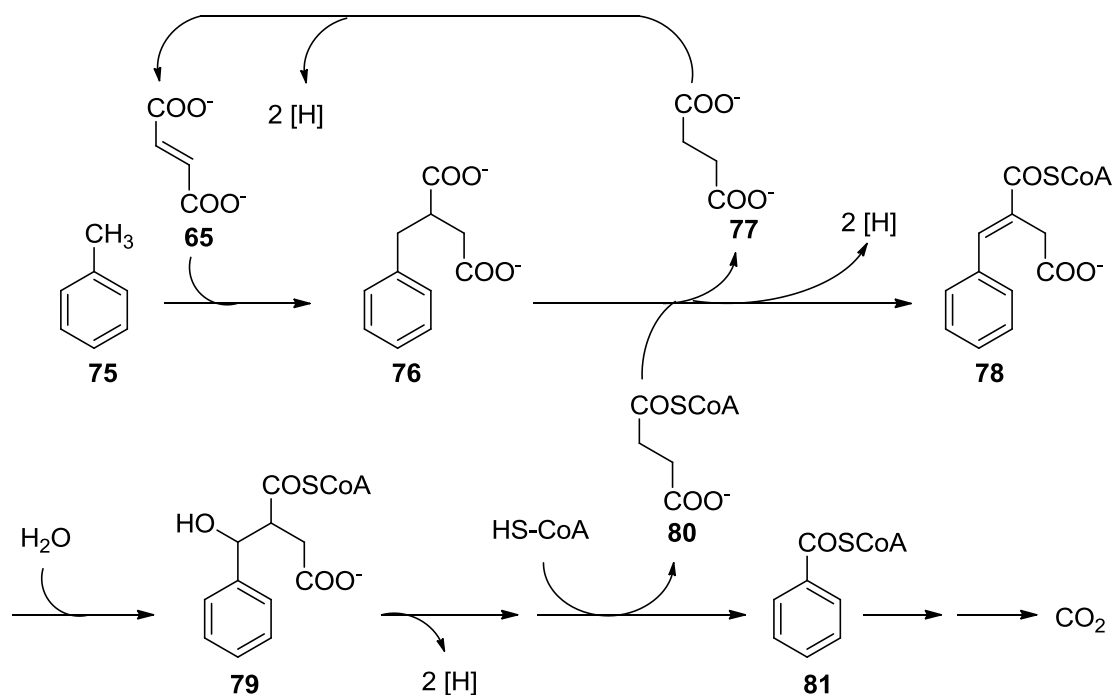
Scheme 19 – Mechanism for the BSS-catalyzed addition of toluene to fumarate.

However, *n*-hexane is not activated at one of the methyl groups (C-1), as indicated by the formed metabolites.⁷⁴ Structural analyses including authentic standard compounds shows that strain HxN1 forms (1-methylpentyl)succinate from *n*-hexane and fumarate as the assumed co-substrate, which indicates that *n*-hexane must have been activated at the C-2 position. Traces of (1-ethylbutyl)succinate are indicative of an additional, alternative activation at C-3 in a side reaction (Fig. 27).⁷⁴



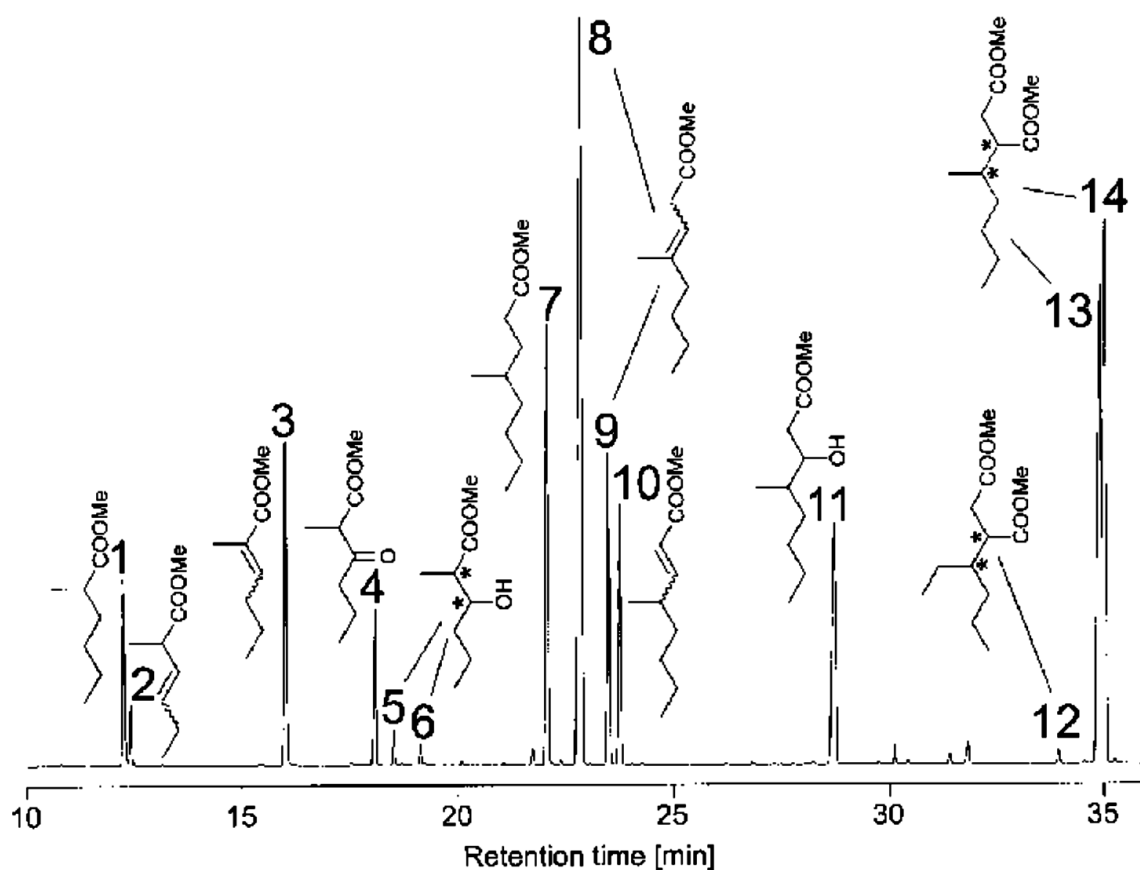
✚ **Figure 27** – Figure adapted from *J. Bacteriol.* **2001**, *183* (5), 1710, Partial gas chromatograms of methylated extracts from heat-treated, acidified cultures of strain HxN1 after anaerobic growth with nitrate as the electron acceptor and with *n*-hexanoate (A) or *n*-hexane (B) as the only organic substrate. By studying the mass spectrometric data compounds 2 and 3 were interpreted as separable diastereomers of (1-methylpentyl)succinate (MPS) dimethyl ester; possible diastereomers of compound 1, (1-ethylbutyl)succinic acid (EBS) dimethyl ester, were not separable on the gas chromatography column. Asterisks (*) indicate chiral carbon atoms; assignment of the absolute stereochemistry of diastereomers was not achieved in this study.

Another unique feature found in the biosynthesis of (1-methylpentyl)succinate, which has two chiral centres, is the formation of both diastereomers in equal amount. Formation of diastereomers is not possible from toluene because benzylosuccinate has only one chiral centre; the enantiomer formed was shown to be (*R*)-2-benzylosuccinic acid (Scheme 19).⁷⁶ After conversion of the latter to benzylosuccinyl-CoA, dehydrogenation and hydration reactions lead to 2-carboxymethyl-3-hydroxyphenylpropionyl-CoA. Hence, the benzyl carbon position (original methyl group of toluene) is converted to a keto group which allows thiolitic cleavage into benzoyl-CoA and acetyl-CoA (Scheme 20).⁷⁷



✚ **Scheme 20** - Pathways of anaerobic toluene degradation in denitrifying bacteria. Only the reactions leading from the hydrocarbons to benzoyl-CoA (or 3-methylbenzoyl-CoA) are shown in detail. **75**, Toluene; **65**, fumarate; **76**, benzylsuccinate; **77**, succinate; **78**, phenylitaconate; **79**, 2-carboxymethyl-3-hydroxyphenylpropionyl-CoA; **80**, succinyl-CoA; **81**, benzoyl-CoA.

An analogous metabolism of an assumed (1-methylpentyl)succinyl-CoA in the anaerobic metabolism of *n*-hexane is not possible. The tertiary carbon atom which forms at the original *n*-alkane chain would prevent oxidation beyond the alcohol level. In 2002 Wilkes et al. grew the strain HxN1 on *n*-hexane in order to assign metabolites specifically to the *n*-hexane metabolism.⁸ The fate of the succinate moiety in (1-methylpentyl)succinate was traced in an experiment in which a culture growing on unlabelled *n*-hexane was reacted with 2,3-*d*₂-fumarate. The results obtained by gas chromatography (GC) (Fig. 85) and electron ionization mass spectrometry (EIMS) showed that the degradation of (1-methylpentyl)succinate (possibly as thioester) in strain HxN1 involves rearrangement of the C-skeleton prior to further oxidation and thus differs in principle from degradation of benzylsuccinate.



🚦 **Figure 28** - Gas chromatograms of methylated extracts from the acidified culture of denitrifying strain HxN1 after anaerobic growth on *n*-hexane. (Figure adapted from Wilkes et al. 2002)⁸

Based on this finding and the identification of a suite of fatty acids specifically formed during growth of strain HxN1 on *n*-hexane, a pathway for the degradation of (1-methylpentyl)succinate (MPS) has been proposed⁸ (Scheme 21). This pathway also accounts for the indispensable regeneration of fumarate, the co-substrate for alkane activation. As shown in Scheme 21, in one round, 1 mol *n*-hexane is converted to 3 mol acetyl-CoA. The compounds that have been identified as methyl esters are followed by the corresponding peak numbers from Fig. 28. 63A, *n*-Hexane; 65B, fumarate; 67C, (1-methylpentyl)succinate (13, 14); 67D, (1-methylpentyl)succinyl-CoA (13, 14); 67E, (2-methylhexyl)malonyl-CoA; 67F, 4-methyloctanoyl-CoA (7); 67G, 4-methyloct-2-enoyl-CoA (10); 67H, 3-hydroxy-4-methyloctanoyl-CoA (11); 67I, 4-methyl-3-oxooctanoyl-CoA; 67J, 2-methylhexanoyl-CoA (1); K, 2-methylhex-2-enoyl-CoA (3); 67L, 3-hydroxy-2-methylhexanoyl-CoA (5, 6); 67M, 2-methyl-3-oxohexanoyl-CoA (4); 67N, propionyl-CoA; 67O, butyryl-CoA; 67P, acetyl-CoA; 67Q, methylmalonyl-CoA; 67R, succinyl-CoA; 67S, succinate.

1.5.1 Possible presence of a glycy radical

The distinct EPR signal in *n*-hexane-grown cells and its virtual absence in *n*-hexanoate-grown cells of strain HxN1 provide evidence for the specific involvement of a radical in the anaerobic initial reaction of *n*-hexane (Fig. 29).⁷⁴ The observed signal is from a radical species which has a strong coupling to a single hydrogen atom. The average *g* value, line shape, and magnitude of the hyperfine coupling is typical for radicals at carbon side chains of amino acids, flavin radicals, or sulfur-centered radicals. There are presently no biochemically purified cell components other than glycy radical enzymes which exhibit such an EPR signal. However, purification of the MPS-forming enzyme from strain HxN1 and structural investigations are needed to prove the assumed involvement of a glycy radical.

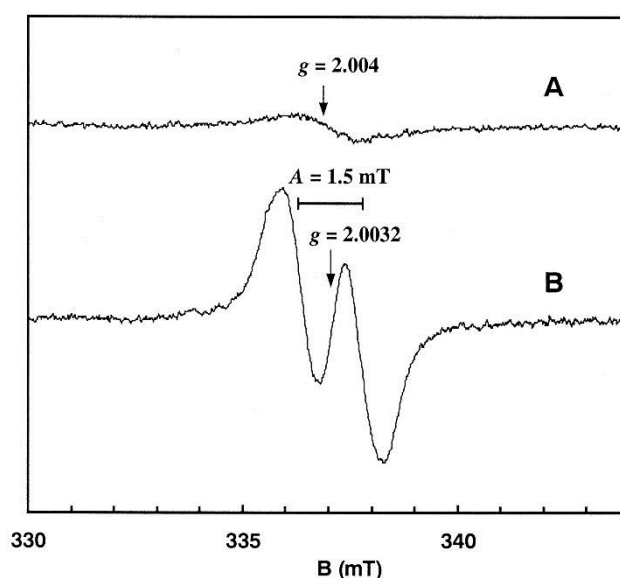
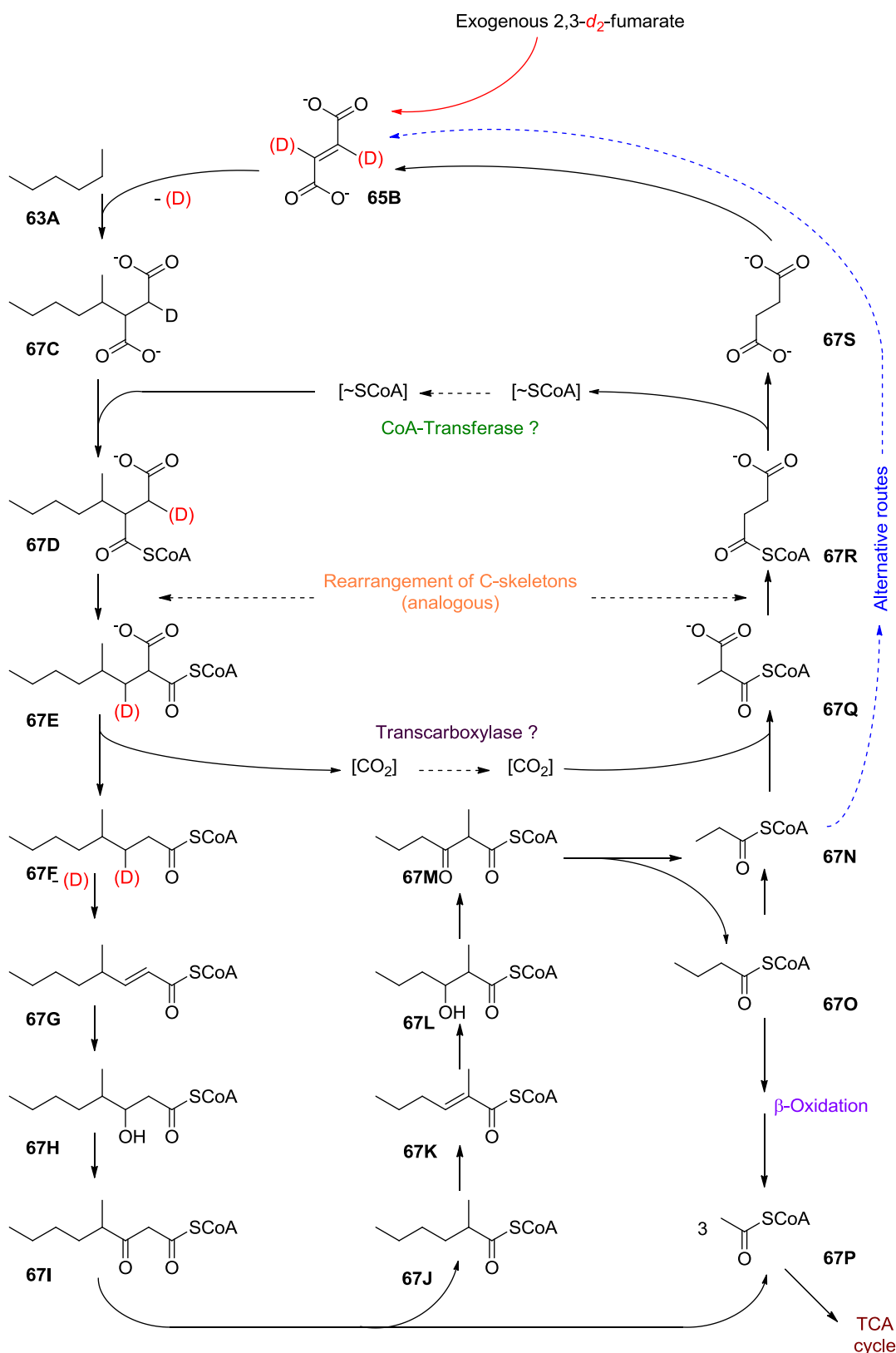
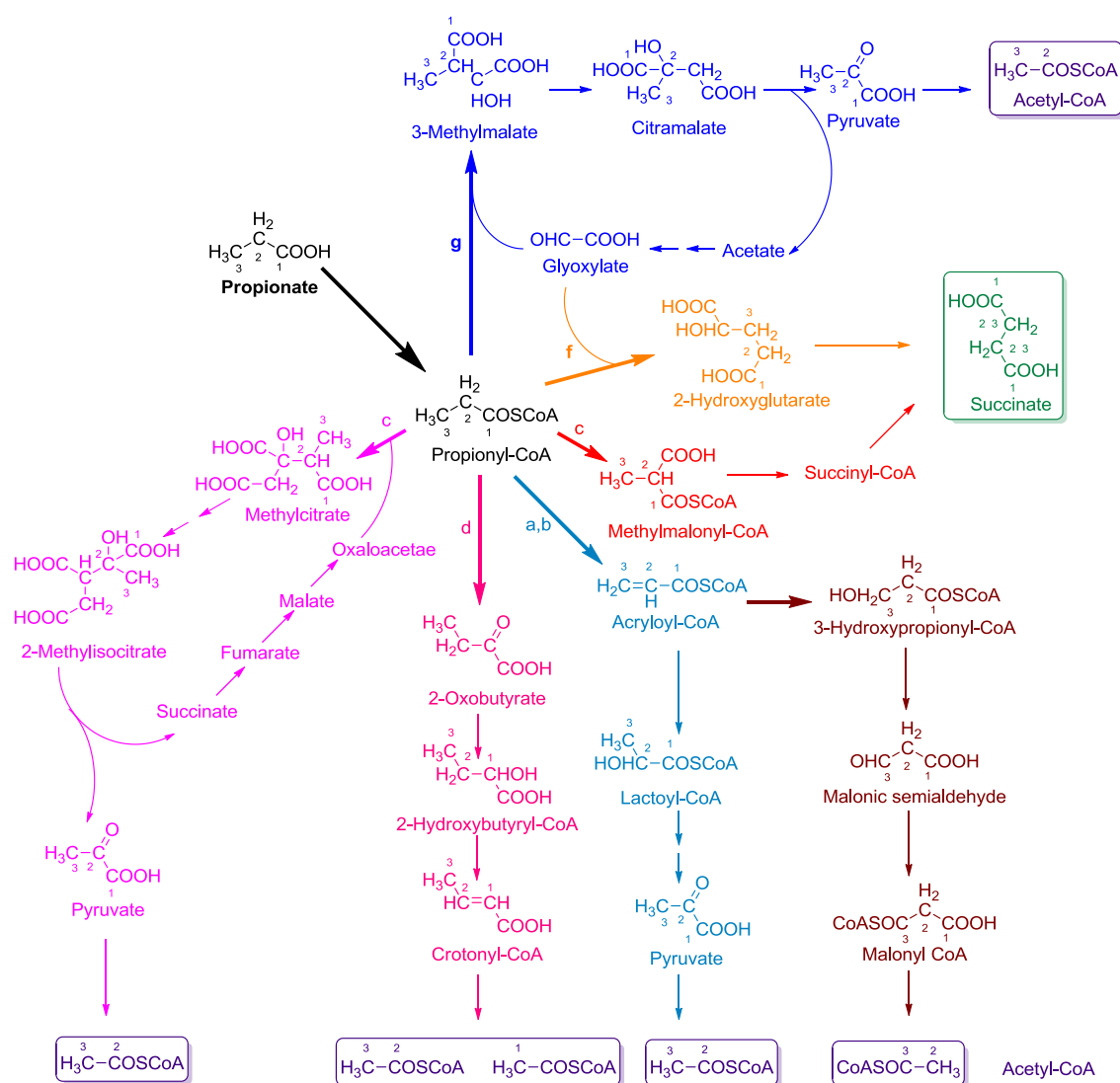


Figure 29 - EPR spectra of suspensions of cells of strain HxN1 grown anaerobically with *n*-hexanoate (A) and *n*-hexane (B) as the only organic substrates and nitrate as the electron acceptor. (Figure adapted from Wilkes et al. 2002)⁸



Scheme 21 – Identified methyl esters are followed by the corresponding peak numbers from Fig. 28. 63A, *n*-Hexane; 65B, fumarate; 67C, (1-methylpentyl)succinate (13, 14); 67D, (1-methylpentyl)succinyl-CoA (13, 14); 67E, (2-methylhexyl)malonyl-CoA; 67F, 4-methyloctanoyl-CoA (7); 67G, 4-methyloct-2-enoyl-CoA (10); 67H, 3-hydroxy-4-methyloctanoyl-CoA (11); 67I, 4-methyl-3-oxooctanoyl-CoA; 67J, 2-methylhexanoyl-CoA (1); K, 2-methylhex-2-enoyl-CoA (3); 67L, 3-hydroxy-2-methylhexanoyl-CoA (5, 6); 67M, 2-methyl-3-oxohexanoyl-CoA (4); 67N, propionyl-CoA; 67O, butyryl-CoA; 67P, acetyl-CoA; 67Q, methylmalonyl-CoA; 67R, succinyl-CoA; 67S, succinate.

Butyryl-CoA is assumed to undergo β -oxidation to acetyl-CoA and final oxidation to CO₂. This assumption is justified because strain HxN1 is able to oxidise organic electron donors including added butyrate or acetate completely to CO₂.⁹ Six pathways are known for propionyl-CoA metabolism (Scheme 22).¹¹ Among these, the methylmalonyl-CoA pathway would regenerate fumarate by involving the least number of reaction steps (Scheme 22-c). This pathway, which is the most common in propionyl-CoA metabolism, starts with α -carboxylation to yield (S)-methylmalonyl-CoA and proceeds via reverse reactions of propionic acid fermentation to free succinate and further to fumarate. The assumption of such a pathway in strain HxN1 leaves open the possibility for carboxylation of propionyl-CoA by transcarboxylation with (2-methylhexyl)malonyl-CoA as carboxyl donor, which would not require energy.



Scheme 22 - Possible pathways for propionate oxidation¹¹: a) α -Oxidation, b) β -Oxidation, c) α -Carboxylation, d) Reductive carboxylation, and e-g) Claisen condensations.

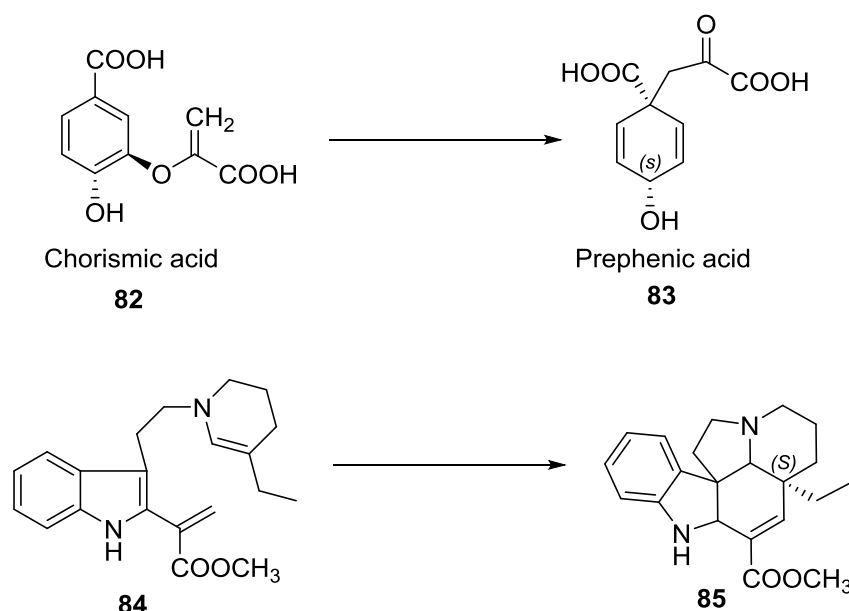
Chapter 2

Introduction to Enzyme Stereospecificity and Isotopic Labelling

2.1 ENZYME STEREOSPECIFICITY

The high degree of stereospecificity which exists within enzymes has been known since the time of Pasteur.⁷⁸ However, the study of this stereospecificity in detail, in terms of the mechanism of reactions and nature of enzyme-substrate complex, has only been endeavoured with in the past few decades.

From this newly acquired knowledge, the one feature that appears to the most interesting is that enzymatic reactions do not proceed with a large degree of concertedness in which all bond breaking and bond making occurs in a single step. The numbers of pericyclic reactions which are found in nature are extremely small; two such reactions are illustrated in Scheme 23, first reaction from primary metabolism and the second one from secondary metabolism.



Scheme 23 – Enzyme-catalysed pericyclic reactions that are probably concerted.

It is worth pointing out that even in these cases (Scheme 23), there is no definite proof that the reactions proceed with concerted mechanisms. Nature appears to prefer to carry reactions out in simple steps, normally involving cleavage or formation of one bond at a time. Therefore, in most cases bonding interactions as a means of controlling the stereospecificity of intermolecular reactions will be of minimal use.

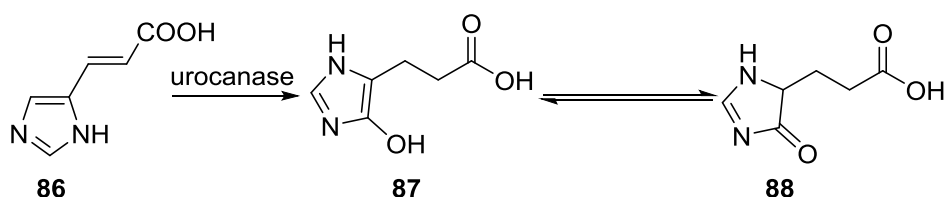
The main basis of enzymatic stereospecificity is non-bonding interactions, i.e., steric control. One of the few reactions which appears to be catalysed by enzymes in a concerted manner is the nucleophilic displacement of S_N2 type. Studies of methyl group transfer from *S*-adenosylmethionine to an acceptor have revealed this type of reaction to occur with inversion at the methyl carbon atom in all cases so far studied.⁷⁹

If enzyme-catalysed reactions proceed in a stepwise manner, this will usually involve the generation of reactive intermediates. However, the enzyme often has complete control over the way which these metastable species react further and this control is exerted while the substrate is bound in the active site of enzyme.

Enzyme stereospecificity is actually the sum of two distinct, although not entirely separable, phenomena. First, is the overall steric course of the reaction as this term is applied to reaction in solution, and secondly, it includes chiral recognition. If the reaction proceeds through a reactive intermediate (e.g., a carbenium ion possessing enantiotopic faces), chiral recognition will occur. Although in solution the intermediacy of such a carbenium ion would almost certainly result in loss of stereospecificity, chiral recognition by the enzyme may still result in stereospecific addition of a nucleophile to only one of the two enantiotopic faces. Likewise, if an enzymatic reaction produced an intermediate that in solution would be torsiosymmetric, torsion may be prevented at the active site, again allowing a stereospecific reaction. Therefore an understanding of the overall steric course, does not allow inferring the existence of a reactive metastable intermediate during an enzymatic reaction in the same way as it does in studies of non-enzymatic reactions. Taking this reasoning into account, the steric course of an enzymatic reaction does not always provide information concerning the mechanism of reaction.

In exceptional cases a loss of stereochemical integrity can be demonstrated during the course of an enzymatic reaction. Such an observation points to one of the two possible occurrences:⁷⁹

- 1) One step in the overall reaction does not come under enzymatic control. I.e., tautomeric conversion of an enol into a ketone, although the enol may be produced enzymatically in a stereocontrolled fashion. If the tautomeric change occurs when the molecule is out of the active site, stereospecificity will be lost (Scheme 24). In the conversion of urocanic acid (**86**) into 3-(4-oxo-4,5-dihydro-1*H*-imidazol-5-yl)propanoic acid (**88**), the true enzymatic product is most likely 3-(4-hydroxy-1*H*-imidazol-5-yl)propanoic acid (**87**), but this spontaneously tautomerizes to afford racemic **88**.⁷⁹



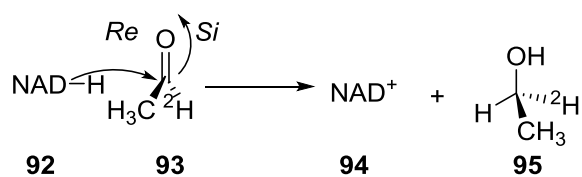
Scheme 24 – The urocanase reaction yields an achiral enolic product which is in equilibrium with its racemic tautomer.

- 2) During the enzymatic reaction a reactive intermediate is generated which possesses homotopic groups or faces. Evidence for the intermediacy of a torsiosymmetric group has been obtained during several of the coenzyme B₁₂ dependent enzymatic rearrangements (see Section 1.2). In many cases the observation of chiral recognition during a reaction does not require any special techniques. I.e., the question of which enantiotopic face of a trigonal centre is attacked by a reagent in an enzymatic reaction is often instantly answered by knowing the absolute configuration of the product (Scheme 25).



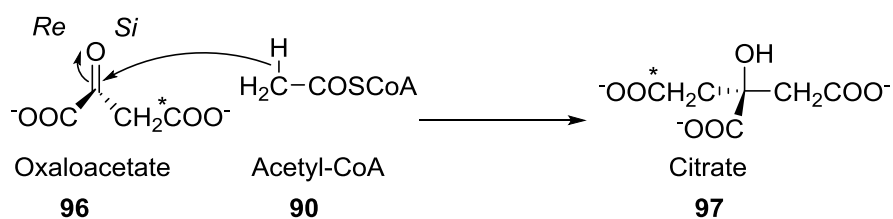
Scheme 25 – (2*S*)-Malate formation.

However, when the approaching reagent is identical with one of the three substituents already at the trigonal centre, isotopic labelling of the chemically equivalent substituents will be useful (Scheme 26). Determining the absolute configuration at the newly formed centre then creates another problem which cannot be solved by conventional methods. However, another enzyme with known stereospecificity may be used for such purpose. I.e., formation of citrate from oxaloacetate and acetyl-CoA in the citrate synthase reaction (Scheme 27 & 28).

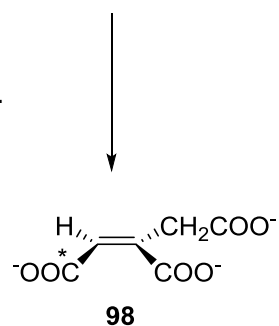


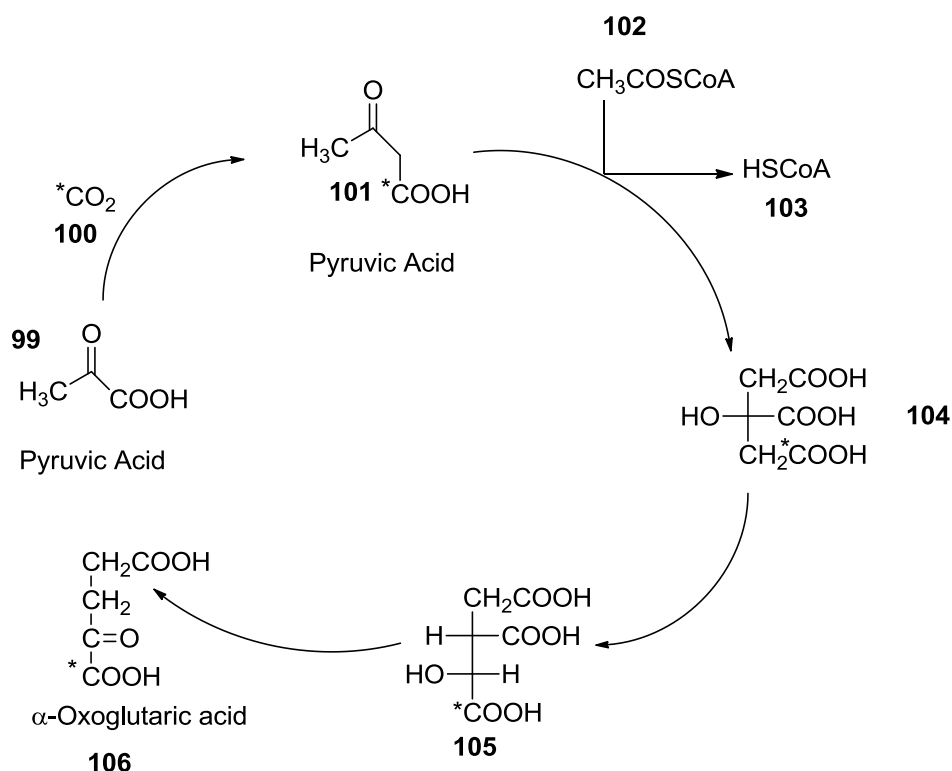
Scheme 26

Starting from isotopically labelled oxaloacetate the enzyme catalyses the formation of citrate containing a label in only one of its carboxymethylene groups. The position of this label was determined by making use of the known steric course of aconitase, which modifies only the $(\text{CH}_2\text{COOH})_{\text{Re}}$ group in a stereospecific dehydration. The results demonstrated that the labelled citrate was (*R*) and hence the enolate of the acetyl-CoA has attacked the *Si*-face of oxaloacetate.



Scheme 27 – Chiral recognition of enantiotopic carboxymethylene groups of citrate by aconitase.





Scheme 28 – The fate of carbon dioxide introduced by pyruvate carboxylase into the citric cycle.

A large amount of difficult and delicate work must often be carried out in order to determine the steric course of an enzyme-catalysed reaction. Furthermore, the knowledge of the steric course actually encompasses a combination of chiral recognition by the enzyme and mechanistic requirements of the reaction. Unravelling these two factors may be difficult. Once stereochemical information has been achieved, data are then sought from other directions, notably from mechanistic investigations and from structural studies on the enzyme in general and on the active site in particular. These pieces of the puzzle should then interlock with knowledge of mechanistic organic chemistry to provide a detailed picture of what happens during an enzyme-catalysed reaction.

2.2 ISOTOPIC LABELLING

The introduction of pulsed Fourier-transform Nuclear Magnetic Resonance (NMR) spectrometers which significantly facilitated the routine ^{13}C NMR assignment of small amounts of natural products, presented a major boost for the study of biosynthetic pathways in the early 1970s. In addition, precursors enriched with ^{13}C and other stable isotopes, e.g. ^2H , ^{18}O , ^{15}N , were becoming more readily available and major gains came from the use of precursors


multiply labelled with ^{13}C or with ^{13}C in conjunction with ^2H , ^{18}O and ^{15}N . The detection of these combinations of isotopic labels by either spin-spin coupling and/or isotopically shifted signals in the NMR spectra of the enriched metabolites allowed the incorporation of whole biosynthetic units to be elucidated for the first time. The biosynthetic unit could be a single bond or, indeed, a multi-atom unit. Thus the integrity of, for example, carbon-carbon, carbon-hydrogen or carbon-oxygen bonds during a complex metabolic pathway could be tested. The course of skeletal and other rearrangements could be traced and, most importantly, the biosynthetic origin of hydrogen, oxygen and nitrogen atoms could be determined and the oxidation levels of the intermediates in the pathway could be established by indirect methods.⁸⁰

2.2.1 Applications of double ^{13}C labelling

[1,2- $^{13}\text{C}_2$] acetate One of the most useful applications in ^{13}C labelling, is to trace the mode of incorporation of intact acetate units into a wide range of metabolites. This has been one of the major developments in biosynthetic methodology and permits information to be obtained which would have been impossible or at best extremely difficult to obtain without isotopic labelling.

The basic concept can be explained using a model polyketide system (Fig. 30). A molecule of acetate in which both carbons are entirely ^{13}C contains two adjacent nuclei of spin 1/2 and so they will couple to each other. If this acetate molecule is incorporated intact into a metabolite then, in any individual molecule, those pairs of carbons derived from an originally intact acetate unit must necessarily both be enriched simultaneously and so will show a mutual ^{13}C - ^{13}C coupling. Thus, if C-1 is enriched, then C-2 must also be enriched. In the resultant ^{13}C NMR spectrum, the natural abundance signal is flanked by ^{13}C - ^{13}C coupling satellites (Fig. 30b). By analysing the coupling patterns, information is obtained on the way in which the precursor molecules are assembled by the enzyme and on the way the polyketide chain folds up prior to condensation and cyclisation. If at any stage in the biosynthesis the bond between two carbons originally derived from an intact acetate unit is broken, then the ^{13}C - ^{13}C coupling is lost and these carbons appear simply as enhanced singlets, as shown for C-3 and C-4 in Fig. 30c. In this way bond cleavage and rearrangement processes occurring during biosynthesis can be detected.

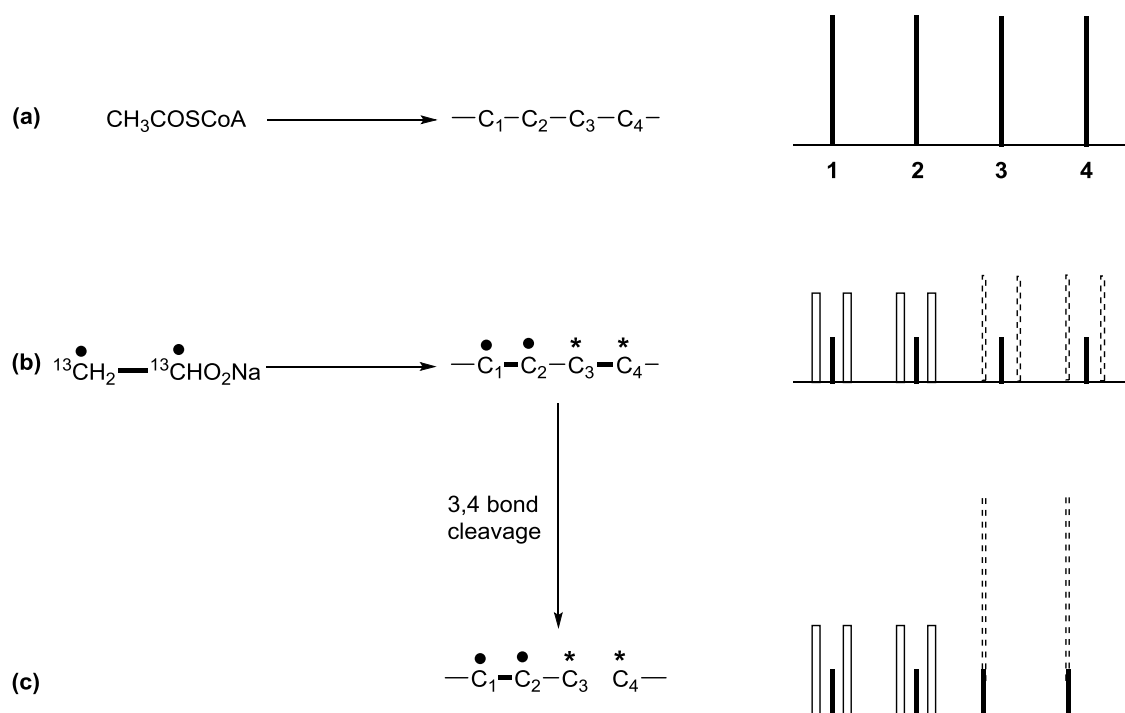
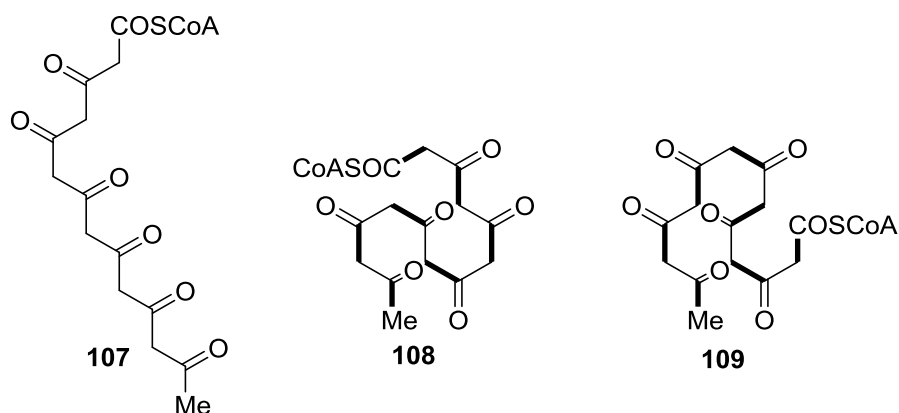


 **Figure 30a–c** - Figure adapted from Simpson et al.⁶ Simulated proton decoupled ^{13}C NMR spectra of a polyketide-derived moiety: **a** at natural abundance; **b** enriched from $[1, 2-^{13}\text{C}_2]$ acetate; **c** after cleavage or rearrangement of an originally intact acetate unit.

Incorporation of $[1, 2-^{13}\text{C}_2]$ acetate is especially useful in distinguishing among alternative foldings of linear polyketide or terpenoid precursors prior to cyclisation and subsequent modifications. For example, from the three possible foldings of the heptaketide precursor of herqueichrysin (**110**), a phenalenone metabolite of *Penicillium herquei*, only one folding is possible.



The specific folding shown below was unambiguously established from the observed ^{13}C - ^{13}C couplings in the ^{13}C NMR spectrum of the enriched metabolite (Fig. 31).⁶

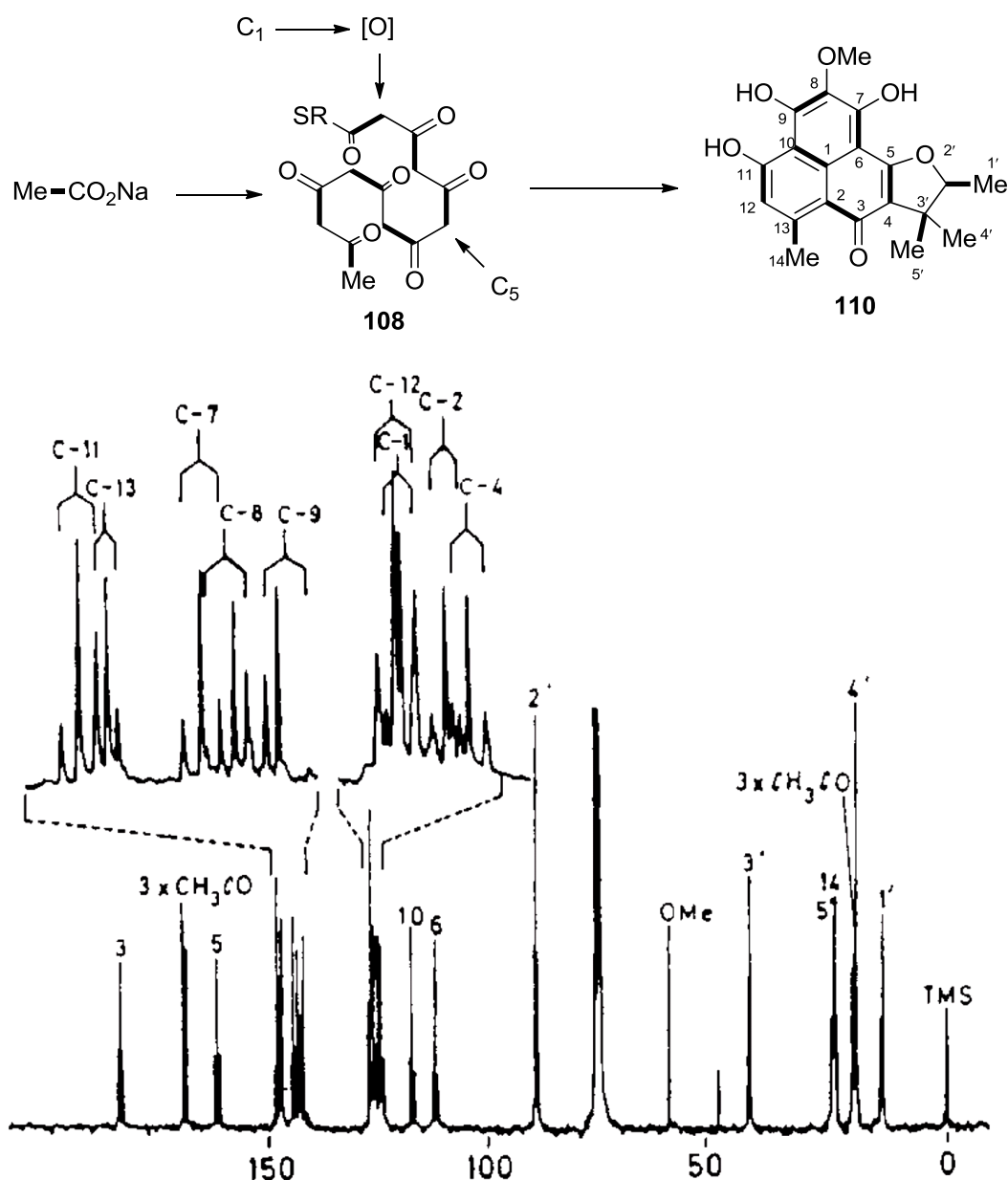


Figure 31 – Figure adapted from Simpson et al.⁶ ^{13}C NMR spectrum of [1, 2- $^{13}\text{C}_2$]acetate enriched herqueichrysin (as its triacetate) determined at 67.89 MHz. Note the severe overlap of the coupled ^{13}C signals in the aromatic region and the second-order ^{13}C - ^{13}C couplings arising from the similarity of the chemical shifts of C-8 and C-9.

Despite their enormous structural diversity, polyketide metabolites are related by their common derivation from highly functionalised carbon chains whose assemblies are controlled by multifunctional enzyme complexes, the polyketide synthases (PKSs) which, like the closely related fatty acid synthases, catalyse repetitious sequences of decarboxylative condensation reactions between

simple acyl thioesters and malonate, as shown in Fig. 32.⁸⁰ Each condensation is followed by a cycle of modifying reactions: ketoreduction, dehydration and enoyl reduction. In contrast to fatty acid biosynthesis where the full cycle of essentially reductive modifications normally follow each condensation reduction, the PKSs can use this sequence in a highly selective and controlled manner to assemble polyketide intermediates with an enormous number of permutations of functionality along the chain. As shown in Fig. 32, the reduction sequence can be largely or entirely omitted to produce the classical polyketide intermediate which bears a carbonyl on every alternate carbon and which normally cyclises to aromatic polyketide metabolites. On the other hand, the reductive sequence can be used fully or partially after each condensation to produce highly functionalised intermediates such as the “reduced polyketide” in Fig. 32.

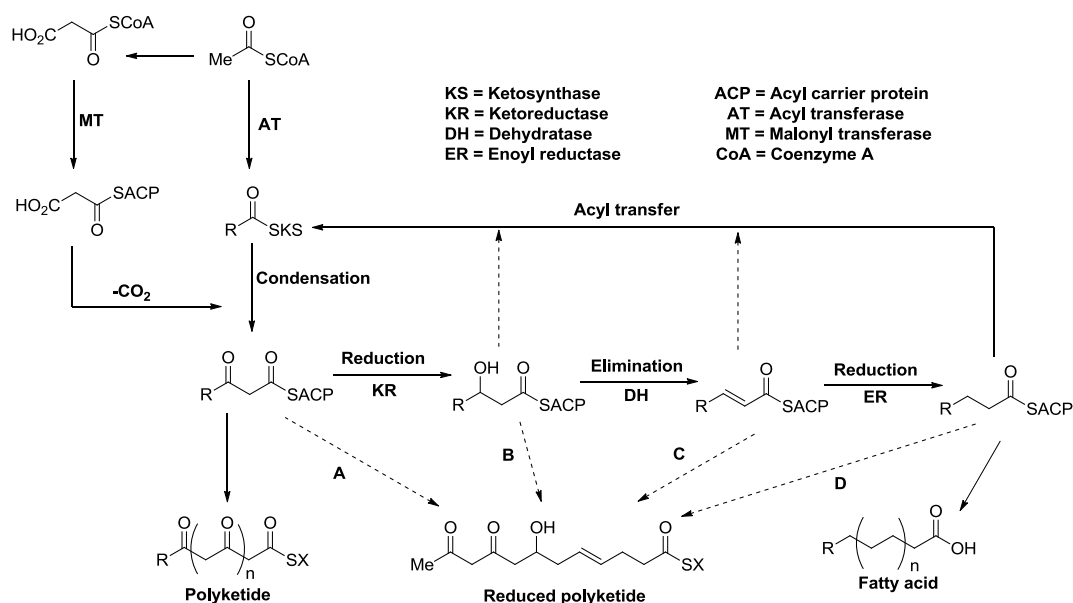


Figure 32 - The assembly of fatty acids, polyketides and reduced polyketides. The “reduced polyketide” intermediate would be formed from an acetate starter by five successive condensation cycles. The first two cycles are condensations and are followed by condensation-ketoreduction, condensation-ketoreduction-elimination, and finally a full condensation-ketoreduction-elimination-enoil reduction cycle. Thus the overall reaction sequence is A, A, AB, ABC, ABCD.

Much of the current understanding of the polyketide metabolites formed via these highly reduced intermediates has come from studies using ²H and ¹⁸O labelled precursors in conjunction with detailed ¹³C and ²H NMR analysis of the enriched metabolites. ²H NMR, despite several inherent disadvantages, has been the nucleus of choice in many biosynthetic studies. Its major limitations

are mainly as a consequence of the low magnetogyric ratio and the relaxation behaviour of the ^2H nucleus. Because it is a quadrupole nucleus (spin 1) and thus very efficiently relaxed, the spectral lines are rather broad and this, coupled with the low magnetogyric constant and the small chemical shift range for hydrogen nuclei, often results in poorly resolved spectra. However, the rapid relaxation and lack of any n.O.e. mean that accurate integration of ^2H NMR spectra is possible so that the relative enrichment at different sites in a metabolite can be accurately assessed. Another major advantage is that as a consequence of its low natural abundance (0.012%), much greater dilutions are tolerable than in the case of ^{13}C -labelling: a 100% ^2H -labelled precursor may be diluted 6000-fold and still result in a doubling of intensity over the corresponding natural abundance signal. This makes ^2H -labelling particularly suitable for studying the incorporation of advanced intermediates on a biosynthetic pathway. The inherent lack of resolution in ^2H NMR can be overcome by the use of isotope-induced shifts in ^{13}C NMR. The use of ^{13}C as a "reporter" nucleus for both hydrogen and oxygen represents one of the great advances in biosynthetic studies with stable isotopes and makes use of the observation that substitution of a proton *alpha* or *beta* to a ^{13}C by deuterium causes a change (usually upfield) in the ^{13}C chemical shift. Similarly, the presence of ^{18}O *alpha* to a ^{13}C atom can be detected by an upfield shift in the ^{13}C NMR spectrum. These effects are summarised in Fig. 33. When the deuterium label is directly attached to a ^{13}C nucleus in the precursor molecule, the proton-noise-decoupled (p.n.d.) ^{13}C NMR spectrum of the enriched metabolite shows, for carbons which have retained deuterium label, a series of signals upfield of the normal resonance. The presence of each deuterium shifts the centre of the resonance by 0.3 - 0.6 ppm and spin-spin coupling ($1J_{\text{CD}}$) produces a characteristic multiplet; hence CD appears (Fig. 33a) as a triplet, whereas CD_2 and CD_3 would give respectively a quintet and septet. Shifted signals arising from carbons which bear no hydrogen suffer reduced signal-to-noise ratio caused by poor relaxation and lack of n.O.e. enhancement, a disadvantage of the method which is compounded by the multiplicities due to coupling. Deuterium decoupling can assist in this by removing the ^{13}C - ^2H coupling (see Fig. 33 below). However, information not obtainable by direct ^2H NMR spectroscopy, such as the distribution of label as CH_2D , CHD_2 and CD_3 and the integrity of carbon-hydrogen bonds during biosynthesis, may be gained. Many of the problems

associated with directly attached deuterium are avoided by placing the deuterium label two bonds away from the ^{13}C reporter nucleus. The isotope shift, although reduced, is still observable, and as β -hydrogens only contribute markedly to the relaxation of non-protonated ^{13}C nuclei, the shifted signals otherwise retain any n.O.e. also experienced by the unshifted signals on proton decoupling. As geminal carbon-proton coupling constants are generally small, and carbon-deuterium couplings are over six times smaller again, the shifted signals are effectively singlets (Fig. 33b), even without deuterium decoupling, and this gives a further increase in the signal to noise ratio compared with the corresponding α -shift experiment. However, neither of these methods provides reliable information on the stereospecificity of deuterium labelling. Although ^2H NMR spectra are disadvantaged by their inherently low dispersion and broad lines, they have the advantage of providing information on the stereospecificity as well as regiospecificity of labelling. ^2H NMR, however, does not prove the number of deuteriums incorporated. The biosynthetic incorporation of ^{18}O can also be detected by the observation of ^{18}O isotope induced shifts in the ^{13}C NMR spectrum, as shown in Fig. 33c,d. The ^{18}O may be conveniently introduced via a doubly labelled precursor or by growth in an $^{18}\text{O}_2$ atmosphere. The resulting shifts are generally not much larger than 0.05 ppm. These are very small effects, the same general size as β - ^2H isotope shifts and are only readily observed with high field spectrometers. As shown in Fig. 33 there are two classes of isotope shifts:

1. Primary (α) – the change in chemical shift of an atom when its isotope is changed, for example, the ^1H chemical shift versus the ^2D chemical shift.
2. Secondary (β)– the change in chemical shift of an atom when the isotope of one of the neighboring atoms is changed, for example, the ^{13}C chemical shift difference between CH_3OH and CH_3OD .

These techniques for elucidation of the origins of hydrogen and oxygen provided the basis for much of the work described below.

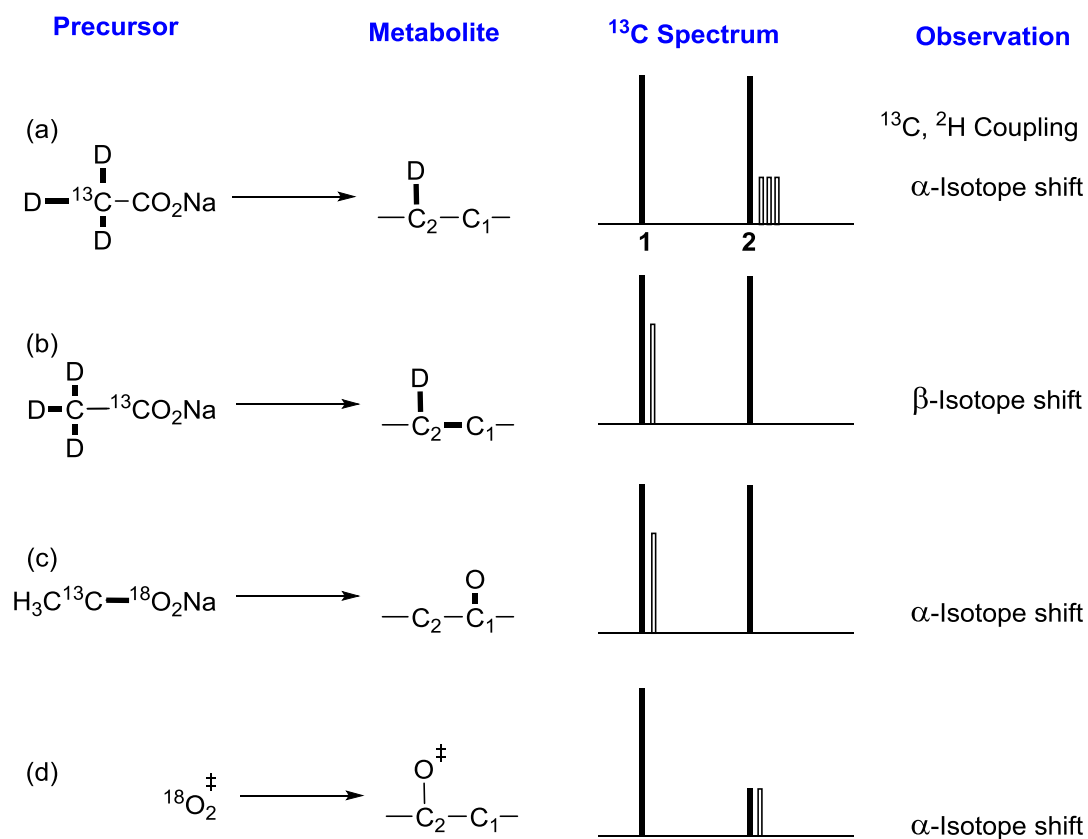


Fig. 33a–d - Simulated proton noise decoupled ^{13}C NMR spectra of a polyketide-derived moiety from: **a** [2- ^{13}C , 2- $^2\text{H}_3$]acetate; **b** [1- ^{13}C , 2- $^2\text{H}_3$]acetate; **c** [1- ^{13}C , $^{18}\text{O}_2$]acetate; **d** $^{18}\text{O}_2$ gas.

Colletodiol (**116**), a macrodiolide containing a 14-membered ring, was originally isolated from the plant pathogen *Colletotrichum capsici* along with a number of related macrodiolides including colletoketol (**117**), which was subsequently isolated (as grahamimycin A) from culture filtrates of *Cytospora* sp. ATCC 20502. Incorporation of ^{13}C -labelled acetates in *C. capsici* established that colletodiol was polyketide-derived and is formed via C_6 and C_8 hydroxyacids of tri- and tetra-ketide origins, respectively, as shown in Scheme 30. Depending on the exact structures of the intermediates, a number of mechanisms can be proposed for the formation of the lactone and 1,2-diol moieties in colletodiol. The origins of all the oxygen and hydrogen atoms have been elucidated by incorporation of [1- ^{13}C , $^2\text{H}_3$]- and [1- ^{13}C , $^{18}\text{O}_2$]acetates and $^{18}\text{O}_2$ gas by cultures of *Cytospora*. The labelling pattern in colletodiol is summarised in Fig. 34. Interestingly, no ^2H isotope-induced shifts could be observed for C-2 or C-8 in the ^{13}C NMR spectrum of the [1- ^{13}C , $^2\text{H}_3$]acetate-enriched colletodiol. It is known

that carbonyl carbons can be poor “reporter” atoms for β - ^2H shifts and the presence of ^2H label was shown by direct ^2H NMR analysis of the enriched metabolite. The level of ^2H incorporation is essentially uniform at all the enriched positions except for C-10 where a very low level was observed. From these results it can be concluded that the lactone ring formation occurs by an acyl substitution mechanism, as shown in Fig. 34 from the thioester intermediates (**112**) and (**113**) to give the macrocyclic triene (**114**). Examination of models suggested that the triene (**114**) would adopt a conformation similar to that observed for colletodiol and in this conformation epoxidation should occur from the more accessible $10R_e$, $11R_e$ face of the Z -alkene to give the $10S,11R$ epoxide (**115**) which on hydrolysis would give colletodiol with the correct $10R,11R$ stereochemistry and the observed origins of the hydroxyl oxygens.

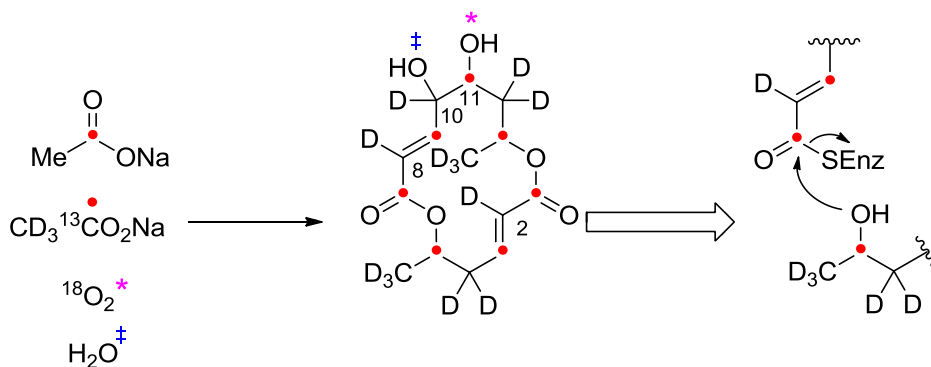
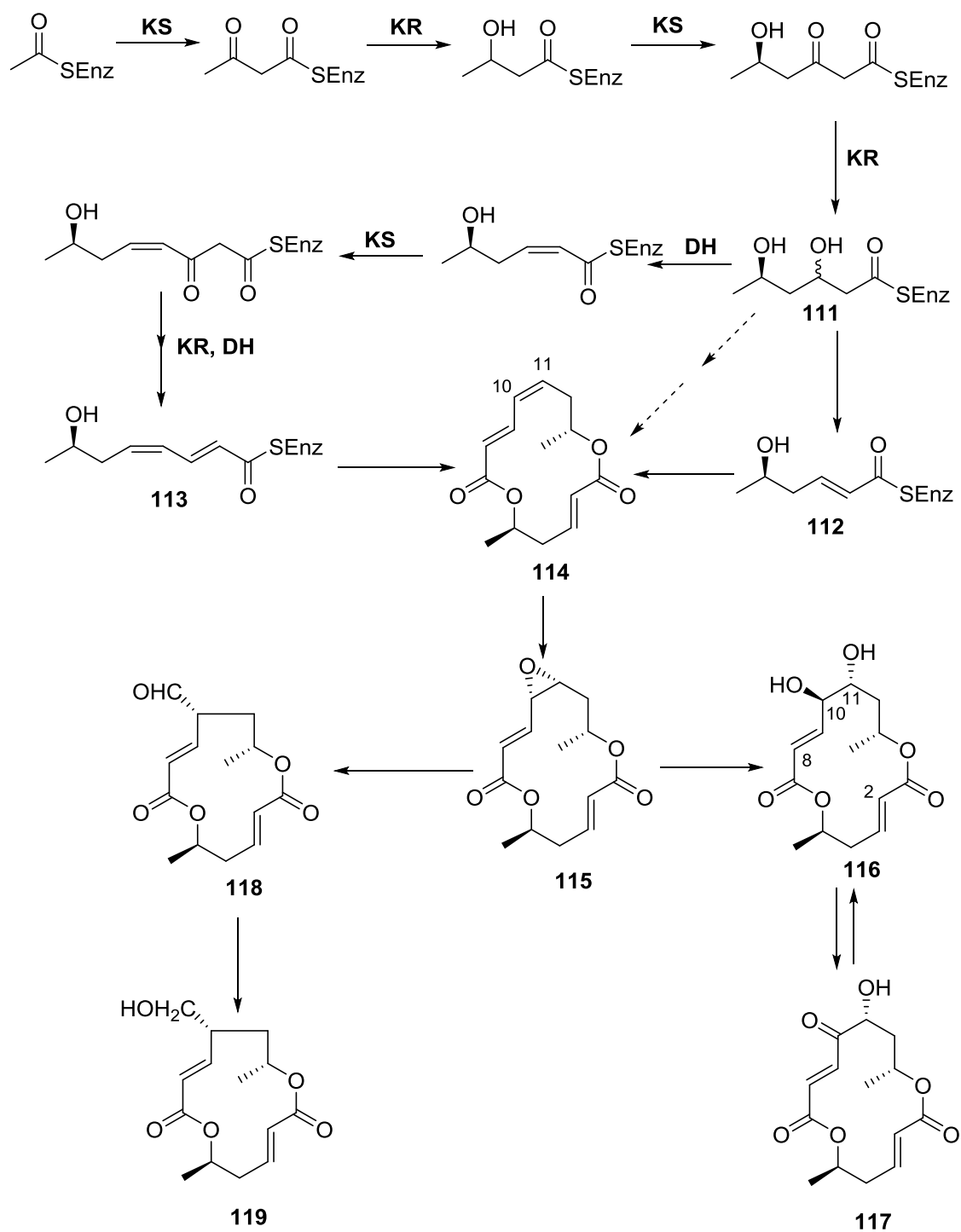
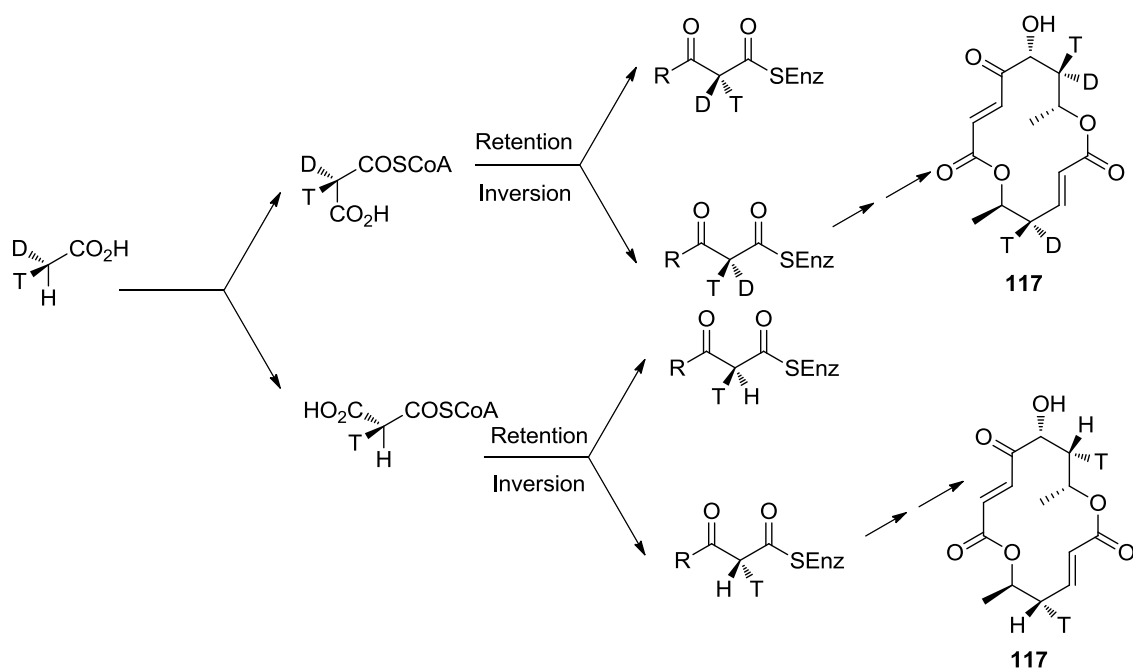


Fig. 34. Incorporation of $[1\text{-}^{13}\text{C}, ^{18}\text{O}_2]$ -, $[1\text{-}^{13}\text{C}, 2\text{-}^2\text{H}_3]$ acetates and $^{18}\text{O}_2$ into colletodiol and an acyl substitution mechanism for macrolactonisation.



Scheme 30

As indicated in Scheme 31 for the (*R*)-acetate, assuming that carboxylation to malonate proceeds with retention of configuration, there are four possible tritiated products from the condensation step. Thus, on subsequent incorporation into the 4- and 12-methylene groups of colletoketol (**117**) all positions where the stereospecific assignments of the diastereotopic hydrogens have been made, the stereochemical outcome can be deduced once it is known which of the prochiral hydrogens is incorporated along with ^2H and which is incorporated along with ^1H . This should be apparent from analysis of the p.n.d. ^3H NMR spectrum in which one ^3H signal should be broadened by coupling to ^2H . The results for incorporation of (*R*)-acetate into colletoketol in *Cytospora* sp ATCC 20502 are shown in Fig. 35. ^3H Label is incorporated most effectively into the methyl positions, but there is significant incorporation into all four methylene hydrogens. Interestingly, there is no observable incorporation into the 2- or 8-alkene positions, in contrast to the results when [$^2\text{H}_3$]acetate is fed. This is difficult to rationalise, but it may be due to a “pool” effect, with the small amount of labelled acetate used in the experiment being entirely consumed by the PKS for the first two condensations, with unlabelled endogenous acetate being used for subsequent condensations. Close examination of the spectrum reveals a sharp singlet at δ 2.54, indicating ^3H label at the 4-pro-*S* position with protium adjacent and a broader signal at δ 2.35, indicating ^3H at the 4-pro-*R* position with deuterium adjacent. This is consistent with inversion of configuration. The results for the 12-methylene group is less clear as both the pro-*R* and pro-*S* hydrogen at δ 2.14 and 1.85 appear as sharp singlets.



Scheme 31

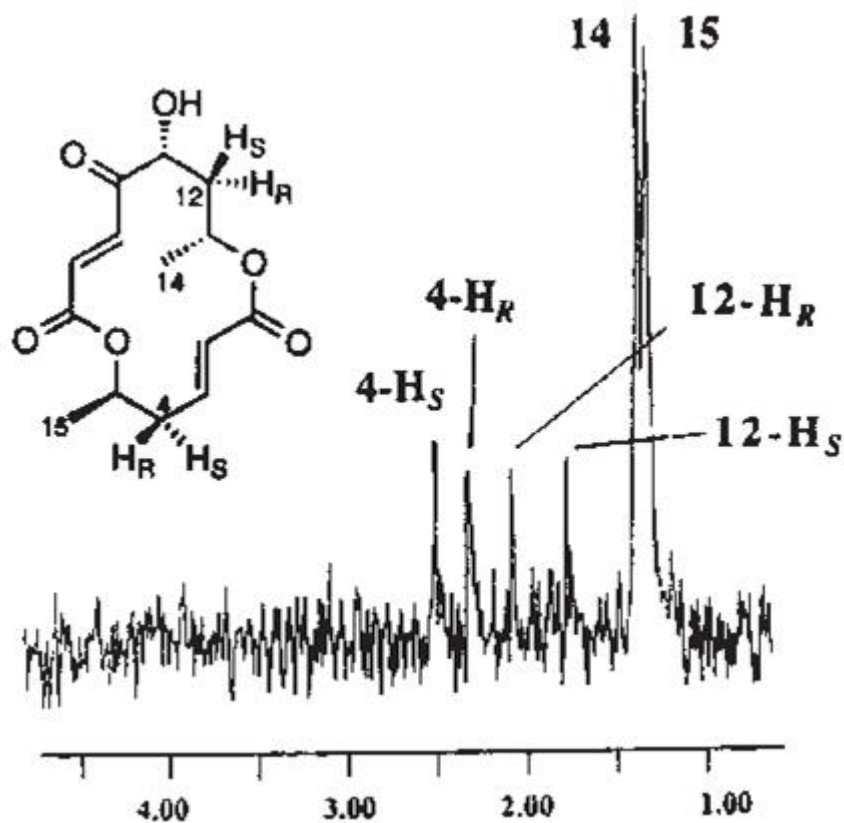


Figure 35 - Figure adapted from Simpson et al.⁶ 533 MHz ^3H NMR spectrum of collettiketol (**117**) enriched from feeding sodium (*R*)-[^3H , ^2H , ^1H]acetate (50 mCi, 36 mCi mmol $^{-1}$) to

2.3 Conclusion

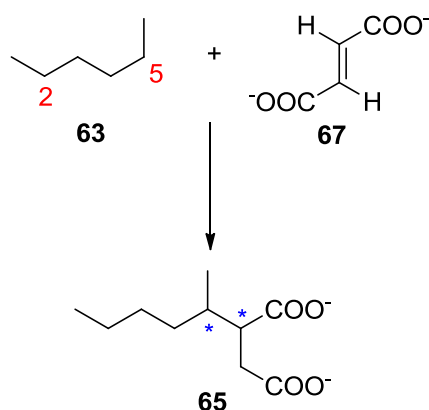
Based on the examples given it is clear that the application of stable isotope labelling methodologies has made a major impact on the elucidation of biosynthetic and metabolic studies in a wide range of systems. As biosynthetic work becomes increasingly focused on studies at the enzymatic level, there will be continued scope for the further development of these applications particularly making use of sensitive mass spectral detection methods rather than the NMR methods which have dominated whole cell studies. These techniques will therefore will be used as the basis for study in Chapter 3.

Chapter 3

Synthesis of Deuterated Substrates for Anaerobic Cultivation with Strain HxN1

3.1 DEUTERATED HEXANES

As mentioned in the introduction, oxidation of *n*-hexane occurs at the C-2 or C-5 position (Scheme 32) forming (1-methylpentyl)succinate (MPS), which possess two chiral centres and exist as four stereoisomers.



Scheme 32 – Asterisks (*) indicate stereogenic centres.

Therefore to examine the formation of MPS in more detail and in order to establish the stereochemistry of the initial hydrogen atom abstraction step, *n*-hexanes stereospecifically deuterated at the C-2 and C-5 position were required (Fig. 36).

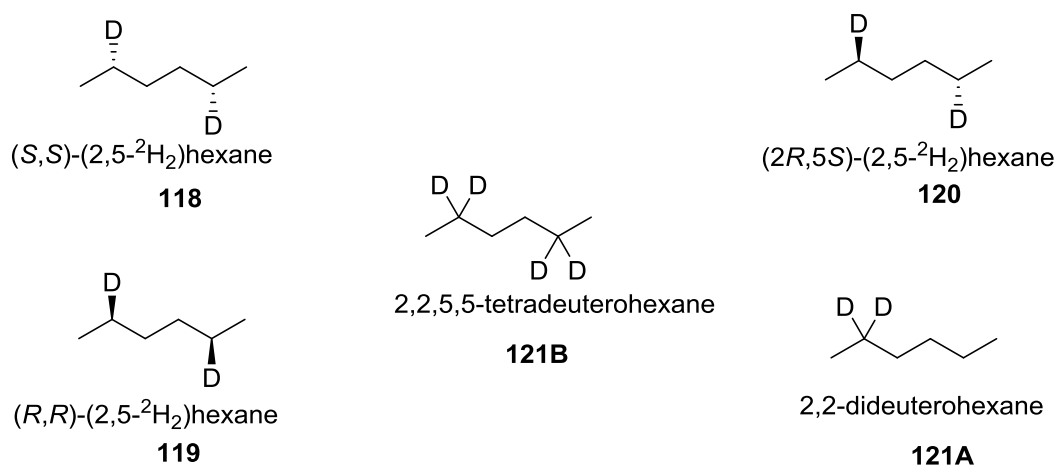
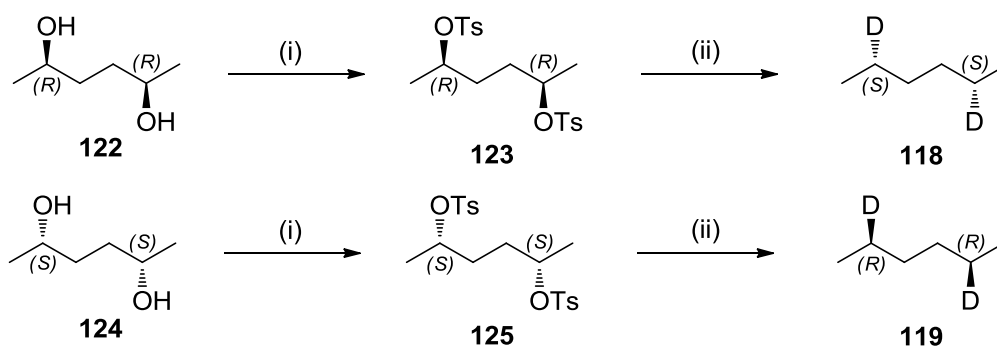


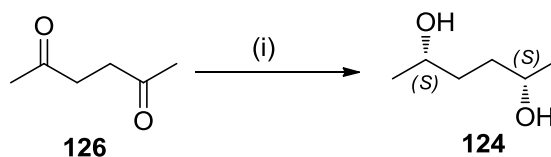
Figure 36 – Target deuterated hexanes.

For this purpose, a strategy for the synthesis of (*R,R*)- and (*S,S*)-(2,5-²H₂)hexane from (*S,S*)- and (*R,R*)-hexane-2,5-diol respectively was developed (Scheme 33).



Scheme 33 - Synthesis of (*R,R*)- (**119**) and (*S,S*)-*n*-(2,5-²H₂)hexane (**118**). (i) *p*-toluenesulfonyl chloride, pyridine in dichloromethane, 0 °C, 72 h; (Ts = *p*-toluenesulfonyl); (ii) LiAlH₄, tetraglyme, 120 °C, 2 h.

(*S,S*)- (**124**) and (*R,R*)-hexane-2,5-diol (**122**) were commercially available. However, in order to reduce costs, (*S,S*)-hexane-2,5-diol was synthesised inexpensively by reducing hexane-2,5-dione (**126**) with baker's yeast (Scheme 33).⁸¹



Scheme 34 – Synthesis of (*S,S*)-hexane-2,5-diol (**124**). (i) Baker's yeast, sucrose, water, RT, 72 h.

Baker's yeast was added to a solution of sucrose in water, followed by addition of the commercially available diketone **126**. Reduction of the diketone **126** yielded optically active diol **124**, which was isolated in 60% yield and 99% ee (from comparison of optical rotation with literature⁸¹). The enantiomeric purity of diol **124** is due to presence of alcohol dehydrogenase enzymes in the baker's yeast, which carry out the reduction of the ketone stereospecifically (Fig. 37).

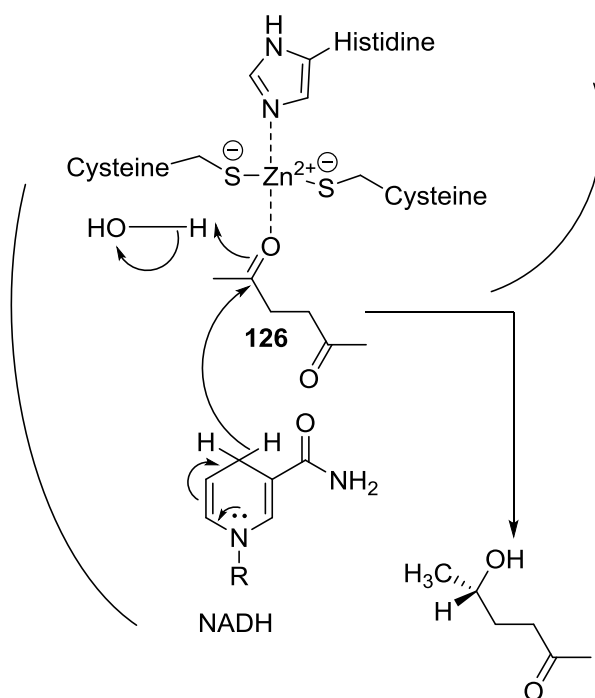


Figure 37 – Typical alcohol dehydrogenase active site.

The transfer of hydride by reduced nicotinamide adenine dinucleotide NADH is driven by the restoration of aromaticity to the pyridinium ring within the product molecule NAD⁺; the enantiospecificity of this reaction becomes apparent as hydride can only be added to the face of the carbonyl ‘recognised’ by the enzyme as the substrate.

Tosylation of the diols **122** and **124** was achieved using *p*-toluenesulfonyl chloride and pyridine as base dissolved in DCM. The crude products were in full recrystallised to afford the pure ditosylates **123** and **125** respectively.⁸¹ ¹³C and ¹H NMR spectra of both enantiomers was identical (See Fig. 38 for the ¹H and ¹³C NMR spectra of (2*R*,5*R*)-hexane-2,5-diol di-*p*-toluenesulfonate). However they did confirm that the corresponding diastereomer (**128**) was not formed, since the ¹³C NMR did not contain double peaks. The absolute configuration of the tosylates was confirmed by X-ray crystallography (Fig. 39 & 40).

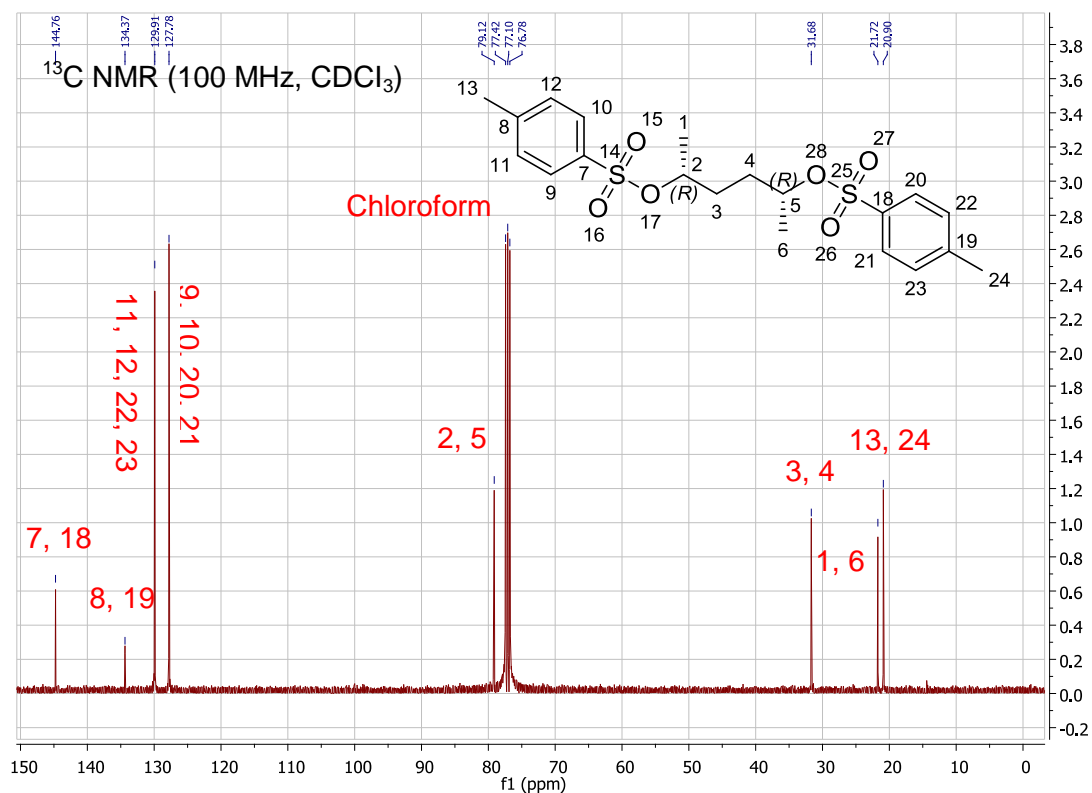
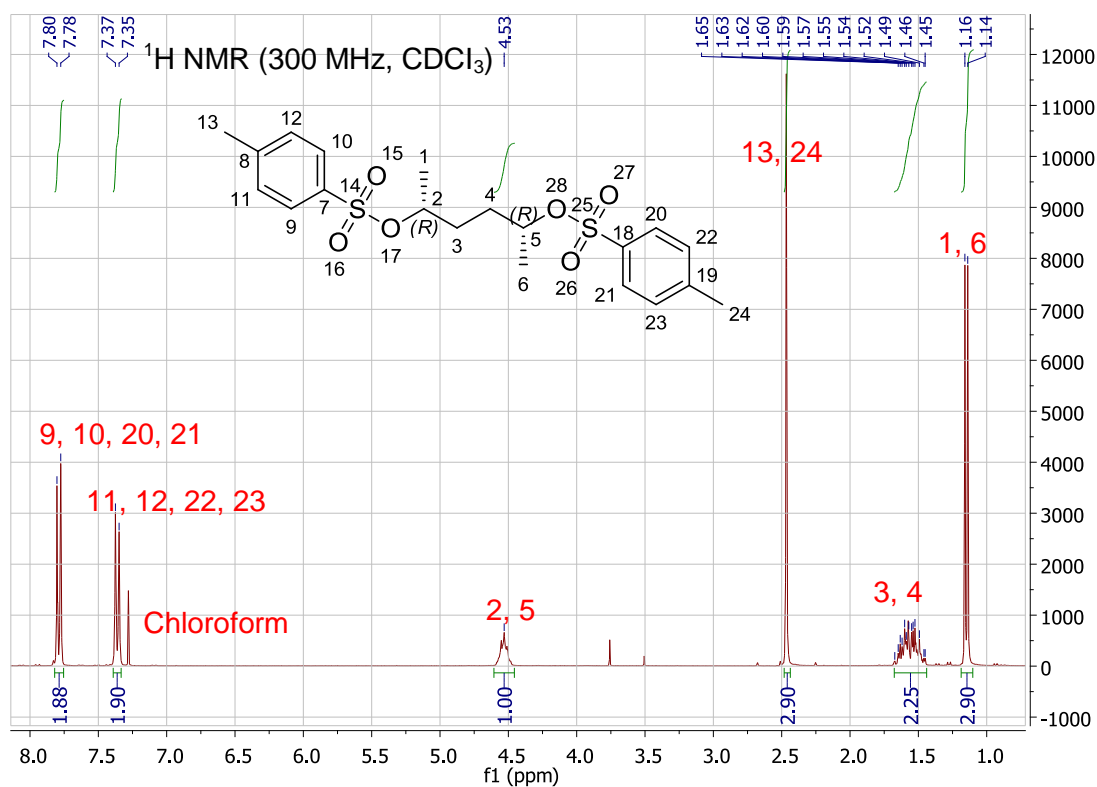
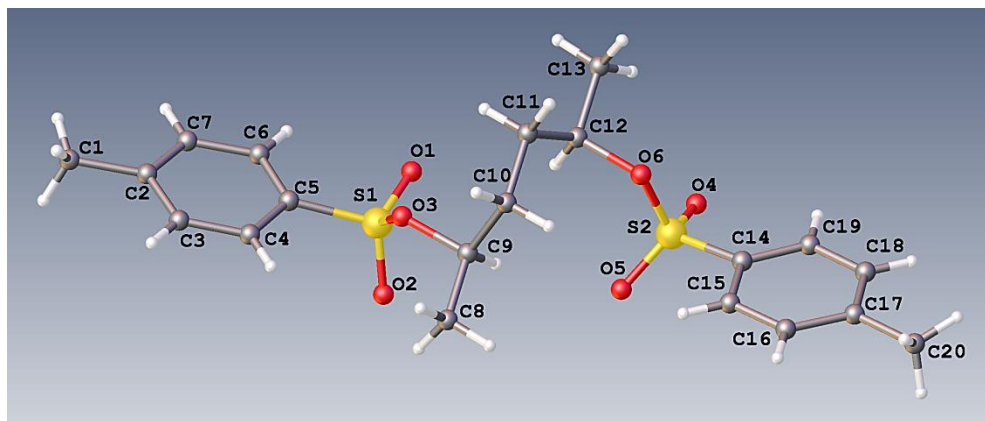
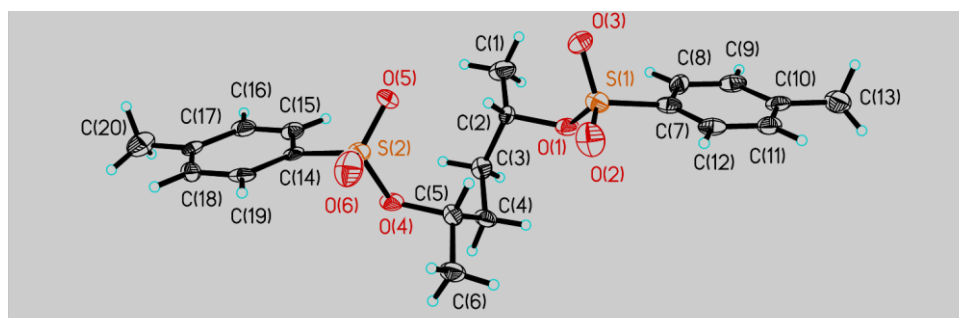


Figure 38 - ¹H and ¹³C NMR spectra of (2*R*,5*R*)-hexane-2,5-diol di-*p*-toluenesulfonate. The (2*S*,5*S*)- isomer had identical NMR spectra. The numbers in red match the peaks with their corresponding atoms.

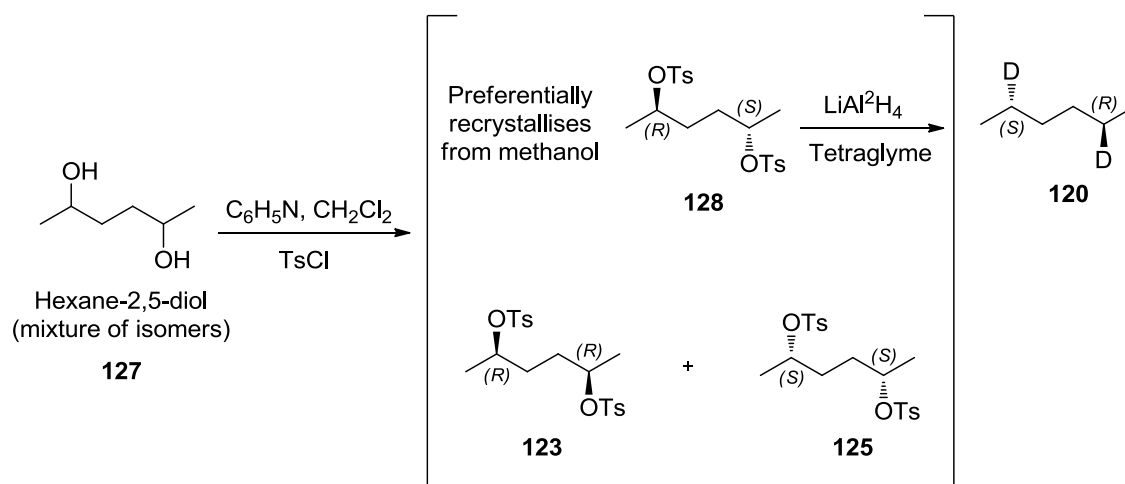


✚ **Figure 39** – (2*R*,5*R*)-Hexane-2,5-diol di-*p*-toluenesulfonate (**123**)



✚ **Figure 40** – (2*S*,5*S*)-Hexane-2,5-diol di-*p*-toluenesulfonate (**125**)

An interesting observation was made during the tosylation of the commercially available hexane-2,5-diol (mixture of isomers) **127** (Scheme 35), which resulted in isomeric mixture of ditosylates (**123**, **125** & **128**). However after recrystallisation, the ^{13}C NMR data (Fig. 41) indicated that only one of the diastereomers had been crystallised due to the fact that each carbon corresponded to a single peak. X-ray crystallography (Fig. 42) confirmed this tosylate to be the (2*R*,5*S*)-hexane-2,5-diol di-*p*-toluenesulfonate (**128**).



Scheme 35 – Synthesis of (2*R*,5*S*)-hexane-2,5-diol di-*p*-toluenesulfonate.

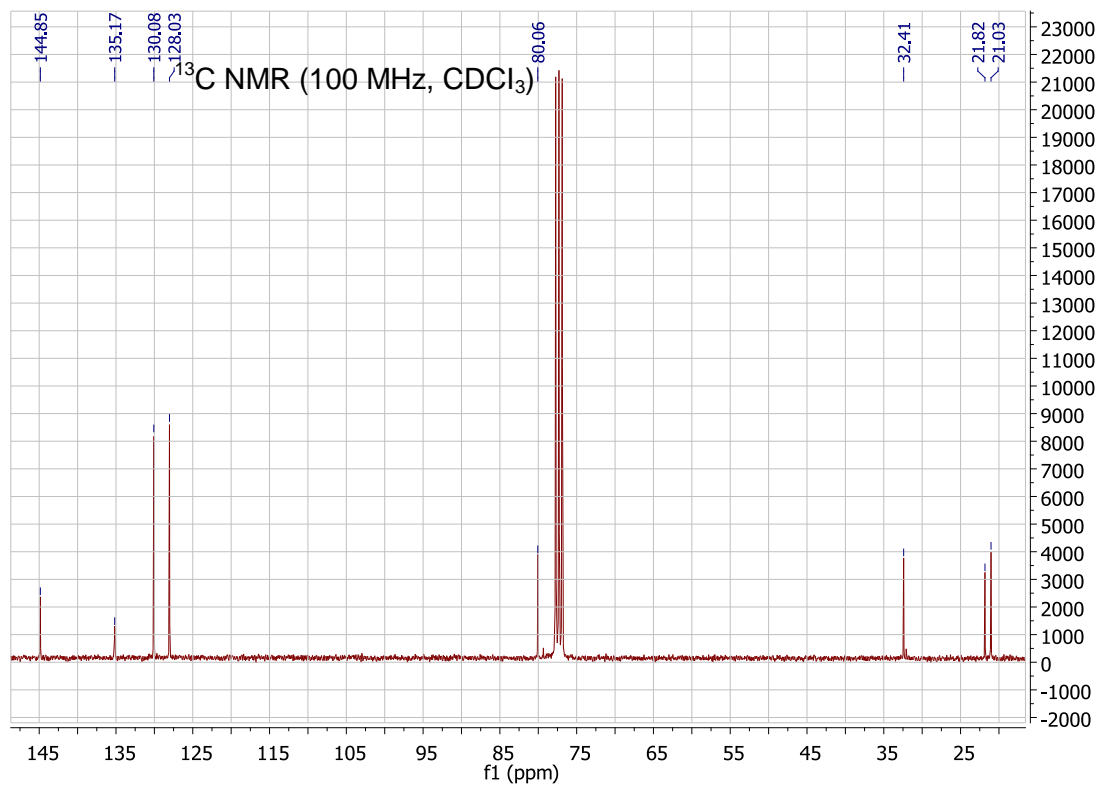
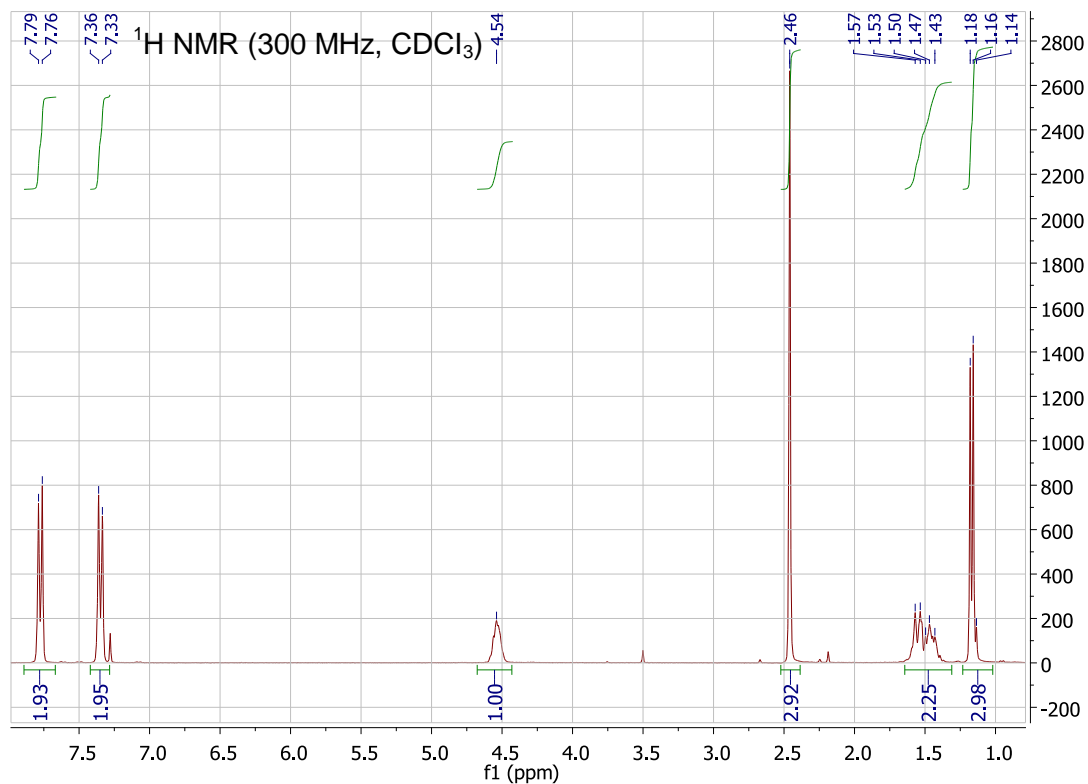


Figure 41 - ¹H and ¹³C NMR of (2*R*,5*S*)-hexane-2,5-diol di-*p*-toluenesulfonate (**128**).

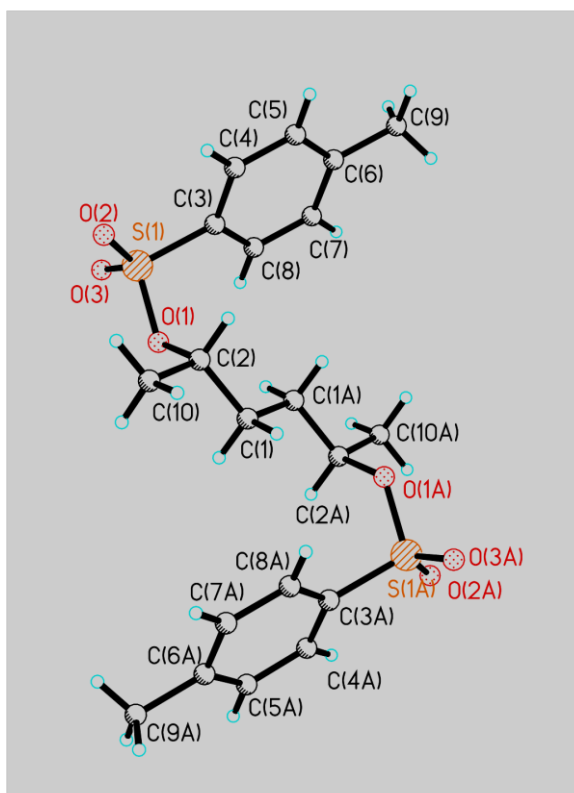
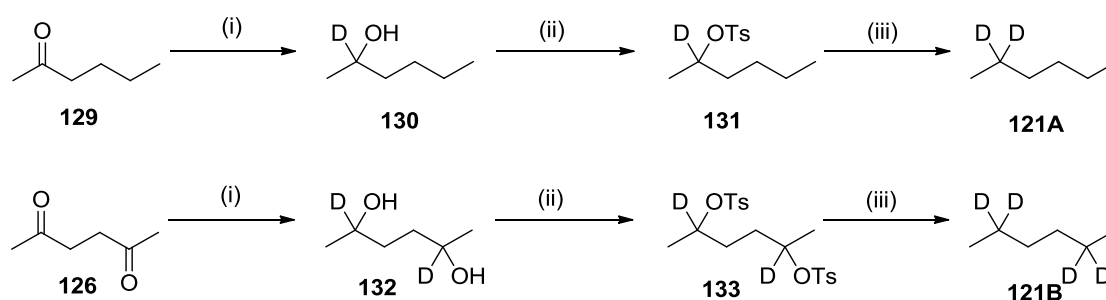


Figure 42 – (2*R*,5*S*)-Hexane-2,5-diol di-*p*-toluenesulfonate (**128**)

Hexan-2-one was reduced with sodium tetradeuteroborohydride in ethanol to afford 2-deuteriohexan-2-ol **129**, which was characterised by ^1H and ^{13}C NMR. Within the limits of detection these spectra showed complete deuteration at C-2. Thus, the resonance at δ 4.0 in the ^1H NMR of hexan-2-ol was completely absent from the spectrum of 2-deuteriohexan-2-ol **130** (Fig. 43). Alcohol **130** was converted into tosylate **131** in the standard way. The tosylate showed lack of a resonance at δ 4.5 confirming the presence of deuterium at C-2 (Fig. 44). Finally, the tosylate was reduced by lithium aluminium deuteride in tetraglyme to give 2,2-dideuteriohexane **121A** (80% yield), which was characterised by EIMS, ^1H , ^2H and ^{13}C NMR.



Scheme 36 – Synthesis of 2,2-dideuteriohexane (**121A**) and 2,2,5,5-tetradeuteriohexane (**121B**). (i) NaB^2H_4 , THF, 60 °C, 3 h; (ii) *p*-Toluenesulfonyl chloride, pyridine in dichloromethane, 0 °C, 72 h; (iii) LiAl^2H_4 , tetraglyme, 120 °C, 2 h.

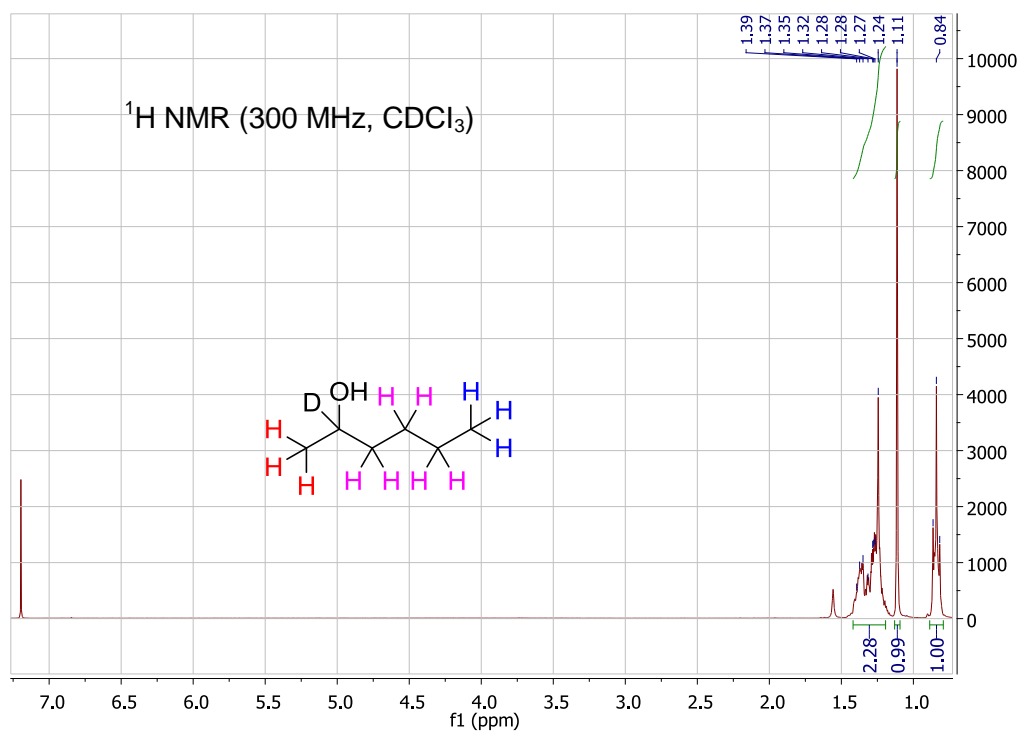


Figure 43 – ¹H NMR of 2-deuteriohexan-2-ol (130).

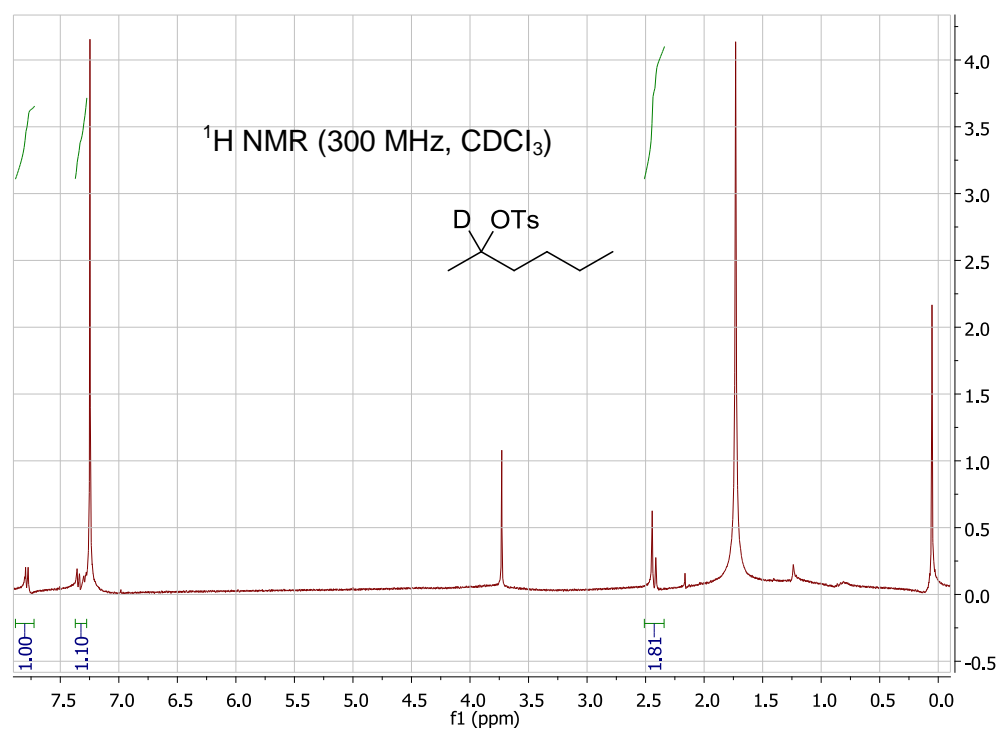


Figure 44 – ¹H NMR of rac-(2-²H)-hexan-2-ol *p*-toluenesulfonate (131),

2,2,5,5-tetradeuterohexane (121B) was prepared following a similar procedure from diketone 126 (See Fig. 45).

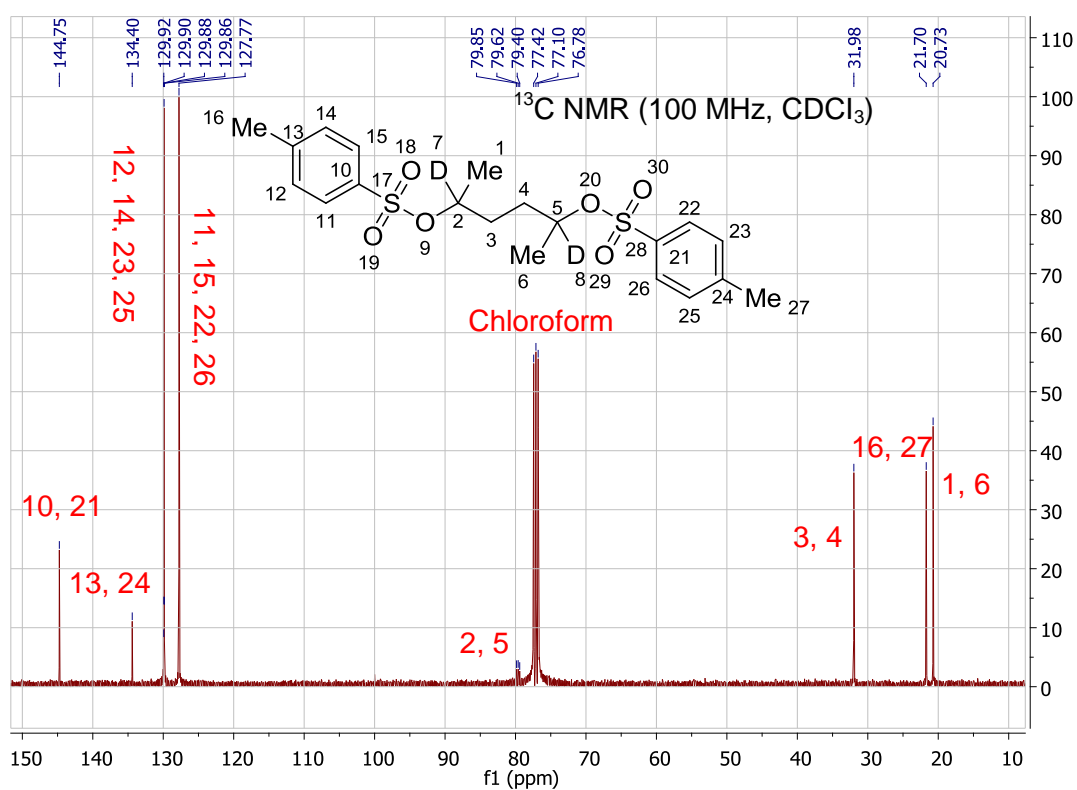
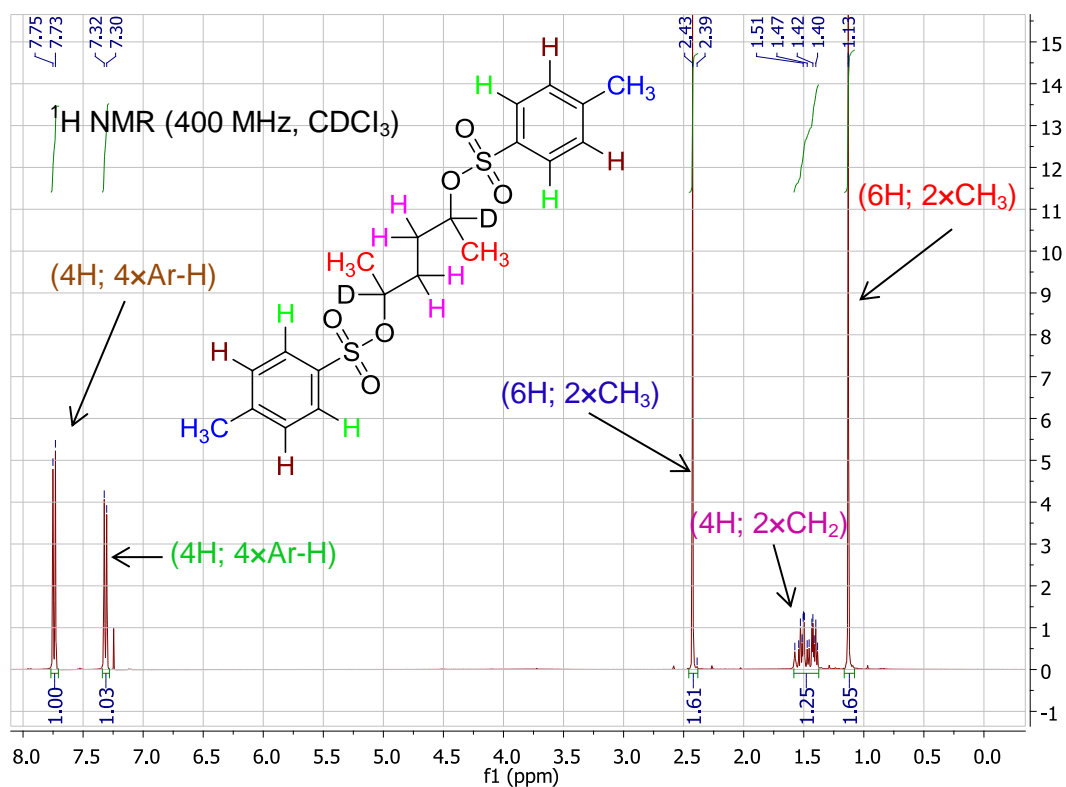


Figure 45 - ¹H and ¹³C NMR of deuterated tosylate 133. *The triplet at δ 79.6 in ¹³C-NMR confirms the presence of CHD group.

The last step of the synthesis involved the use of tetraglyme (tetraethyleneglycol dimethyl ether) (**134**), a high boiling solvent (bp 275 °C), to facilitate (using direct distillation) the isolation of the labelled hexane following reduction of an intermediate tosylate by lithium aluminum deuteride.

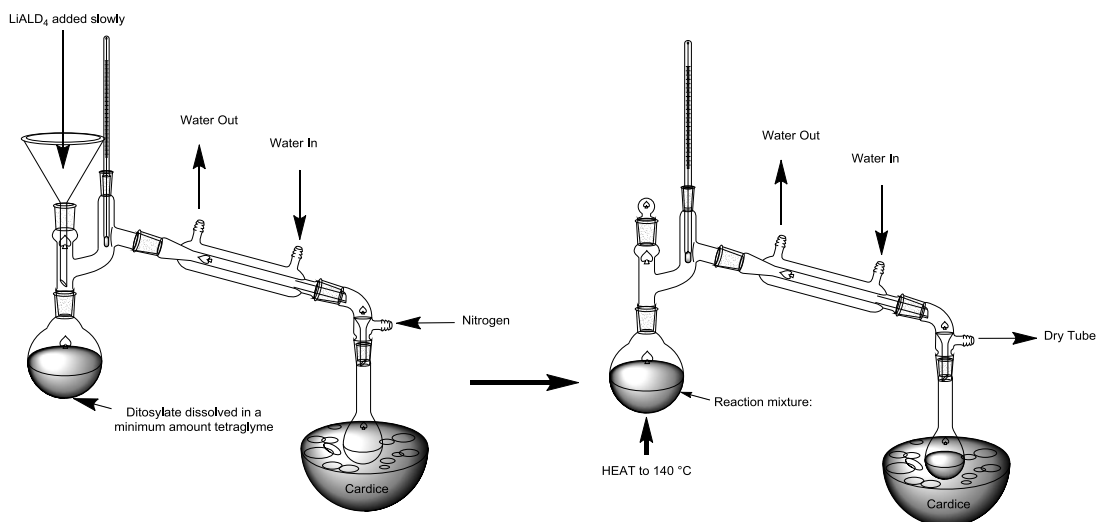
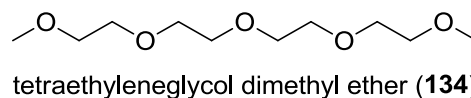


Figure 46 – Isolation of the labelled hexane by direct distillation.

The synthesised tosylates were dissolved in a minimum amount of tetraglyme in a flask attached to a distillation system, which was connected to a nitrogen line. Lithium aluminium deuteride (2 equiv.) was added at room temperature (0 °C for large-scale). The nitrogen line was removed and replaced with a drying tube. The reaction flask was heated up to 140°C and the dideuterated hexanes were collected in the flask placed in dry ice in 75 – 85% (Fig. 46). Due to the low boiling point of hexane (69°C), the afforded products were then transferred into an ampoule and sealed using a heat gun in order to minimise the loss of product due to evaporation.

3.1.1 Confirmation of deuteration

The complete deuteration of the hexanes was confirmed by ^1H -, ^2H - and ^{13}C -spectroscopy (Fig. 47-53). The ^1H NMR of **120** (Fig. 48) indicate that the ratio of terminal hydrogens to non-terminal hydrogens is 1:1, in contrast to the ratio of hydrogens in non-deuterated n-hexane (Fig. 47) which is 6:8. ^2H -NMR spectroscopy was also performed to confirm the deuteration.

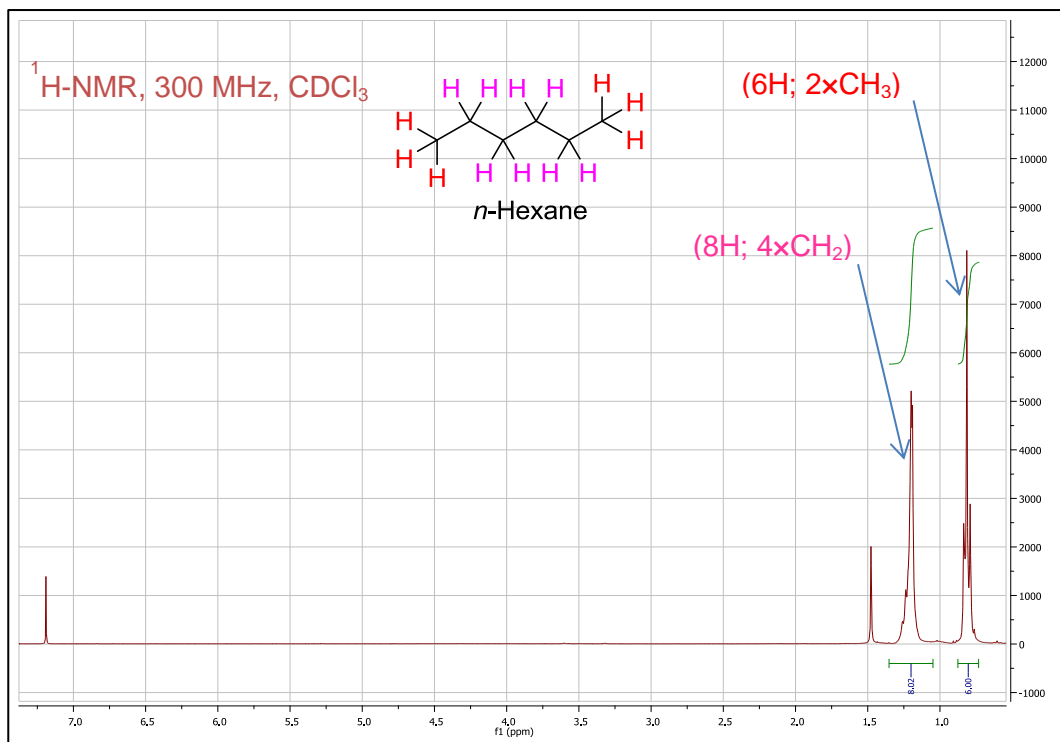


Figure 47 – ¹H-NMR of *n*-hexane.

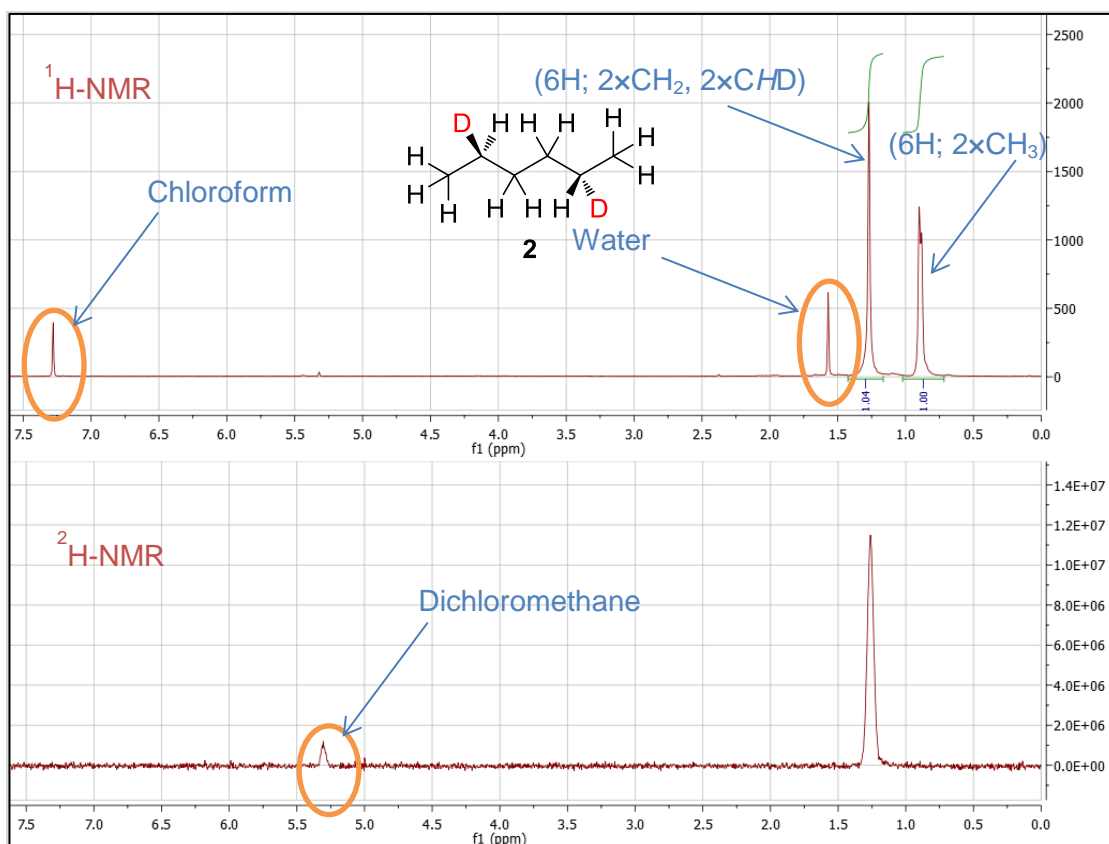


Figure 48 – ¹H- and ²H-NMR of (2*R*,5*S*)-(2,5-²H₂)hexane (**120**).

However, the most unique feature of the deuterated compounds is indicated in their ^{13}C -NMR. The introduction of deuterium into a molecule has a distinct effect on its NMR spectra. ^1H NMR spectra are simplified, as the extent of coupling resulting from deuterium atoms is $1/6^{\text{th}}$ that of hydrogen atoms, and as such they do not significantly split the signals of adjacent protons. However, protons in geminal CHD groups are split by deuterium atoms into triplets as a result of deuterium having spin $I = 1$. This splitting was not visible on the spectra of most of the deuterated compounds synthesised in this project, possibly as a result of broadening of signals.

As mentioned in chapter 2, ^{13}C NMR spectra become more complicated, as deuterium atoms do split the signals of directly bonded ^{13}C atoms, and this splitting shows up on a normal proton-decoupled spectrum, from which splitting from ^1H atoms is removed. Splitting of a ^{13}C signal by deuterium follows the rule multiplicity = $2I + 1$, where I is the number of directly-bonded deuterium atoms. Hence, a carbon atom bonded to one deuterium will show as triplet, and a carbon atom bonded to two deuterium atoms will show as a quintet.⁸²

For example in deuterated hexane **120** only one deuterium is bonded to the carbon at C-2 and therefore the multiplicity = $(2 \times 1) + 1 = 3$, which is shown as a triplet in ^{13}C -NMR (Fig. 39). However, CD_2 in the hexane **121B** has a multiplicity of 5 and exhibits a quintet (Fig. 53).

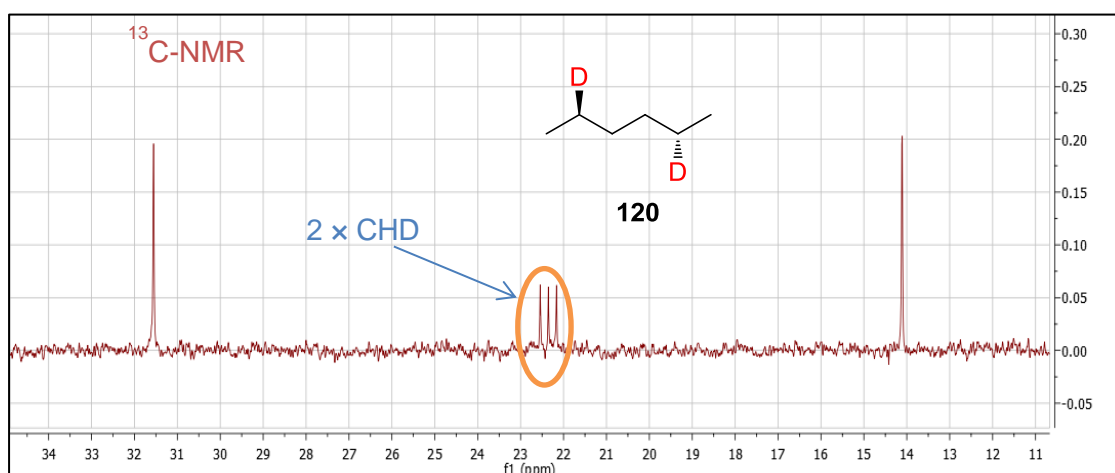


Figure 49 – ^{13}C -NMR of $(2R,5S)$ -($2,5$ - $^2\text{H}_2$)hexane (**120**).

These features were present in the NMR spectra of all other deuterated hexanes, which is shown in figures 50 – 52.

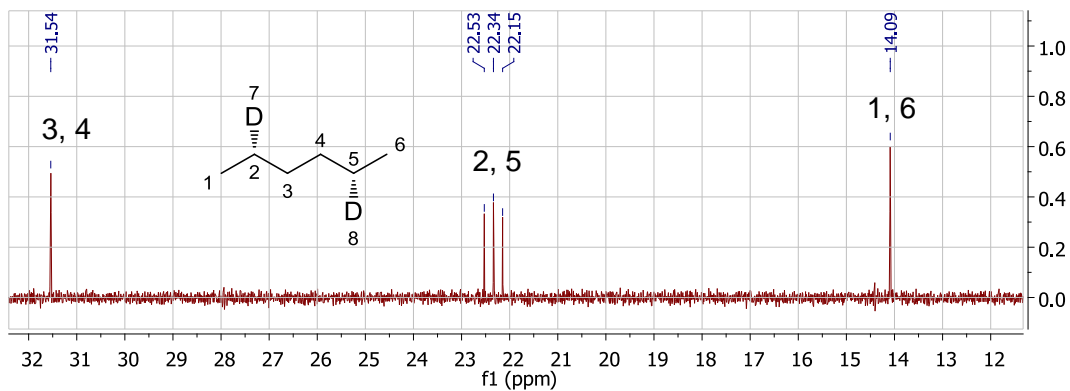
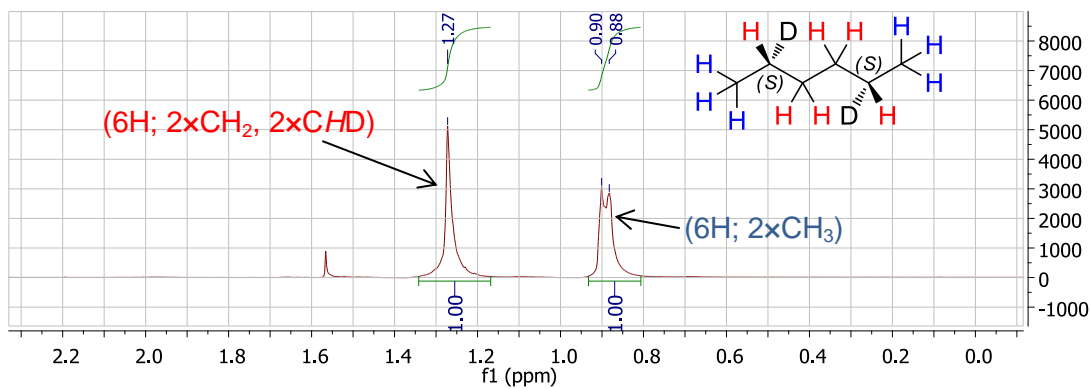


Figure 50 – ^1H and ^{13}C -NMR of (2*S*,5*S*)-(2,5- $^2\text{H}_2$)hexane (**120**).

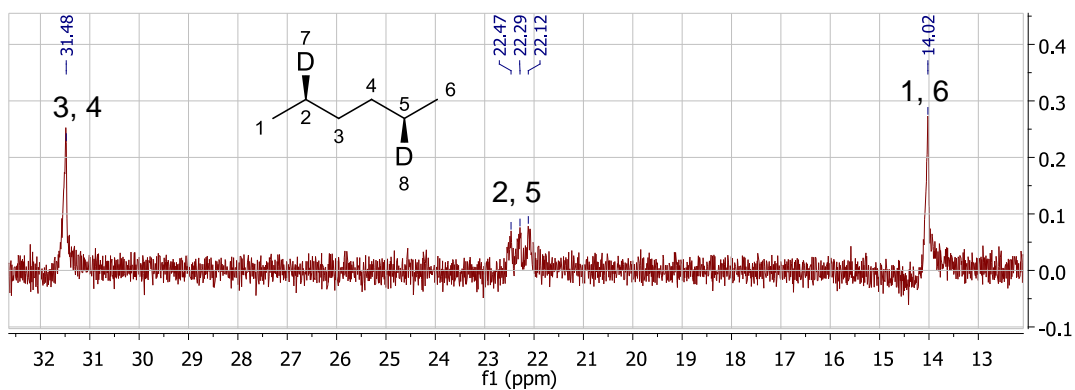
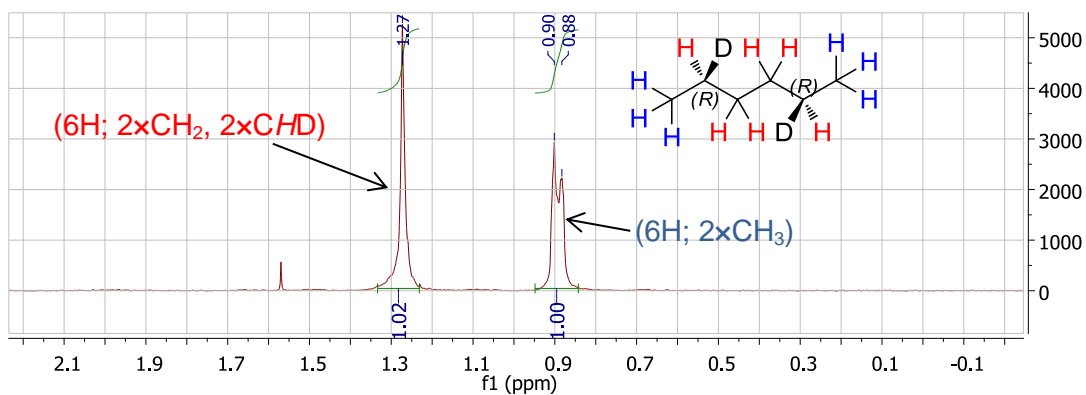


Figure 51 – ^1H - and ^{13}C -NMR of (2*R*,5*R*)-(2,5- $^2\text{H}_2$)hexane (**119**).

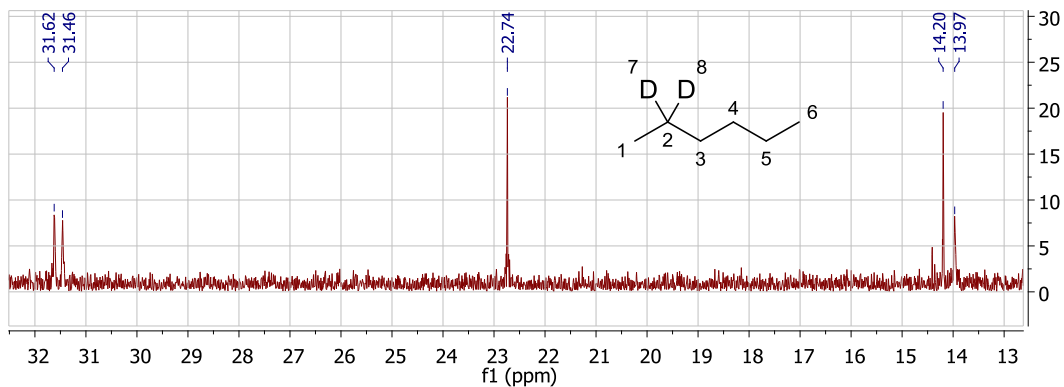
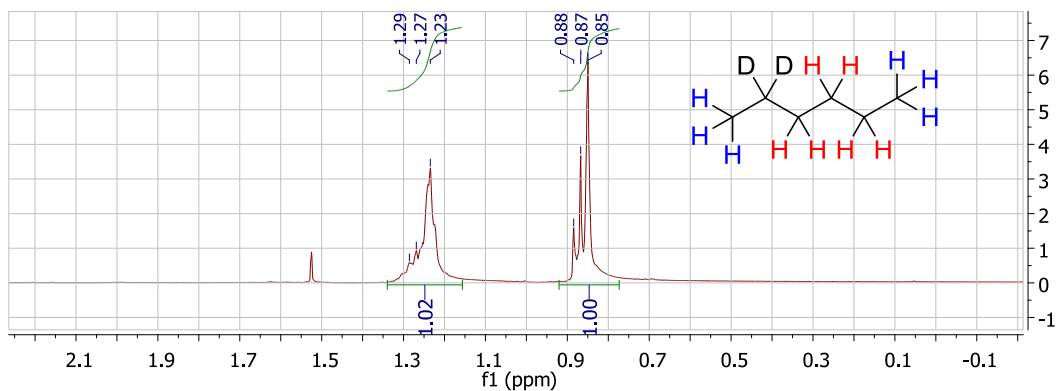


Figure 52 – ^1H and ^{13}C -NMR of 2,2-dideuterohexane (121A).

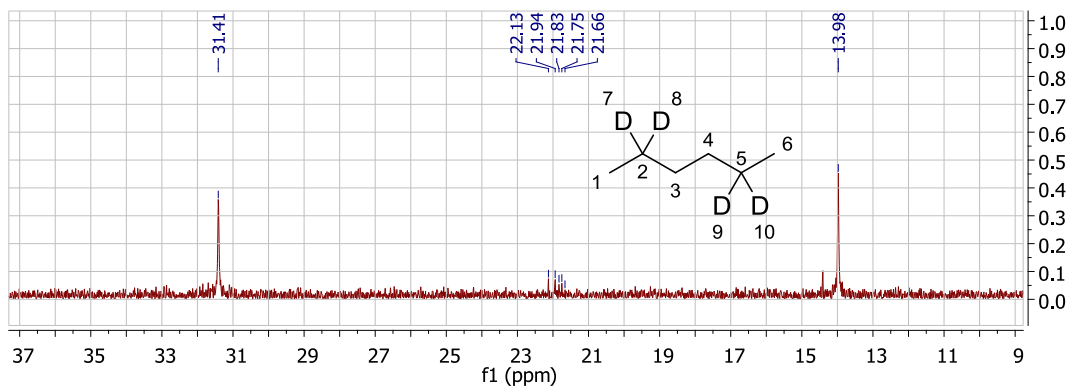
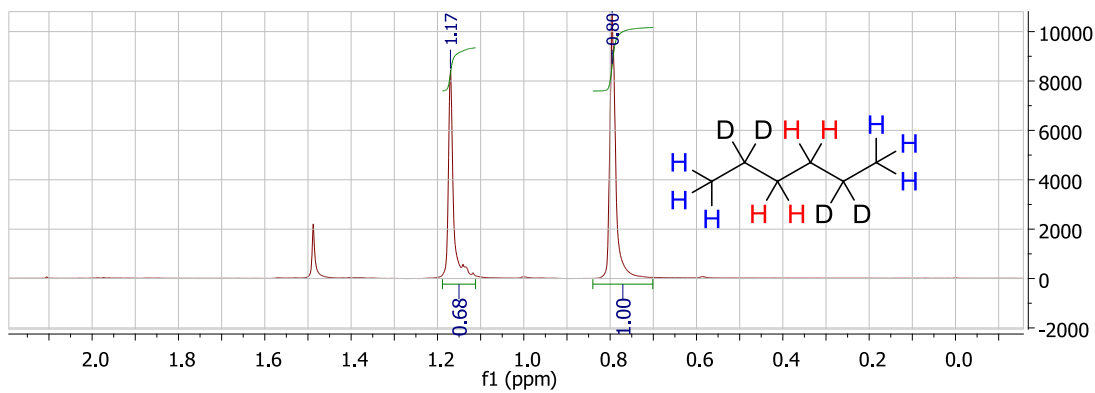
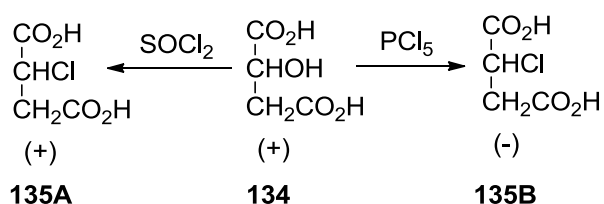


Figure 53 – ^1H - and ^{13}C -NMR of 2,2,5,5-tetradeuterohexane (121B).

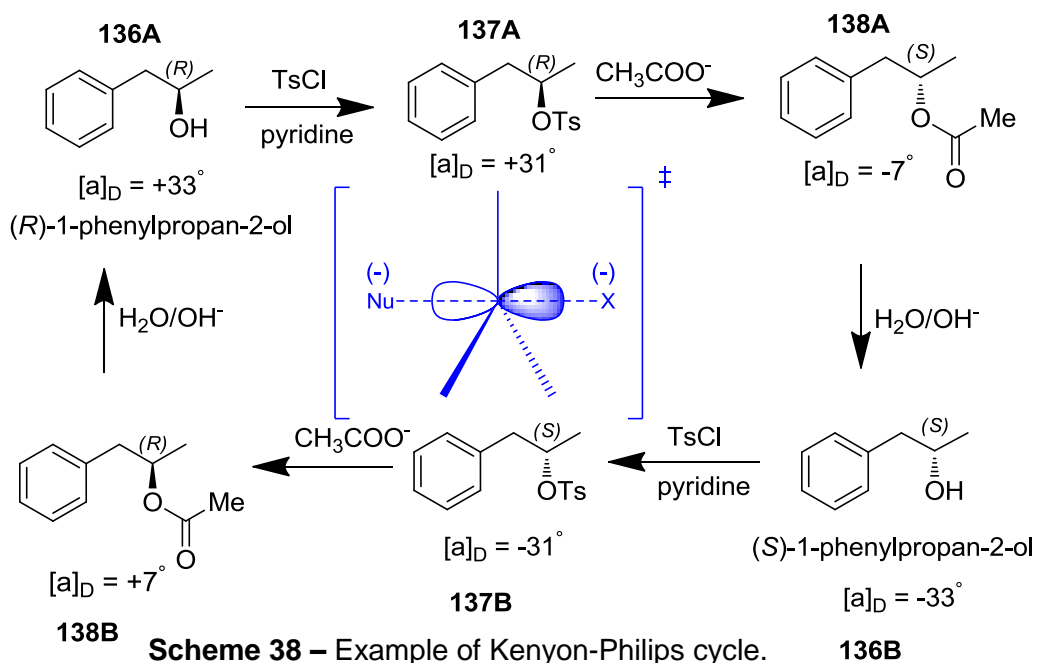
3.1.2 Inversion of configuration (S_N2) following reduction by $LiAlH_4$

The reduction of the tosylates by $LiAlH_4$ is a S_N2 reaction and proceeds via inversion of configuration at each stereocentre.⁸³ This process was first observed by P. Walden⁸⁴ in 1896 when he noticed that compounds can invert their configuration as a result of substitution reactions. He reacted hydroxysuccinic acid with $SOCl_2$ and PCl_5 and realised that one of the steps during the reactions was associated with inversion of the configuration, whereas, the other proceeded with retention, but at the time he was unable to specify which (Scheme 37).

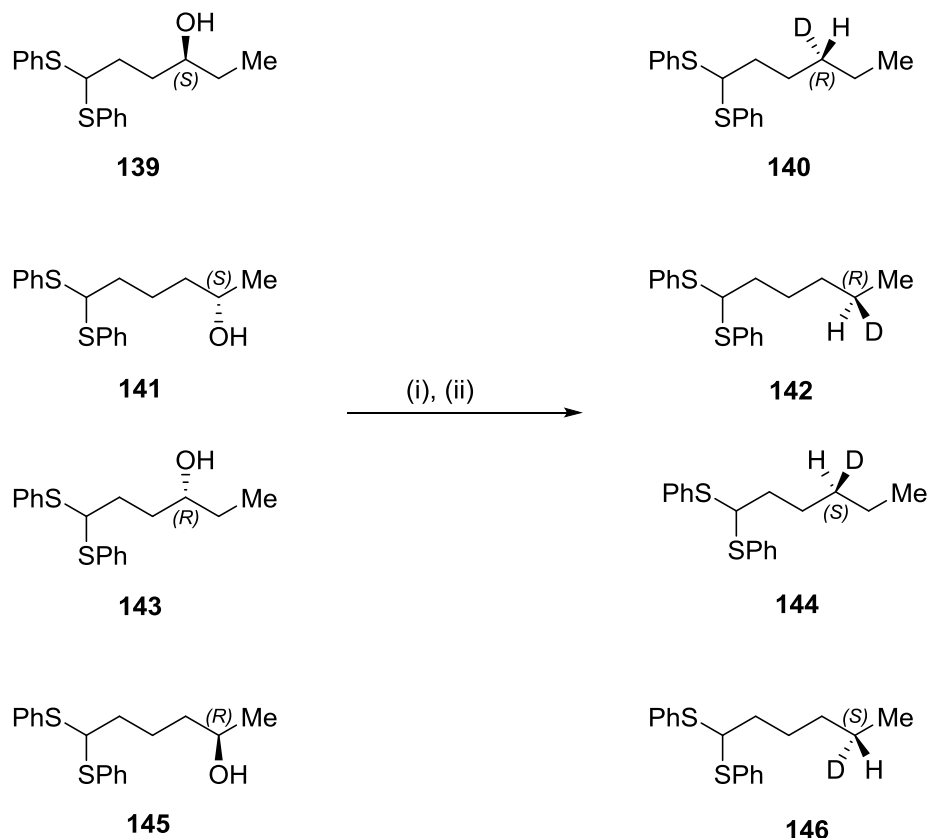


Scheme 37

Proof that an S_N2 reaction proceeds with inversion of configuration was provided by Kenyon et al (Kenyon-Philips cycle) in a three-step reaction sequence in which the starting material and the product were enantiomers (Scheme 38).⁸⁵



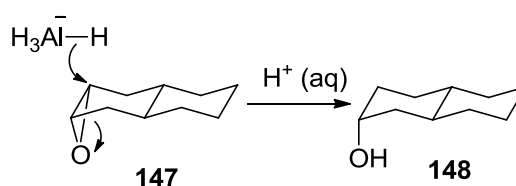
The deuteride anion behaves in the same way as acetate and approaches the electrophilic carbon at an angle of 180° from the leaving group (tosylate), resulting in inversion of configuration. The examples below are from published studies carried out by Baillif et al⁸³ that confirm the S_N2 stereochemistry of lithium aluminium deuteride on tosylates (Scheme 39):



Scheme 39 – Reagents and conditions: (i) TsCl, pyr.; (ii) LiAl²H₄, Et₂O

Assigning the absolute configuration for each step illustrated that configurations remained unchanged after tosylation, however it was inverted following reduction with LiAl²H₄.

A common reaction which can be used as evidence to confirm the S_N2 reactivity of LiAlH₄ is the reduction of epoxides. The epoxide on the cyclohexane ring shown below cleaves in such a direction as to give an axial alcohol, which is expected for a S_N2 reaction (Scheme 40).⁸⁶



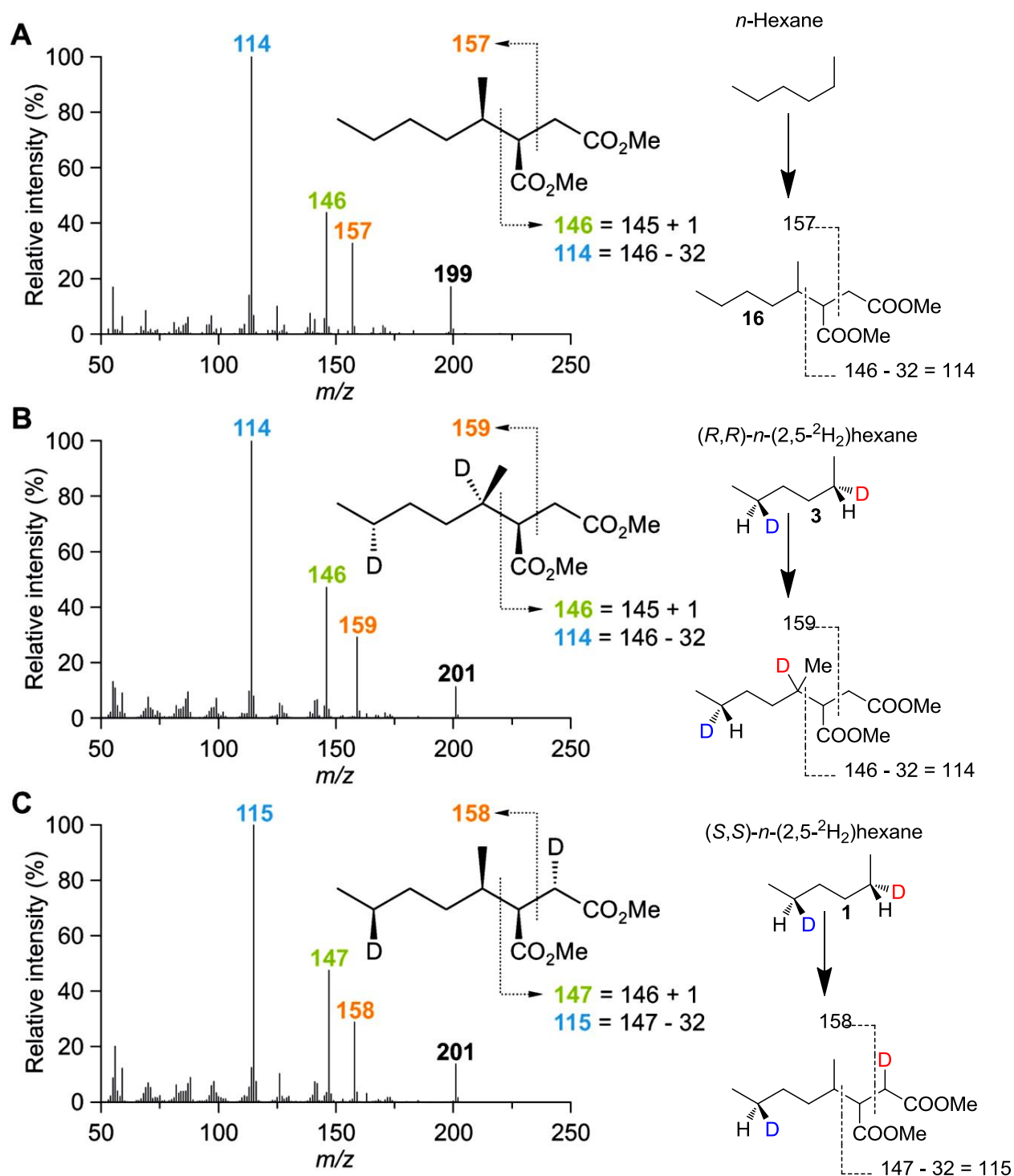
Scheme 40 – Reduction of epoxide by LiAlH₄.

3.1.3 Analysis of the metabolites

The deuterated hexanes prepared as described above, were transferred to glass ampoules, thermally sealed and sent to Prof. R. Rabus (Oldenburg university) laboratory to be used as growth substrates for strain HxN1. Rotational symmetry of the *n*-(2,5-²H₂)hexane isomers forces the enzyme to attack a configurationally defined CHD center and simplifies the product analysis.

Mass spectrometric analysis of metabolites formed during anaerobic growth of strain HxN1 in the presence of deuterated hexanes **1** and **3** were performed. Complete transfer of a deuterium atom to the succinate moiety of **16** was observed upon addition of **1**, while essentially no deuterium transfer occurred with **3** (Fig. 38).

As shown in figure 54 the fragment ion at *m/z* 199 resulting from loss of OCH₃ from one of the methyl ester moieties in spectrum **(A)** is shifted to *m/z* 201 in **(B)** and **(C)**, indicating the presence of two deuterium atoms. The fragment ion at *m/z* 157 in **(A)** is shifted to *m/z* 159 and *m/z* 158 in **(B)** and **(C)**, respectively. The fragment ions at *m/z* 114 and *m/z* 146 in **(A)** are shifted to *m/z* 115 and *m/z* 147, respectively, in **(C)**, while no shift is observed in **(B)**. Thus, exclusively the pro-S hydrogen atom is abstracted from the *n*-hexane.



✚ **Figure 54** – Figure adapted from Jarling et al.⁷ Mass spectra showing the labelling patterns of deuterated isotopologues of **16** (as dimethyl esters after derivatisation with diazomethane) formed during anaerobic growth of strain HxN1 in the presence of stereospecifically deuterated *n*-hexanes. **A**) **16** formed from non-deuterated *n*-hexane, **B**) (1',4'-²H₂)-**16** formed from **3**, **C**) (3,4'-²H₂)-**16** formed from **1**.



Mass spectrometric analysis of (1-methylpentyl)succinic acid formed during anaerobic growth of strain HxN1 in the presence of (2*R*,5*S*)-*n*-(2,5-²H₂)hexane (*meso*) revealed the presence of a ~ 3:1 mixture of the (1',4'-²H₂)- and (3,4'-²H₂)-isotopologues, while in the presence of *n*-(2,2-²H₂)hexane a ~ 5:1 mixture of the (4',4'-²H₂)- and (3,1'-²H₂)-isotopologues was observed. This shows that hydrogen abstraction from *n*-hexane has a primary kinetic isotope effect ≥ 3.

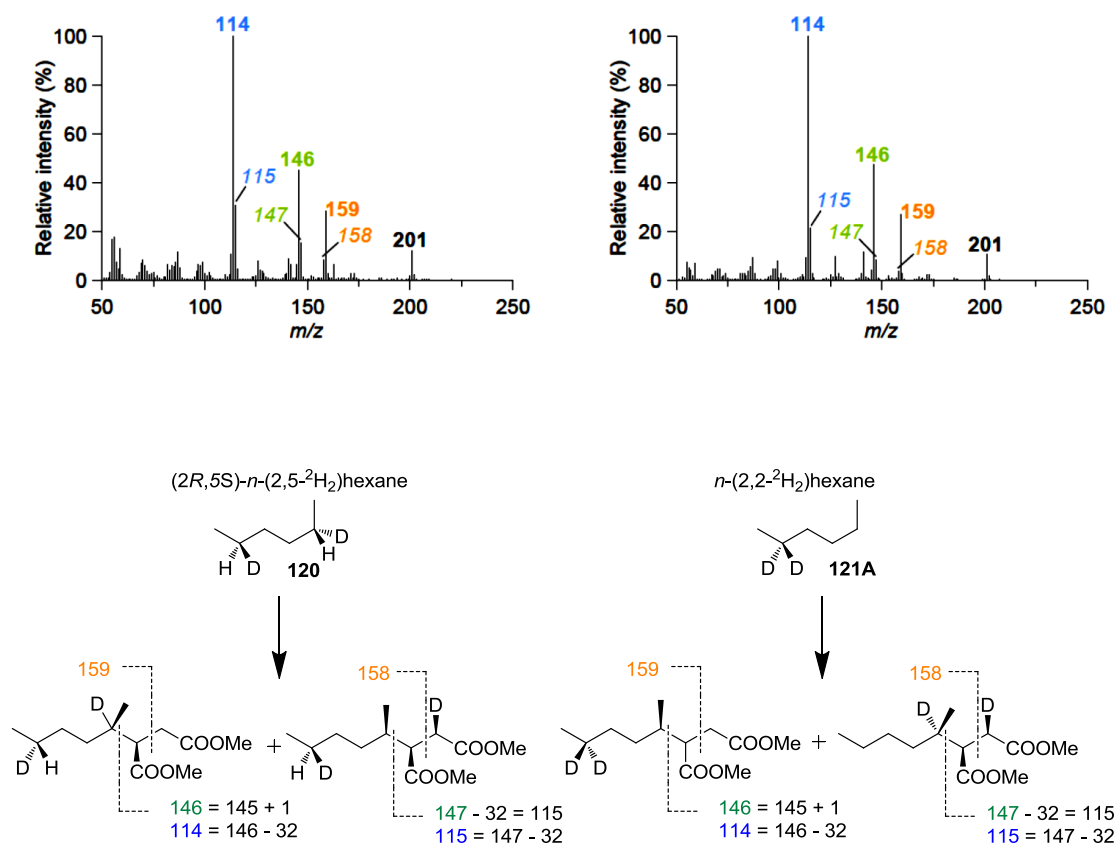
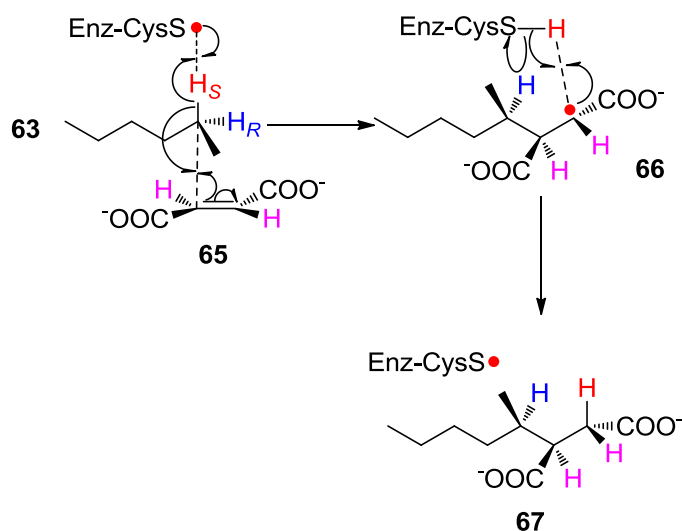


Figure 55 – Mass spectra showing the labelling pattern of deuterated isotopologues of (1-methylpentyl)succinic acid (as dimethyl esters after derivatisation with diazomethane) formed in the presence of (2*R*,5*S*)-*n*-(2,5-²H₂)hexane (left) or *n*-(2,2-²H₂)hexane (right).

3.1.4 Proposed mechanism

The observed results proves that in the initial step of the catalytic cycle of the (1-methylpentyl)succinate-forming enzyme exclusively the pro-*S* hydrogen atom is abstracted from C-2 of *n*-hexane. Subsequently, the secondary alkyl species binds with a fumarate molecule on the face opposite to that from which the

hydrogen atom was abstracted, resulting in the 1'*R* configuration of **67**. Thus, an overall inversion of configuration at C-2 of *n*-hexane takes place. The formation of **67** is completed by back transfer of the originally abstracted hydrogen atom, which regenerates the cysteinyl radical. The hydrogen abstraction and addition to fumarate may even occur in a concerted manner, similar to an S_N2 reaction. Hence, a modified mechanism for the initial abstraction of hydrogen was proposed (Scheme 42).



Scheme 42 – Proposed concerted mechanism of the (1-methylpentyl)succinate forming enzyme reaction. The active form of the enzyme is generated by abstraction of a hydrogen atom from an adjacent cysteine residue by the glycol storage radical.

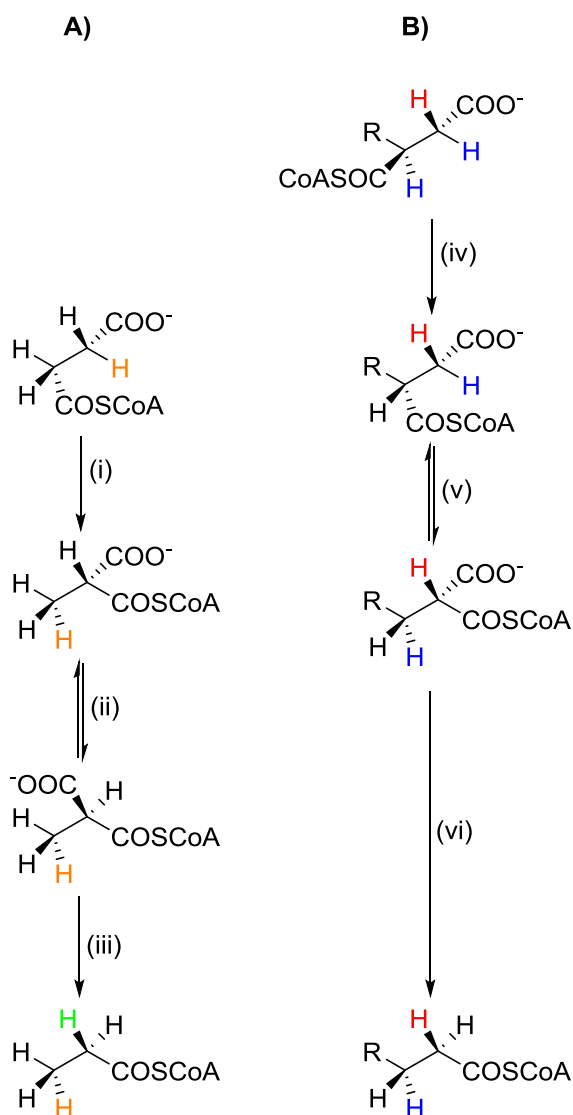
3.1.5 Summary

In order to avoid the formation of unlabelled **67**, incubation experiments were performed with cultures of strain HxN1 that had been adapted to *n*-heptane using a mixture of *n*-heptane and a dideuterated *n*-hexane (8:1). Rotational symmetry of the *n*-(2,5-²H₂)hexane isomers causes the enzyme to attack a configurationally defined CHD center and makes the product analysis simpler. Upon the addition of **118**, the complete transfer of a deuterium atom to the succinate moiety of **67** was observed, while no deuterium transfer occurred with **119** (Figure 38). This proves that in the initial step of the catalytic cycle of the (1-methylpentyl)succinate-forming enzyme exclusively the pro-*S* hydrogen atom is abstracted from C-2 of unlabelled hexane **65**. Afterwards, the secondary alkyl species binds with a fumarate molecule on the face opposite to that from which

the hydrogen atom was abstracted, resulting in the 1'*R* configuration of MPS **67**. Therefore, an overall inversion of configuration at C-2 of **1** takes place. The formation of **67** is completed by back transfer of the originally abstracted hydrogen atom, which regenerates the cysteinyl radical. The hydrogen abstraction and addition to fumarate may even occur in a concerted manner, similar to an S_N2 reaction (Scheme 42). Such a mechanism could explain how the high difference in bond dissociation energy (BDE) between a thiol (RS-H) and a C-H bond of a methylene group in an alkane ($\Delta\text{BDE} \approx 40 \text{ kJ mol}^{-1}$) could be overcome.⁸⁷ Hence, the highly energetic hex-2-yl radical may not exist as a single enzyme-bound species. The only detectable radical in this reaction would be that at C3 of the succinate moiety stabilised by the adjacent carboxylate, similar to the radical detected in the carbon-skeleton rearrangement catalyzed by glutamate mutase.⁸⁸ With **120** and **121A**, mixtures of dideuterated isotopologues of **67** were formed in which the main product was formed by the transfer of the pro-*S* hydrogen atom from C2 and C5, respectively (see the Supporting Information). This indicates a significant primary kinetic isotope effect (≥ 3) for the abstraction of the hydrogen atom.

3.1.6 Comparison of the known transformation of succinyl-CoA to propionyl-CoA via methylmalonyl-CoA with the present pathway

The fate of deuterium atoms from labeled substrates was used to elucidate the overall stereochemical course of the (1-methylpentyl)succinate-forming reaction and subsequent steps in the degradation pathway (Scheme 43). This was based on assumed similarities to the known transformation of succinyl-CoA to propionyl-CoA. In the latter pathway an epimerisation is required as (*R*)-methylmalonyl-CoA formed from succinyl-CoA by methylmalonyl-CoA mutase is not a substrate of (*S*)-methylmalonyl-CoA decarboxylase. A corresponding step appears to be absent in the transformation of (2-methylhexyl)malonyl-CoA to (*R*)-4-methyloctanoyl-CoA as no exchange of the hydrogen atom at C-2 with external hydrogen was observed .



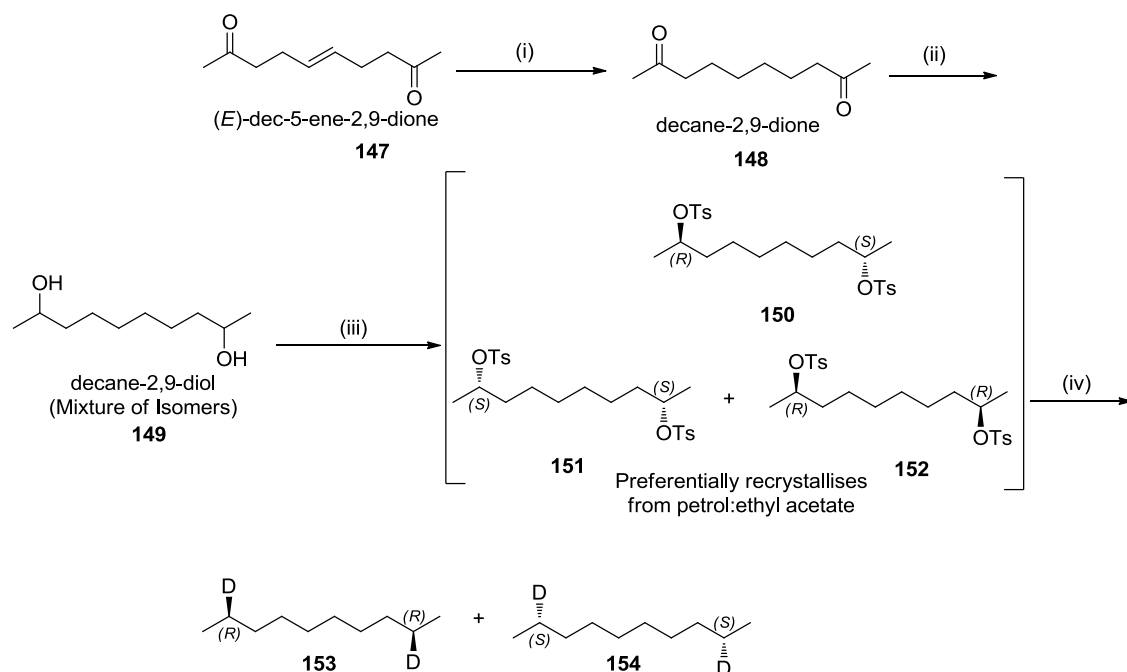
Scheme 43 - Comparison of the known transformation of succinyl-CoA to propionyl-CoA via methylmalonyl-CoA with the corresponding reactions in the pathway of anaerobic oxidation of n-hexane in strain HxN1. i, methylmalonyl-CoA mutase; ii, methylmalonyl-CoA epimerase; iii, (S)-methylmalonyl-CoA decarboxylase, iv, postulated (1-methylalkyl)succinyl-CoA epimerase; v, (2-methylalkyl)malonyl-CoA mutase; vi, (2-methylalkyl)malonyl-CoA decarboxylase; R = hex-2-yl.

3.2 DEUTERATED DECANES

In order to verify that the same mechanism applies to initial abstraction of hydrogen in $> C_6$ alkanes, synthesis of deuterated decanes as substrates was also required. This section was not completed due to time factors, however two methods were developed for the synthesis of deuterated decanes.

3.2.1 Synthesis of decane-2,9-diol di-*p*-toluenesulfonates

The initial method involved hydrogenation of commercially available **147** to afford diketone **148**, which was further reduced by sodium borohydride to afford diol **149**, which was tosylated in the same manner as hexane-2,5-diol (**127**), subsequent fractional recrystallisation of the ditosylate mixture preferentially afforded a mixture of (2*S*,9*S*)- and (2*R*,9*R*)-decane-2,9-diol di-*p*-toluenesulfonates (**151** and **152**), which were fully characterised by 1H and ^{13}C NMR (Fig. 57). The relative configuration of the mixture was achieved using X-ray crystallography (Fig. 56).



Scheme 44 – Synthesis of (2*S*,9*S*)- and (2*R*,9*R*)-2,9-dideuteriodecane. (i) H_2 , 10% Pd/C, THF, RT, 24 h; (ii) $NaBH_4$, CH_3OH , $0^\circ C$, 2 h; (iii) C_6H_5N , TsCl, CH_2Cl_2 , $0^\circ C$, 72 h; (iv) $LiAl^2H_4$, tetraglyme.

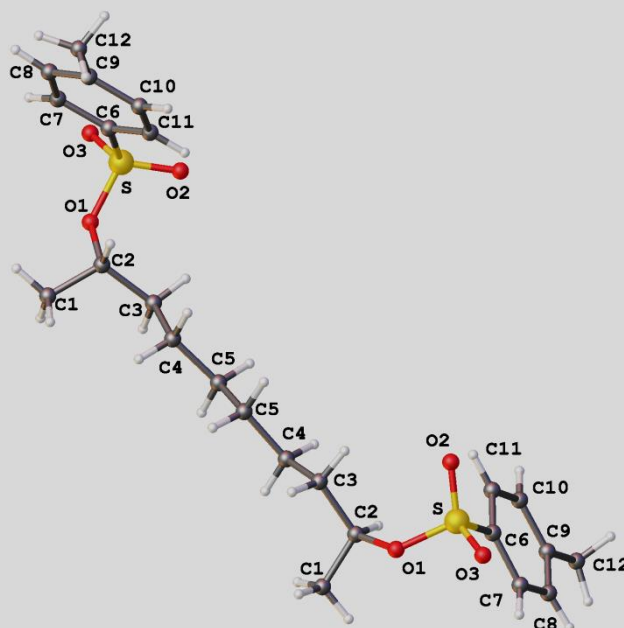
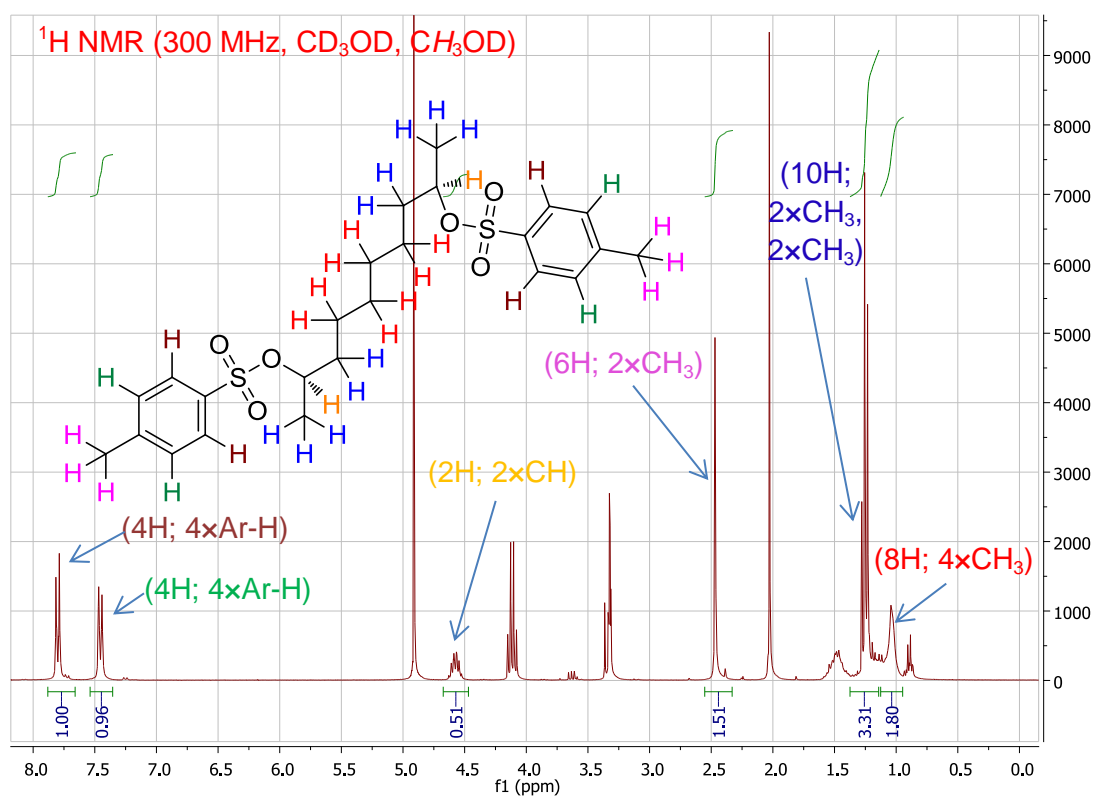


Figure 56 - (2*S*,9*S*)- and (2*R*,9*R*)-decane-2,9-diol di-*p*-toluenesulfonates (151 and 152)

A racemic mixture of (2*S*,9*S*)- and (2*R*,9*R*)-2,9-dideuteriodecane was obtained, using the same method for obtaining deuterated hexanes. This mixture will be used as a reference standard for comparison of NMR spectra (Fig. 58).



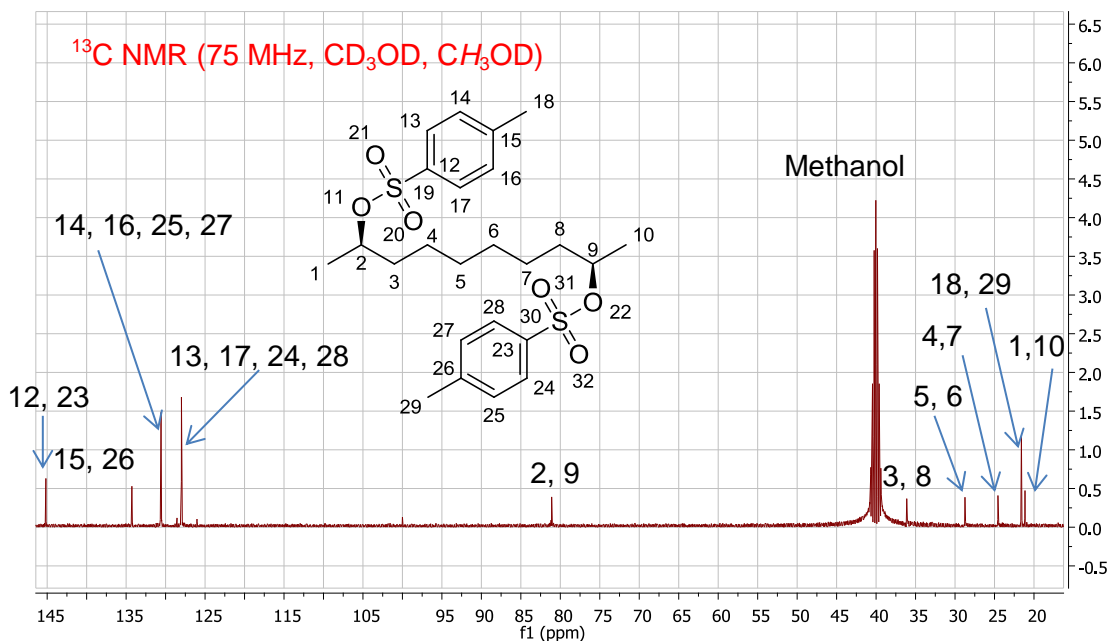


Figure 57 - ¹H and ¹³C NMR spectra of ditosylates **151** and **152**.

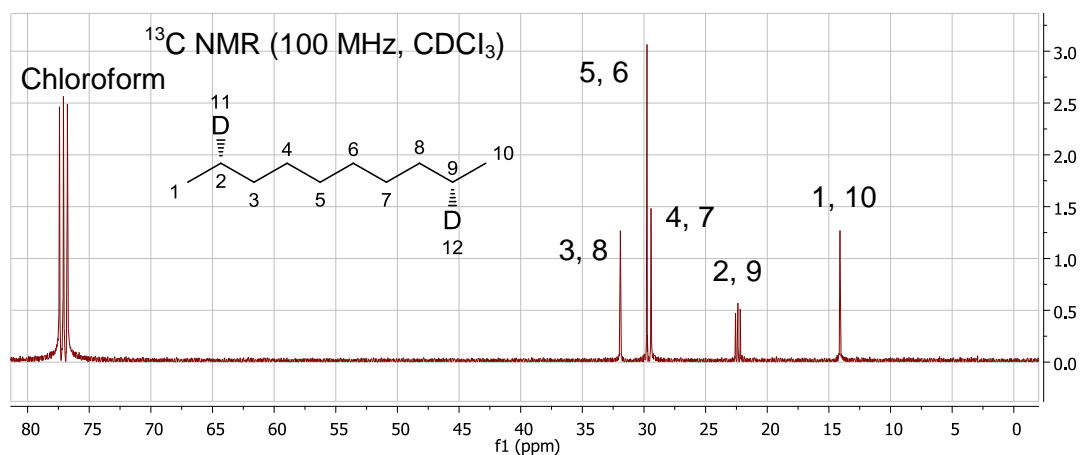
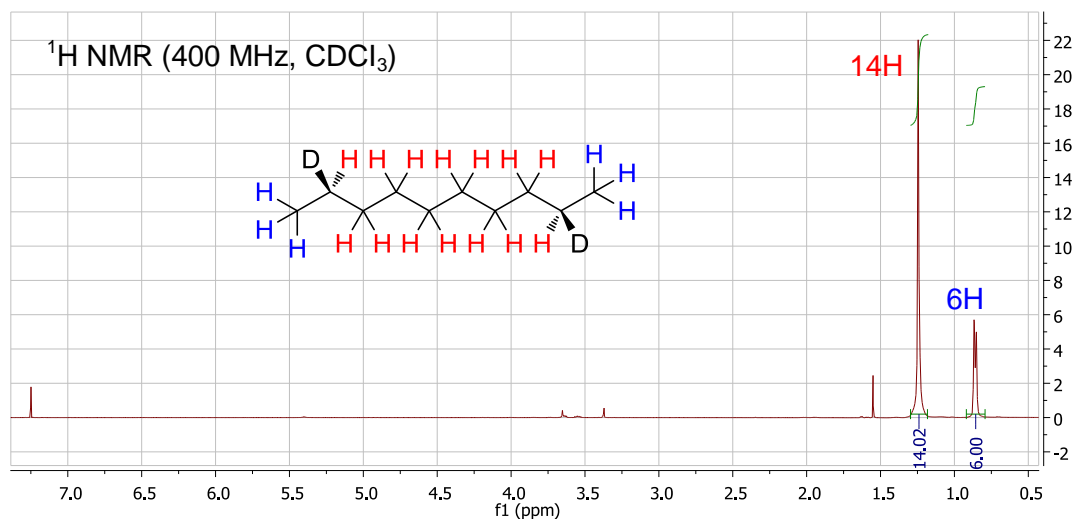
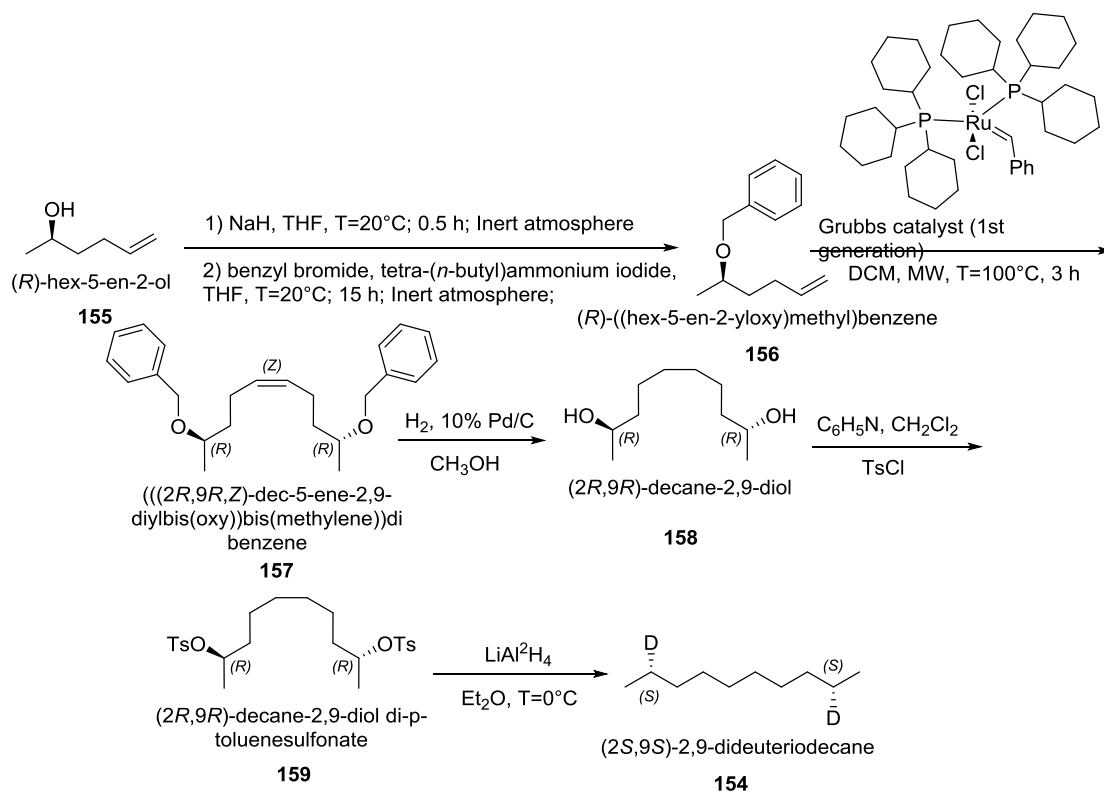


Figure 58 - ¹H and ¹³C NMR spectra of (2*S*,9*S*)- and (2*R*,9*R*)-2,9-dideuteriododecane (**153** and **154**).

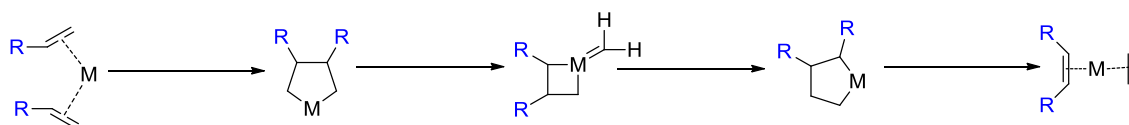
3.2.2 (2S,9S)-2,9-dideuteriodecane

Protection of hydroxyl group in **155** using sodium hydride and benzyl bromide, was followed by olefin metathesis of **156** using Grubbs' catalyst (1st generation) to afford **157** (see ¹H NMR spectra; Fig. 59).



Scheme 45 – Synthesis of (2S,9S)-2,9-dideuteriodecane.

Grubbs' catalyst operates by redistribution of fragments of alkenes (olefins) by the scission and regeneration of carbon-carbon double bonds (Scheme 46).



Scheme 46 – Mechanism of action of Grubbs' catalyst.

Subsequently, **157** was hydrogenated to afford diol **158**, tosylated using the same method as before, and reduced by LiAl²H₄ to give (2S,9S)-2,9-dideuteriodecane (see ¹³C-NMR spectra; Fig. 60).

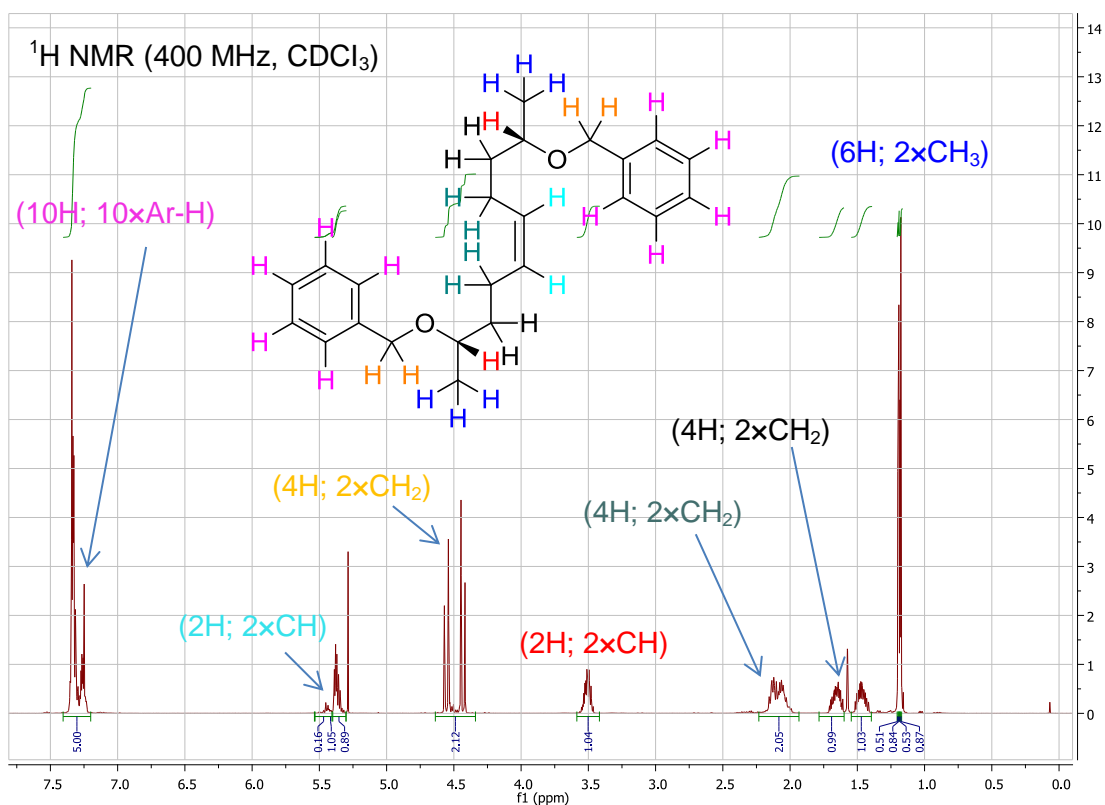


Figure 59 - ¹H NMR spectra of **157**.

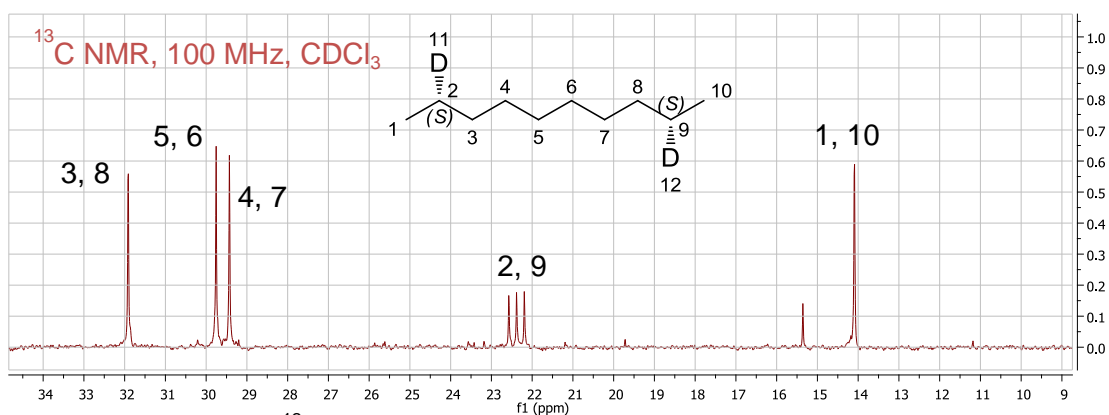


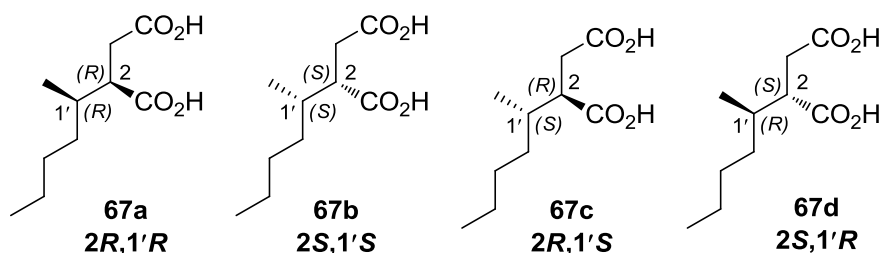
Figure 60 - ¹³C NMR spectra of (2S,9S)-2,9-dideuteriodecane (**154**).

Chapter 4

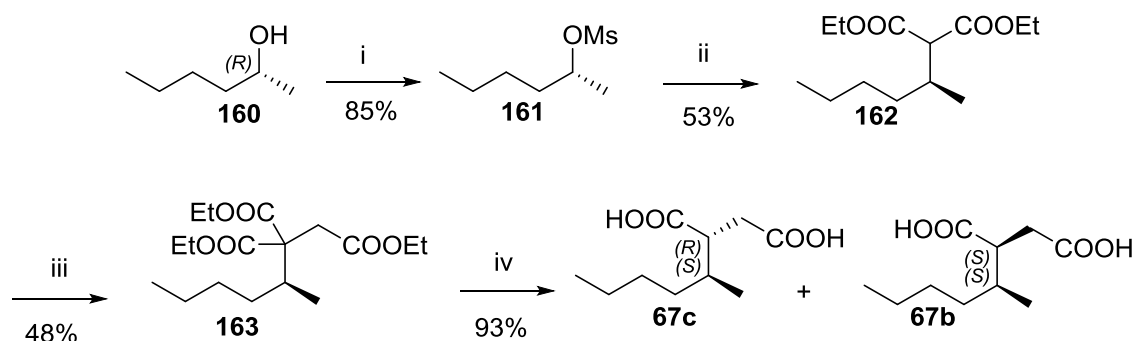
Synthesis of Succinic Acid Metabolites Produced by Strain HxN1 During Anaerobic Growth with Hexane

4.1 ASSIGNMENT OF CONFIGURATION OF STEREOCENTERS IN (1-METHYLPENTYL)SUCCINIC ACID ISOMERS PRODUCED BY STRAIN HxN1 DURING ANAEROBIC GROWTH WITH *n*-HEXANE

Structures **67a-d** of (1-methylpentyl)succinic acid (MPS) are formed following anaerobic degradation of hexane by strain HxN1. These structures have two chiral centres and therefore can exist as four possible stereoisomers. To explain the configuration at the newly formed stereocentres, synthesis of all four stereoisomers of **67** (a - d) was required in order to use them as standards for comparison with metabolites from strain HxN1.



The synthesis of these stereoisomers was achieved from racemic and pure (*R*)- and (*S*)-hexan-2-ol through activation of the hydroxy group and displacement with diethyl malonate, followed by alkylation with ethyl bromoacetate, hydrolysis of the ester groups, and decarboxylation with hydrochloric acid to give the desired MPS in an overall 20% yield (Scheme 47).



Scheme 47 - Synthesis of a mixture of (2*R*,1'*S*)- and (2*S*,1'*S*)-(1-methylpentyl)succinic acid. i, Methanesulfonyl chloride, triethylamine in dichloromethane (methanesulfonyl = Ms)³; ii, sodium hydride followed by diethyl malonate in 1,2-dimethoxyethane³; iii, sodium hydride followed by ethyl bromoacetate in tetrahydrofuran; iv, concentrated hydrochloric acid, reflux for 48 h.

(*R*)- and (*S*)-hexan-2-ol are both commercially available. However, in order to reduce costs (*S*)-hexan-2-ol was also synthesised via reduction of hexan-2-one by carrots⁸⁹ in a similar procedure as to that described in chapter 3 using baker's yeast. The general feature of these reductions is, for most cases, well

afforded the (2*R*,1'*S*)/(2*S*,1'*R*) isomers (**67c** and **67d**) in a pure form. The relative configurations were confirmed by X-ray crystallography (Fig. 63). The mixture of (2*R*,1'*R*)/(2*S*,1'*S*) isomers (**67a** and **67b**) was obtained (90% purity) by evaporation of the mother liquor.

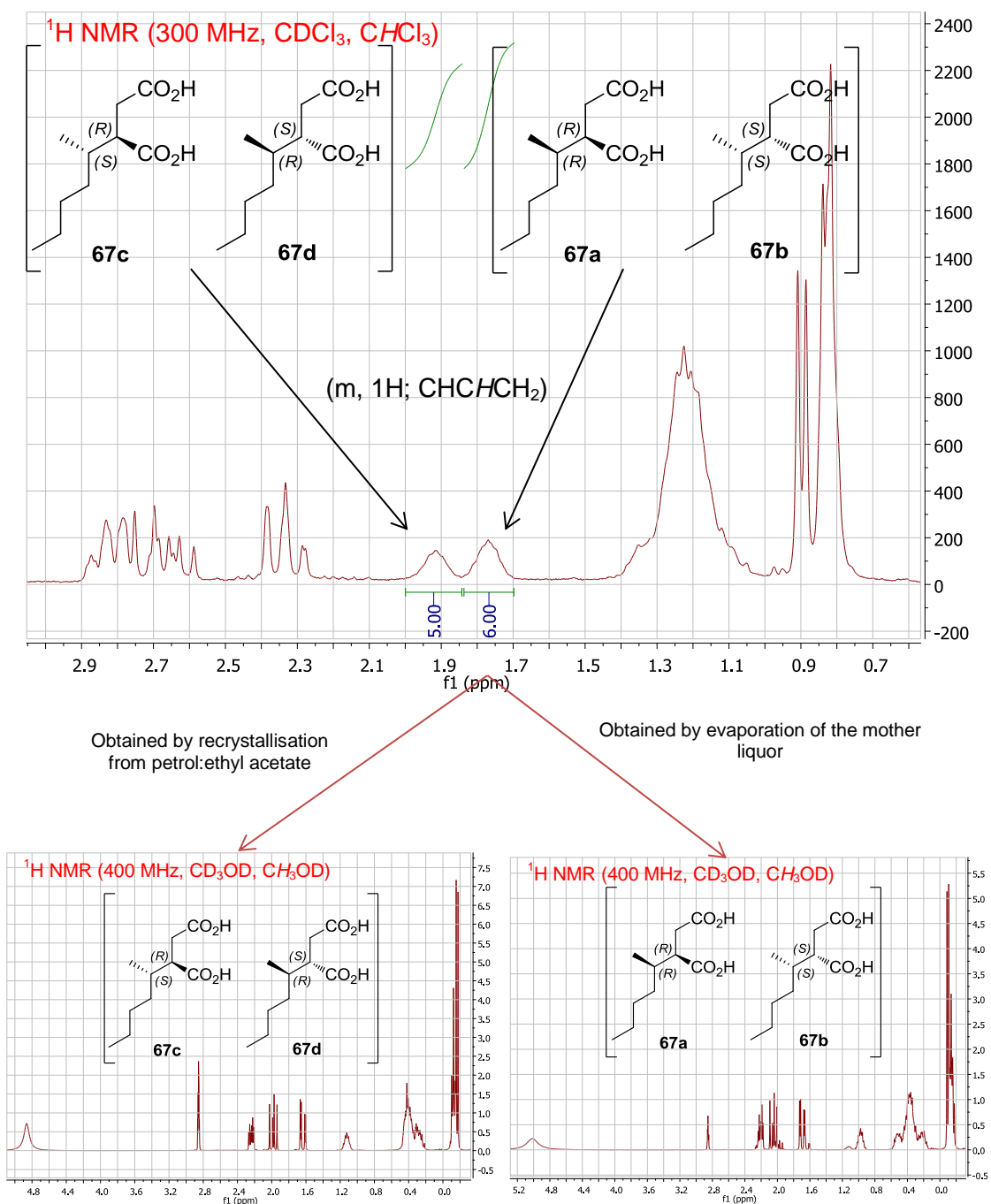


Figure 62 – Comparison of the ¹H-NMR of the two sets of succinic acid diastereomers confirms a successful separation.

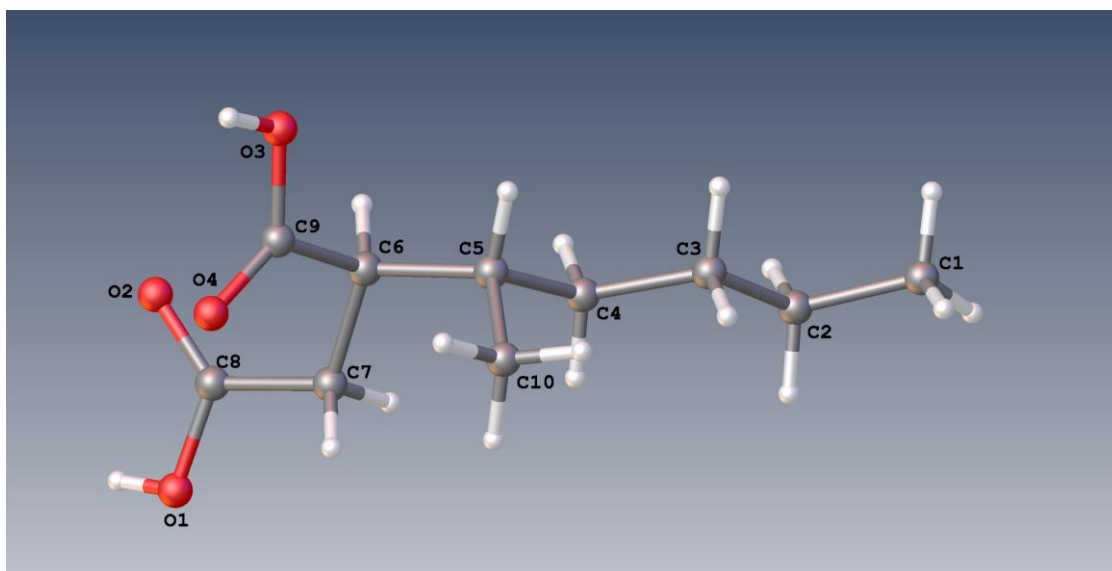


Figure 63 – X-ray crystallography of (2*R*,1'*S*)/(2*S*,1'*R*) isomers (**67c** and **67d**).

Display of single peaks in the ^{13}C NMR of mixtures 2 and 4, further confirms the separation of diastereomers (Fig. 64A and B).

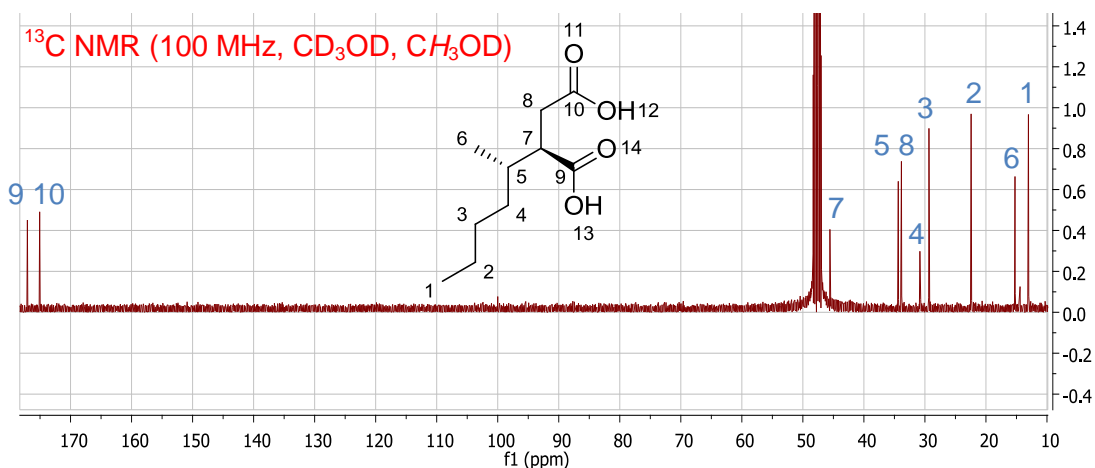


Figure 64A – ^{13}C NMR of mixture 2 (**67c** and **67d**).

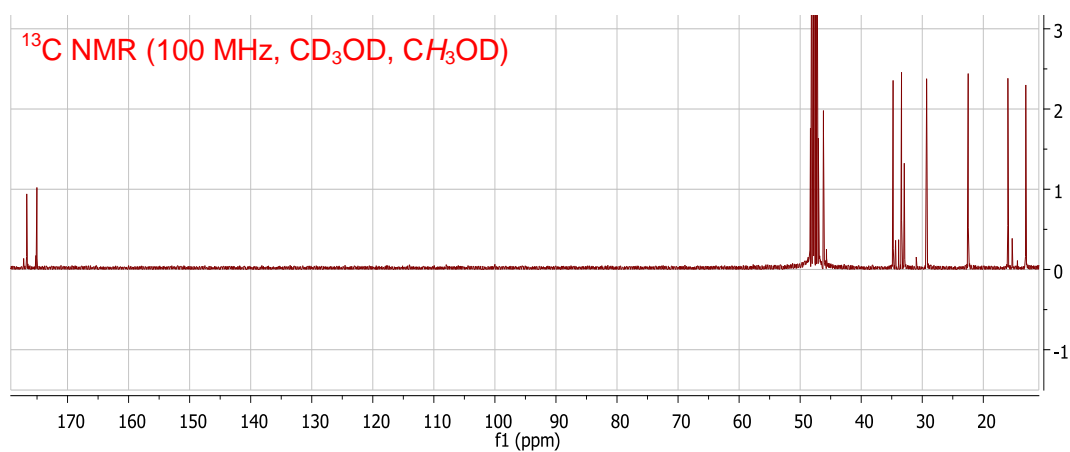


Figure 64B – ^{13}C NMR of mixture 4 (**67a** and **67b**).

Ultimately, mixtures 1 - 4 were isolated (Fig. 61). However, in order for the MPS mixtures (**67a-d**) to be analysed by gas chromatography (GC), they were derivatized to 3-(1-methylpentyl)-1-(1-phenylethyl)pyrrolidine-2,5-diones / *N*-(1-phenylethyl) 3-(1-methylpentyl)succinimides using (*R*)-(+)-1-phenylethylamine. Subsequently the chromatographs were compared with the chromatographs of products formed by strain HxN1 during anaerobic growth with *n*-hexane (Fig. 65).

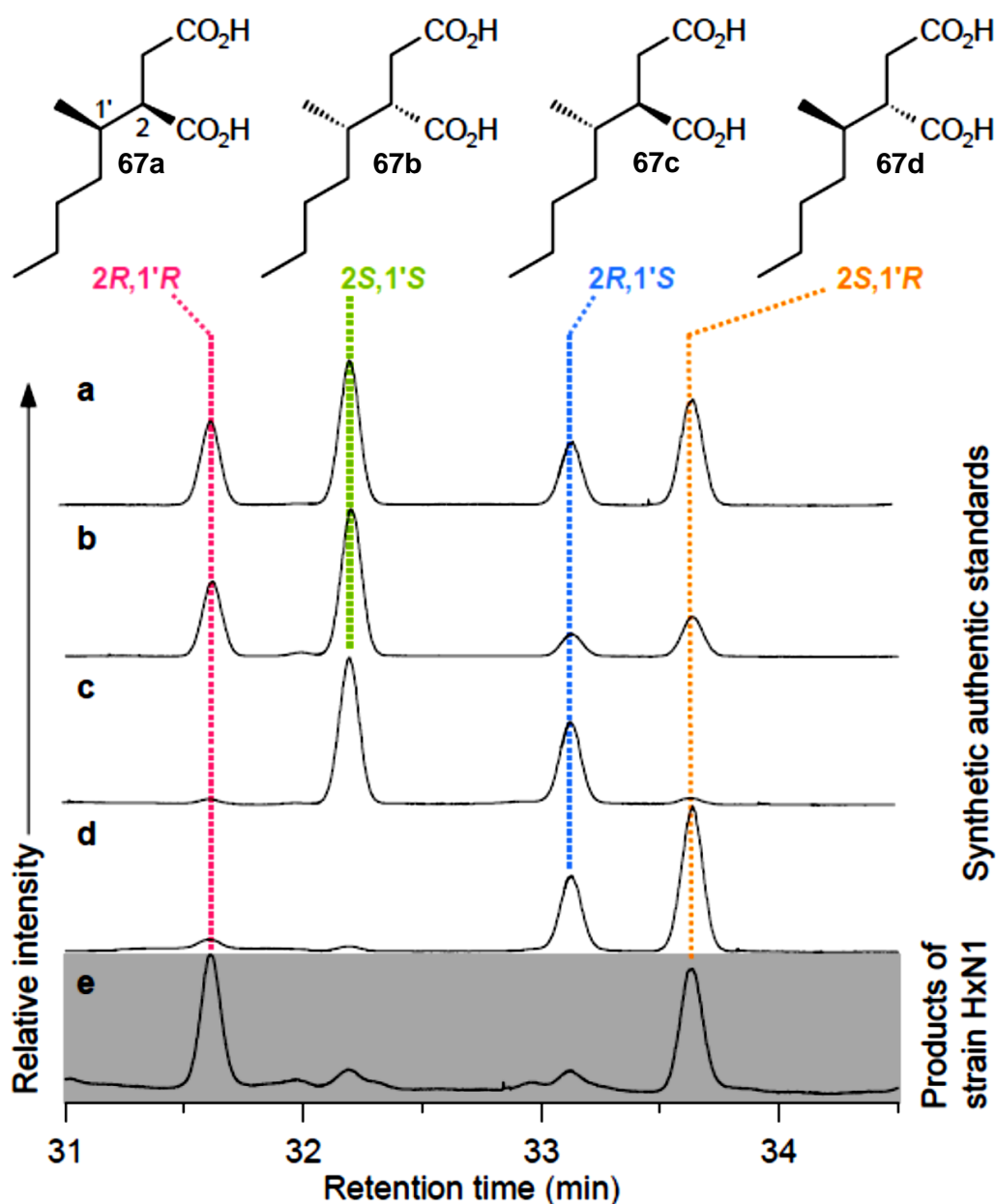
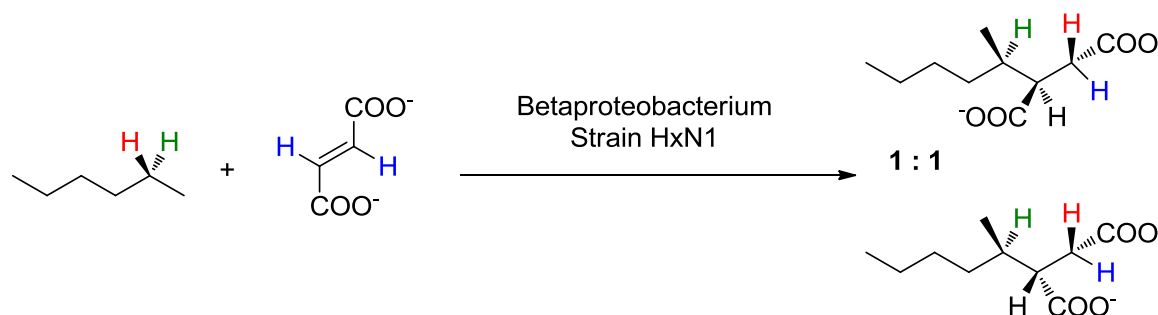


Figure 65 – Gas chromatograms showing the specific formation of the (*2R,1'R*)- and (*2S,1'R*)-isomers of **67** during anaerobic growth of strain HxN1 with *n*-hexane **A**) Mixture of all four stereoisomers; **B**) (*2R,1'R*)/(*2S,1'S*); **C**) (*2R,1'S*)/(*2S,1'R*); **D**) (*2S,1'S*)/(*2R,1'S*); **E**) (*2R,1'R*)/(*2S,1'R*); **F**) products formed by strain HxN1 during anaerobic growth with *n*-hexane.

As shown in Fig. 65, strain HxN1 specifically forms equal amounts of **67a** and **67d** during anaerobic growth with hexane. This demonstrates that both configurations at C-2 in the succinate moiety are present. However, the stereocenter at C-1' in the products (C-2 of the hydrocarbon substrate) has exclusively the *R* configuration (Scheme 48).



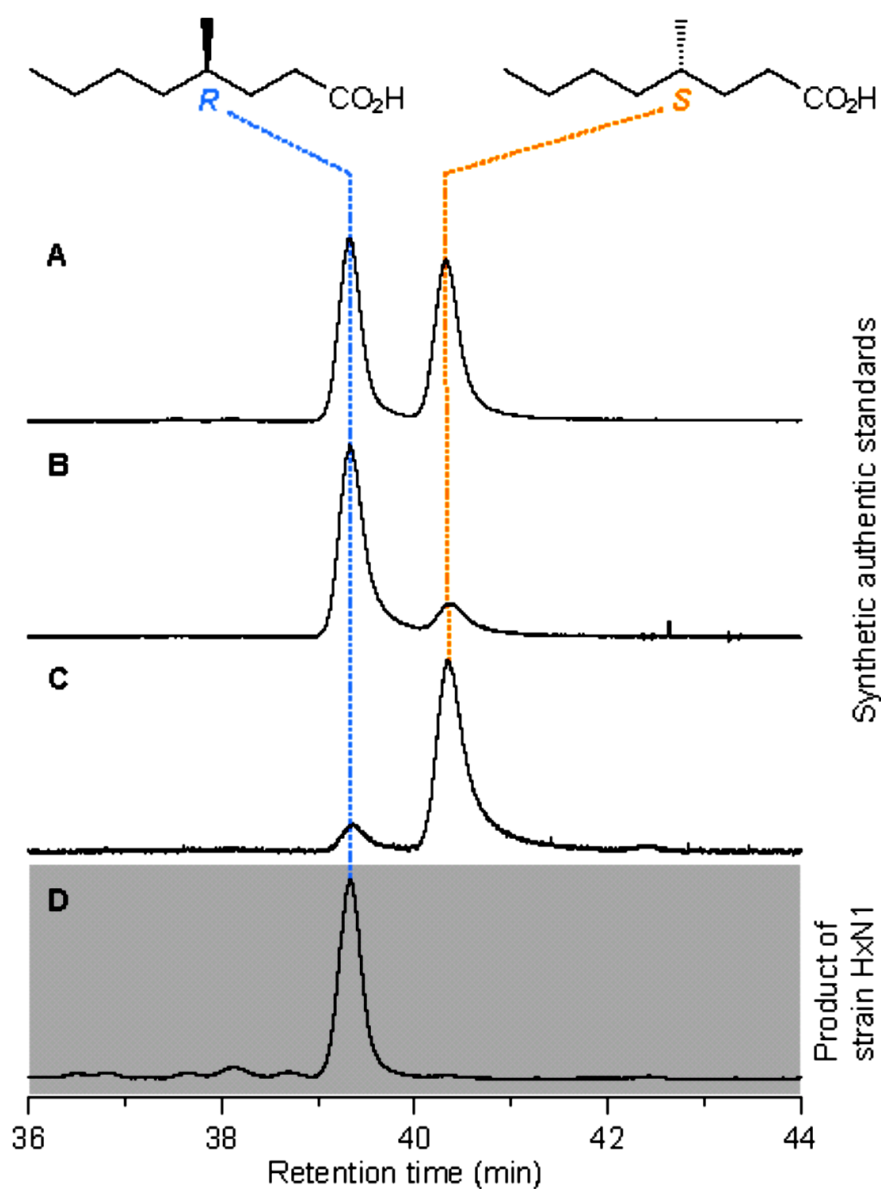
Scheme 49 – Formation of equal amounts of **67a** and **67d** during anaerobic growth with hexane.

4.2 Assignment of Configuration of 4-Methyloctanoic Acid Produced by Strain HxN1 During Anaerobic Growth with *n*-Hexane

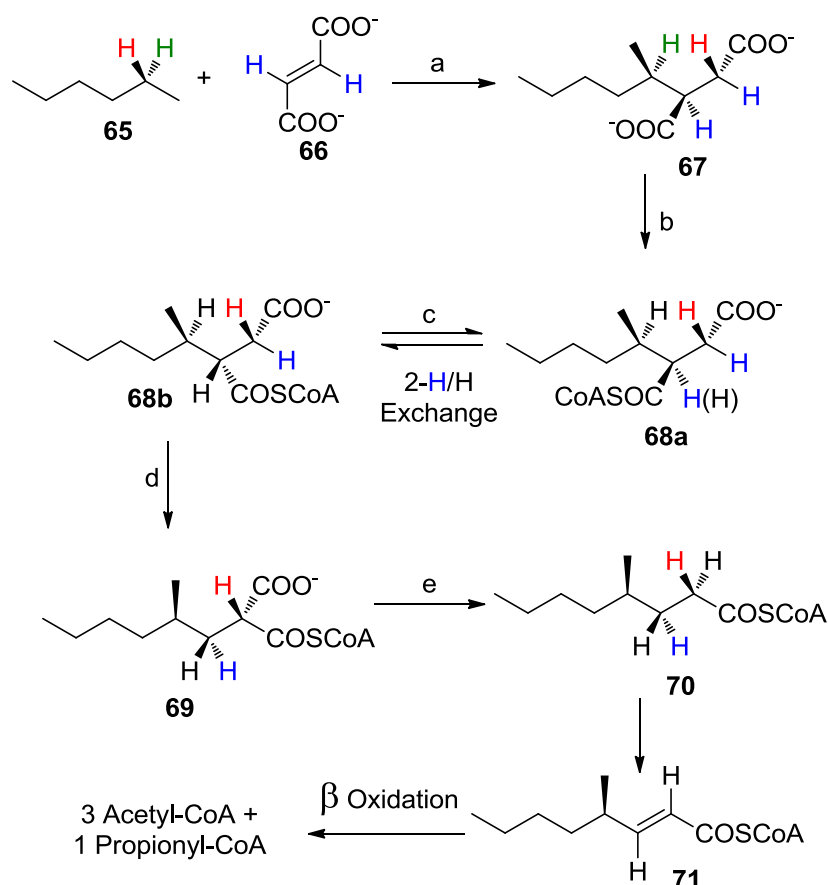
Using the (*R*) and (*S*)-4-methyloctanoic acid which were synthesised by my colleague Marta Drozdowska,⁷ assignment of the configuration of 4-methyloctanoic acid which is further produced by strain HxN1 during anoxic growth with *n*-hexane, was possible using comparison in Gas chromatography. This confirms that only the (*R*)-enantiomer is formed (Fig. 66), which is in agreement with the results obtained for (1-methylpentyl)succinate.

4.3 Conclusion

Using the information gathered from analysis of the metabolites from deuterated hexanes and also GC comparison of metabolites with synthesised isomers, the following pathway is proposed for the Initial steps of the anaerobic oxidation of *n*-hexane in the denitrifying strain HxN1 (Scheme 50).



✚ **Figure 66** - Gas chromatograms showing the specific formation of (*R*)-4-methyloctanoic acid during anaerobic growth of strain HxN1 with *n*-hexane. A) Racemate; B) (*R*)-4-methyloctanoic acid; C) (*S*)-4-methyloctanoic acid; D) product formed by strain HxN1 during anaerobic growth with *n*-hexane.



Scheme 50 - Initial steps of the anaerobic oxidation of *n*-hexane in the denitrifying strain HxN1 including the proposed stereochemistry of the reactions involved as elucidated in this study. a) (1-Methylalkyl)-succinate synthase; b) (1-methylalkyl)succinate-CoA ligase; c) (1-methylalkyl) succinyl-CoA epimerase; d) (2-methylalkyl)malonyl-CoA mutase; e) (2-methylalkyl)malonyl-CoA decarboxylase; f) 4-methylalkanoyl-CoA dehydrogenase.

4.4 Discussion

Mechanistically, this reaction appears to be similar to the formation of benzylsuccinate from toluene catalyzed by the glycyl radical enzyme benzylsuccinate synthase.⁹² Indeed, EPR spectroscopy provided strong evidence for the presence of a glycyl radical enzyme in cells of the denitrifying betaproteobacterium “*Aromatoleum*” strain HxN1 anaerobically grown with *n*-hexane.² A tentative (1-methylalkyl)succinate synthase similar to benzylsuccinate synthase has been identified.⁵¹ However, abstraction of a hydrogen atom from any C–H bond of an *n*-alkane is intrinsically more difficult than such a process at the methyl group of toluene.⁸⁷ To better understand the

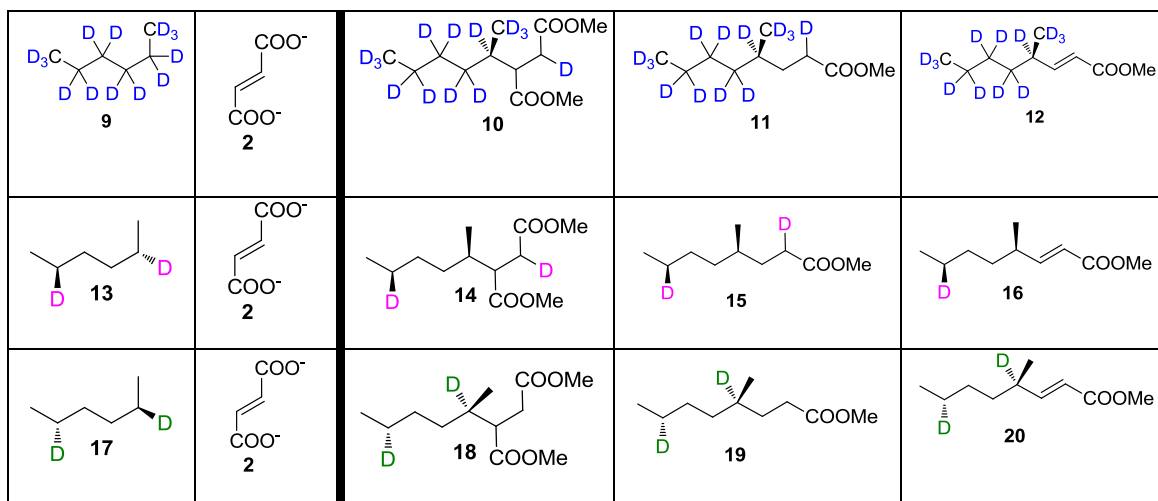
mechanism of *n*-alkane functionalization under anoxic conditions, we have studied the stereochemical features of this defining example of C–H activation.

Analysis of metabolites present in cells of strain HxN1 anaerobically grown with *n*-hexane (**65**) had shown that the formed (1-methylpentyl)succinate (**67**) consists of two diastereoisomers (Scheme 49), indicating an apparent imperfect stereoselectivity of the enzymatic reaction. The analogous formation of benzylsuccinate from toluene by benzylsuccinate synthase yields exclusively the *R* enantiomer (Scheme 19). Anaerobic incubation of strain HxN1 with perdeuterated *n*-hexane revealed that the hydrogen atom abstracted from C-2 of the *n*-alkane is transferred to C-3 of the succinate moiety. It has been suggested that subsequent degradation of **67** by means of activation as a coenzyme A thioester, intramolecular rearrangement to (2-methylhexyl)malonyl-CoA (**69**), and decarboxylation leads to 4-methyloctanoyl-CoA (**70**), which is then further degraded by dehydrogenation and β -oxidation (Scheme 50).

4.5 Labeling patterns of other metabolites detected upon anaerobic growth of strain HxN1 with various deuterium-labelled substrates

The labelling patterns of metabolites detected upon anaerobic growth of strain HxN1 with various deuterium-labelled substrates were assigned based on interpretation of their mass spectrometric fragmentation patterns (Table 6 & 7). The observed labelling patterns imply fates of specific hydrogen atoms, which are fully in accord with the proposed stereochemistry of the enzyme reactions involved in *n*-hexane oxidation by strain HxN1 as discussed in Scheme 50.

Substrates		Products		



❖ **Table 6⁷** – Labeling patterns of metabolites detected upon anaerobic growth of strain HxN1 with various deuterium-labeled substrates. **1**, *n*-Hexane; **2**, fumarate; **3**, (1'*R*)-(1-methylpentyl)succinic acid dimethyl ester; **4**, (*R*)-4-methyloctanoic acid methyl ester; **5**, (*R*)-4-methyloct-2-enoic acid methyl ester; **6**, (2,3-²H₂)fumarate; **7**, (1'*R*)-(3-²H)(1-methylpentyl)succinic acid dimethyl ester; **8**, (*R*)-(3-²H)4-methyloctanoic acid methyl ester; **9**, *n*-(²H₁₄)hexane; **10**, (1'*R*)-(3,1',2',2',3',3',4',4',5',5',5',6',6',6',6'-²H₁₄)(1-methylpentyl)succinic acid dimethyl ester; **11**, (*R*)-(2,4,5,5,6,6,7,7,8,8,8,1',1',1'-²H₁₄)4-methyloctanoic acid methyl ester; **12**, (*R*)-(4,5,5,6,6,7,7,8,8,8,1',1',1'-²H₁₃)4-methyloct-2-enoic acid methyl ester; **13**, (2*S*,5*S*)-*n*-(2,5-²H₂)hexane; **14**, (1'*R*,4'*S*)-(3,4'-²H₂)(1-methylpentyl)succinic acid dimethyl ester; **15**, (4*R*,7*S*)-(2,7'-²H₂)4-methyloctanoic acid methyl ester; **16**, (4*R*,7*S*)-(7'-²H)4-methyloct-2-enoic acid methyl ester; **17**, (2*R*,5*R*)-*n*-(2,5-²H₂)hexane; **18**, (1'*R*,4'*R*)-(1',4'-²H₂)(1-methylpentyl)succinic acid dimethyl ester; **19**, (4*R*,7*R*)-(4,7'-²H₂)4-methyloctanoic acid methyl ester; **20**, (4*R*,7*R*)-(4,7'-²H₂)4-methyloct-2-enoic acid methyl ester. (Metabolites **16** and **20** were not detected)

❖ **Table 7** - Mass spectrometric data of unlabeled and deuterated metabolites detected upon anaerobic growth of strain HxN1 with various unlabeled and deuterium-labeled substrates. The *m/z* values of key fragment ions used for the assignment of labeling patterns are given in bold numbers.

No	Metabolite	Substrate		Key Ions <i>m/z</i> (% relative intensity)
1.1	(1' <i>R</i>)-(1-methylpentyl)succinate		<i>all</i> -(¹ H)	<i>all</i> -(¹ H)
2.1		3-(² H)	<i>all</i> -(¹ H)	2,3-(² H ₂)
3.1		2,3-(¹ H ²),(² H ₁₄)	<i>all</i> -(² H)	<i>all</i> -(¹ H)

M⁺ absent, **199** (14.5), 183 (1.3), 171 (2.2), 170 (1.8), **157** (33.9), **146** (48.7), 141 (6.2), 139 (9.1), 125 (8.6), **114** (100), 97 (5.1), 87 (6.0), 74 (1.8), 69 (5.5), 59 (5.3), 55 (10.4)

M⁺ absent, **200** (12.9), 184 (0.8), 172 (1.8), 171 (2.1), **157** (29.7), **147** (41.1), 142 (7.2), 140 (7.8), 125 (9.8), **115** (100), 97 (8.1), 88 (9.6), 75 (2.1), 70 (4.4), 69 (4.9), 59 (8.0), 56 (10.6), 55 (10.9)

M⁺ absent, **213** (13.9), 194 (1.0), 185 (1.8), 183 (1.2), **170** (24.7), 152 (7.2), **148** (46.6),

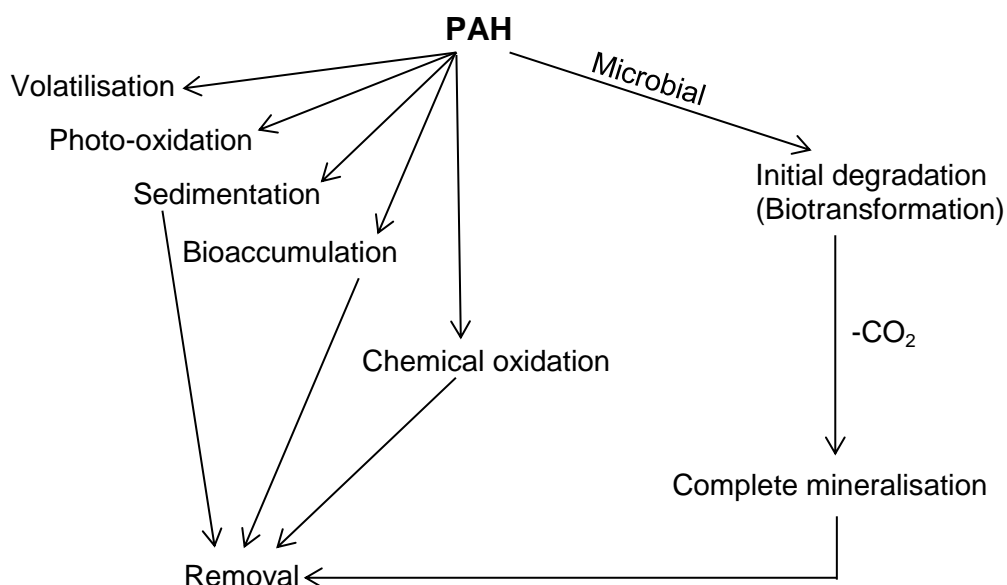
				138 (3.2), 137 (5.6), 118 (4.7), 115 (100), 109 (7.0), 90 (3.5), 89 (9.8), 77 (3.7), 62 (6.8), 59 (6.8), 56 (6.6)
4.1	(4'S)-3,4'-(² H ₂)	(2S,5S)-2,5-(² H ₂)	<i>all</i> -(¹ H)	M ⁺ absent, 201 (13.9), 185 (0.7), 173 (1.8), 172 (1.8), 158 (29.0), 147 (47.6), 142 (6.8), 141 (7.4), 126 (10.4), 115 (100), 98 (7.6), 97 (6.0), 88 (8.9), 87 (6.8), 82 (6.3), 71 (5.4), 70 (7.0), 69 (5.4), 59 (12.3), 56 (20.3), 55 (8.9)
5.1	(4'R)-1',4'-(² H ₂)	(2R,5R)-2,5-(² H ₂)	<i>all</i> -(¹ H)	M ⁺ absent, 201 (11.4), 185 (0.7), 173 (1.3), 171 (2.0), 159 (29.3), 146 (47.2), 142 (6.7), 141 (6.4), 127 (4.6), 126 (5.5), 114 (100), 99 (7.2), 87 (9.6), 86 (7.0), 82 (4.6), 74 (2.6), 70 (7.7), 59 (9.2), 56 (11.0), 55 (13.2)
6.1 a	(4'S)-1',4'-(² H ₂)	(2R,5S)-2,5-(² H ₂)	<i>all</i> -(¹ H)	M ⁺ absent, 201 (13.0), 185 (0.7), 173 (1.8), 172 (0.7), 171 (1.5), 159 (25.2), 158 (7.9), 147 (19.2), 146 (45.9), 142 (7.4), 141 (9.2), 127 (5.4), 126 (8.1), 115 (33.4), 114 (100), 99 (8.5), 98 (5.0), 97 (5.2), 88 (4.8), 87 (11.7), 86 (6.6), 82 (6.0), 74 (3.7), 71 (5.1), 70 (9.7), 69 (4.6), 59 (13.2), 57 (9.2), 56 (18.3), 55 (15.2)
6.1 b	(4'R)-3,4'-(² H ₂)	(2R,5S)-2,5-(² H ₂)	<i>all</i> -(¹ H)	


Chapter 5

Anaerobic Degradation of Naphthalene

5.1 INTRODUCTION TO POLYCYCLIC AROMATIC HYDROCARBONS

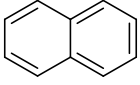
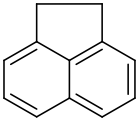
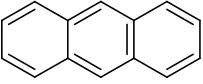
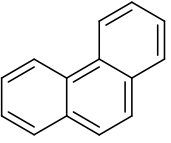
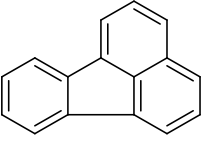
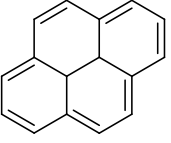
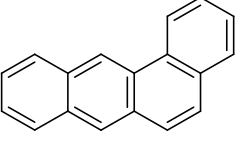
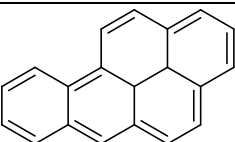
Polycyclic aromatic hydrocarbons (PAHs) are among the most toxic and widespread contaminants in nature. Exposure to PAHs creates a significant risk for people living in industrialised areas of the world. Due to their hydrophobicity and strong adsorption to sediments they are poorly soluble in water and therefore have only a limited bioavailability in natural environments. For these reasons PAHs are very slowly degraded by microorganisms and remain in the environment over a long period of time until they are degraded, resuspended, bioaccumulated, or removed by dredging. The lipophilicity, environmental persistence, and genotoxicity increase as the molecular size of PAHs increases up to 4 or 5 fused benzene rings (Table 8) and toxicological concern shifts towards chronic toxicity, primarily carcinogenesis.⁹³ The possible fates of PAHs in the environment include volatilisation, photooxidation, chemical oxidation, bioaccumulation, adsorption to soil particles, leaching and microbial degradation (Fig. 67).⁹³



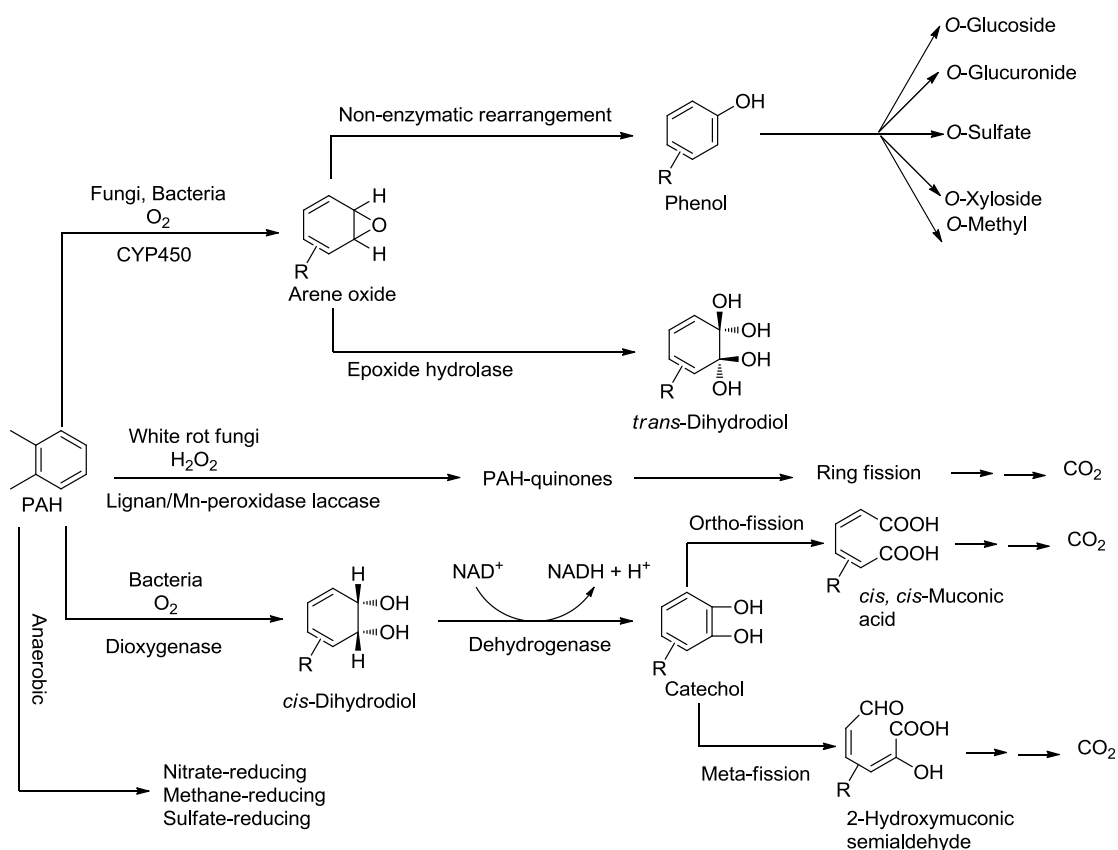
 **Figure 67** - Schematic representation of the environmental fate of PAHs.

Aerobic PAH-degrading bacteria make intensive use of dioxygen as a co-substrate for ring hydroxylating/cleaving oxygenases, however, when saturated sediments are exposed to high carbon loads, e.g. by tar oils containing high amounts of PAHs, they rapidly turn anoxic due to the depletion of dioxygen. Under such conditions, the degradation of PAHs has to be performed by

anaerobic bacteria and specific anaerobic biochemical pathways are involved (Scheme 51).⁹³

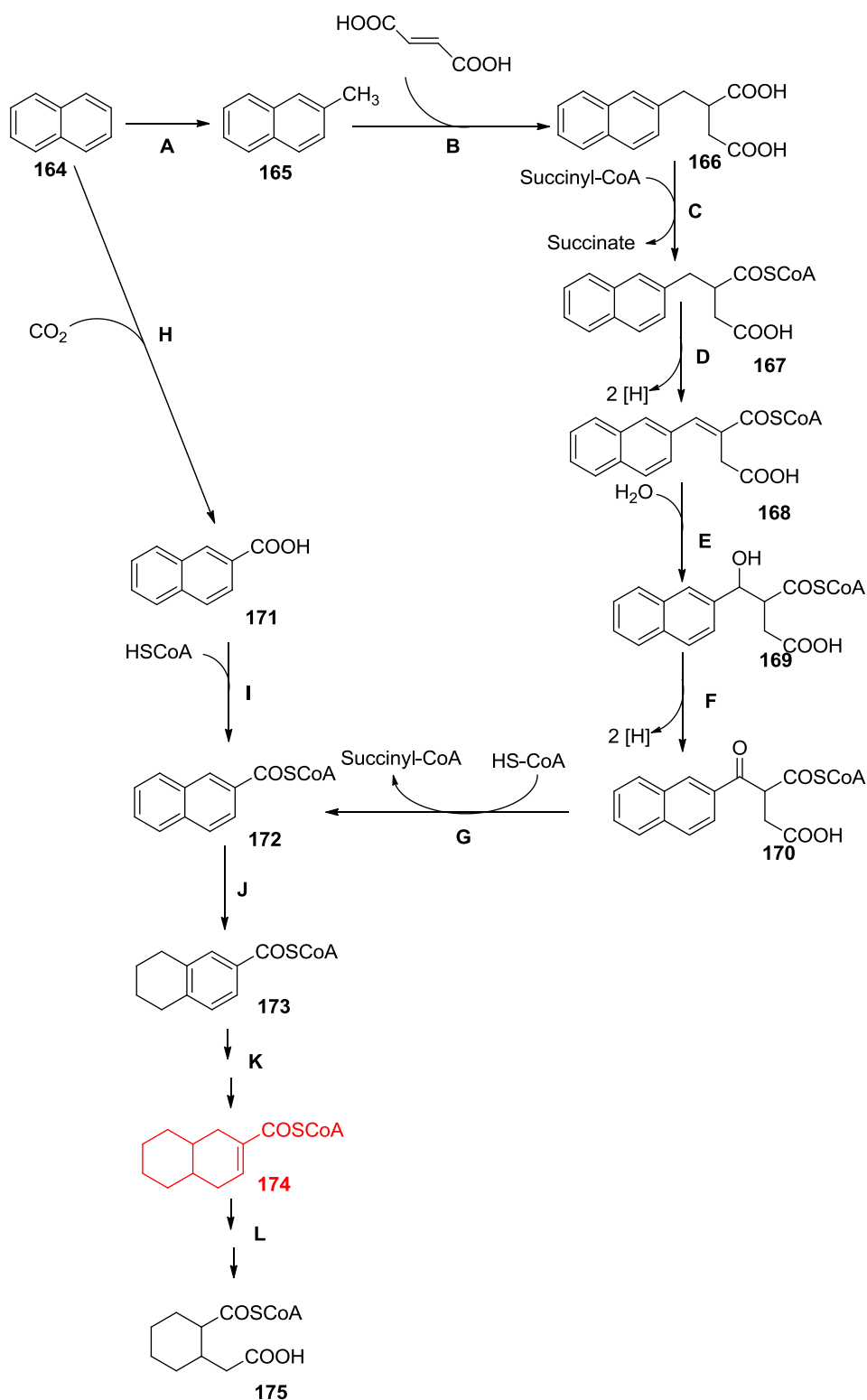
Recalcitrance	PAH	MW (g/mol)	Solubility (mg/dm ³)	Genotoxicity
	 Naphthalene	128.2	32
	 Acenaphthene	154.2	4	+ Ames
	 Anthracene	178.2	0.070
	 Phenanthrene	178.2	1.300
	 Fluoranthene	202.3	0.260	Weak Carcinogen
	 Pyrene	202.3	0.140	± Ames + UDS + SCE
	 Benz[a]anthracene	228.3	0.002	+ Ames + CA + SCE + Carcinogen
	 Benzo[a]pyrene	252.3	0.003	+ Ames + CA + UDS + DA + SCE + Carcinogen

❖ **Table 8** - Chemical structures, physical and toxicological characteristics of polycyclic aromatic hydrocarbons. The symbols are: (DA) DNA adducts, (SCE) sister chromatid exchange, (CA) chromosomal aberrations, (Ames) *Salmonella Typhimurium* reversion assay, (UDS) unscheduled DNA synthesis, (-) not genotoxic.



Scheme 51 - Pathways for the microbial catabolism of polycyclic aromatic hydrocarbons.

In recent years, anaerobic microorganisms have successfully been cultivated with 2-methylnaphthalene, naphthalene or phenanthrene as sole carbon and electron source with different electron acceptors.⁹⁴ These cultures reveal extremely slow growth rates greatly hampering *in vitro* studies of the degradation pathways. The best investigated anaerobic PAH-degrading cultures comprise the sulfate-reducing highly enriched culture N47⁹⁵ and the pure culture NaphS2⁹⁶, which both degrade naphthalene with sulfate as electron acceptor. These studies have suggested a preliminary degradation pathway of naphthalene with two possible main routes to activate the ring in position 2, either carboxylation or methylation followed by fumarate addition (Scheme 52). The carbon atom in position 2 is the most electron rich, which would foster an electrophilic substitution reaction.⁹⁴

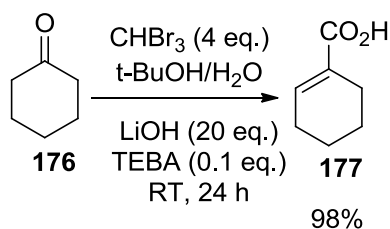


Scheme 52 - Proposed naphthalene and 2-methylnaphthalene degradation pathways. Enzymes involved in the pathway are as follows: (A) naphthalene methyl-transferase; (B) naphthyl-2-methylsuccinyl synthase; (C) naphthyl-2-methyl-succinyl-CoA transferase; (D) naphthyl-2-methyl-succinyl-CoA dehydrogenase; (E) naphthyl-2-methylene succinyl-CoA hydratase; (F) naphthyl-2-hydroxymethyl-succinyl-CoA dehydrogenase; (G) naphthyl-2-oxomethyl-succinyl-CoA thiolase; (H) naphthoate carboxylase; (I) naphthoyl-CoA ligase; (J and K) 2-naphthoyl-CoA reductase; (L) enoyl-CoA hydratase. Cis-2-carboxycyclo-hexylacetic acid is then further degraded to form acetyl-CoA and CO₂.

5.1.1 Synthesis of intermediates

In order to confirm and study the proposed pathway, synthesis of 1,4,4a,5,6,7,8,8a-octahydro-2-naphthoyl-CoA (**174**) was required.

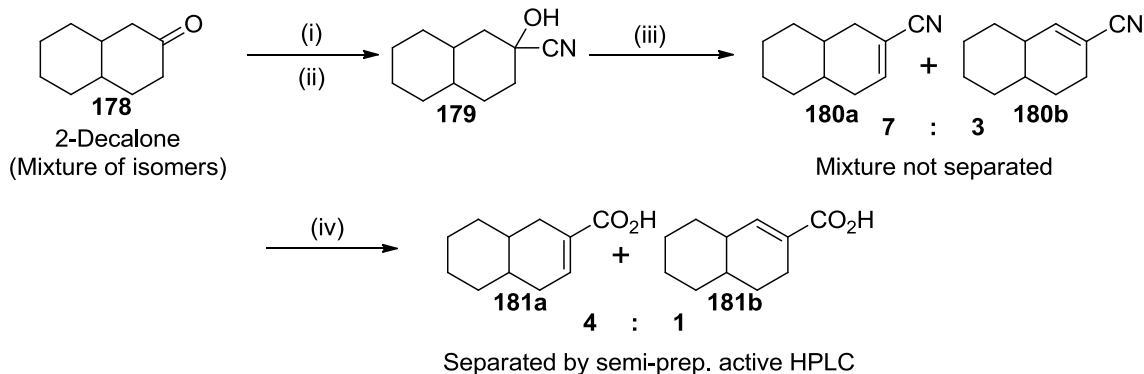
Initial attempts for the synthesis of this intermediate followed a similar procedure to the published synthesis of cyclohexene-1-carboxylic Acid (**14**) from cyclohexanone (**13**) using bromoform (Scheme 53).⁹⁷



TEBA = benzyltriethylammonium chloride

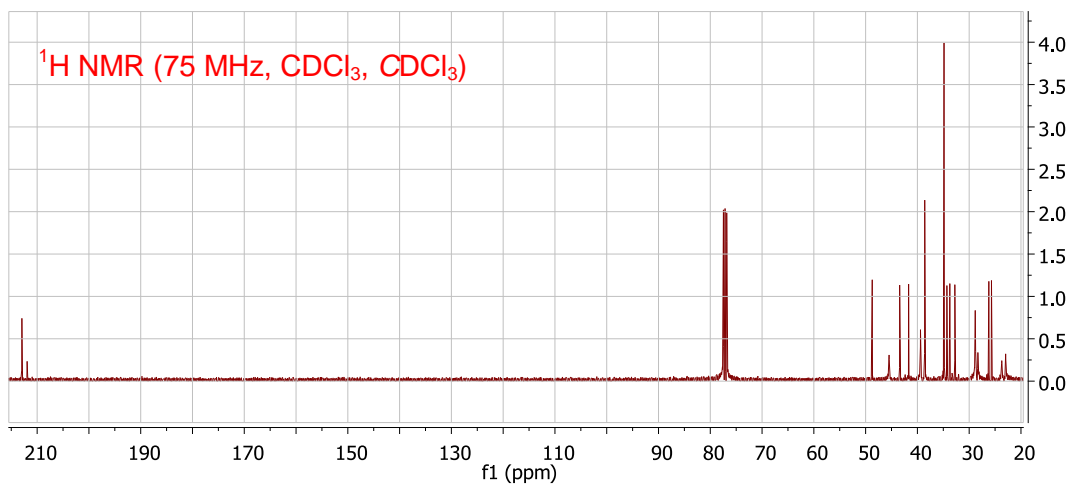
Scheme 53

However, when this procedure was attempted with the commercially available 2-decalone (mixture of isomers) (**178**) as starting material, only a 3% yield of the conjugated acid (**181a**) was obtained. A second method also using the commercially available 2-decalone (**178**) was explored (Scheme 54).⁹⁸



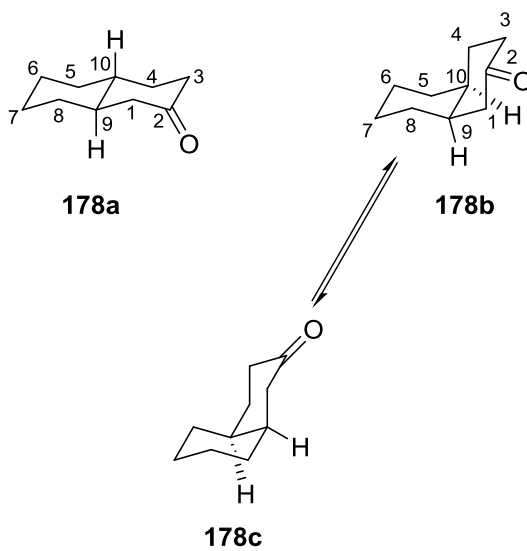
Scheme 54 – Synthesis of 1,4,4a,5,6,7,8,8a-octahydronaphthalene-2-carboxylic acid (**181a**) and 3,4,4a,5,6,7,8,8a-octahydronaphthalene-2-carboxylic acid (**181b**). (i) H_2SO_4 , MeOH, (ii) NaCN, H_2O , RT, 5 h; (iii) 2,6-lutidine, SOCl_2 , Et_2O , 60 °C, 12 h; (iv) H_2SO_4 , H_2O , 110 °C, 24 h.

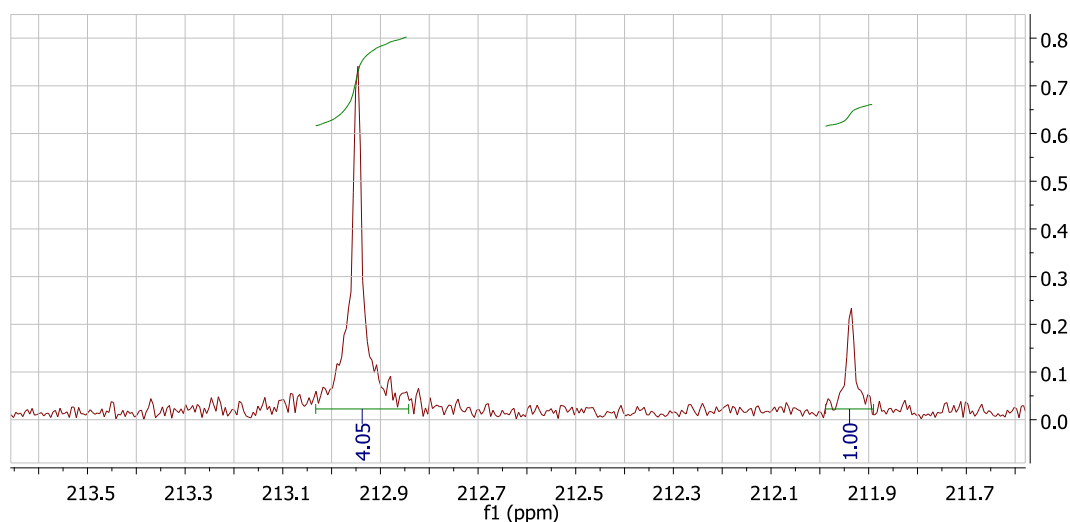
In order to measure the ration *cis*- to *trans*-isomer in the purchased 2-decalone (**178**), ^{13}C -NMR of **178** was obtained and compared with the literature values⁹⁹ reported (Table 9).



❖ **Table 9**

Carbon atom	¹³ C chemical shifts (ppm) of <i>trans</i> -decal-2-ones (in CDCl ₃)	¹³ C chemical shifts (ppm) of <i>cis</i> -decal-2-ones (in CDCl ₃)
C-1	48.65	45.55
C-2	211.93	213.42
C-3	41.62	39.47
C-4	33.68	28.87
C-5	34.25	28.36
C-6	25.64	22.99
C-7	26.15	23.74
C-8	32.72	28.87
C-9	43.38	38.65
C-10	41.69 (d)	34.92 (s)





Nucleophilic addition of the cyanide anion to the ketone **178** afforded the cyanohydrin **179** in high yield (95%). Treatment of cyanohydrin **179** with thionyl chloride using 2,6 lutidine as a bulky base afforded a mixture of nitriles **180a** and **180b** (63% yield) in a ratio of 7:3. Finally, the nitrile mixture **180** was hydrolysed using sulfuric acid to afford a mixture of the corresponding carboxylic acids **181a** and **181b** (4:1 ratio based on ^1H NMR spectra; see fig. 68) in 95% yield.

Two different methods were used to separate the carboxylic acids. The first one using a semi-prep. HPLC, although this method was time consuming and could only be applied to a small quantity of material. However it resulted in a partial separation of isomers.

Due to small quantity of material that was obtained using semi-prep HPLC, purification of the crude product by crystallisation followed by recrystallisation using different solvent mixtures was attempted, recrystallisation from absolute ethanol at 5 °C produced some ball-shaped crystals which were isolated. The comparison of ^1H -NMR of the vinyl hydrogens in the isomers obtained in method 1 and 2, revealed some interesting results.

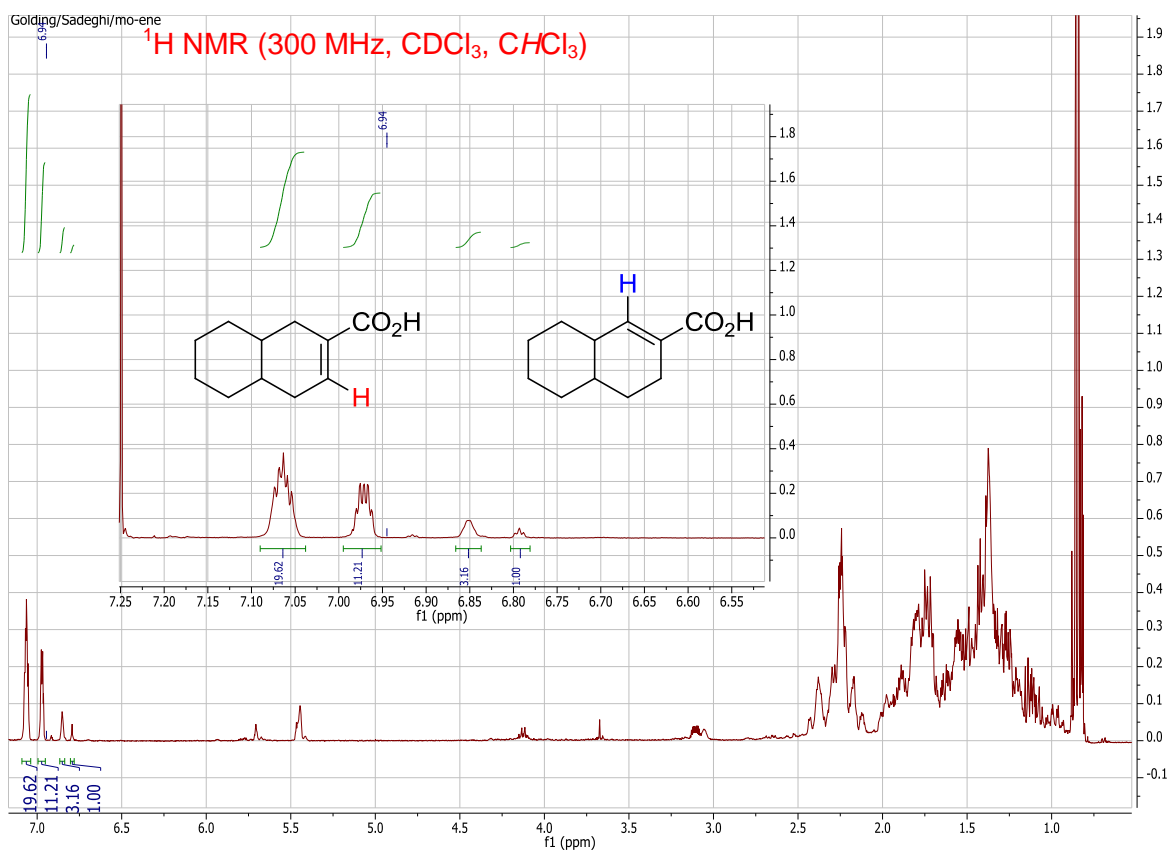


Figure 68 – ¹H-NMR of the crude mixture of **181a** and **181b** carboxylic

Following the separation of the two isomers by semi-prep HPLC, assigning the correct isomer to its corresponding ¹H-NMR could not be done with certainty, X-ray crystallography of the crystals (Fig. 70) obtained from recrystallisation assisted the assignment of ¹H-NMR spectra (Fig. 69). The absolute configuration by X-ray crystallography confirms that the purified crystals are (4a*S*,8a*R*)-1,4,4a,5,6,7,8,8a-octahydronaphthalene-2-carboxylic acid (*cis*-isomer).

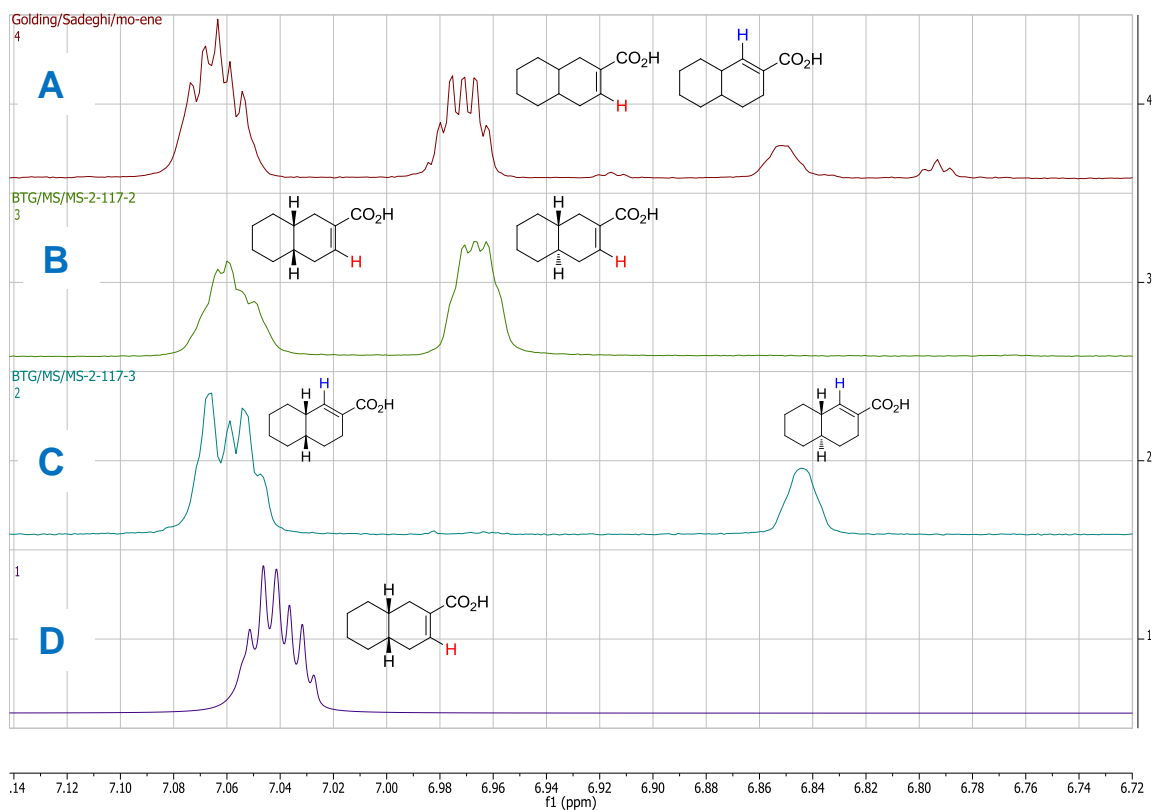


Figure 69 – Comparison of the $^1\text{H-NMR}$ s of the isolated carboxylic acids; **A**, crude product, **B & C**, separated by HPLC, **D**, Obtained via recrystallisation.

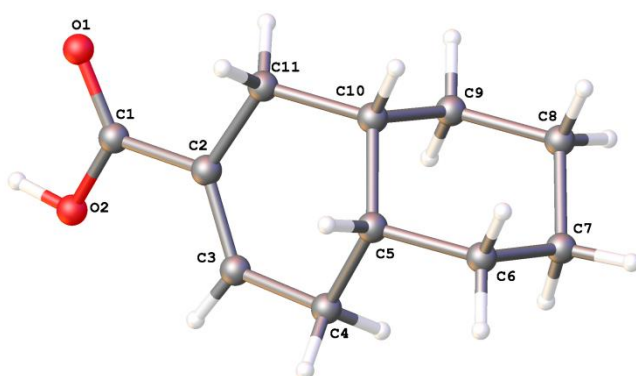


Figure 70 – X-ray crystallography of the crystals obtained via method 2.

5.2 In vitro assay

The synthesised carboxylic acids (**181a & b**) were sent for biological testing in the laboratories of Prof. M. Boll and Prof. R. Meckenstock.¹⁰⁰

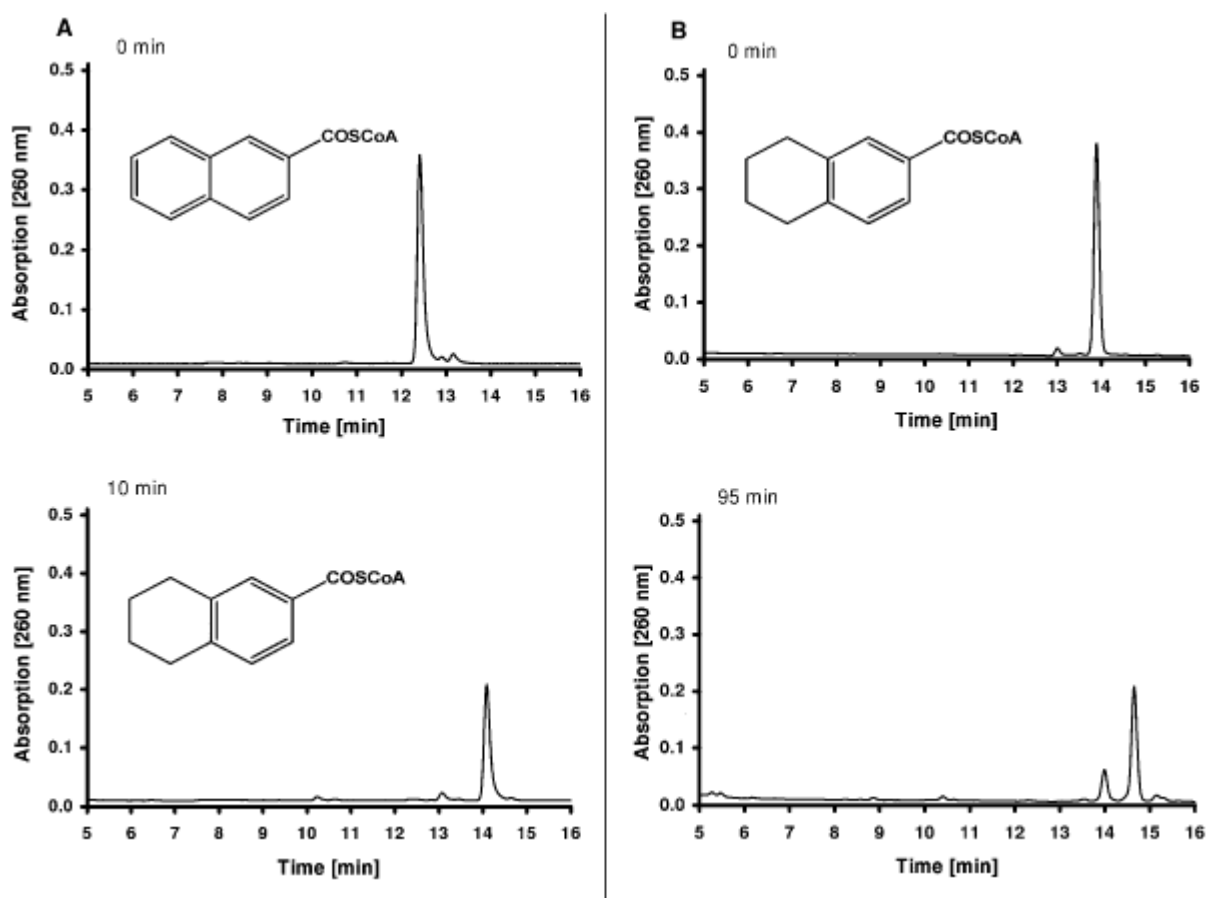
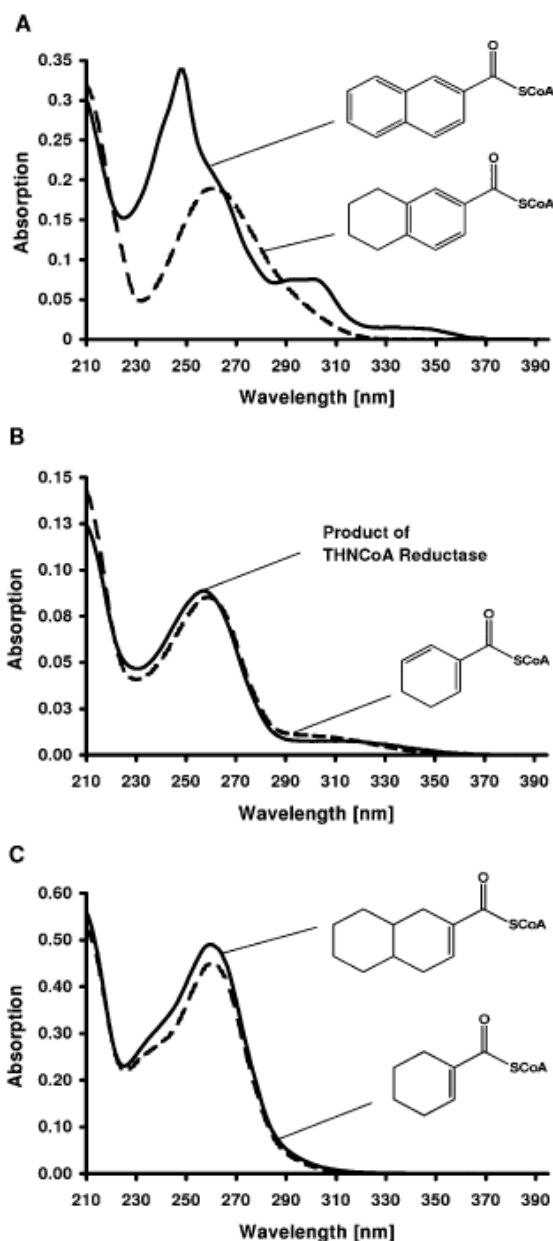


Figure 71 - HPLC analysis of *in vitro* conversion of NCoA and THNCoA by extracts from N47 grown on naphthalene.

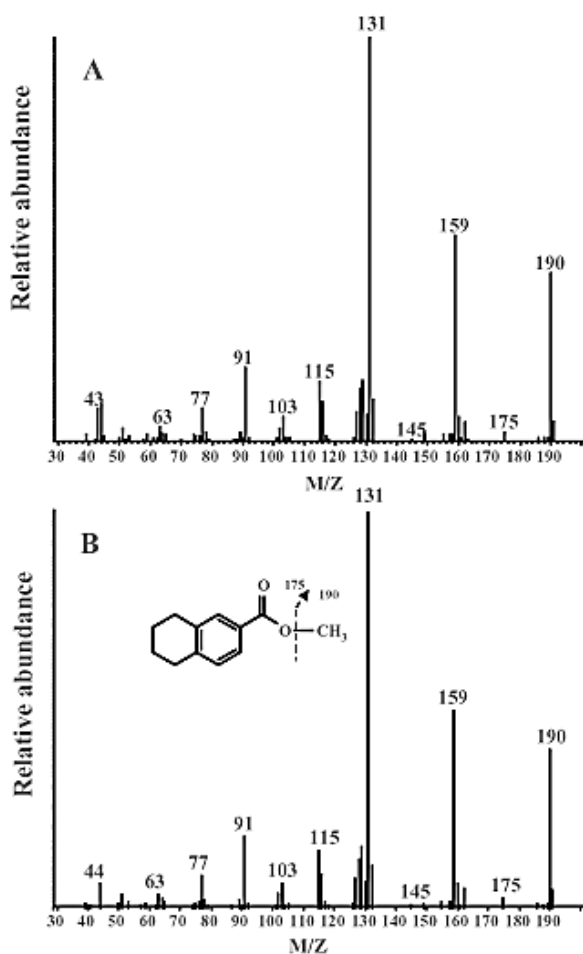
Previous studies with the sulfate-reducing enrichment culture N47 have indicated that naphthalene is initially converted to 2-naphthoic acid via a carboxylation reaction.⁹⁴ The product formed is then assumed to be activated by an ATP-dependent 2-naphthoic acid CoA ligase or by a CoA transferase. In order to study the subsequent anticipated reductive dearomatisation steps, cell extracts from culture N47 anaerobically grown on naphthalene and sulfate as electron donor and acceptor respectively, were reacted with 2-naphthoyl-CoA (NCoA) in anoxic *in vitro* assays. The NCoA used in these studies was chemically synthesised from 2-naphthoic acid and CoA via the corresponding succinimidyl ester. When extracts from strain N47 grown on naphthalene/sulfate were anaerobically incubated with 0.2 mM NCoA, the time-, protein- and sodiumdithionite-(5 mM) dependent decrease of NCoA and the concomitant

formation of a major more apolar product was observed by reversed phase HPLC analysis (Fig. 71). The product co-migrated with an authentic 5,6,7,8-tetrahydro-2-NCoA (THNCoA) standard and displayed an identical UV/vis spectrum (Fig. 72A). GC-MS analysis of the hydrolysed and methyl-ester derivatised sample showed similar retention time and mass fragments as the methyl-ester derivative of authentic 5,6,7,8-tetrahydro-2-naphthoic acid (m/z ion fragments of m/z 77, 91, 103, 115, 131, 159, 175 and 190 for the methyl-ester derivative) (Fig. 73).



✚ **Figure 72** – Figure adapted from Eberlein et. al.⁴ UV/vis spectra of substrates/products of NCoA reductase and THNCoA reductase. **A.** NCoA (solid line) and THNCoA (dotted line) standards; the UV spectrum of product formed by NCoA reductase was identical to that of an authentic THNCoA standard. **B.** The predicted HHNCoA product (solid line) and cyclohexa-1,5-diene-1-carboxyl-CoA (dotted line); the latter is the conjugated two-electron reduced product formed from benzoyl-CoA by benzoyl-CoA reductases. **C.** 1,4,4a,5,6,7,8,8a-octahydro-2-naphthoyl-CoA (**181a**) (solid line) and Cyclohex-1-en-1-carboxyl-CoA (dotted line).

Virtually no product was identified in the initial phase of the reaction that could be assigned to a two electron reduced intermediate. Such a compound was expected to elute from the reversed phase HPLC column used between NCoA (retention time 12.5 min) and THNCoA (retention time 14 min). Thus, NCoA reductase is suggested to catalyse a four-electron reduction of the substrate without release of a two-electron reduced dihydro-NCoA intermediate. The product formed from THNCoA exhibited a UV/vis spectrum highly similar to that of the fully conjugated cyclic dienoyl-CoA compound cyclohexa-1,5-diene-1-carboxyl-CoA, the product of ATP-dependent BCR (Fig. 72B). This spectrum is characterised by a shoulder at 310 nm caused by the dienoyl-CoA moiety indicating that the product formed from THNCoA is a hexahydronaphthoyl-CoA compound. In contrast, a conjugated octahydro-2-naphthoyl-CoA product has a clearly distinct UV spectrum that is very similar to that of a cyclic, conjugated monoenoil-CoA compound (Fig. 72C). LC-MS-MS analysis of the free carboxylic acid of the THNCoA reductase product obtained after alkaline hydrolysis of the CoA-ester revealed a mass pair ion of 177.1–133.1 with a retention time of 22.04 min corresponding to hexahydro-2-naphthoic acid

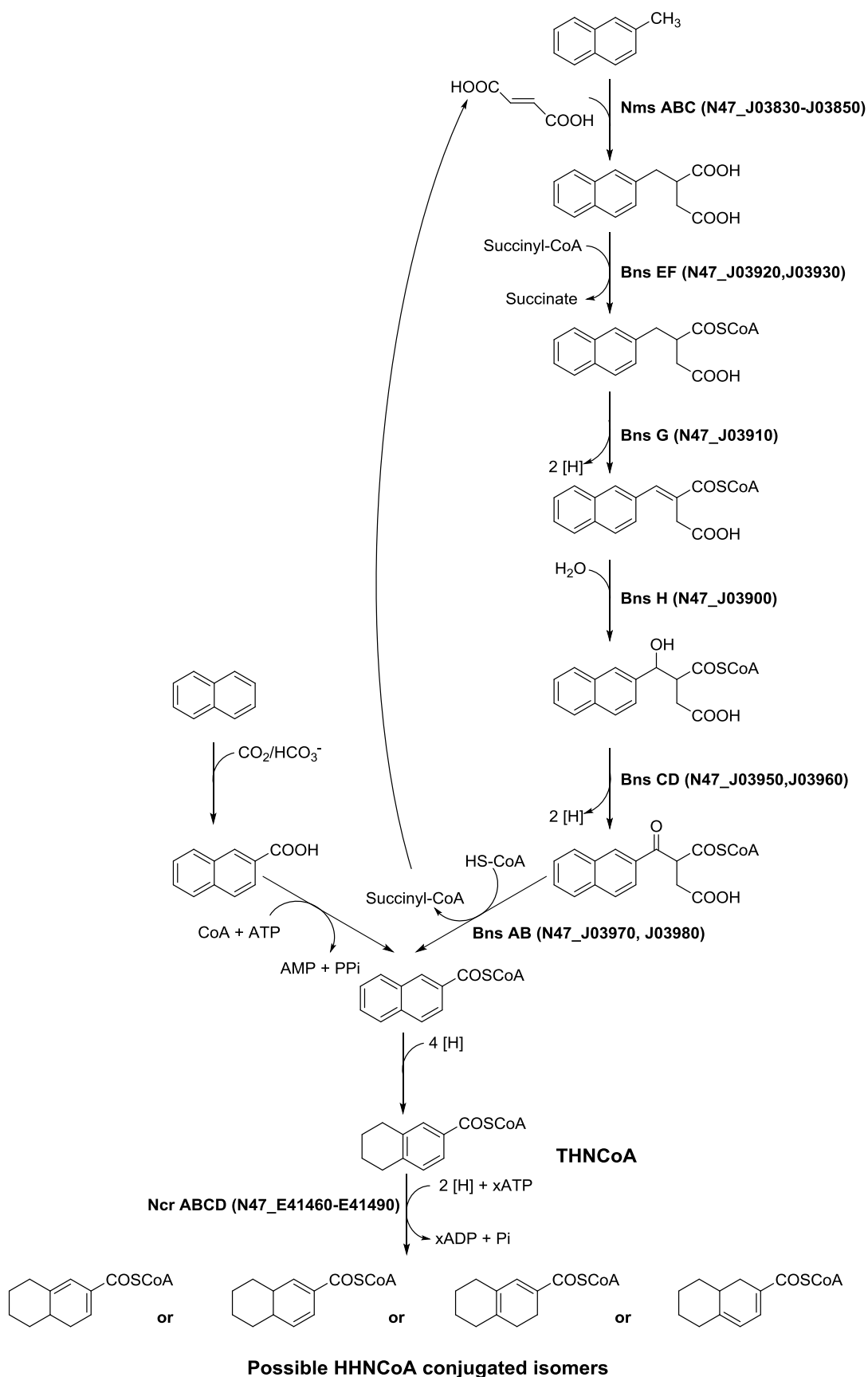


(HHN). These values were two mass units lower than that of a 3,4,4a,5,6,7,8,8a-octahydro-2-naphthoic acid (**181a**) chemical standard with a mass pair ion of 179.05–135.05 with a retention time of 22.45 min (Fig. 7). These findings suggest that THNCoA was reduced by a two electron reduction to a conjugated hexahydro-NCoA (HHNCoA) product.

Figure 73 – Figure adapted from Eberlein et al.⁴ Mass spectrum profiles of the methyl-ester derivative detected at the retention time of 27.7 min from (A) *in vitro* conversion of NCoA by extracts from N47 grown on naphthalene after hydrolysis of the CoA ester with 1 N NaOH; and (B) methyl-ester derivative of 5,6,7,8-tetrahydro-2-naphthoic acid authentic chemical

5.2 Conclusion

As shown in Scheme 55, there are four possible isomers of hexahydro-2-naphthoic acid with a fully conjugated system of the two olefinic bonds and the carbonyl moiety. In bold, are the putative genes coding for the enzymes catalysing the corresponding reactions, in parenthesis, their respective locus tags on the N47 genome. NmsABC, naphthyl-2-methyl-succinate synthase; BnsEF, naphthyl-2-methyl-succinate CoA transferase; BnsG, naphthyl-2-methyl-succinyl-CoA dehydrogenase; BnsH, naphthyl-2-methylene-succinyl-CoA hydratase; BnsCD, naphthyl-2-hydroxymethyl-succinyl-CoA dehydrogenase; BnsAB, naphthyl-2-oxomethyl-succinyl-CoA thiolase; NcrABCD, THNCoA reductase (Selesi *et al.*, 2010). Abbreviations THNCoA and HHNCoA stand for 5,6,7,8-tetrahydro-2-naphthoyl-CoA and hexahydro-2-naphthoyl-CoA respectively.



Scheme 55 - Proposed peripheral pathways for anaerobic naphthalene and 2-methylnaphthalene degradation to naphthoic acid and the central naphthoyl-CoA pathway in enrichment culture N47.

Chapter 6

Experimental

6.1 General information

Melting points were determined on a Stuart SMP3 hot stage apparatus and are uncorrected. Infrared spectra were recorded on a Varian 800 FT-IR Scimitar Series infrared spectrometer. Mass spectra were recorded on Waters ACQUITY UPLC™ LCT premier MS in positive ion mode. Accurate mass analyses were measured using a Finnigan MAT95 or MAT900 by the EPSRC National Mass Spectrometry Service Centre, Grove Building, Swansea University, Singleton Park, Swansea, Wales, UK, SA2 8PP. ¹H NMR spectra were recorded on a Brüker Avance 300 MHz or Jeol ESC 400 MHz or Jeol Lambda/Eclipse 500 MHz spectrometers at ambient temperatures in deuterated chloroform or methanol with tetramethylsilane as internal standard. Data for ¹H spectra are reported as follows: chemical shifts are measured in ppm from internal tetramethylsilane on the δ scale, integration, multiplicity (br = broad, s = singlet, d = doublet, t = triplet, q = quartet, dd = doublet of doublets, ddd = doublet of doublet of doublets, dt = doublet of triplets, ddt = doublet of doublet of triplets and m = multiplet), coupling constants (*J*) are given in Hz, integration and assignment where possible. ¹³C NMR was recorded on a Brüker Avance (75.5 MHz) or Jeol ESC (100.5 MHz) or Jeol Lambda/Eclipse (125 MHz) spectrometers at ambient temperature. Chemical shifts are reported in ppm from tetramethylsilane on the δ scale, using solvent resonance as the internal standard [deuterated chloroform (CDCl₃) at 77.0 ppm]. Optical rotations were measured on a PolAAR 2001 digital polarimeter using a 1.0 dm cell at ambient temperature and are reported as follows [α]_D^T (c g/100 mL, solvent).

Thin layer chromatography was performed on EM reagent 0.25 mm silica gel 60F plates. Visualisation was accomplished with UV light and aqueous potassium permanganate (VII) solution. Medium pressure ('flash') column chromatography was performed on Fluorochem LC3025 (40-63 μ m) silica gel, eluting with the indicated solvent under forced flow.

Chemicals were purchased from the Aldrich, Alfa Aesar or Fluorochem companies and were used as supplied except where indicated. All reactions were carried out under an atmosphere of nitrogen in pre-dried glassware. Where necessary, solvents were dried prior to use.

6.2 Details of microbiological experiments

The deuterated hexanes were transferred to separate glass ampoules, thermally sealed and sent to the microbiology laboratory to be used as growth substrates for strain HxN1.

The following work was carried out by Prof. Rene Jarling's team⁷ and is as follows:

The *n*-alkane-degrading betaproteobacterium strain HxN1 was anaerobically cultivated in chemically defined, bicarbonate-buffered, ascorbate-reduced (4 mM) and nitrate-containing (9 mM) medium.⁹ Flat glass bottles (500 mL), containing 400 mL of medium and sealed with butyl rubber stoppers under a head space of N₂-CO₂ (90:10, vol/vol), were used for cultivation. *n*-Heptane, *n*-hexane and *n*-(²H₂)hexane stereoisomers were added to the medium diluted (0.1–5%, vol/vol) in sterile, deaerated 2,2,4,4,6,8,8-heptamethylnonane as an inert carrier phase (10 mL of mixture per bottle), using N₂-flushed syringes. To scavenge possible traces of dioxygen with the reductant, the freshly prepared, *n*-alkane/carrier phase-containing medium was then preincubated for > 24 h prior to inoculation. Growing cultures of strain HxN1, passaged > 5 times with *n*-heptane as sole organic substrate, were used for inoculation. Cultures were incubated at 28°C on a slowly rotating shaker (50 rpm) in nearly horizontal position, avoiding contact of the *n*-alkane/carrier phase mixture with the stoppers. Cultures were subjected to metabolite extraction immediately after depletion of nitrate and formed nitrite, both of which were monitored with disposable test strips (Merck, Darmstadt, Germany).

Metabolite extraction was essentially performed as described. Cultures for metabolite analysis were heated in closed bottles in a water bath to 85°C for 15 min to inactivate eventually present enzymes that may catalyse reactions with dioxygen during further handling in the air. In the *n*-hexane-grown cultures, the aqueous phase was separated from the overlying carrier phase via a separatory funnel. The heated cells were removed by centrifugation (7,000 3 *g*, 20 min) to avoid possible interference with phase separation during subsequent ether extraction. After heat inactivation, the culture broth was separated from the

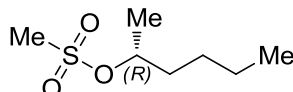
carrier phase, acidified with HCl and extracted 3 times with 50 mL diethyl ether. The combined ether extracts were dried over anhydrous Na₂SO₄ and stored at 4°C in glass bottles sealed with Teflon-coated screw caps.

n-Heptane (5%, vol/vol) was used as growth substrate instead of *n*-hexane to avoid the formation of *n*-hexane-derived metabolites subsequently interfering with the analysis of the targeted *n*-(²H₂)hexane-derived metabolites and also in order to use the smallest amounts of *n*-(²H₂)hexane stereoisomers per incubation experiment due to little availability of deuterated hexanes.

A pre-experiment with *n*-heptane (5%, vol/vol) and rising amounts of *n*-hexane (0.1–1%, vol/vol) was conducted to determine the lowest *n*-hexane concentration still allowing for recording an optimal metabolite profile. The main Incubation experiments were performed with cultures of strain HxN1 that had been adapted to *n*-heptane using a mixture of *n*-heptane and a dideuterated *n*-hexane (8:1).

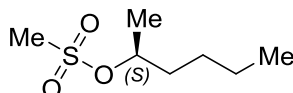
3. Synthesis of (1-methylpentyl)succinic acid stereoisomers

(*R*)-Hexan-2-ol *O*-methanesulfonate (**161a**)³



To (*R*)-hexan-2-ol (1.00 g, 1.2 mL, 9.8 mmol) and triethylamine (1.29 g, 1.8 mL, 12.7 mmol) in dichloromethane (2.0 mL) stirred under nitrogen at 0 °C was added dropwise methanesulfonyl chloride (1.46 g, 1.0 mL, 12.7 mmol). Within 30 min a white precipitate was formed and the mixture was stirred for a further 60 min at 0°C. Saturated aqueous NaHCO₃ (6 mL) was added and stirring was continued for 15 min. After separation of the phases the organic layer was washed with water (6 mL), dried (MgSO₄) and concentrated to afford the title compound (1.51 g, 85% yield) as a yellow oil. ¹H NMR (300 MHz, CDCl₃, CHCl₃): δ=4.78-4.67 ppm (m, 1H; CH), 2.93 (s, 3H; SCH₃), 1.35 (d, 3J(H,H)=6.3 Hz, 3H; CHCH₃), 1.33-1.25 (m, 6H; 3×CH₂), 0.85 (m, 3H; CH₂CH₃).

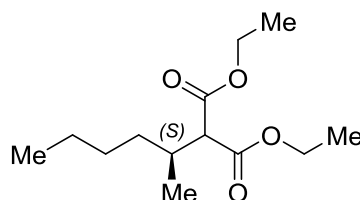
(*S*)-Hexan-2-ol *O*-methanesulfonate (**161b**)



Prepared following the same procedure as **161a**, from (*S*)-hexan-2-ol. ¹H NMR (300 MHz, CDCl₃, CHCl₃): δ=4.78-4.67 ppm (m, 1H; CH), 2.93 (s, 3H; SCH₃),

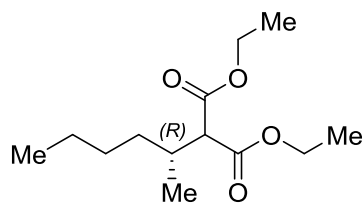
1.35 (d, $^3J(\text{H,H})=6.3$ Hz, 3H; CHCH_3), 1.33-1.25 (m, 6H; $3\times\text{CH}_2$), 0.85 (m, 3H; CH_2CH_3).

Diethyl (*S*)-(1-methylpentyl)malonate (162a)³



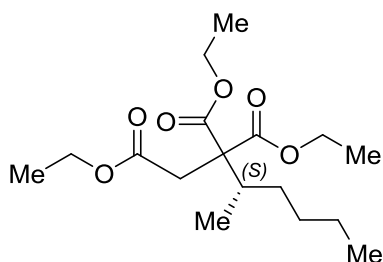
To a suspension of sodium hydride (0.23 g, 5.8 mmol, 60% in mineral oil) in dry 1,2-dimethoxyethane (4.0 mL) at room temperature was added dropwise diethyl malonate (0.91 g, 0.86 mL, 5.7 mmol) over 30 min. Hydrogen was evolved and the cloudy mixture became clear. The solution was stirred for 30 min after which (*R*)-hexan-2-ol *O*-methanesulfonate (0.85 g, 4.24 mmol) was added dropwise. The mixture was stirred at 85°C for 5 h and allowed to cool to room temperature. Diethyl ether (5.5 mL) and saturated ammonium chloride (4.5 mL) were added. After phase separation, the organic layer was washed with water (5 mL), dried (MgSO_4) and concentrated to afford a crude oil. The oil was purified by medium pressure liquid chromatography on silica eluting with petrol – diethyl ether (9:1, v/v) to afford the title compound (0.76 g, 73%) as a colourless oil. *R*_f 0.6 petrol – diethyl ether (5:1, v/v). In a scale-up synthesis, the diester (53%) was purified by fractional distillation: bp 86-89°C (0.5 Torr) [diethyl malonate and the precursor mesylate were collected at bp 28-32°C and 60-64°C, respectively]. ^1H NMR (300 MHz, CDCl_3 , CHCl_3): $\delta=4.12$ ppm (q, $^3J(\text{H,H})=7.1$ Hz, 4H; $2\times\text{OCH}_2$), 3.16 (d, $^3J(\text{H,H})=8.2$ Hz, 1H; COCH), 2.16 (m, 1H; CH_3CH), 1.39–1.07 (m, 12H; $2\times\text{OCH}_2\text{CH}_3$, $3\times\text{CH}_2$), 0.91 (d, $^3J(\text{H,H})=6.8$ Hz, 3H; CHCH_3), 0.82 (t, $^3J(\text{H,H})=6.8$ Hz, 3H; CH_2CH_3).

Diethyl (*R*)-(1-methylpentyl)malonate (162b)



Prepared following the same procedure as **162a**, from (*S*)-hexan-2-ol *O*-methanesulfonate. ^1H NMR (300 MHz, CDCl_3 , CHCl_3): δ =4.12 ppm (q, $^3J(\text{H,H})=7.1$ Hz, 4H; 2 \times OCH $_2$), 3.16 (d, $^3J(\text{H,H})=8.2$ Hz, 1H; COCH), 2.16 (m, 1H; CH $_3$ CH), 1.39–1.07 (m, 12H; 2 \times OCH $_2$ CH $_3$, 3 \times CH $_2$), 0.91 (d, $^3J(\text{H,H})=6.8$ Hz, 3H; CHCH $_3$), 0.82 (t, $^3J(\text{H,H})=6.8$ Hz, 3H; CH $_2$ CH $_3$).

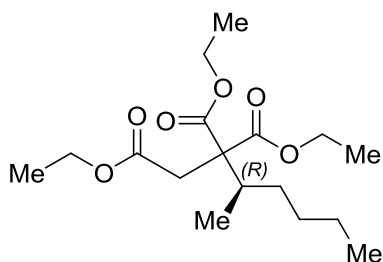
Triethyl (*S*)-3-methylheptane-1,2,2-tricarboxylate (**163a**)



A suspension of sodium hydride (30 mg, 0.75 mmol, 60% in mineral oil) in dry tetrahydrofuran (5.0 mL) was cooled to 0°C and to this was added diethyl (*S*)-(1-methylpentyl)malonate (190 mg, 0.80 mmol) dropwise over a period of 30 min. The reaction mixture was allowed to warm up to room temperature and stirred for 1.5 h. The mixture was cooled to 0°C and ethyl bromoacetate (0.12 mg, 77 μL , 0.71 mmol) was added dropwise over a period of 30 min. After stirring for 48 h the mixture was poured into 1.5 M hydrochloric acid (65 μL) and ice (1.2 g). Extraction with dichloromethane (4 \times 2 mL), drying (MgSO_4) and removal of the solvent gave the crude product as light brown oil. The oil was purified by medium-pressure liquid chromatography on silica eluting with petrol – ethyl acetate (10:1, v/v) to afford triethyl (*S*)-3-methylheptane-1,2,2-

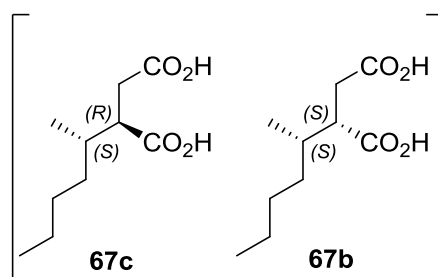
tricarboxylate (161 mg, 61%) as a colourless oil. *R_f* 0.2 petrol – ethyl acetate (5:1, v/v). In a scale-up reaction most of the excess of diester was removed by distillation (bp 86-89°C, 0.5 Torr) and a short path silica column was performed to give the triester (48%). ¹H NMR (300 MHz, CDCl₃, CHCl₃): δ=4.14 ppm (m, 4H; 2×COOCH₂), 4.05 (q, ³*J*(H,H)=7.1 Hz, 2H; CH₂COOCH₂), 2.82 (s, 2H; CCH₂), 2.03 (m, 1H; CH₃CH), 1.46–0.95 (m, 15H; 3×OCH₂CH₃, 3×CH₂), 0.90 (d, ³*J*(H,H)=6.8 Hz, 3H; CHCH₃), 0.81 (t, ³*J*(H,H)=6.9 Hz, 3H; CH₂CH₃); ¹³C NMR (100 MHz, CDCl₃, CDCl₃): δ=171.1 ppm, 170.4, 61.7, 61.3, 60.9, 60.1, 38.8, 37.7, 32.0, 30.3, 22.7, 15.0, 14.1; LC-MS (ESI⁺): *m/z* 331([M+H]⁺); IR: 2350, 1766, 902, 722, 649, 514 cm⁻¹.

Triethyl (*R*)-3-methylheptane-1,2,2-tricarboxylate (**163b**)



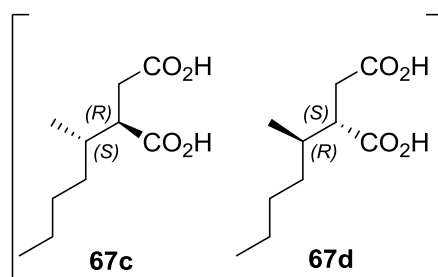
Prepared following the same procedure as **163a**, from (*R*)-(1-methylpentyl)malonate. ¹H NMR (300 MHz, CDCl₃, CHCl₃): δ=4.14 ppm (m, 4H; 2×COOCH₂), 4.05 (q, ³*J*(H,H)=7.1 Hz, 2H; CH₂COOCH₂), 2.82 (s, 2H; CCH₂), 2.03 (m, 1H; CH₃CH), 1.46–0.95 (m, 15H; 3×OCH₂CH₃, 3×CH₂), 0.90 (d, ³*J*(H,H)=6.8 Hz, 3H; CHCH₃), 0.81 (t, ³*J*(H,H)=6.9 Hz, 3H; CH₂CH₃).

(2*R*,1'*S*)- and (2*S*,1'*S*)-(1-Methylpentyl)succinic acid (**67b** and **67c** mixture)



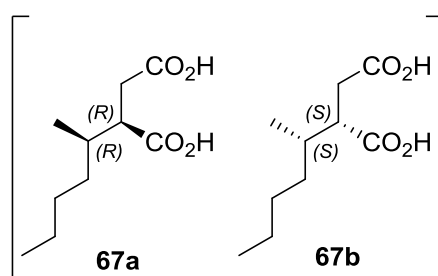
Triethyl (S)-3-methylheptane-1,2,2-tricarboxylate (150 mg, 0.45 mmol) was boiled at reflux with concentrated hydrochloric acid (150 mL) for 48 h. The resulting mixture was concentrated to afford (2*R*,1'*S*)- and (2*S*,1'*S*)-(1-methylpentyl)succinic acid (ca. 1:1 mixture, 85 mg, 93%) as a yellow sticky solid. ¹H NMR (300 MHz, CDCl₃, CHCl₃): δ=3.18-2.40 ppm (m, 3H; H at C-2 and C-3), 1.98-1.85 (m, 0.5H; CHCHCH₃, 2*R*,1'*S*), 1.83-1.71 (m, 0.5H; CHCHCH₃, 2*S*,1'*S*), 1.35-1.05 (m, 6H; 3×CH₂), 0.92-0.79 (m, 6H; CH₂CH₃, CHCH₃); ¹³C NMR (100 MHz, CDCl₃, CDCl₃): δ=181.5 ppm, 180.8, 179.5, 179.4, 46.4, 45.8, 34.9, 34.2, 33.5, 31.3, 29.5, 29.4, 22.8, 17.1, 16.1, 14.1; LC-MS (ESI): *m/z* 201 ([M-H]). The above synthetic route was also applied to (S)-hexan-2-ol and racemic hexan-2-ol. The former gave a mixture of (2*S*,1'*R*)- and (2*R*,1'*R*)-(1-methylpentyl)succinic acid, whereas the latter gave a mixture of all four product stereoisomers. The racemic mixture of (2*S*,1'*R*)- and (2*R*,1'*S*)-(1-methylpentyl)succinic acid was obtained by preferential crystallization (vapour diffusion) of all four isomers from petrol/ethyl acetate. The relative configuration was confirmed by X-ray crystallography (we thank Dr. R. Harrington, Newcastle University, for this result). The mother liquor was concentrated to afford a mixture enriched in (2*R*,1'*R*)- and (2*S*,1'*S*)-(1-methylpentyl)succinic acid.

(2*S*,1'*R*)- and (2*R*,1'*S*)-(1-Methylpentyl)succinic acid (67c and 67d mixture)



Mp 143 – 144°C; ¹H NMR (400 MHz, CD₃OD, CH₃OD): δ=2.83-2.23 ppm (m, 3H; H at C-2 and C-3), 1.95-1.84 (m, 1H; CHCHCH₂), 1.41-1.16 (m, 6H; 3×CH₂), 0.90 (t, ³J(H,H)=7.0 Hz, 3H; CH₂CH₃), 0.86 (d, ³J(H,H)=6.9 Hz, 3H; CHCH₃); ¹³C NMR (100 MHz, CD₃OD, CH₃OD): δ=177.1 ppm, 175.1, 45.6, 34.4, 33.9, 30.8, 29.4, 22.4, 15.2, 13.0; LCMS (ESI⁻): *m/z* 201 ([M-H]⁻).

(2R,1'R)- and (2S,1'S)-(1-Methylpentyl)succinic acid (67a and 67b mixture)



Mp 87 – 89°C; ¹H NMR (400 MHz, CD₃OD, CH₃OD): δ=2.80-2.31 ppm (m, 3H; H at C-2 and C-3), 1.83-1.71 (m, 1H; CHCHCH₂), 1.47-1.08 (m, 6H; 3×CH₂), 0.90 (d, ³J(H,H)=6.9 Hz, 3H; CHCH₃), 0.88 (t, ³J(H,H)=4.9 Hz, 3H; CH₂CH₃); ¹³C NMR (100 MHz, CD₃OD, CH₃OD): δ=178.3 ppm, 176.6, 36.6, 35.2, 34.9, 31.0, 24.1, 17.7, 17.1, 14.6; LCMS: *m/z* (ESI⁻): 201 ([M-H]⁻).

4. Assignment of configuration of stereocenters in (1-methylpentyl)succinic acid isomers produced by strain HxN1 during anaerobic growth with *n*-hexane

a) Derivatization of (1-methylpentyl)succinic acid

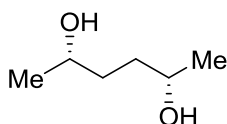
Derivatization of (1-methylpentyl)succinic acid to 3-(1-methylpentyl)-1-(1-phenylethyl)pyrrolidine-2,5-diones / *N*-(1-phenylethyl) 3-(1-methylpentyl)succinimides was performed using a modification of the procedure described that was suitable for small sample sizes.[3] (1-Methylpentyl)succinic acid (0.75 mg, 0.004 mmol) or a solvent-free extract of HxN1 (from 400 mL culture, acidified and extracted with diethyl ether), 2 mg (*R*)-1-phenylethylamine (2 μ L, 0.017 mmol), 1 mL toluene and no more than 4 pellets of 3Å molecular sieve were heated at reflux for 2 h. After removal of the solvent under reduced pressure the residue was taken up in 0.5 mL dichloromethane (GC grade) for analysis by gas chromatography (GC).

b) Gas chromatographic separation of 3-(1-methylpentyl)-1-(1-phenylethyl)pyrrolidine-2,5-diones / N-(1-phenylethyl) 3-(1-methylpentyl)succinimides

This was performed using an Agilent 6890A gas chromatograph equipped with a PTV injection system, a flame ionisation detector and a HP-INNOWax fused silica capillary column (Agilent; length 30 m, inner diameter 0.25 mm, film thickness 0.25 μ m). Helium was used as carrier gas at a constant flow of 1.5 mL/min. Upon sample injection at an injector temperature of 250°C the injector was set to splitless mode for 120 s. The GC oven temperature was programmed from 60°C (hold time 1 min) to 200°C at a heating rate of 10°C/min and further to 250°C (hold time 40 min) at a heating rate of 8°C/min. The resulting chromatograms are shown in Supporting Figure 1. The results were confirmed by separation of the same samples using the same gas chromatograph, however, equipped with a BPX5 fused silica capillary column (SGE; length 50 m, inner diameter 0.22 mm, film thickness 0.25 μ m) or a DB-FFAP fused silica capillary column (Agilent; length 60 m, inner diameter 0.25 mm, film thickness 0.25 μ m). For these analyses the GC oven temperature was programmed from 50°C (initial hold time 1 min) to 310°C (final hold time 30 min) at a heating rate of 3°C/min or from 120°C to 240°C (final hold time 25 min) at a heating rate of 8°C/min, respectively.

7. Synthesis and analytical characterization of deuterated *n*-hexanes

(2*S*,5*S*)-Hexan-2,5-diol (124) ¹⁰¹

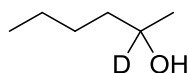


Baker's yeast (60 g) was added to a stirred solution of sucrose (100 g, 0.29 mol) in H₂O (520 mL) and allowed to stir for 1 h and acetyl acetone (2.85 g, 2.9 mL, 25 mmol) was added and additional solution of sucrose (75 g, 0.22 mol) in H₂O (330 mL) was added to the mixture after 24 h, followed by addition of another portion of acetyl acetone (2.85 g, 2.9 mL, 25 mmol) 1 h later, after 72 h an additional portion of yeast (20 g) and sucrose (40 g, 0.17 mol) in H₂O (150 mL) were added and the mixture was stirred for another 72 h. The mixture was suction filtered through a thin layer of celite (30 g), followed by removal of the water under reduced pressure to afford a crude yellow solid, ethyl acetate (500 mL) was added to the crude residue and the mixture was allowed to stir overnight.

The mixture was filtered again through celite (15g), dried (MgSO₄) and concentrated to afford a yellow oil, the residue was dissolved in a minimum amount of ethyl acetate at reflux and allowed to cool slowly to room temperature, then stored at 5 °C overnight. Collection by suction filtration and drying under vacuum at room temperature afforded the diol (3.31 g, 28.0 mmol, 56 %) as a white crystalline solid.

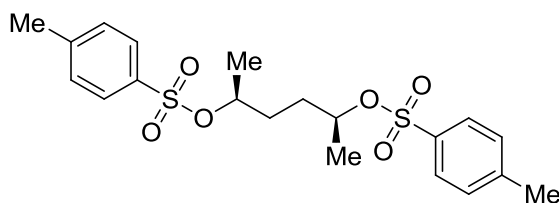
¹H NMR (300 MHz, CDCl₃, CHCl₃) δ=3.76 ppm (m, 2H, CH), 2.51 (br s, 2H, OH), 1.48 (m, 4H, 2 × CH₂), 1.14 (d, ³J(H,H)=6.2 HZ, 6H, CH₃).

2-deuteriohexan-2-ol (130)



^1H NMR (300 MHz, CDCl_3 , CHCl_3) δ =1.44-1.15 ppm (m, 6H, 3 \times CH_2), 1.11 (m, 3H, CDOHCH_3), 0.84 (m, 3H, CH_3).

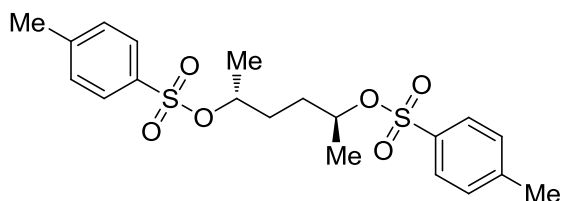
(2*S*,5*S*)-Hexane-2,5-diol di-*p*-toluenesulfonate (125)



To (2*S*,5*S*)-hexane-2,5-diol (1.18 g, 10.0 mmol) in dichloromethane (30 mL) containing pyridine (1.58 g, 20.0 mmol) cooled to 0°C and stirred was added *p*-toluenesulfonyl chloride (3.80 g, 20.0 mmol) in small portions over a period of 1 h. The mixture was stirred for 72 h, after which the white suspension was diluted with dichloromethane (20 mL) and washed with 10% aqueous hydrochloric acid (10 mL). The organic layer was separated and the aqueous layer was extracted further with dichloromethane (2 \times 10 mL). The combined organic layers were washed with another portion of 10% aqueous hydrochloric acid (10 mL), saturated aqueous NaHCO_3 , dried (MgSO_4) and concentrated under reduced pressure to afford a white solid. This was dissolved in a minimum amount of methanol at reflux and the solution was allowed to cool slowly to room temperature, and then stored at 5°C for 1 week. The resulting solid was collected by filtration and dried in vacuo at room temperature to afford the ditosylate (3.48 g, 82%) as a white crystalline solid, mp 92-95 °C (lit.⁸¹ 94.5-97 °C); ^1H NMR (300 MHz, CDCl_3 , CHCl_3): δ =7.77 ppm (d, $^3J(\text{H},\text{H})=8.3$ Hz, 4H;

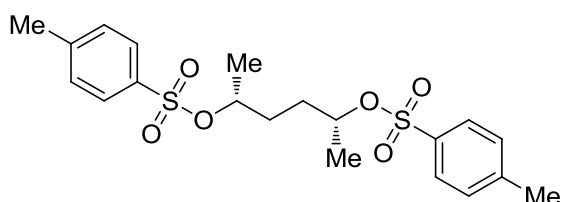
4x Ar-H), 7.28 (d, $^3J(\text{H,H})=8.1$ Hz, 4H; 4x Ar-H), 4.45 (m, 2H; 2x CH), 2.38 (s, 6H; 2xAr-CH₃), 1.47 (m, 4H; 2xCH₂), 1.06 (d, $^3J(\text{H,H})=6.3$ Hz, 6H; 2xCHCH₃).

(2R,5S)-Hexane-2,5-diol di-O-*p*-toluenesulfonate (128)



The *meso*-ditosylate was prepared following a similar procedure to that above from hexane-2,5-diol [mixture of (2*R*,5*R*)-, (2*S*,5*S*)- and *meso*-isomer] (1.18 g, 10.0 mmol). Four recrystallizations from methanol afforded (2*R*,5*S*)-hexane-2,5-diol di-*O-p*-toluenesulfonate (1.86 g, 44% yield), mp 114 - 116°C (lit.¹⁰² 115.5 - 117°C); ¹H NMR (300 MHz, CDCl₃, CHCl₃): δ=7.78 ppm (d, $^3J(\text{H,H})=8.0$ Hz, 4H; 4x Ar-H), 7.35 (d, $^3J(\text{H,H})=8.0$ Hz, 4H; 4x Ar-H), 4.53 (m, 2H; 2x CH), 2.38 (s, 6H; 2xAr-CH₃), 1.49 (m, 4H; 2xCH₂), 1.08 (m, 6H; 2xCHCH₃).

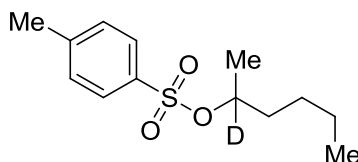
(2R,5R)-Hexane-2,5-diol di-*p*-toluenesulfonate (123)



The ditosylate was prepared following a similar procedure to that above from (2*R*,5*R*)-hexane-2,5-diol (purchased from Alfa Aesar, Heysham LA3 2XY, UK) (1.18 g, 10.0 mmol). Recrystallisations from methanol yielded (2*R*,5*R*)-hexane-2,5-diol di-*O-p*-toluenesulfonate (3.35 g, 79% yield), mp 89 – 92°C (lit.¹⁰³ 81 – 91°C); ¹H NMR (300 MHz, CDCl₃, CHCl₃): δ=7.79 ppm (d, $^3J(\text{H,H})=8.3$ Hz, 4H;

4x Ar-H), 7.36 (d, $^3J(\text{H,H})=8.1$ Hz, 4H; 4x Ar-H), 4.53 (m, 2H; 2x CH), 2.47 (s, 6H; 2xArCH₃), 1.55 (m, 4H; 2xCH₂), 1.15 (d, $^3J(\text{H,H})=6.3$ Hz, 6H; 2xCHCH₃).

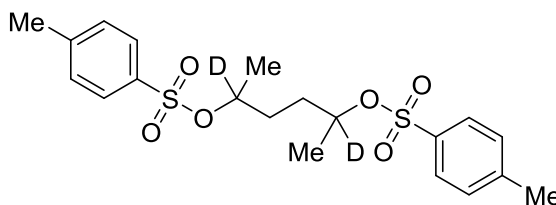
rac-(2-²H)-Hexan-2-ol *p*-toluenesulfonate (131)



Hexan-2-one was reduced with sodium borodeuteride in tetrahydrofuran and the resulting (2-²H)-hexan-2-ol was converted into the *p*-toluenesulfonate by the above procedure.

¹H NMR (300 MHz, CD₃OD, CH₃OD): $\delta=7.74$ ppm (d, $^3J(\text{H,H})=8.0$ Hz, 2H; 2 x Ar-H), 7.28 (d, $^3J(\text{H,H})=8.0$ Hz, 2H; 2 x Ar-H), 4.53 (m, 2H; 2x CH), 2.38 (s, 6H; 2xAr-CH₃), 1.49 (m, 4H; 2xCH₂), 1.08 (m, 6H; 2xCHCH₃).

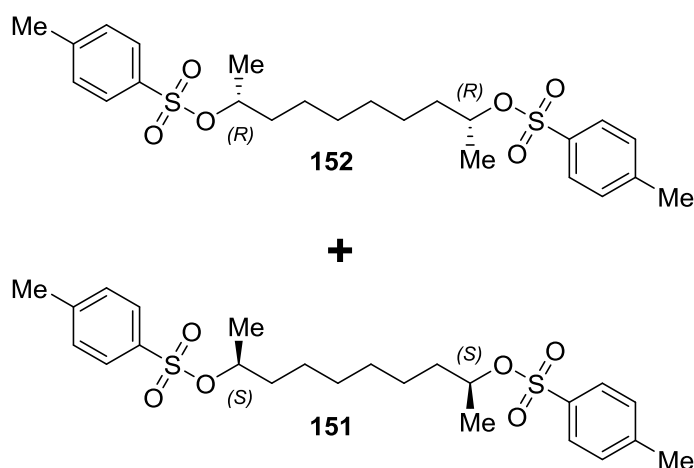
2,5-dideuteriohexane-2,5-diyl bis(4-methylbenzenesulfonate) (133)



¹H NMR (300 MHz, CDCl₃) $\delta=7.69$ ppm (d, $^3J(\text{H,H})=8.3$ Hz, 4H, Ar-H), 7.27 (d, $^3J(\text{H,H})=8.3$ Hz, 4H, Ar-H), 2.38 (s, 6H, 2 x Ar-CH₃), 1.42 (m, 4H, 2 x CH₂), 1.06 (d, $^3J(\text{H,H})=6.3$ Hz, 6H, 2 x CH-CH₃), ¹³C NMR (100 MHz, CDCl₃) $\delta=144.75$ ppm

(2 × Me-Ar-C), 134.40 (2 × S-Ar-C), 129.88 (4 × Ar-CH₂), 127.77 (4 × Ar-CH₂), 79.62 (t, *J* = 22.7, 2 × D-C), 31.98 (2 × CH₂), 21.71 (2 × Ph-CH₃), 20.74 (2 × CH₃).

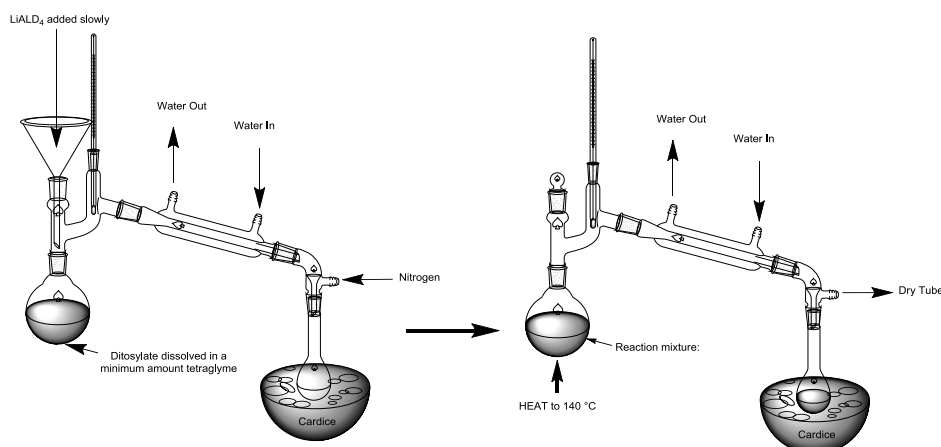
(2R,9R)- and (2S,9S)-decane-2,9-diyl bis(4-methylbenzenesulfonate) (151 and 152 mixture)



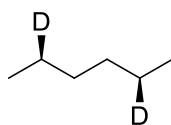
¹H NMR (300 MHz, CDCl₃) δ=7.80 ppm (d, ³*J*(H,H)=8.3 Hz, 4H, Ar-H), 7.45 (d, ³*J*(H,H)=8.1 Hz, 4H, Ar-H), 4.65-4.50 (m, 2H; 2 × CH), 2.49 (s, 6H, 2 × Ar-CH₃), 1.60-1.40 (m, 10H, 2 × CHCH₂ & 2 × CH₃), 1.25-1.00 (m, 8H, 4 × CH₂), ¹³C NMR (100 MHz, CDCl₃) δ=144.6 ppm, 133.7, 130.0, 127.5, 80.0, 38.9, 24.0, 21.1.

General procedure for preparation of dideuterated *n*-hexanes from tosylates

As shown in the figure below, the ditosylate or rac-(2-²H)hexan-2-ol *p*-toluenesulphonate was dissolved in a minimum amount of tetraethyleneglycol dimethyl ether (tetraglyme) in a round-bottomed flask. The flask was attached to a distillation system, which was connected to a nitrogen line. LiAlD₄ (2 equiv.) was added at 0°C or room temperature. The nitrogen line was removed and replaced with a drying tube. The reaction flask was heated up to 140°C (bath temperature) with the collecting flask placed in Cardice. The dideuterated hexane was collected over a period of up to 2 h in 75-85% yield.

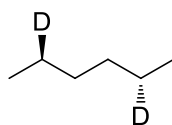


(2*R*,5*R*)-*n*-(2,5-²H₂)Hexane (119)



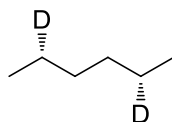
¹H NMR (300 MHz, CDCl₃, CHCl₃): δ=1.27 ppm (br s, 6H; 2×CH₂, 2×CHD), 0.89 (d, ³J(H,H)=5.5 Hz, 6H; 2×CH₃); ¹³C NMR (100 MHz, CDCl₃, CDCl₃): δ=31.5 ppm (2×CH₂), 22.3 (t, ¹J(C,D)=18.4 Hz; 2×CHD), 14.1 (2×CH₃); 2H NMR (76.8 MHz, dichloromethane): δ=1.29 ppm (relative to CHDCl₂ at δ=5.33 ppm; br s; 2×CHD).

(2*R*,5*S*)-*n*-(2,5-²H₂)Hexane (120)



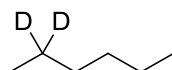
^1H NMR (300 MHz, CDCl_3 , CHCl_3): $\delta=1.27$ ppm (br s, 6H; $2\times\text{CH}_2$, $2\times\text{CHD}$), 0.89 (d, $^3J(\text{H,H})=5.0$ Hz, 6H; $2\times\text{CH}_3$); ^{13}C NMR (100 MHz, CDCl_3 , CDCl_3): $\delta=31.56$ ppm ($2\times\text{CH}_2$), 22.35 (t, $^1J(\text{C,D})=19.1$ Hz; $2\times\text{CHD}$), 14.11 ($2\times\text{CH}_3$); ^2H NMR (76.8 MHz, dichloromethane): $\delta=1.28$ ppm (relative to CHDCl_2 at $\delta=5.33$ ppm; br s; $2\times\text{CHD}$).

(2S,5S)-*n*-(2,5- $^2\text{H}_2$)Hexane (118)



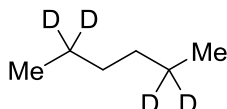
^1H NMR (300 MHz, CDCl_3 , CHCl_3): $\delta=1.27$ ppm (br s, 6H; $2\times\text{CH}_2$, $2\times\text{CHD}$), 0.89 (d, $^3J(\text{H,H})=5.5$ Hz, 6H; $2\times\text{CH}_3$); ^{13}C NMR (100 MHz, CDCl_3 , CDCl_3): $\delta=31.55$ ppm ($2\times\text{CH}_2$), 22.34 (t, $^1J(\text{C,D})=18.4$ Hz, $2\times\text{CHD}$), 14.09 ($2\times\text{CH}_3$); ^2H NMR (76.8 MHz, dichloromethane): $\delta=1.29$ ppm (relative to CHDCl_2 at $\delta=5.33$ ppm; br s; $2\times\text{CHD}$).

***n*-(2,2- $^2\text{H}_2$)Hexane (121A)**



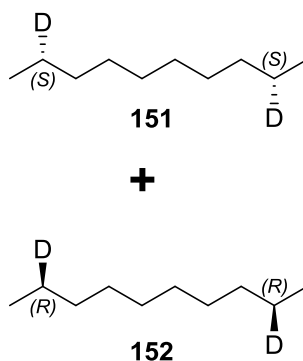
^1H NMR (300 MHz, CDCl_3 , CHCl_3): δ =1.26 ppm (br s, 6H; $3\times\text{CH}_2$), 0.87 (m, 6H; $2\times\text{CH}_3$); ^{13}C NMR (100 MHz, CDCl_3 , CDCl_3): δ =31.62 ppm, 31.47, 22.75, 14.20, 13.98; ^2H NMR (76.8 MHz, dichloromethane): δ =1.27 ppm (relative to CHDCl_2 at δ =5.33 ppm; br s; CD_2).

Preparation of 2,2,5,5-tetradeuteriohexane (121B)



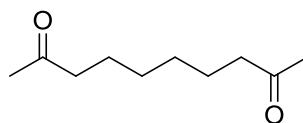
^1H NMR (300 MHz, CDCl_3) δ 0.80 (s, 6H, $2\times\text{CH}_3$), 1.17 (s, 4H, $2\times\text{CH}_2$). ^{13}C NMR (100 MHz, CDCl_3) δ 31.56 ($2\times\text{CH}_2$), 21.66 (qn, $^1J(\text{C},\text{D})=19.1$ Hz, $2\times\text{CD}_2$), 13.98 ($2\times\text{CH}_3$). D NMR (500 MHz, dichloromethane) 1.31 (s, 4D, $2\times\text{CD}_2$).

(2S,9S)- and (2R,9R)-2,9-dideuteriododecane (151 and 152 mixture)



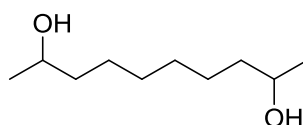
^1H NMR (300 MHz, CDCl_3 , CHCl_3): δ =1.27 ppm (br s, 14H; $6\times\text{CH}_2$, $2\times\text{CHD}$), 0.85 (d, $^3J(\text{H},\text{H})=6.4$ Hz, 6H; $2\times\text{CH}_3$); ^{13}C NMR (100 MHz, CDCl_3 , CDCl_3): δ =31.8 ppm ($2\times\text{CHCH}_2$), 29.7 ($2\times\text{CH}_2$), 29.3 ($2\times\text{CH}_2$), 22.5 (t, $^1J(\text{C},\text{D})=19.1$ Hz, $2\times\text{CHD}$), 14.09 ($2\times\text{CH}_3$).

Decane-2,9-dione (148)



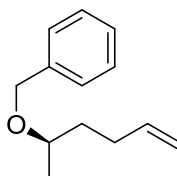
Prepared following the above procedure, by hydrogenation of commercially available (E)-dec-5-ene-2,9-dione (3.0 g, 17.8 mmol) dissolved in 25.0 mL of tetrahydrofuran (THF), using 1.0g of Pd/C as catalyst. This afforded 2.85 g of decane-2,9-dione (95% yield) as a white solid. ^1H NMR (300 MHz, CDCl_3 , CHCl_3): δ =2.40 ppm (t, 4H, $^3J(\text{H,H})=7.3$ Hz), 2.12 (s, 6H), 1.58-1.52 (m, 4H), 1.30-1.26 (m, 4H). ^{13}C NMR (CDCl_3 , 100 MHz) : δ =209.1 ppm, 43.7, 29.9, 29.0, 23.7.

rac-Decane-2,9-diol (149)



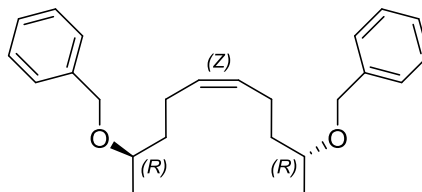
^1H NMR (300 MHz, CDCl_3 , CHCl_3): δ =3.74 (m, 2H, 2 x CH_3CH), 2.44 (t, 4H, 2 x CHCH_2), 1.36 (m, 12H, 6 x CH_2), 1.18 (d, $^3J(\text{H,H})=6.2$ Hz, 2x CH_3).

(R)-((hex-5-en-2-yloxy)methyl)benzene (156)



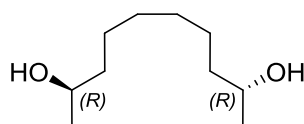
^1H NMR (300 MHz, CDCl_3 , CHCl_3): δ =7.35 ppm (m, 5H, 5xAr-H), 5.75 (m, CHCH_2), 5.0 (m, 2H, CH_2), 4.55 (m, 2H, O- CH_2), 3.55 (m, H, CH_3CH), 2.15 (m, 2H, CH_2CHCH_2), 1.80-1.50 (m, 2H, CHCH_2CH_2), 1.23 (d, 3H, $^3J(\text{H,H})=6.1$ Hz, CH_3).

(((2*R*,9*R*,*Z*)-dec-5-ene-2,9-diylbis(oxy))bis(methylene))dibenzene (157)



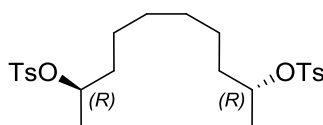
^1H NMR (300 MHz, CDCl_3 , CHCl_3): δ =7.37-7.23 ppm (m, 10H, 10 \times Ar-H), 5.37 (m, 2H, CHCH), 4.50 (dd, 4H, $^3J(\text{H,H})=11.8$ Hz, 49.4 Hz, 2 \times O-CH₂), 3.50 (m, 2H, 10 \times CH), 2.05 (m, 4H, CH₂CHCHCH₂), 1:1 ratio 1.72-1.55 & 1.52-1.40 (m, 4H, 2 \times CHCH₂CH₂), 1.18 (double doublets, 6H, $^3J(\text{H,H})=6.1$ Hz, CH₃).

(2*R*,9*R*)-decane-2,9-diol (158)



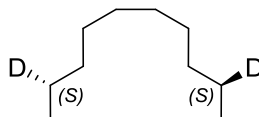
^1H NMR (300 MHz, CDCl_3 , CHCl_3): δ =3.72 ppm (m, 2H, 2 \times CH), 2:1 ratio 1.45-1.30 & 1.29-1.15 (m, 12H, 6 \times CH₂), 1.12 (dd, 6H, $^3J(\text{H,H})=6.2$ Hz, 1.0 Hz, 2 \times CH₃).

(2*R*,9*R*)-decane-2,9-diol di-*p*-toluenesulfonate (159)



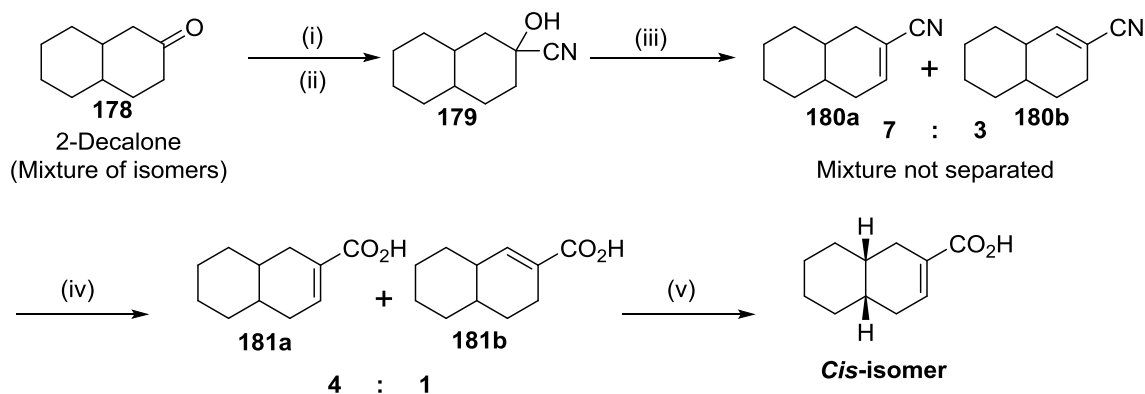
^1H NMR (300 MHz, CDCl_3 , CHCl_3): δ =7.70 ppm (d, $^3J(\text{H,H})=8.3$ Hz, 4H; 4 \times Ar-H), 7.25 (d, $^3J(\text{H,H})=8.0$ Hz, 4H; 4 \times Ar-H), 4.50 (m, 2H, 2 \times CH_3CH), 2.37 (s, 6H, 2 \times Ar- CH_3), 1.52 (m, 4H, 2 \times CHCH_2), 1.15 (d, 6H, $^3J(\text{H,H})=6.3$ Hz, 2 \times CH_3).

(2S,9S)-decane-2,9-diol di-*p*-toluenesulfonate (154)



^1H NMR (300 MHz, CDCl_3 , CHCl_3): δ =1.25 ppm (br s, 14H; 6 \times CH_2 , 2 \times CHD), 0.85 (d, $^3J(\text{H,H})=5.9$ Hz, 6H; 2 \times CH_3); ^{13}C NMR (100 MHz, CDCl_3 , CDCl_3): δ =31.93 ppm (2 \times CHCH_2), 29.77 ($\text{CH}_2\text{CH}_2\text{CH}_2\text{CH}_2$), 29.45 (2 \times CHCH_2CH_2), 22.4 (t, $^1J(\text{C,D})=19.1$ Hz, 2 \times CHD), 14.07 (2 \times CH_3).

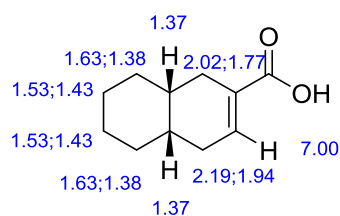
Synthesis of 1,4,4a,5,6,7,8,8a-octahydronaphthalene-2-carboxylic acid (181)



Scheme 54 – Synthesis of 1,4,4a,5,6,7,8,8a-octahydronaphthalene-2-carboxylic acid (**181a**) and 3,4,4a,5,6,7,8,8a-octahydronaphthalene-2-carboxylic acid (**181b**). (i) H_2SO_4 , MeOH, (ii) NaCN, H_2O , RT, 5 h; (iii) 2,6-lutidine, SOCl_2 , Et_2O , 60 °C, 12 h; (iv) H_2SO_4 , H_2O , 110 °C, 24 h; (v) Recrystallisation from ethanol.

Following a literature procedure⁹⁸, a mixture of 1,4,4a,5,6,7,8,8a-octahydronaphthalene-2-carbonitrile and 3,4,4a,5,6,7,8,8a-octahydronaphthalene-2-carbonitrile was prepared from 2-decalone (4:1 mixture of *cis*- and *trans*-isomers) and then hydrolysed with aqueous sulfuric acid. Fractional recrystallisation of the 1,4,4a,5,6,7,8,8a-octahydronaphthalene-2-carboxylic acid from ethanol gave a single isomer, mp 142–143°C, which using X-ray Crystallography, was shown to possess *cis* stereochemistry at the ring junction.

¹H NMR (400 MHz, CDCl₃, CHCl₃): δ=7.04 ppm (m, H; CH), 2.3-1.2 (m, Fig. 74); ¹³C NMR (100 MHz, CDCl₃, CDCl₃): δ=172.0 ppm, 140.9, 127.8, 100.0, 58.6, 50.9, 32.6, 32.2, 28.8, 18.5, -20.1.



References

1. So, C. M.; Young, L. Y., Isolation and characterization of a sulfate-reducing bacterium that anaerobically degrades alkanes. *Applied and environmental microbiology* **1999**, 65 (7), 2969-76.
2. Rabus, R.; Wilkes, H.; Behrends, A.; Armstroff, A.; Fischer, T.; Pierik, A. J.; Widdel, F., Anaerobic initial reaction of n-alkanes in a denitrifying bacterium: evidence for (1-methylpentyl)succinate as initial product and for involvement of

an organic radical in n-hexane metabolism. *Journal of bacteriology* **2001**, 183 (5), 1707-15.

3. CONSORTIUM FUER ELEKTROCHEMISCHE INDUSTRIE GMBH, Method for the Production of Optically Active 3-Alkyl Carboxylic Acids and the Intermediate Products Thereof. *US2007/225519 A1* **2007**.

4. Eberlein, C.; Johannes, J.; Mouttaki, H.; Sadeghi, M.; Golding, B. T.; Boll, M.; Meckenstock, R. U., ATP-dependent/-independent enzymatic ring reductions involved in the anaerobic catabolism of naphthalene. *Environmental Microbiology* **2013**, n/a-n/a.

5. Head, I. M.; Jones, D. M.; Larter, S. R., Biological activity in the deep subsurface and the origin of heavy oil. *Nature* **2003**, 426 (6964), 344-352.

6. Simpson, T. J., Carbon-13 nuclear magnetic resonance structural and biosynthetic studies on deoxyherqueinone and herqueichrysin, phenalenone metabolites of *Penicillium herquei*. *Journal of the Chemical Society, Perkin Transactions 1* **1979**, 0 (0), 1233-1238.

7. Jarling, R.; Sadeghi, M.; Drozdowska, M.; Lahme, S.; Buckel, W.; Rabus, R.; Widdel, F.; Golding, B. T.; Wilkes, H., Stereochemical Investigations Reveal the Mechanism of the Bacterial Activation of n-Alkanes without Oxygen. *Angewandte Chemie International Edition* **2012**, 51 (6), 1334-1338.

8. Wilkes, H.; Rabus, R.; Fischer, T.; Armstroff, A.; Behrends, A.; Widdel, F., Anaerobic degradation of n-hexane in a denitrifying bacterium: further degradation of the initial intermediate (1-methylpentyl)succinate via C-skeleton rearrangement. *Arch. Microbiol.* **2002**, 177 (3), 235-243.

9. Ehrenreich, P.; Behrends, A.; Harder, J.; Widdel, F., Anaerobic oxidation of alkanes by newly isolated denitrifying bacteria. *Archives of Microbiology* **2000**, 173 (1), 58-64.

10. Muyzer, G.; Stams, A. J., The ecology and biotechnology of sulphate-reducing bacteria. *Nature reviews. Microbiology* **2008**, 6 (6), 441-54.

11. Textor, S.; Wendisch, V. F.; De Graaf, A. A.; Muller, U.; Linder, M. I.; Linder, D.; Buckel, W., Propionate oxidation in *Escherichia coli*: evidence for operation of a methylcitrate cycle in bacteria. *Arch Microbiol* **1997**, *168* (5), 428-36.
12. So, C. M.; Phelps, C. D.; Young, L. Y., Anaerobic transformation of alkanes to fatty acids by a sulfate-reducing bacterium, strain Hxd3. *Applied and environmental microbiology* **2003**, *69* (7), 3892-900.
13. Heider, J., Adding handles to unhandy substrates: anaerobic hydrocarbon activation mechanisms. *Current opinion in chemical biology* **2007**, *11* (2), 188-94.
14. Kapuscinski, J., DAPI: a DNA-specific fluorescent probe. *Biotechnic & histochemistry : official publication of the Biological Stain Commission* **1995**, *70* (5), 220-33.
15. Kniemeyer, O.; Musat, F.; Sievert, S. M.; Knittel, K.; Wilkes, H.; Blumenberg, M.; Michaelis, W.; Classen, A.; Bolm, C.; Joye, S. B.; Widdel, F., Anaerobic oxidation of short-chain hydrocarbons by marine sulphate-reducing bacteria. *Nature* **2007**, *449* (7164), 898-901.
16. (a) van Beilen, J.; Funhoff, E., Alkane hydroxylases involved in microbial alkane degradation. *Applied Microbiology and Biotechnology* **2007**, *74* (1), 13-21; (b) Wentzel, A.; Ellingsen, T.; Kotlar, H.-K.; Zotchev, S.; Throne-Holst, M., Bacterial metabolism of long-chain n-alkanes. *Applied Microbiology and Biotechnology* **2007**, *76* (6), 1209-1221.
17. Rosenberg, E., Exploiting microbial growth on hydrocarbons — new markets. *Trends in Biotechnology* **1993**, *11* (10), 419-424.
18. Harayama, S.; Kasai, Y.; Hara, A., Microbial communities in oil-contaminated seawater. *Current Opinion in Biotechnology* **2004**, *15* (3), 205-214.

19. Margesin, R.; Labbe, D.; Schinner, F.; Greer, C. W.; Whyte, L. G., Characterization of hydrocarbon-degrading microbial populations in contaminated and pristine Alpine soils. *Appl Environ Microbiol* **2003**, *69* (6), 3085-92.
20. (a) Head, I. M.; Jones, D. M.; Roling, W. F. M., Marine microorganisms make a meal of oil. *Nat Rev Micro* **2006**, *4* (3), 173-182; (b) Wang, Y.; Yu, M.; Austin, B.; Zhang, X.-H., *Oleispira lenta* sp. nov., a novel marine bacterium isolated from Yellow sea coastal seawater in Qingdao, China. *Antonie van Leeuwenhoek* **2012**, *101* (4), 787-794.
21. Yakimov, M. M.; Golyshin, P. N.; Lang, S.; Moore, E. R. B.; Abraham, W.-R.; Lünsdorf, H.; Timmis, K. N., *Alcanivorax borkumensis* gen. nov., sp. nov., a new, hydrocarbon-degrading and surfactant-producing marine bacterium. *International Journal of Systematic Bacteriology* **1998**, *48* (2), 339-348.
22. (a) Hara, A.; Syutsubo, K.; Harayama, S., *Alcanivorax* which prevails in oil-contaminated seawater exhibits broad substrate specificity for alkane degradation. *Environmental microbiology* **2003**, *5* (9), 746-53; (b) Harayama, S.; Kasai, Y.; Hara, A., Microbial communities in oil-contaminated seawater. *Curr Opin Biotechnol* **2004**, *15* (3), 205-14; (c) Kasai, Y.; Kishira, H.; Sasaki, T.; Syutsubo, K.; Watanabe, K.; Harayama, S., Predominant growth of *Alcanivorax* strains in oil-contaminated and nutrient-supplemented sea water. *Environmental microbiology* **2002**, *4* (3), 141-7; (d) McKew, B. A.; Coulon, F.; Yakimov, M. M.; Denaro, R.; Genovese, M.; Smith, C. J.; Osborn, A. M.; Timmis, K. N.; McGenity, T. J., Efficacy of intervention strategies for bioremediation of crude oil in marine systems and effects on indigenous hydrocarbonoclastic bacteria. *Environmental microbiology* **2007**, *9* (6), 1562-71; (e) Yakimov, M. M.; Timmis, K. N.; Golyshin, P. N., Obligate oil-degrading marine bacteria. *Curr Opin Biotechnol* **2007**, *18* (3), 257-66.
23. Yakimov, M. M.; Giuliano, L.; Denaro, R.; Crisafi, E.; Chernikova, T. N.; Abraham, W. R.; Luensdorf, H.; Timmis, K. N.; Golyshin, P. N., *Thalassolituus oleivorans* gen. nov., sp. nov., a novel marine bacterium that obligately utilizes

hydrocarbons. *International journal of systematic and evolutionary microbiology* **2004**, 54 (Pt 1), 141-8.

24. Golyshin, P. N.; Chernikova, T. N.; Abraham, W. R.; Lünsdorf, H.; Timmis, K. N.; Yakimov, M. M., Oleiphilaceae fam. nov., to include *Oleiphilus messinensis* gen. nov., sp. nov., a novel marine bacterium that obligately utilizes hydrocarbons. *International journal of systematic and evolutionary microbiology* **2002**, 52 (Pt 3), 901-911.

25. Yakimov, M. M.; Giuliano, L.; Gentile, G.; Crisafi, E.; Chernikova, T. N.; Abraham, W. R.; Lunsdorf, H.; Timmis, K. N.; Golyshin, P. N., *Oleispira antarctica* gen. nov., sp. nov., a novel hydrocarbonoclastic marine bacterium isolated from Antarctic coastal sea water. *International journal of systematic and evolutionary microbiology* **2003**, 53 (Pt 3), 779-85.

26. Eastcott, L.; Shiu, W. Y.; Mackay, D., Environmentally relevant physical-chemical properties of hydrocarbons: A review of data and development of simple correlations. *Oil and Chemical Pollution* **1988**, 4 (3), 191-216.

27. Ron, E. Z.; Rosenberg, E., Biosurfactants and oil bioremediation. *Current Opinion in Biotechnology* **2002**, 13 (3), 249-252.

28. Schmitz, C.; Goebel, I.; Wagner, S.; Vomberg, A.; Klinner, U., Competition between n-alkane-assimilating yeasts and bacteria during colonization of sandy soil microcosms. *Appl Microbiol Biotechnol* **2000**, 54 (1), 126-32.

29. Green, J.; Dalton, H., Substrate specificity of soluble methane monooxygenase. Mechanistic implications. *The Journal of biological chemistry* **1989**, 264 (30), 17698-703.

30. Siegbahn, P. E. M.; Crabtree, R. H.; Nordlund, P., Mechanism of methane monooxygenase – a structural and quantum chemical perspective. *JBIC* **1998**, 3 (3), 314-317.

31. van Beilen, J. B.; Panke, S.; Lucchini, S.; Franchini, A. G.; Röthlisberger, M.; Witholt, B., Analysis of *Pseudomonas putida* alkane-degradation gene clusters and flanking insertion sequences: evolution and regulation of the alk genes. *Microbiology* **2001**, *147* (6), 1621-1630.
32. van Beilen, J. B.; Marin, M. M.; Smits, T. H.; Rothlisberger, M.; Franchini, A. G.; Witholt, B.; Rojo, F., Characterization of two alkane hydroxylase genes from the marine hydrocarbonoclastic bacterium *Alcanivorax borkumensis*. *Environmental microbiology* **2004**, *6* (3), 264-73.
33. van Beilen, J. B.; Funhoff, E. G.; van Loon, A.; Just, A.; Kaysser, L.; Bouza, M.; Holtackers, R.; Rothlisberger, M.; Li, Z.; Witholt, B., Cytochrome P450 alkane hydroxylases of the CYP153 family are common in alkane-degrading eubacteria lacking integral membrane alkane hydroxylases. *Appl Environ Microbiol* **2006**, *72* (1), 59-65.
34. Funhoff, E. G.; Bauer, U.; Garcia-Rubio, I.; Witholt, B.; van Beilen, J. B., CYP153A6, a soluble P450 oxygenase catalyzing terminal-alkane hydroxylation. *Journal of bacteriology* **2006**, *188* (14), 5220-7.
35. Iida, T.; Sumita, T.; Ohta, A.; Takagi, M., The cytochrome P450ALK multigene family of an n-alkane-assimilating yeast, *Yarrowia lipolytica*: cloning and characterization of genes coding for new CYP52 family members. *Yeast (Chichester, England)* **2000**, *16* (12), 1077-87.
36. Tani, A.; Ishige, T.; Sakai, Y.; Kato, N., Gene structures and regulation of the alkane hydroxylase complex in *Acinetobacter* sp. strain M-1. *Journal of bacteriology* **2001**, *183* (5), 1819-23.
37. Throne-Holst, M.; Wentzel, A.; Ellingsen, T. E.; Kotlar, H. K.; Zotchev, S. B., Identification of novel genes involved in long-chain n-alkane degradation by *Acinetobacter* sp. strain DSM 17874. *Appl Environ Microbiol* **2007**, *73* (10), 3327-32.
38. Feng, L.; Wang, W.; Cheng, J.; Ren, Y.; Zhao, G.; Gao, C.; Tang, Y.; Liu, X.; Han, W.; Peng, X.; Liu, R.; Wang, L., Genome and proteome of long-chain

alkane degrading *Geobacillus thermodenitrificans* NG80-2 isolated from a deep-subsurface oil reservoir. *Proceedings of the National Academy of Sciences of the United States of America* **2007**, *104* (13), 5602-7.

39. Prieto, M. A., From oil to bioplastics, a dream come true? *Journal of bacteriology* **2007**, *189* (2), 289-90.

40. (a) Vogel, T. M.; Grbic-Galic, D., Incorporation of Oxygen from Water into Toluene and Benzene during Anaerobic Fermentative Transformation. *Applied and environmental microbiology* **1986**, *52* (1), 200-2; (b) Grbic-Galic, D.; Vogel, T. M., Transformation of toluene and benzene by mixed methanogenic cultures. *Applied and environmental microbiology* **1987**, *53* (2), 254-60.

41. Bryant, D. A.; Frigaard, N.-U., Prokaryotic photosynthesis and phototrophy illuminated. *Trends in Microbiology* **2006**, *14* (11), 488-496.

42. Dobrinski, K. P.; Longo, D. L.; Scott, K. M., The carbon-concentrating mechanism of the hydrothermal vent chemolithoautotroph *Thiomicrospira crunogena*. *Journal of bacteriology* **2005**, *187* (16), 5761-6.

43. (a) Helgeson, H. C.; Owens, C. E.; Knox, A. M.; Richard, L., Calculation of the Standard Molal Thermodynamic Properties of Crystalline, Liquid, and Gas Organic Molecules at High Temperatures and Pressures. *Geochimica et Cosmochimica Acta* **1998**, *62* (6), 985-1081; (b) Thauer, R. K.; Jungermann, K.; Decker, K., Energy conservation in chemotrophic anaerobic bacteria. *Bacteriological reviews* **1977**, *41* (1), 100-80; (c) Hanselmann, K. W., Microbial energetics applied to waste repositories. *Cellular and Molecular Life Sciences* **1991**, *47* (7), 645-687.

44. Jones, D. M.; Head, I. M.; Gray, N. D.; Adams, J. J.; Rowan, A. K.; Aitken, C. M.; Bennett, B.; Huang, H.; Brown, A.; Bowler, B. F. J.; Oldenburg, T.; Erdmann, M.; Larter, S. R., Crude-oil biodegradation via methanogenesis in subsurface petroleum reservoirs. *Nature* **2008**, *451* (7175), 176-180.

45. Mbadinga, S. M.; Wang, L.-Y.; Zhou, L.; Liu, J.-F.; Gu, J.-D.; Mu, B.-Z., Microbial communities involved in anaerobic degradation of alkanes. *International Biodeterioration & Biodegradation* **2011**, *65* (1), 1-13.
46. Valentine, D. L.; Chidthaisong, A.; Rice, A.; Reeburgh, W. S.; Tyler, S. C., Carbon and hydrogen isotope fractionation by moderately thermophilic methanogens. *Geochimica et Cosmochimica Acta* **2004**, *68* (7), 1571-1590.
47. Rabus, R.; Widdel, F., Utilization of Alkylbenzenes during Anaerobic Growth of Pure Cultures of Denitrifying Bacteria on Crude Oil. *Appl Environ Microbiol* **1996**, *62* (4), 1238-41.
48. Rabus, R.; Widdel, F., Anaerobic degradation of ethylbenzene and other aromatic hydrocarbons by new denitrifying bacteria. *Arch Microbiol* **1995**, *163* (2), 96-103.
49. Zedelius, J.; Rabus, R.; Grundmann, O.; Werner, I.; Brodkorb, D.; Schreiber, F.; Ehrenreich, P.; Behrends, A.; Wilkes, H.; Kube, M.; Reinhardt, R.; Widdel, F., Alkane degradation under anoxic conditions by a nitrate-reducing bacterium with possible involvement of the electron acceptor in substrate activation. *Environmental microbiology reports* **2011**, *3* (1), 125-135.
50. Scott, C. C.; Finnerty, W. R., Characterization of intracytoplasmic hydrocarbon inclusions from the hydrocarbon-oxidizing *Acinetobacter* species HO1-N. *Journal of bacteriology* **1976**, *127* (1), 481-9.
51. Grundmann, O.; Behrends, A.; Rabus, R.; Amann, J.; Halder, T.; Heider, J.; Widdel, F., Genes encoding the candidate enzyme for anaerobic activation of n-alkanes in the denitrifying bacterium, strain HxN1. *Environmental Microbiology* **2008**, *10* (2), 376-385.
52. Buckel, W.; Golding, B. T., Radical enzymes in anaerobes. *Annu. Rev. Microbiol.* **2006**, *60*, 27-49.

53. Selmer, T.; Pierik, A. J.; Heider, J., New glycol radical enzymes catalysing key metabolic steps in anaerobic bacteria. *Biological chemistry* **2005**, *386* (10), 981-8.
54. Rabus, R.; Jarling, R.; Lahme, S.; Kühner, S.; Heider, J.; Widdel, F.; Wilkes, H., Co-metabolic conversion of toluene in anaerobic n-alkane-degrading bacteria. *Environmental Microbiology* **2011**, *13* (9), 2576-2586.
55. Callaghan, A. V.; Wawrik, B.; Ni Chadhain, S. M.; Young, L. Y.; Zylstra, G. J., Anaerobic alkane-degrading strain AK-01 contains two alkylsuccinate synthase genes. *Biochemical and biophysical research communications* **2008**, *366* (1), 142-8.
56. Zedelius, J.; Rabus, R.; Grundmann, O.; Werner, I.; Brodkorb, D.; Schreiber, F.; Ehrenreich, P.; Behrends, A.; Wilkes, H.; Kube, M.; Reinhardt, R.; Widdel, F., Alkane degradation under anoxic conditions by a nitrate-reducing bacterium with possible involvement of the electron acceptor in substrate activation. *Environmental Microbiology Reports* **2011**, *3* (1), 125-135.
57. Widdel, F.; Knittel, K.; Galushko, A., Anaerobic Hydrocarbon-Degrading Microorganisms: An Overview. In *Handbook of Hydrocarbon and Lipid Microbiology*, Timmis, K., Ed. Springer Berlin Heidelberg: 2010; pp 1997-2021.
58. Grossi, V.; Cravo-Laureau, C.; Guyoneaud, R.; Ranchou-Peyruse, A.; Hirschler-Réa, A., Metabolism of n-alkanes and n-alkenes by anaerobic bacteria: A summary. *Organic Geochemistry* **2008**, *39* (8), 1197-1203.
59. Cravo-Laureau, C.; Matheron, R.; Cayol, J. L.; Joulian, C.; Hirschler-Rea, A., *Desulfatibacillum aliphaticivorans* gen. nov., sp. nov., an n-alkane- and n-alkene-degrading, sulfate-reducing bacterium. *International journal of systematic and evolutionary microbiology* **2004**, *54* (Pt 1), 77-83.
60. Davidova, I. A.; Duncan, K. E.; Choi, O. K.; Suflita, J. M., *Desulfoglaeba alkanexedens* gen. nov., sp. nov., an n-alkane-degrading, sulfate-reducing bacterium. *International journal of systematic and evolutionary microbiology* **2006**, *56* (Pt 12), 2737-42.

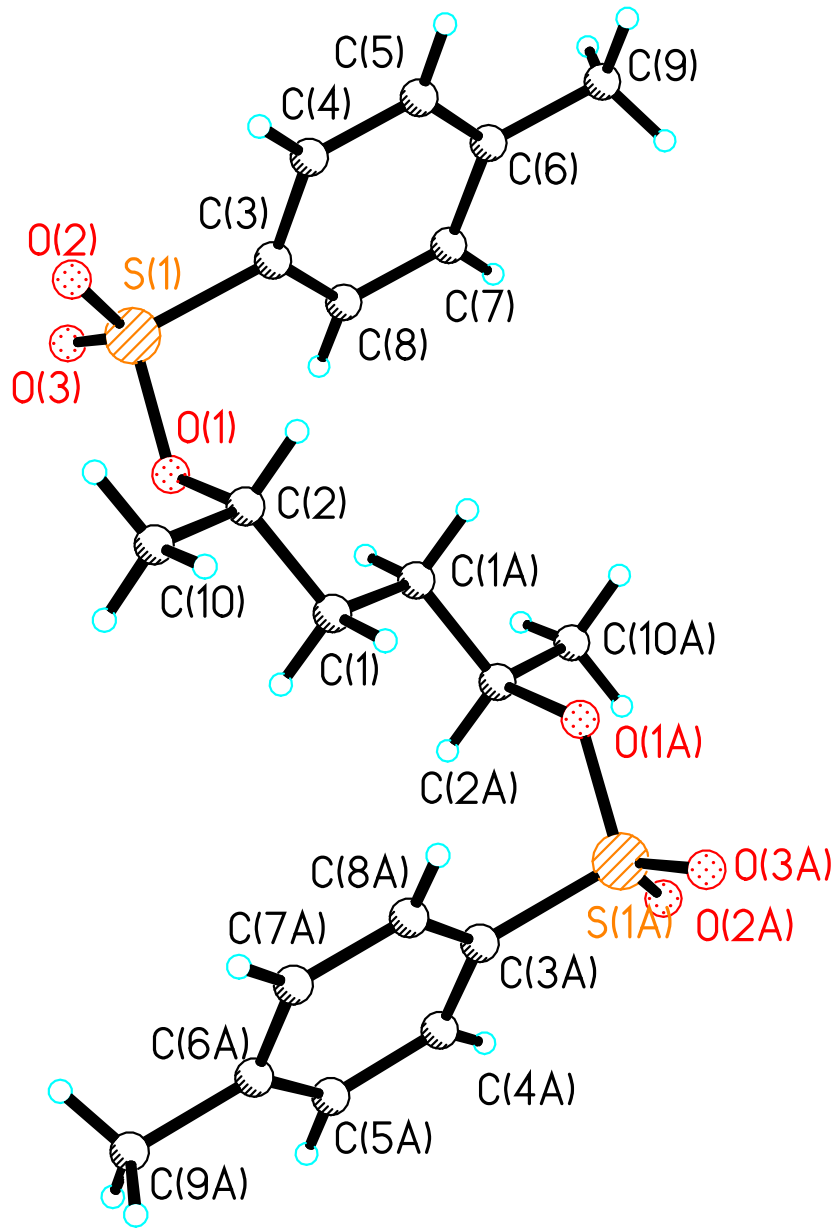
61. Higashioka, Y.; Kojima, H.; Nakagawa, T.; Sato, S.; Fukui, M., A novel n-alkane-degrading bacterium as a minor member of p-xylene-degrading sulfate-reducing consortium. *Biodegradation* **2009**, *20* (3), 383-90.
62. Rueter, P., Rabus, R., Wilkes, H., Aeckersberg, F., Rainey, F. A., Jannasch, H. W. & Widdel, F., Anaerobic oxidation of hydrocarbons in crude oil by new types of sulphate-reducing bacteria. *Nature* **1994**, *372* (6505), 455-8.
63. Cravo-Laureau, C.; Grossi, V.; Raphel, D.; Matheron, R.; Hirschler-Rea, A., Anaerobic n-alkane metabolism by a sulfate-reducing bacterium, *Desulfatibacillum aliphaticivorans* strain CV2803T. *Applied and environmental microbiology* **2005**, *71* (7), 3458-67.
64. Callaghan, A. V.; Gieg, L. M.; Kropp, K. G.; Suflita, J. M.; Young, L. Y., Comparison of mechanisms of alkane metabolism under sulfate-reducing conditions among two bacterial isolates and a bacterial consortium. *Applied and environmental microbiology* **2006**, *72* (6), 4274-82.
65. Townsend, G. T.; Prince, R. C.; Suflita, J. M., Anaerobic biodegradation of alicyclic constituents of gasoline and natural gas condensate by bacteria from an anoxic aquifer. *FEMS microbiology ecology* **2004**, *49* (1), 129-35.
66. Widdel, F.; Rabus, R., Anaerobic biodegradation of saturated and aromatic hydrocarbons. *Curr. Opin. Biotechnol.* **2001**, *12* (3), 259-76.
67. Aeckersberg, F.; Bak, F.; Widdel, F., Anaerobic oxidation of saturated hydrocarbons to CO₂ by a new type of sulfate-reducing bacterium. *Arch Microbiol* **1991**, *156* (1), 5-14.
68. Buckel, W.; Kratky, C.; Golding, B. T., Stabilisation of Methylene Radicals by Cob(II)alamin in Coenzyme B12 Dependent Mutases. *Chemistry – A European Journal* **2006**, *12* (2), 352-362.
69. Layer, G.; Heinz, D. W.; Jahn, D.; Schubert, W.-D., Structure and function of radical SAM enzymes. *Current Opinion in Chemical Biology* **2004**, *8* (5), 468-476.

70. Chirpich, T. P.; Zappia, V.; Costilow, R. N.; Barker, H. A., Lysine 2,3-aminomutase. Purification and properties of a pyridoxal phosphate and S-adenosylmethionine-activated enzyme. *The Journal of biological chemistry* **1970**, *245* (7), 1778-89.
71. Eklund, H.; Fontecave, M., Glycyl radical enzymes: a conservative structural basis for radicals. *Structure* **1999**, *7* (11), R257-R262.
72. Knappe, J.; Neugebauer, F. A.; Blaschkowski, H. P.; Gänzler, M., Post-translational activation introduces a free radical into pyruvate formate-lyase. *Proceedings of the National Academy of Sciences* **1984**, *81* (5), 1332-1335.
73. Buis, J. M.; Broderick, J. B., Pyruvate formate-lyase activating enzyme: elucidation of a novel mechanism for glycyl radical formation. *Archives of Biochemistry and Biophysics* **2005**, *433* (1), 288-296.
74. Rabus, R.; Wilkes, H.; Behrends, A.; Armstroff, A.; Fischer, T.; Pierik, A. J.; Widdel, F., Anaerobic initial reaction of n-alkanes in a denitrifying bacterium: evidence for (1-methylpentyl)succinate as initial product and for involvement of an organic radical in n-hexane metabolism. *J. Bacteriol.* **2001**, *183* (5), 1707-1715.
75. Aeckersberg, F.; Rainey, F. A.; Widdel, F., Growth, natural relationships, cellular fatty acids and metabolic adaptation of sulfate-reducing bacteria that utilize long-chain alkanes under anoxic conditions. *Arch Microbiol* **1998**, *170* (5), 361-9.
76. Qiao, C.; Marsh, E. N. G., Mechanism of Benzylsuccinate Synthase: Stereochemistry of Toluene Addition to Fumarate and Maleate. *Journal of the American Chemical Society* **2005**, *127* (24), 8608-8609.
77. Spormann, A. M. W., F., Metabolism of alkylbenzenes, alkanes, and other hydrocarbons in anaerobic bacteria. *Biodegradation* **11** **2000**, 85-105.
78. Manchester, K. L., Louis Pasteur (1822–1895) — chance and the prepared mind. *Trends in Biotechnology* **1995**, *13* (12), 511-515.

79. Bryce, C. F. A., Stereospecificity in organic chemistry and enzymology: By J Rétey and J A Robinson, pp 324. Verlag Chemie, Weinheim. 1982. DM 138 ISBN 3-527-25905-8. *Biochemical Education* **1984**, 12 (1), 44-44.
80. Simpson, T., Application of Isotopic Methods to Secondary Metabolic Pathways. In *Biosynthesis*, Leeper, F.; Vederas, J., Eds. Springer Berlin Heidelberg: 1998; Vol. 195, pp 1-48.
81. McKinstry, L., Livinghouse, T., An efficient procedure for the synthesis of C-chiral bisphosphines. *Tetrahedron* **1995**, 51 (28), 7655-7666.
82. Wesener, J. R.; Schmitt, P.; Guenther, H., Spin-echo carbon-13 NMR spectroscopy for the analysis of deuterated carbon compounds. *Journal of the American Chemical Society* **1984**, 106 (1), 10-13.
83. Baillif, V.; Robins, R. J.; Billault, I.; Lesot, P., Assignment of absolute configuration of natural abundance deuterium signals associated with (R)- and (S)-enantiomers in a fatty acid aligned in a chiral liquid crystal: enantioselective synthesis and NMR analysis. *J Am Chem Soc* **2006**, 128 (34), 11180-7.
84. Buchanan, J. G.; Diggle, R. A.; Ruggiero, G. D.; Williams, I. H., The Walden cycle revisited: a computational study of competitive ring closure to [small alpha]- and [small beta]-lactones. *Chemical Communications* **2006**, 0 (10), 1106-1108.
85. Smith, M. B.; March, J., *March's Advanced Organic Chemistry: Reactions, Mechanisms, and Structure*. Wiley: 2007.
86. Healy, E. F.; Lewis, J. D.; Minniear, A. B., A study of the aluminum hydride reduction of unsaturated cyclic epoxides. *Tetrahedron Letters* **1994**, 35 (36), 6647-6648.
87. Hioe, J.; Zipse, H., Radical stability and its role in synthesis and catalysis. *Organic & biomolecular chemistry* **2010**, 8 (16), 3609-17.

88. Bothe, H.; Darley, D. J.; Albracht, S. P.; Gerfen, G. J.; Golding, B. T.; Buckel, W., Identification of the 4-glutamyl radical as an intermediate in the carbon skeleton rearrangement catalyzed by coenzyme B12-dependent glutamate mutase from *Clostridium cochlearium*. *Biochemistry* **1998**, *37* (12), 4105-13.
89. Yadav, J. S.; Nanda, S.; Reddy, P. T.; Rao, A. B., Efficient Enantioselective Reduction of Ketones with *Daucus carota* Root. *The Journal of Organic Chemistry* **2002**, *67* (11), 3900-3903.
90. Prelog, V., Specification of the stereospecificity of some oxidoreductases by diamond lattice sections. *Pure Appl. Chem.* **1964**, *9* (1), 119-130.
91. Sih, C. J. Z., B.; Gopalan, A. S.; Shieh, W. R.; VanMiddlesworth, F, Selectivity, a Goal for Synthetic Efficiency. *Proceedings of the Fourteenth Workshop Conference Hoechst, SchloB Reisingburg 18-22 September 1983*.
92. Leuthner, B.; Leutwein, C.; Schulz, H.; Hörth, P.; Haehnel, W.; Schiltz, E.; Schägger, H.; Heider, J., Biochemical and genetic characterization of benzylsuccinate synthase from *Thauera aromatica*: a new glyceryl radical enzyme catalysing the first step in anaerobic toluene metabolism. *Molecular Microbiology* **1998**, *28* (3), 615-628.
93. Cerniglia, C., Biodegradation of polycyclic aromatic hydrocarbons. *Biodegradation* **1992**, *3* (2-3), 351-368.
94. Meckenstock, R. U.; Mouttaki, H., Anaerobic degradation of non-substituted aromatic hydrocarbons. *Current Opinion in Biotechnology* **2011**, *22* (3), 406-414.
95. Bergmann, F.; Selesi, D.; Weinmaier, T.; Tischler, P.; Rattei, T.; Meckenstock, R. U., Genomic insights into the metabolic potential of the polycyclic aromatic hydrocarbon degrading sulfate-reducing Deltaproteobacterium N47. *Environmental Microbiology* **2011**, *13* (5), 1125-1137.

96. DiDonato, R. J., Jr.; Young, N. D.; Butler, J. E.; Chin, K.-J.; Hixson, K. K.; Mouser, P.; Lipton, M. S.; DeBoy, R.; Methé, B. A., Genome Sequence of the Deltaproteobacterial Strain NaphS2 and Analysis of Differential Gene Expression during Anaerobic Growth on Naphthalene. *PLoS ONE* **2010**, *5* (11), e14072.
97. Vitnik, V. D.; Ivanović, M. D.; Vitnik, Ž. J.; Đorđević, J. B.; Žižak, Ž. S.; Juranić, Z. D.; Juranić, I. O., One-Step Conversion of Ketones to Conjugated Acids Using Bromoform. *Synthetic Communications* **2009**, *39* (8), 1457-1471.
98. Vaughan, W. R.; Caple, R., β -Bromo Acids. I. Stereochemistry and Mechanism of the Hydrobromination of α,β -Unsaturated Cyclohexenecarboxylic Acids. *Journal of the American Chemical Society* **1964**, *86* (22), 4928-4937.
99. Di Maio, G.; Migneco, L. M.; Vecchi, E.; Iavarone, C., Analysis of ^1H and ^{13}C NMR spectra of cis- and trans-10-substituted decal-2-ones by 2D NMR techniques. *Magnetic Resonance in Chemistry* **2000**, *38* (2), 108-114.
100. Eberlein, C.; Johannes, J.; Mouttaki, H.; Sadeghi, M.; Golding, B. T.; Boll, M.; Meckenstock, R. U., ATP-dependent/-independent enzymatic ring reductions involved in the anaerobic catabolism of naphthalene. *Environmental microbiology* **2013**.
101. Lieser, J. K., A Simple Synthesis of (S,S)-2,5-Hexanediol. *Synthetic Communications* **1983**, *13* (9), 765-767.
102. Eliel, E. L.; Hutchins, R. O.; Mebane, R.; Willer, R. L., Endocyclic vs. exocyclic attack in nucleophilic displacement reactions on five- and six-membered cyclic onium salts. *The Journal of Organic Chemistry* **1976**, *41* (6), 1052-1057.
103. Dodson, R. M.; Nelson, V. C., Correlation of the chirality of the disulfide group with its molecular ellipticity. *The Journal of Organic Chemistry* **1968**, *33* (10), 3966-3968.



Crystal data and structure refinement for btg81.

Identification code	btg81	
Chemical formula (moiety)	$C_{20}H_{26}O_6S_2$	
Chemical formula (total)	$C_{20}H_{26}O_6S_2$	
Formula weight	426.53	
Temperature	293(2) K	
Radiation, wavelength	MoK α , 0.71073 Å	
Crystal system, space group	orthorhombic, Pbc a	
Unit cell parameters	$a = 7.6411(2)$ Å	$\alpha = 90^\circ$
	$b = 16.2167(4)$ Å	$\beta = 90^\circ$
	$c = 16.6447(4)$ Å	$\gamma = 90^\circ$
Cell volume	2062.50(9) Å ³	
Z	4	
Calculated density	1.374 g/cm ³	
Absorption coefficient μ	0.292 mm ⁻¹	
F(000)	904	
Crystal colour and size	colourless, 0.40 × 0.40 × 0.40 mm ³	
Reflections for cell refinement	5430 (θ range 2.9 to 28.5°)	
Data collection method diffractometer	Oxford Diffraction Gemini A Ultra	
	thick-slice ω scans	
θ range for data collection	3.2 to 28.6°	
Index ranges	h -7 to 10, k -19 to 15, l -21 to 18	
Completeness to $\theta = 26.0^\circ$	98.8 %	
Reflections collected	9227	
Independent reflections	2301 ($R_{int} = 0.0228$)	
Reflections with $F^2 > 2\sigma$	1860	
Absorption correction	semi-empirical from equivalents	

Min. and max. transmission	0.8922 and 0.8922
Structure solution	direct methods
Refinement method	Full-matrix least-squares on F^2
Weighting parameters a, b	0.0512, 0.1031
Data / restraints / parameters	2301 / 0 / 130
Final R indices [$F^2 > 2\sigma$]	R1 = 0.0308, wR2 = 0.0853
R indices (all data)	R1 = 0.0402, wR2 = 0.0882
Goodness-of-fit on F^2	1.108
Extinction coefficient	0.0010(6)
Largest and mean shift/su	0.000 and 0.000
Largest diff. peak and hole	0.35 and -0.33 e \AA^{-3}

Table 2. Atomic coordinates and equivalent isotropic displacement parameters (\AA^2) for btg81. U_{eq} is defined as one third of the trace of the orthogonalized U^{ij} tensor.

	x	y	z	U_{eq}
S(1)	0.87901(4)	0.11708(2)	0.60182(2)	0.02038(13)
O(1)	0.74464(12)	0.10293(5)	0.53174(5)	0.0199(2)
O(2)	0.83542(13)	0.19007(6)	0.64548(6)	0.0274(3)
O(3)	1.04563(13)	0.11148(6)	0.56337(6)	0.0295(3)
C(1)	0.46778(18)	0.04400(8)	0.49549(8)	0.0208(3)
C(2)	0.55496(18)	0.10563(8)	0.55051(8)	0.0206(3)
C(3)	0.84902(17)	0.03191(8)	0.66539(8)	0.0190(3)
C(5)	0.78429(18)	-0.02455(9)	0.79425(8)	0.0238(3)
C(4)	0.80244(17)	0.04344(8)	0.74471(8)	0.0220(3)
C(6)	0.80861(19)	-0.10399(8)	0.76518(8)	0.0228(3)
C(7)	0.85222(18)	-0.11390(8)	0.68449(9)	0.0238(3)
C(8)	0.87554(17)	-0.04716(9)	0.63465(8)	0.0219(3)
C(9)	0.7892(2)	-0.17828(10)	0.81818(9)	0.0334(4)
C(10)	0.4872(2)	0.19213(9)	0.53817(9)	0.0320(4)

Table 3. Bond lengths [Å] and angles [°] for btg81.

S(1)–O(1)	1.5709(10)	S(1)–O(2)	1.4284(10)
S(1)–O(3)	1.4279(11)	S(1)–C(3)	1.7550(13)
O(1)–C(2)	1.4833(16)	C(1)–C(1A)	1.517(3)
C(1)–H(1A)	0.970	C(1)–H(1B)	0.970
C(1)–C(2)	1.5104(18)	C(2)–H(2A)	0.980
C(2)–C(10)	1.5093(19)	C(3)–C(4)	1.3800(19)
C(3)–C(8)	1.3953(18)	C(5)–H(3A)	0.930
C(5)–C(4)	1.3840(19)	C(5)–C(6)	1.3886(19)
C(4)–H(4A)	0.930	C(6)–C(7)	1.393(2)
C(6)–C(9)	1.5006(19)	C(7)–H(7A)	0.930
C(7)–C(8)	1.3753(19)	C(8)–H(8A)	0.930
C(9)–H(9A)	0.960	C(9)–H(9B)	0.960
C(9)–H(9C)	0.960	C(10)–H(10A)	0.960
C(10)–H(10B)	0.960	C(10)–H(10C)	0.960
O(1)–S(1)–O(2)	110.27(6)	O(1)–S(1)–O(3)	103.92(6)
O(1)–S(1)–C(3)	104.32(6)	O(2)–S(1)–O(3)	119.26(6)
O(2)–S(1)–C(3)	108.36(6)	O(3)–S(1)–C(3)	109.67(6)
S(1)–O(1)–C(2)	118.55(8)	C(1A)–C(1)–H(1A)	108.6
C(1A)–C(1)–H(1B)	108.6	C(1A)–C(1)–C(2)	114.79(14)
H(1A)–C(1)–H(1B)	107.5	H(1A)–C(1)–C(2)	108.6
H(1B)–C(1)–C(2)	108.6	O(1)–C(2)–C(1)	106.48(10)
O(1)–C(2)–H(2A)	109.5	O(1)–C(2)–C(10)	109.52(11)
C(1)–C(2)–H(2A)	109.5	C(1)–C(2)–C(10)	112.40(11)
H(2A)–C(2)–C(10)	109.5	S(1)–C(3)–C(4)	120.25(10)
S(1)–C(3)–C(8)	118.89(10)	C(4)–C(3)–C(8)	120.86(12)
H(3A)–C(5)–C(4)	119.4	H(3A)–C(5)–C(6)	119.4
C(4)–C(5)–C(6)	121.20(12)	C(3)–C(4)–C(5)	119.20(12)

C(3)–C(4)–H(4A)	120.4	C(5)–C(4)–H(4A)	120.4
C(5)–C(6)–C(7)	118.36(12)	C(5)–C(6)–C(9)	121.79(13)
C(7)–C(6)–C(9)	119.85(12)	C(6)–C(7)–H(7A)	119.3
C(6)–C(7)–C(8)	121.45(13)	H(7A)–C(7)–C(8)	119.3
C(3)–C(8)–C(7)	118.89(12)	C(3)–C(8)–H(8A)	120.6
C(7)–C(8)–H(8A)	120.6	C(6)–C(9)–H(9A)	109.5
C(6)–C(9)–H(9B)	109.5	C(6)–C(9)–H(9C)	109.5
H(9A)–C(9)–H(9B)	109.5	H(9A)–C(9)–H(9C)	109.5
H(9B)–C(9)–H(9C)	109.5	C(2)–C(10)–H(10A)	109.5
C(2)–C(10)–H(10B)	109.5	C(2)–C(10)–H(10C)	109.5
H(10A)–C(10)–H(10B)	109.5	H(10A)–C(10)–H(10C)	109.5
H(10B)–C(10)–H(10C)	109.5		

Symmetry operations for equivalent atoms

A $-x+1, -y, -z+1$

Table 4. Anisotropic displacement parameters (\AA^2) for btg81. The anisotropic displacement factor exponent takes the form: $-2\pi^2[h^2a^2U^{11} + \dots + 2hka^*b^*U^{12}]$

	U^{11}	U^{22}	U^{33}	U^{23}	U^{13}	U^{12}
S(1)	0.0186(2)	0.01888(19)	0.0237(2)	-0.00078(13)	-0.00043(14)	-0.00359(12)
O(1)	0.0186(5)	0.0214(5)	0.0195(5)	-0.0011(4)	0.0007(4)	-0.0011(4)
O(2)	0.0332(6)	0.0187(5)	0.0304(5)	-0.0050(4)	-0.0024(5)	-0.0043(4)
O(3)	0.0198(6)	0.0341(6)	0.0347(6)	0.0033(4)	0.0034(5)	-0.0046(4)
C(1)	0.0190(7)	0.0188(7)	0.0248(6)	-0.0012(5)	-0.0015(6)	0.0008(5)
C(2)	0.0173(7)	0.0204(7)	0.0241(7)	-0.0025(5)	0.0011(6)	0.0003(5)
C(3)	0.0149(6)	0.0204(7)	0.0216(6)	-0.0001(5)	-0.0020(5)	-0.0009(5)
C(5)	0.0198(7)	0.0305(8)	0.0210(6)	-0.0012(6)	-0.0006(6)	0.0020(6)
C(4)	0.0188(7)	0.0224(7)	0.0248(7)	-0.0058(5)	-0.0006(6)	0.0013(6)
C(6)	0.0177(7)	0.0258(7)	0.0250(7)	0.0025(6)	-0.0037(6)	0.0010(6)
C(7)	0.0234(7)	0.0195(7)	0.0286(7)	-0.0040(6)	-0.0033(6)	0.0029(5)
C(8)	0.0211(7)	0.0238(7)	0.0209(7)	-0.0034(6)	-0.0008(6)	0.0021(6)
C(9)	0.0368(9)	0.0299(8)	0.0334(8)	0.0077(6)	-0.0024(7)	0.0035(7)
C(10)	0.0295(8)	0.0221(8)	0.0445(9)	-0.0081(6)	-0.0057(7)	0.0050(6)

Table 5. Hydrogen coordinates and isotropic displacement parameters (\AA^2) for btg81.

	x	y	z	U
H(1A)	0.4862	0.0613	0.4403	0.025
H(1B)	0.3428	0.0450	0.5056	0.025
H(2A)	0.5365	0.0892	0.6065	0.025
H(3A)	0.7553	-0.0169	0.8480	0.029
H(4A)	0.7835	0.0963	0.7646	0.026
H(7A)	0.8659	-0.1668	0.6639	0.029
H(8A)	0.9084	-0.0546	0.5813	0.026
H(9A)	0.7405	-0.1619	0.8689	0.050
H(9B)	0.9019	-0.2030	0.8267	0.050
H(9C)	0.7129	-0.2175	0.7929	0.050
H(10A)	0.5500	0.2294	0.5724	0.048
H(10B)	0.3648	0.1940	0.5511	0.048
H(10C)	0.5036	0.2079	0.4831	0.048

Table 6. Torsion angles [°] for btg81.

O(2)–S(1)–O(1)–C(2)	–50.42(10)	O(3)–S(1)–O(1)–C(2)	–179.34(8)
C(3)–S(1)–O(1)–C(2)	65.75(9)	S(1)–O(1)–C(2)–C(1)	–146.16(9)
S(1)–O(1)–C(2)–C(10)	92.07(12)	C(1A)–C(1)–C(2)–O(1)	59.41(18)
C(1A)–C(1)–C(2)–C(10)	179.34(15)	O(1)–S(1)–C(3)–C(4)	–121.47(11)
O(1)–S(1)–C(3)–C(8)	59.45(12)	O(2)–S(1)–C(3)–C(4)	–3.99(13)
O(2)–S(1)–C(3)–C(8)	176.94(10)	O(3)–S(1)–C(3)–C(4)	127.74(11)
O(3)–S(1)–C(3)–C(8)	–51.34(12)	S(1)–C(3)–C(4)–C(5)	–178.21(10)
C(8)–C(3)–C(4)–C(5)	0.8(2)	C(6)–C(5)–C(4)–C(3)	–1.3(2)
C(4)–C(5)–C(6)–C(7)	0.1(2)	C(4)–C(5)–C(6)–C(9)	–179.95(13)
C(5)–C(6)–C(7)–C(8)	1.7(2)	C(9)–C(6)–C(7)–C(8)	–178.28(13)
C(6)–C(7)–C(8)–C(3)	–2.2(2)	S(1)–C(3)–C(8)–C(7)	179.93(10)
C(4)–C(3)–C(8)–C(7)	0.9(2)		

Symmetry operations for equivalent atoms

A $-x+1, -y, -z+1$

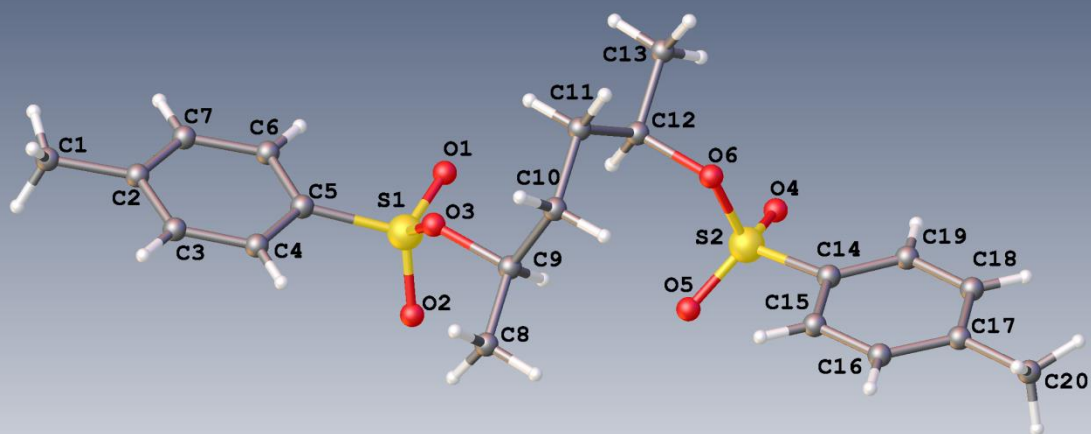


Table 1. Crystal data and structure refinement for btg86.

Identification code	btg86	
Chemical formula (moiety)	$C_{40}H_{52}O_{12}S_4$	
Chemical formula (total)	$C_{40}H_{52}O_{12}S_4$	
Formula weight	853.06	
Temperature	150(2) K	
Radiation, wavelength	MoK α , 0.71073 Å	
Crystal system, space group	monoclinic, P12 $_1$ 1	
Unit cell parameters	$a = 6.07920(10)$ Å	$\alpha = 90^\circ$
	$b = 7.2085(2)$ Å	$\beta = 92.103(2)^\circ$
	$c = 23.3865(5)$ Å	$\gamma = 90^\circ$
Cell volume	$1024.15(4)$ Å ³	
Z	1	
Calculated density	1.383 g/cm ³	
Absorption coefficient μ	0.294 mm ⁻¹	
F(000)	452	
Crystal colour and size	colourless, 0.30 × 0.20 × 0.20 mm ³	
Reflections for cell refinement	6622 (θ range 2.8 to 28.5°)	
Data collection method	Xcalibur, Atlas, Gemini ultra thick-slice ω scans	
θ range for data collection	3.0 to 28.5°	
Index ranges	h -8 to 8, k -8 to 9, l -30 to 29	
Completeness to $\theta = 26.0^\circ$	98.7 %	
Reflections collected	9186	
Independent reflections	4252 ($R_{int} = 0.0202$)	
Reflections with $F^2 > 2\sigma$	3834	
Absorption correction	semi-empirical from equivalents	
Min. and max. transmission	0.9170 and 0.9435	
Structure solution	direct methods	
Refinement method	Full-matrix least-squares on F^2	
Weighting parameters a, b	0.0348, 0.0000	
Data / restraints / parameters	4252 / 1 / 258	
Final R indices [$F^2 > 2\sigma$]	R1 = 0.0250, wR2 = 0.0560	
R indices (all data)	R1 = 0.0296, wR2 = 0.0570	
Goodness-of-fit on F^2	0.978	
Absolute structure parameter	-0.03(4)	
Extinction coefficient	0.0050(12)	
Largest and mean shift/su	0.001 and 0.000	
Largest diff. peak and hole	0.27 and -0.26 e Å ⁻³	

Table 2. Atomic coordinates and equivalent isotropic displacement parameters (\AA^2) for btg86. U_{eq} is defined as one third of the trace of the orthogonalized U^{ij} tensor.

	x	y	z	U_{eq}
S(1)	0.13446(7)	0.46561(6)	0.635959(16)	0.02535(10)
S(2)	0.03462(6)	0.30026(5)	0.870089(15)	0.02329(10)
O(1)	-0.0474(2)	0.3462(2)	0.64469(5)	0.0448(4)
O(2)	0.1123(2)	0.65493(18)	0.65320(5)	0.0392(3)
O(3)	0.34748(18)	0.38155(16)	0.66493(4)	0.0248(3)
O(4)	-0.19321(19)	0.2551(2)	0.87339(5)	0.0406(3)
O(5)	0.0904(2)	0.47141(17)	0.84301(5)	0.0386(3)
O(6)	0.15918(17)	0.13790(15)	0.84055(4)	0.0218(2)
C(1)	0.3673(3)	0.4722(3)	0.38702(7)	0.0380(4)
C(2)	0.3107(3)	0.4653(2)	0.44937(6)	0.0252(3)
C(3)	0.4589(3)	0.5307(2)	0.49150(7)	0.0272(4)
C(4)	0.4098(3)	0.5270(2)	0.54870(7)	0.0252(4)
C(5)	0.2082(2)	0.4551(2)	0.56391(6)	0.0212(3)
C(6)	0.0581(3)	0.3884(2)	0.52364(7)	0.0243(3)
C(7)	0.1101(3)	0.3945(2)	0.46572(7)	0.0271(4)
C(8)	0.5600(3)	0.5729(3)	0.73173(8)	0.0344(4)
C(9)	0.3913(3)	0.4204(2)	0.72712(6)	0.0216(4)
C(10)	0.4727(3)	0.2399(2)	0.75276(6)	0.0242(4)
C(11)	0.3144(3)	0.0773(2)	0.74893(6)	0.0231(3)
C(12)	0.0998(3)	0.1000(2)	0.77926(6)	0.0206(3)
C(13)	-0.0401(3)	-0.0722(2)	0.77648(7)	0.0310(4)
C(14)	0.1606(2)	0.2917(2)	0.93861(6)	0.0185(3)
C(15)	0.3717(3)	0.3634(2)	0.94704(7)	0.0231(3)
C(16)	0.4635(3)	0.3701(2)	1.00174(7)	0.0236(3)
C(17)	0.3497(2)	0.3061(2)	1.04856(6)	0.0215(3)
C(18)	0.1397(3)	0.2344(2)	1.03900(6)	0.0225(3)
C(19)	0.0437(3)	0.2257(2)	0.98412(6)	0.0209(3)
C(20)	0.4545(3)	0.3154(3)	1.10785(7)	0.0352(4)

Table 3. Bond lengths [Å] and angles [°] for btg86.

S(1)–O(1)	1.4222(14)	S(1)–O(2)	1.4308(13)
S(1)–O(3)	1.5617(12)	S(1)–C(5)	1.7612(14)
S(2)–O(4)	1.4275(13)	S(2)–O(5)	1.4331(13)
S(2)–O(6)	1.5680(11)	S(2)–C(14)	1.7517(14)
O(3)–C(9)	1.4955(17)	O(6)–C(12)	1.4907(17)
C(1)–H(1A)	0.980	C(1)–H(1B)	0.980
C(1)–H(1C)	0.980	C(1)–C(2)	1.511(2)
C(2)–C(3)	1.393(2)	C(2)–C(7)	1.388(2)
C(3)–H(3A)	0.950	C(3)–C(4)	1.382(2)
C(4)–H(4A)	0.950	C(4)–C(5)	1.389(2)
C(5)–C(6)	1.374(2)	C(6)–H(6A)	0.950
C(6)–C(7)	1.403(2)	C(7)–H(7A)	0.950
C(8)–H(8A)	0.980	C(8)–H(8B)	0.980
C(8)–H(8C)	0.980	C(8)–C(9)	1.504(2)
C(9)–H(9A)	1.000	C(9)–C(10)	1.509(2)
C(10)–H(10A)	0.990	C(10)–H(10B)	0.990
C(10)–C(11)	1.517(2)	C(11)–H(11A)	0.990
C(11)–H(11B)	0.990	C(11)–C(12)	1.517(2)
C(12)–H(12A)	1.000	C(12)–C(13)	1.505(2)
C(13)–H(13A)	0.980	C(13)–H(13B)	0.980
C(13)–H(13C)	0.980	C(14)–C(15)	1.390(2)
C(14)–C(19)	1.385(2)	C(15)–H(15A)	0.950
C(15)–C(16)	1.378(2)	C(16)–H(16A)	0.950
C(16)–C(17)	1.395(2)	C(17)–C(18)	1.388(2)
C(17)–C(20)	1.506(2)	C(18)–H(18A)	0.950
C(18)–C(19)	1.392(2)	C(19)–H(19A)	0.950
C(20)–H(20A)	0.980	C(20)–H(20B)	0.980
C(20)–H(20C)	0.980		
O(1)–S(1)–O(2)	117.07(8)	O(1)–S(1)–O(3)	109.85(8)
O(1)–S(1)–C(5)	109.75(8)	O(2)–S(1)–O(3)	109.46(7)
O(2)–S(1)–C(5)	109.92(7)	O(3)–S(1)–C(5)	99.33(6)
O(4)–S(2)–O(5)	117.75(8)	O(4)–S(2)–O(6)	109.81(7)
O(4)–S(2)–C(14)	109.58(7)	O(5)–S(2)–O(6)	108.79(6)
O(5)–S(2)–C(14)	109.38(8)	O(6)–S(2)–C(14)	100.06(6)
S(1)–O(3)–C(9)	117.69(9)	S(2)–O(6)–C(12)	117.17(9)
H(1A)–C(1)–H(1B)	109.5	H(1A)–C(1)–H(1C)	109.5
H(1A)–C(1)–C(2)	109.5	H(1B)–C(1)–H(1C)	109.5
H(1B)–C(1)–C(2)	109.5	H(1C)–C(1)–C(2)	109.5
C(1)–C(2)–C(3)	120.46(15)	C(1)–C(2)–C(7)	120.75(16)
C(3)–C(2)–C(7)	118.79(14)	C(2)–C(3)–H(3A)	119.3
C(2)–C(3)–C(4)	121.41(15)	H(3A)–C(3)–C(4)	119.3
C(3)–C(4)–H(4A)	120.7	C(3)–C(4)–C(5)	118.63(15)
H(4A)–C(4)–C(5)	120.7	S(1)–C(5)–C(4)	119.14(12)
S(1)–C(5)–C(6)	119.01(11)	C(4)–C(5)–C(6)	121.68(13)
C(5)–C(6)–H(6A)	120.5	C(5)–C(6)–C(7)	118.90(14)
H(6A)–C(6)–C(7)	120.5	C(2)–C(7)–C(6)	120.58(15)
C(2)–C(7)–H(7A)	119.7	C(6)–C(7)–H(7A)	119.7
H(8A)–C(8)–H(8B)	109.5	H(8A)–C(8)–H(8C)	109.5
H(8A)–C(8)–C(9)	109.5	H(8B)–C(8)–H(8C)	109.5
H(8B)–C(8)–C(9)	109.5	H(8C)–C(8)–C(9)	109.5
O(3)–C(9)–C(8)	107.66(12)	O(3)–C(9)–H(9A)	110.2
O(3)–C(9)–C(10)	105.62(11)	C(8)–C(9)–H(9A)	110.2
C(8)–C(9)–C(10)	112.89(14)	H(9A)–C(9)–C(10)	110.2
C(9)–C(10)–H(10A)	108.2	C(9)–C(10)–H(10B)	108.2

C(9)–C(10)–C(11)	116.42(14)	H(10A)–C(10)–H(10B)	107.3
H(10A)–C(10)–C(11)	108.2	H(10B)–C(10)–C(11)	108.2
C(10)–C(11)–H(11A)	108.2	C(10)–C(11)–H(11B)	108.2
C(10)–C(11)–C(12)	116.35(13)	H(11A)–C(11)–H(11B)	107.4
H(11A)–C(11)–C(12)	108.2	H(11B)–C(11)–C(12)	108.2
O(6)–C(12)–C(11)	106.69(12)	O(6)–C(12)–H(12A)	109.8
O(6)–C(12)–C(13)	108.02(12)	C(11)–C(12)–H(12A)	109.8
C(11)–C(12)–C(13)	112.66(13)	H(12A)–C(12)–C(13)	109.8
C(12)–C(13)–H(13A)	109.5	C(12)–C(13)–H(13B)	109.5
C(12)–C(13)–H(13C)	109.5	H(13A)–C(13)–H(13B)	109.5
H(13A)–C(13)–H(13C)	109.5	H(13B)–C(13)–H(13C)	109.5
S(2)–C(14)–C(15)	119.14(11)	S(2)–C(14)–C(19)	119.70(12)
C(15)–C(14)–C(19)	121.02(14)	C(14)–C(15)–H(15A)	120.5
C(14)–C(15)–C(16)	119.03(13)	H(15A)–C(15)–C(16)	120.5
C(15)–C(16)–H(16A)	119.3	C(15)–C(16)–C(17)	121.42(15)
H(16A)–C(16)–C(17)	119.3	C(16)–C(17)–C(18)	118.47(14)
C(16)–C(17)–C(20)	120.19(15)	C(18)–C(17)–C(20)	121.34(14)
C(17)–C(18)–H(18A)	119.4	C(17)–C(18)–C(19)	121.15(14)
H(18A)–C(18)–C(19)	119.4	C(14)–C(19)–C(18)	118.92(14)
C(14)–C(19)–H(19A)	120.5	C(18)–C(19)–H(19A)	120.5
C(17)–C(20)–H(20A)	109.5	C(17)–C(20)–H(20B)	109.5
C(17)–C(20)–H(20C)	109.5	H(20A)–C(20)–H(20B)	109.5
H(20A)–C(20)–H(20C)	109.5	H(20B)–C(20)–H(20C)	109.5

Table 4. Anisotropic displacement parameters (\AA^2) for btg86. The anisotropic displacement factor exponent takes the form: $-2\pi^2[h^2a^*2U^{11} + \dots + 2hka^*b^*U^{12}]$

	U^{11}	U^{22}	U^{33}	U^{23}	U^{13}	U^{12}
S(1)	0.0261(2) 0.00521(19)	0.0326(2)	0.01751(17)	0.00154(18)	0.00279(15)	
S(2)	0.0285(2) 0.00848(18)	0.0256(2)	0.01574(17)	-0.00197(16)	-0.00061(15)	
O(1)	0.0339(7) -0.0126(7)	0.0705(11)	0.0306(6)	0.0048(7)	0.0082(5)	
O(2)	0.0571(8)	0.0375(7)	0.0232(6)	-0.0029(5)	0.0024(6)	0.0241(6)
O(3)	0.0329(6)	0.0267(6)	0.0148(5)	-0.0028(4)	0.0002(5)	0.0080(5)
O(4)	0.0246(6)	0.0721(10)	0.0247(6)	-0.0111(6)	-0.0038(5)	0.0103(6)
O(5)	0.0712(9)	0.0249(6)	0.0199(5)	0.0029(5)	0.0021(6)	0.0112(7)
O(6)	0.0266(6)	0.0229(6)	0.0159(5)	-0.0020(5)	-0.0003(5)	0.0058(5)
C(1)	0.0585(12) 0.0032(10)	0.0354(10)	0.0203(7)	0.0017(8)	0.0034(8)	
C(2)	0.0389(9)	0.0184(7)	0.0184(7)	-0.0003(7)	0.0028(7)	0.0055(8)
C(3)	0.0275(9) -0.0044(7)	0.0277(9)	0.0269(9)	0.0023(7)	0.0060(7)	
C(4)	0.0284(8) -0.0039(7)	0.0248(9)	0.0221(8)	-0.0023(6)	-0.0022(7)	
C(5)	0.0261(8)	0.0209(8)	0.0167(7)	-0.0004(7)	0.0018(6)	0.0012(7)
C(6)	0.0246(8) -0.0026(7)	0.0228(8)	0.0254(8)	0.0021(7)	-0.0017(7)	
C(7)	0.0346(9)	0.0252(9)	0.0208(8)	-0.0023(7)	-0.0093(7)	0.0011(7)
C(8)	0.0412(11) -0.0074(9)	0.0337(10)	0.0286(9)	-0.0056(8)	0.0040(8)	
C(9)	0.0269(8)	0.0259(10)	0.0122(7)	-0.0026(6)	0.0030(6)	0.0002(7)
C(10)	0.0224(8)	0.0328(9)	0.0173(7)	0.0011(7)	-0.0010(6)	0.0028(7)
C(11)	0.0278(8)	0.0236(8)	0.0177(7)	0.0004(6)	0.0001(7)	0.0061(7)
C(12)	0.0260(8)	0.0213(8)	0.0141(7)	-0.0005(6)	-0.0029(6)	0.0022(7)
C(13)	0.0361(9) -0.0069(8)	0.0291(10)	0.0278(9)	-0.0009(7)	0.0009(7)	
C(14)	0.0235(7)	0.0174(7)	0.0147(6)	-0.0009(6)	0.0006(6)	0.0040(7)
C(15)	0.0238(8)	0.0234(8)	0.0225(8)	0.0013(7)	0.0070(7)	0.0006(7)
C(16)	0.0201(8) -0.0009(7)	0.0222(8)	0.0284(8)	-0.0028(7)	-0.0009(7)	
C(17)	0.0270(8)	0.0186(7)	0.0188(7)	-0.0035(7)	-0.0013(6)	0.0042(7)
C(18)	0.0282(8)	0.0212(8)	0.0187(7)	0.0017(6)	0.0075(7)	0.0012(7)
C(19)	0.0208(8) -0.0007(7)	0.0194(8)	0.0226(8)	-0.0024(7)	0.0031(6)	
C(20)	0.0430(10) 0.0065(10)	0.0392(10)	0.0230(8)	-0.0059(9)	-0.0060(7)	

Table 5. Hydrogen coordinates and isotropic displacement parameters (\AA^2) for btg86.

	x	y	z	U
H(1A)	0.2622	0.3963	0.3645	0.057
H(1B)	0.5165	0.4240	0.3826	0.057
H(1C)	0.3599	0.6008	0.3735	0.057
H(3A)	0.5967	0.5790	0.4807	0.033
H(4A)	0.5119	0.5726	0.5770	0.030
H(6A)	-0.0786	0.3389	0.5348	0.029
H(7A)	0.0072	0.3499	0.4374	0.033
H(8A)	0.5040	0.6830	0.7114	0.052
H(8B)	0.6965	0.5315	0.7147	0.052
H(8C)	0.5895	0.6034	0.7721	0.052
H(9A)	0.2527	0.4598	0.7454	0.026
H(10A)	0.5127	0.2617	0.7936	0.029
H(10B)	0.6090	0.2042	0.7336	0.029
H(11A)	0.2791	0.0522	0.7080	0.028
H(11B)	0.3910	-0.0335	0.7648	0.028
H(12A)	0.0152	0.2071	0.7625	0.025
H(13A)	-0.1753	-0.0511	0.7971	0.047
H(13B)	0.0418	-0.1759	0.7941	0.047
H(13C)	-0.0779	-0.1019	0.7364	0.047
H(15A)	0.4513	0.4071	0.9155	0.028
H(16A)	0.6074	0.4195	1.0077	0.028
H(18A)	0.0600	0.1906	1.0705	0.027
H(19A)	-0.0996	0.1754	0.9780	0.025
H(20A)	0.6088	0.2769	1.1066	0.053
H(20B)	0.3760	0.2324	1.1333	0.053
H(20C)	0.4467	0.4428	1.1222	0.053

Table 6. Torsion angles [°] for btg86.

O(1)–S(1)–O(3)–C(9)	–85.03(12)	O(2)–S(1)–O(3)–C(9)	44.82(12)
C(5)–S(1)–O(3)–C(9)	159.92(11)	O(4)–S(2)–O(6)–C(12)	65.59(11)
O(5)–S(2)–O(6)–C(12)	–64.61(12)	C(14)–S(2)–O(6)–C(12)	–179.22(10)
C(1)–C(2)–C(3)–C(4)	179.51(16)	C(7)–C(2)–C(3)–C(4)	–0.2(2)
C(2)–C(3)–C(4)–C(5)	0.4(2)	C(3)–C(4)–C(5)–S(1)	–175.18(13)
C(3)–C(4)–C(5)–C(6)	0.0(2)	O(1)–S(1)–C(5)–C(4)	–165.59(13)
O(1)–S(1)–C(5)–C(6)	19.12(16)	O(2)–S(1)–C(5)–C(4)	64.29(15)
O(2)–S(1)–C(5)–C(6)	–111.01(14)	O(3)–S(1)–C(5)–C(4)	–50.46(14)
O(3)–S(1)–C(5)–C(6)	134.24(13)	S(1)–C(5)–C(6)–C(7)	174.72(13)
C(4)–C(5)–C(6)–C(7)	–0.4(2)	C(1)–C(2)–C(7)–C(6)	–179.99(16)
C(3)–C(2)–C(7)–C(6)	–0.2(2)	C(5)–C(6)–C(7)–C(2)	0.6(2)
S(1)–O(3)–C(9)–C(8)	–100.86(14)	S(1)–O(3)–C(9)–C(10)	138.30(11)
O(3)–C(9)–C(10)–C(11)	–61.47(16)	C(8)–C(9)–C(10)–C(11)	–178.85(12)
C(9)–C(10)–C(11)–C(12)	–61.75(19)	S(2)–O(6)–C(12)–C(11)	134.10(11)
S(2)–O(6)–C(12)–C(13)	–104.53(13)	C(10)–C(11)–C(12)–O(6)	–57.85(17)
C(10)–C(11)–C(12)–C(13)	–176.23(14)	O(4)–S(2)–C(14)–C(15)	–168.30(13)
O(4)–S(2)–C(14)–C(19)	7.31(15)	O(5)–S(2)–C(14)–C(15)	–37.83(14)
O(5)–S(2)–C(14)–C(19)	137.78(13)	O(6)–S(2)–C(14)–C(15)	76.33(14)
O(6)–S(2)–C(14)–C(19)	–108.06(13)	S(2)–C(14)–C(15)–C(16)	174.84(12)
C(19)–C(14)–C(15)–C(16)	–0.7(2)	C(14)–C(15)–C(16)–C(17)	0.3(2)
C(15)–C(16)–C(17)–C(18)	0.0(2)	C(15)–C(16)–C(17)–C(20)	–179.97(16)
C(16)–C(17)–C(18)–C(19)	0.2(2)	C(20)–C(17)–C(18)–C(19)	–179.86(15)
S(2)–C(14)–C(19)–C(18)	–174.64(11)	C(15)–C(14)–C(19)–C(18)	0.9(2)
C(17)–C(18)–C(19)–C(14)	–0.6(2)		

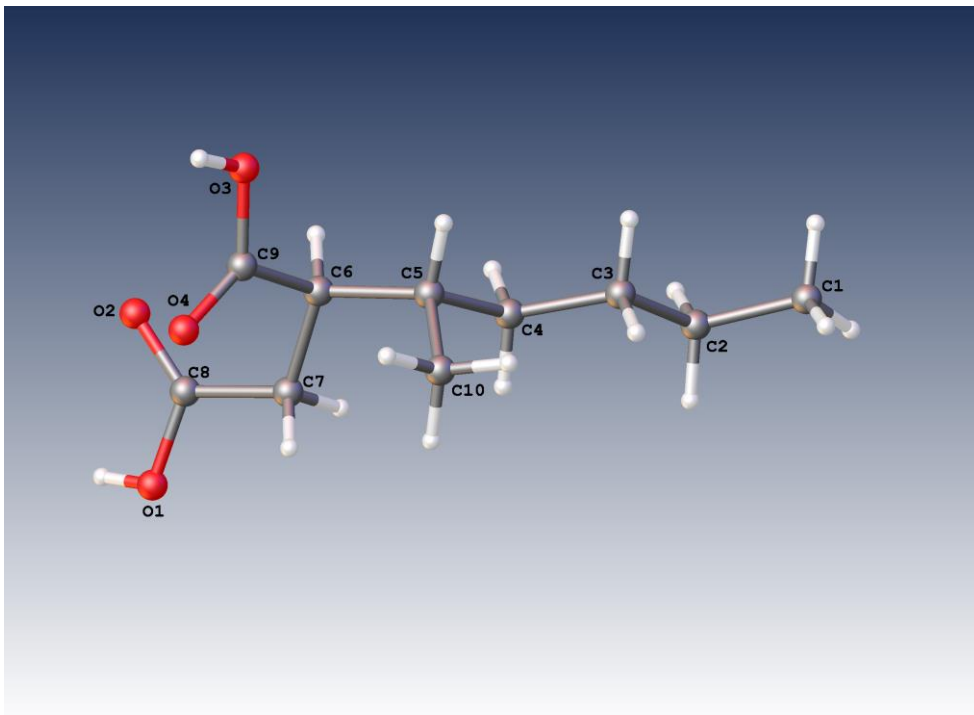


Table 1. Crystal data and structure refinement for btg84.

Identification code	btg84	
Chemical formula (moiety)	$C_{10}H_{18}O_4$	
Chemical formula (total)	$C_{10}H_{18}O_4$	
Formula weight	202.24	
Temperature	150(2) K	
Radiation, wavelength	CuK α , 1.54178 Å	
Crystal system, space group	monoclinic, P12 ₁ /c1	
Unit cell parameters	a = 9.1729(18) Å	$\alpha = 90^\circ$
	b = 11.7134(16) Å	$\beta = 105.94(2)^\circ$
	c = 10.748(2) Å	$\gamma = 90^\circ$
Cell volume	1110.4(3) Å ³	
Z	4	
Calculated density	1.210 g/cm ³	
Absorption coefficient μ	0.766 mm ⁻¹	
F(000)	440	
Crystal colour and size	colourless, 0.30 × 0.10 × 0.10 mm ³	
Reflections for cell refinement	2118 (θ range 3.8 to 63.0°)	
Data collection method	Xcalibur, Atlas, Gemini ultra thick-slice ω scans	
θ range for data collection	8.4 to 50.4°	
Index ranges	h -9 to 9, k -11 to 11, l -10 to 10	
Completeness to $\theta = 50.4^\circ$	99.6 %	
Reflections collected	5154	
Independent reflections	1154 ($R_{int} = 0.0573$)	
Reflections with $F^2 > 2\sigma$	988	
Absorption correction	semi-empirical from equivalents	
Min. and max. transmission	0.8027 and 0.9273	
Structure solution	direct methods	
Refinement method	Full-matrix least-squares on F^2	
Weighting parameters a, b	0.2000, 0.0000	
Data / restraints / parameters	1154 / 0 / 138	
Final R indices [$F^2 > 2\sigma$]	R1 = 0.0878, wR2 = 0.2816	
R indices (all data)	R1 = 0.0984, wR2 = 0.3299	
Goodness-of-fit on F^2	1.560	
Extinction coefficient	0.017(7)	
Largest and mean shift/su	0.000 and 0.000	
Largest diff. peak and hole	0.38 and -0.37 e Å ⁻³	

Table 2. Atomic coordinates and equivalent isotropic displacement parameters (\AA^2) for btg84. U_{eq} is defined as one third of the trace of the orthogonalized U^{ij} tensor.

	x	y	z	U_{eq}
O(1)	0.0812(4)	0.1576(3)	-0.0050(4)	0.0645(14)
O(2)	0.3054(4)	0.1975(2)	0.1339(3)	0.0659(14)
O(3)	0.3596(4)	0.1251(3)	0.4952(4)	0.0694(14)
O(4)	0.1358(4)	0.1724(3)	0.3590(3)	0.0664(14)
C(1)	0.3417(7)	-0.5279(4)	0.3266(5)	0.0805(18)
C(2)	0.3124(6)	-0.4126(4)	0.2631(5)	0.0678(16)
C(3)	0.2970(5)	-0.3164(3)	0.3512(5)	0.0620(15)
C(4)	0.2811(5)	-0.2012(3)	0.2852(5)	0.0587(15)
C(5)	0.2494(5)	-0.1007(3)	0.3653(4)	0.0557(15)
C(6)	0.2727(5)	0.0148(4)	0.3035(4)	0.0589(16)
C(7)	0.1691(6)	0.0295(3)	0.1662(4)	0.0628(16)
C(8)	0.1933(6)	0.1360(4)	0.0995(5)	0.0575(16)
C(9)	0.2491(7)	0.1117(4)	0.3865(5)	0.0618(16)
C(10)	0.0931(6)	-0.1106(4)	0.3889(5)	0.0691(17)

Table 3. Bond lengths [Å] and angles [°] for btg84.

O(1)–C(8)	1.323(6)	O(1)–H(1)	0.79(7)
O(2)–C(8)	1.226(5)	O(3)–H(3)	0.87(6)
O(3)–C(9)	1.328(6)	O(4)–C(9)	1.227(5)
C(1)–H(1A)	0.980	C(1)–H(1B)	0.980
C(1)–H(1C)	0.980	C(1)–C(2)	1.503(6)
C(2)–H(2A)	0.990	C(2)–H(2B)	0.990
C(2)–C(3)	1.503(6)	C(3)–H(3A)	0.990
C(3)–H(3B)	0.990	C(3)–C(4)	1.513(6)
C(4)–H(4A)	0.990	C(4)–H(4B)	0.990
C(4)–C(5)	1.533(6)	C(5)–H(5A)	1.000
C(5)–C(6)	1.547(6)	C(5)–C(10)	1.527(7)
C(6)–H(6A)	1.000	C(6)–C(7)	1.530(6)
C(6)–C(9)	1.495(6)	C(7)–H(7A)	0.990
C(7)–H(7B)	0.990	C(7)–C(8)	1.485(6)
C(10)–H(10A)	0.980	C(10)–H(10B)	0.980
C(10)–H(10C)	0.980		
C(8)–O(1)–H(1)	106(4)	H(3)–O(3)–C(9)	110(4)
H(1A)–C(1)–H(1B)	109.5	H(1A)–C(1)–H(1C)	109.5
H(1A)–C(1)–C(2)	109.5	H(1B)–C(1)–H(1C)	109.5
H(1B)–C(1)–C(2)	109.5	H(1C)–C(1)–C(2)	109.5
C(1)–C(2)–H(2A)	108.5	C(1)–C(2)–H(2B)	108.5
C(1)–C(2)–C(3)	115.1(4)	H(2A)–C(2)–H(2B)	107.5
H(2A)–C(2)–C(3)	108.5	H(2B)–C(2)–C(3)	108.5
C(2)–C(3)–H(3A)	109.0	C(2)–C(3)–H(3B)	109.0
C(2)–C(3)–C(4)	112.8(4)	H(3A)–C(3)–H(3B)	107.8
H(3A)–C(3)–C(4)	109.0	H(3B)–C(3)–C(4)	109.0
C(3)–C(4)–H(4A)	108.4	C(3)–C(4)–H(4B)	108.4
C(3)–C(4)–C(5)	115.5(3)	H(4A)–C(4)–H(4B)	107.5
H(4A)–C(4)–C(5)	108.4	H(4B)–C(4)–C(5)	108.4
C(4)–C(5)–H(5A)	107.1	C(4)–C(5)–C(6)	111.1(3)
C(4)–C(5)–C(10)	111.5(3)	H(5A)–C(5)–C(6)	107.1
H(5A)–C(5)–C(10)	107.1	C(6)–C(5)–C(10)	112.6(3)
C(5)–C(6)–H(6A)	107.9	C(5)–C(6)–C(7)	113.0(3)
C(5)–C(6)–C(9)	110.4(3)	H(6A)–C(6)–C(7)	107.9
H(6A)–C(6)–C(9)	107.9	C(7)–C(6)–C(9)	109.7(4)
C(6)–C(7)–H(7A)	108.5	C(6)–C(7)–H(7B)	108.5
C(6)–C(7)–C(8)	115.1(4)	H(7A)–C(7)–H(7B)	107.5
H(7A)–C(7)–C(8)	108.5	H(7B)–C(7)–C(8)	108.5
O(1)–C(8)–O(2)	122.4(4)	O(1)–C(8)–C(7)	112.7(5)
O(2)–C(8)–C(7)	124.9(5)	O(3)–C(9)–O(4)	122.3(4)
O(3)–C(9)–C(6)	114.4(5)	O(4)–C(9)–C(6)	123.2(5)
C(5)–C(10)–H(10A)	109.5	C(5)–C(10)–H(10B)	109.5
C(5)–C(10)–H(10C)	109.5	H(10A)–C(10)–H(10B)	109.5
H(10A)–C(10)–H(10C)	109.5	H(10B)–C(10)–H(10C)	109.5

Table 4. Anisotropic displacement parameters (\AA^2) for btg84. The anisotropic displacement factor exponent takes the form: $-2\pi^2[h^2a^{*2}U^{11} + \dots + 2hka^*b^*U^{12}]$

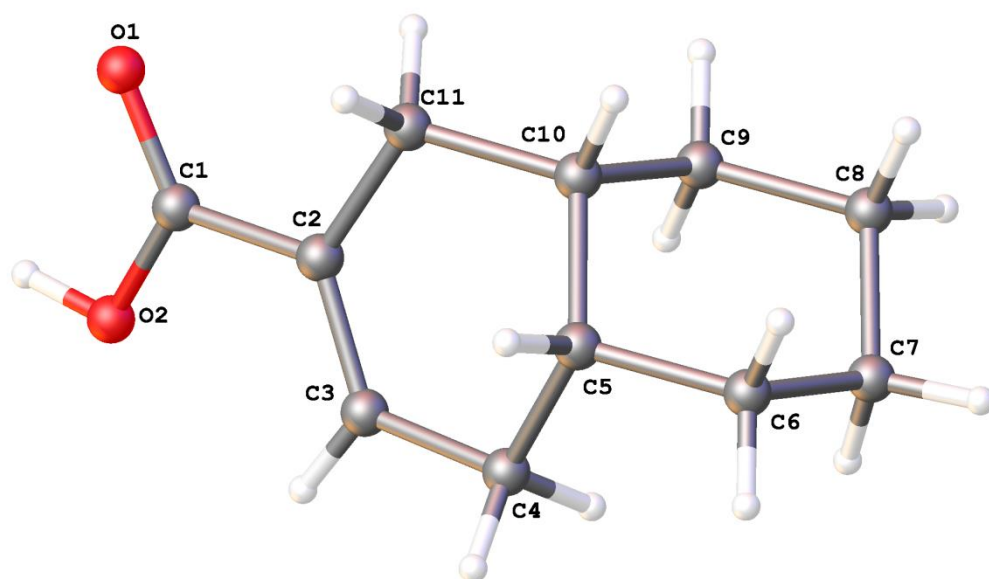
	U^{11}	U^{22}	U^{33}	U^{23}	U^{13}	U^{12}
O(1)	0.076(3)	0.053(2)	0.073(3)	0.0064(16)	0.035(2)	
	-0.0031(18)					
O(2)	0.078(2)	0.056(2)	0.072(2)	0.0055(15)	0.0337(19)	
	-0.0077(18)					
O(3)	0.081(3)	0.059(2)	0.073(3)	-0.0143(17)	0.030(2)	0.0035(17)
O(4)	0.074(3)	0.056(2)	0.076(2)	-0.0074(15)	0.0314(19)	
	0.0061(16)					
C(1)	0.110(4)	0.054(3)	0.088(4)	-0.004(3)	0.045(3)	0.001(3)
C(2)	0.080(3)	0.054(3)	0.081(3)	-0.002(2)	0.041(3)	-0.001(2)
C(3)	0.075(3)	0.051(3)	0.069(3)	0.004(2)	0.036(3)	0.004(2)
C(4)	0.070(3)	0.050(3)	0.068(3)	-0.003(2)	0.039(3)	
	-0.0030(19)					
C(5)	0.065(3)	0.049(3)	0.062(3)	0.0015(19)	0.033(2)	
	-0.0006(18)					
C(6)	0.075(3)	0.051(3)	0.064(3)	-0.001(2)	0.041(3)	
	-0.0022(19)					
C(7)	0.089(3)	0.046(3)	0.065(3)	-0.006(2)	0.043(3)	-0.008(2)
C(8)	0.072(3)	0.047(3)	0.065(3)	0.001(2)	0.039(3)	0.003(2)
C(9)	0.079(4)	0.050(3)	0.071(4)	0.001(2)	0.046(3)	-0.006(3)
C(10)	0.082(3)	0.055(3)	0.087(4)	0.000(2)	0.051(3)	0.002(2)

Table 5. Hydrogen coordinates and isotropic displacement parameters (\AA^2) for btg84.

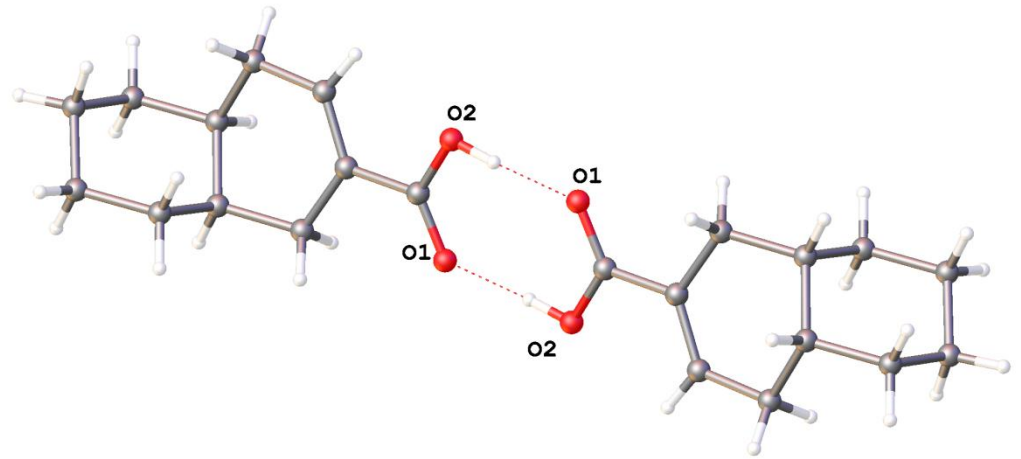
	x	y	z	U
H(3)	0.338(6)	0.181(5)	0.541(6)	0.083(17)
H(1A)	0.3368	-0.5865	0.2605	0.121
H(1B)	0.2648	-0.5437	0.3721	0.121
H(1C)	0.4425	-0.5286	0.3885	0.121
H(2A)	0.2181	-0.4169	0.1912	0.081
H(2B)	0.3965	-0.3945	0.2251	0.081
H(3A)	0.3873	-0.3153	0.4271	0.074
H(3B)	0.2070	-0.3302	0.3831	0.074
H(4A)	0.1978	-0.2057	0.2042	0.070
H(4B)	0.3757	-0.1849	0.2610	0.070
H(5A)	0.3259	-0.1045	0.4518	0.067
H(6A)	0.3800	0.0179	0.2990	0.071
H(7A)	0.1841	-0.0364	0.1135	0.075
H(7B)	0.0625	0.0278	0.1699	0.075
H(10A)	0.0882	-0.1808	0.4372	0.104
H(10B)	0.0151	-0.1128	0.3057	0.104
H(10C)	0.0756	-0.0446	0.4389	0.104
H(1)	0.110(7)	0.209(6)	-0.041(6)	0.10(2)

Table 6. Torsion angles [°] for btg84.

C(1)–C(2)–C(3)–C(4)	175.1(4)	C(2)–C(3)–C(4)–C(5)	174.2(4)
C(3)–C(4)–C(5)–C(6)	166.6(4)	C(3)–C(4)–C(5)–C(10)	–66.9(5)
C(4)–C(5)–C(6)–C(7)	59.8(5)	C(4)–C(5)–C(6)–C(9)	–177.0(4)
C(10)–C(5)–C(6)–C(7)	–66.2(5)	C(10)–C(5)–C(6)–C(9)	57.0(5)
C(5)–C(6)–C(7)–C(8)	–176.5(3)	C(9)–C(6)–C(7)–C(8)	59.9(5)
C(6)–C(7)–C(8)–O(1)	–165.6(4)	C(6)–C(7)–C(8)–O(2)	15.9(6)
C(5)–C(6)–C(9)–O(3)	72.5(5)	C(5)–C(6)–C(9)–O(4)	–105.6(5)
C(7)–C(6)–C(9)–O(3)	–162.4(3)	C(7)–C(6)–C(9)–O(4)	19.5(5)



Asymmetric unit for BTG105



Hydrogen Bonding in BTG105

Table 1. Crystal data and structure refinement for btg105.

Identification code	btg105	
Chemical formula (moiety)	$C_{44}H_{64}O_8$	
Chemical formula (total)	$C_{44}H_{64}O_8$	
Formula weight	720.95	
Temperature	150(2) K	
Radiation, wavelength	MoK α , 0.71073 Å	
Crystal system, space group	monoclinic, P12 ₁ /c1	
Unit cell parameters	a = 10.7054(9) Å	$\alpha = 90^\circ$
	b = 6.9447(4) Å	$\beta = 106.339(7)^\circ$
	c = 13.3775(9) Å	$\gamma = 90^\circ$
Cell volume	954.39(12) Å ³	
Z	1	
Calculated density	1.254 g/cm ³	
Absorption coefficient μ	0.084 mm ⁻¹	
F(000)	392	
Reflections for cell refinement	1630 (θ range 2.9 to 28.5°)	
Data collection method	Xcalibur, Atlas, Gemini ultra thick-slice ω scans	
θ range for data collection	3.2 to 28.6°	
Index ranges	h -12 to 12, k -6 to 9, l -14 to 17	
Completeness to $\theta = 25.0^\circ$	99.9 %	
Reflections collected	4437	
Independent reflections	1992 ($R_{int} = 0.0315$)	
Reflections with $F^2 > 2\sigma$	1529	
Absorption correction	semi-empirical from equivalents	
Min. and max. transmission	0.82940 and 1.00000	
Structure solution	direct methods	
Refinement method	Full-matrix least-squares on F^2	
Weighting parameters a, b	0.0381, 0.1708	
Data / restraints / parameters	1992 / 0 / 123	
Final R indices [$F^2 > 2\sigma$]	R1 = 0.0484, wR2 = 0.0983	
R indices (all data)	R1 = 0.0688, wR2 = 0.1094	
Goodness-of-fit on F^2	1.070	
Extinction coefficient	0.0048(18)	
Largest and mean shift/su	0.000 and 0.000	
Largest diff. peak and hole	0.22 and -0.18 e Å ⁻³	

Table 2. Atomic coordinates and equivalent isotropic displacement parameters (\AA^2) for btg105. U_{eq} is defined as one third of the trace of the orthogonalized U^{ij} tensor.

	x	y	z	U_{eq}
O(1)	0.01422(11)	0.13106(16)	0.40469(8)	0.0310(3)
O(2)	0.10550(12)	0.19282(18)	0.57314(8)	0.0346(3)
C(1)	0.08232(14)	0.2334(2)	0.47314(11)	0.0253(4)
C(2)	0.14344(14)	0.4103(2)	0.44836(11)	0.0247(4)
C(3)	0.20167(15)	0.5338(2)	0.52315(12)	0.0287(4)
C(4)	0.26250(17)	0.7171(2)	0.50318(12)	0.0323(4)
C(5)	0.23046(16)	0.7713(2)	0.38783(12)	0.0294(4)
C(6)	0.32396(17)	0.9235(3)	0.36844(13)	0.0359(4)
C(7)	0.45995(17)	0.8438(3)	0.38230(13)	0.0378(5)
C(8)	0.45739(18)	0.6670(3)	0.31568(14)	0.0404(5)
C(9)	0.36542(16)	0.5136(2)	0.33584(13)	0.0343(4)
C(10)	0.22903(15)	0.5944(2)	0.31923(11)	0.0275(4)
C(11)	0.13185(16)	0.4460(2)	0.33543(11)	0.0307(4)

Table 3. Bond lengths [Å] and angles [°] for btg105.

O(1)–C(1)	1.2244(18)	O(2)–C(1)	1.3204(18)
O(2)–H(2)	0.89(2)	C(1)–C(2)	1.473(2)
C(2)–C(3)	1.332(2)	C(2)–C(11)	1.501(2)
C(3)–H(3A)	0.950	C(3)–C(4)	1.488(2)
C(4)–H(4A)	0.990	C(4)–H(4B)	0.990
C(4)–C(5)	1.531(2)	C(5)–H(5A)	1.000
C(5)–C(6)	1.527(2)	C(5)–C(10)	1.531(2)
C(6)–H(6A)	0.990	C(6)–H(6B)	0.990
C(6)–C(7)	1.519(2)	C(7)–H(7A)	0.990
C(7)–H(7B)	0.990	C(7)–C(8)	1.513(3)
C(8)–H(8A)	0.990	C(8)–H(8B)	0.990
C(8)–C(9)	1.525(2)	C(9)–H(9A)	0.990
C(9)–H(9B)	0.990	C(9)–C(10)	1.521(2)
C(10)–H(10A)	1.000	C(10)–C(11)	1.522(2)
C(11)–H(11A)	0.990	C(11)–H(11B)	0.990
C(1)–O(2)–H(2)	106.9(13)	O(1)–C(1)–O(2)	122.46(15)
O(1)–C(1)–C(2)	121.62(14)	O(2)–C(1)–C(2)	115.92(13)
C(1)–C(2)–C(3)	120.79(14)	C(1)–C(2)–C(11)	116.63(13)
C(3)–C(2)–C(11)	122.54(14)	C(2)–C(3)–H(3A)	118.2
C(2)–C(3)–C(4)	123.52(14)	H(3A)–C(3)–C(4)	118.2
C(3)–C(4)–H(4A)	108.8	C(3)–C(4)–H(4B)	108.8
C(3)–C(4)–C(5)	113.95(13)	H(4A)–C(4)–H(4B)	107.7
H(4A)–C(4)–C(5)	108.8	H(4B)–C(4)–C(5)	108.8
C(4)–C(5)–H(5A)	107.6	C(4)–C(5)–C(6)	111.69(13)
C(4)–C(5)–C(10)	111.63(13)	H(5A)–C(5)–C(6)	107.6
H(5A)–C(5)–C(10)	107.6	C(6)–C(5)–C(10)	110.50(14)
C(5)–C(6)–H(6A)	109.2	C(5)–C(6)–H(6B)	109.2
C(5)–C(6)–C(7)	112.24(14)	H(6A)–C(6)–H(6B)	107.9
H(6A)–C(6)–C(7)	109.2	H(6B)–C(6)–C(7)	109.2
C(6)–C(7)–H(7A)	109.3	C(6)–C(7)–H(7B)	109.3
C(6)–C(7)–C(8)	111.46(14)	H(7A)–C(7)–H(7B)	108.0
H(7A)–C(7)–C(8)	109.3	H(7B)–C(7)–C(8)	109.3
C(7)–C(8)–H(8A)	109.3	C(7)–C(8)–H(8B)	109.3
C(7)–C(8)–C(9)	111.60(14)	H(8A)–C(8)–H(8B)	108.0
H(8A)–C(8)–C(9)	109.3	H(8B)–C(8)–C(9)	109.3
C(8)–C(9)–H(9A)	109.4	C(8)–C(9)–H(9B)	109.4
C(8)–C(9)–C(10)	110.97(14)	H(9A)–C(9)–H(9B)	108.0
H(9A)–C(9)–C(10)	109.4	H(9B)–C(9)–C(10)	109.4
C(5)–C(10)–C(9)	111.16(13)	C(5)–C(10)–H(10A)	107.2
C(5)–C(10)–C(11)	110.48(13)	C(9)–C(10)–H(10A)	107.2
C(9)–C(10)–C(11)	113.34(14)	H(10A)–C(10)–C(11)	107.2
C(2)–C(11)–C(10)	112.88(12)	C(2)–C(11)–H(11A)	109.0
C(2)–C(11)–H(11B)	109.0	C(10)–C(11)–H(11A)	109.0
C(10)–C(11)–H(11B)	109.0	H(11A)–C(11)–H(11B)	107.8

Table 4. Anisotropic displacement parameters (\AA^2) for btg105. The anisotropic displacement factor exponent takes the form: $-2\pi^2[h^2a^2U^{11} + \dots + 2hka^*b^*U^{12}]$

	U^{11}	U^{22}	U^{33}	U^{23}	U^{13}	U^{12}
O(1)	0.0375(7)	0.0276(6)	0.0264(6)	-0.0002(5)	0.0062(5)	
	-0.0083(5)					
O(2)	0.0441(7)	0.0329(7)	0.0253(6)	0.0026(5)	0.0074(5)	
	-0.0121(6)					
C(1)	0.0249(8)	0.0263(9)	0.0244(8)	0.0008(7)	0.0064(6)	0.0036(7)
C(2)	0.0239(8)	0.0247(8)	0.0252(8)	-0.0005(7)	0.0064(6)	
	-0.0003(7)					
C(3)	0.0314(9)	0.0302(9)	0.0258(8)	-0.0006(7)	0.0101(6)	
	-0.0009(8)					
C(4)	0.0392(10)	0.0278(9)	0.0322(9)	-0.0088(7)	0.0136(7)	
	-0.0061(8)					
C(5)	0.0317(9)	0.0226(9)	0.0328(9)	0.0013(7)	0.0071(7)	0.0005(7)
C(6)	0.0474(11)	0.0253(9)	0.0327(9)	-0.0001(8)	0.0077(7)	
	-0.0068(8)					
C(7)	0.0407(10)	0.0401(11)	0.0326(9)	0.0010(8)	0.0102(7)	
	-0.0152(9)					
C(8)	0.0382(10)	0.0446(12)	0.0425(10)	0.0002(9)	0.0180(8)	
	-0.0060(9)					
C(9)	0.0406(10)	0.0296(9)	0.0363(9)	-0.0022(8)	0.0168(7)	0.0000(8)
C(10)	0.0337(9)	0.0255(9)	0.0223(8)	0.0004(7)	0.0060(6)	
	-0.0051(7)					
C(11)	0.0362(9)	0.0273(9)	0.0273(8)	-0.0015(7)	0.0066(7)	
	-0.0073(8)					

Table 5. Hydrogen coordinates and isotropic displacement parameters (\AA^2) for btg105.

	x	y	z	U
H(3A)	0.2045	0.5033	0.5930	0.034
H(4A)	0.3582	0.7060	0.5317	0.039
H(4B)	0.2331	0.8224	0.5411	0.039
H(5A)	0.1410	0.8281	0.3671	0.035
H(6A)	0.2897	0.9740	0.2967	0.043
H(6B)	0.3286	1.0320	0.4174	0.043
H(7A)	0.5149	0.9439	0.3631	0.045
H(7B)	0.4993	0.8102	0.4564	0.045
H(8A)	0.5463	0.6129	0.3308	0.049
H(8B)	0.4292	0.7042	0.2412	0.049
H(9A)	0.3622	0.4035	0.2882	0.041
H(9B)	0.3988	0.4661	0.4082	0.041
H(10A)	0.1979	0.6380	0.2451	0.033
H(11A)	0.0425	0.4911	0.3003	0.037
H(11B)	0.1456	0.3232	0.3024	0.037
H(2)	0.063(2)	0.085(3)	0.5773(15)	0.053(6)

Table 6. Torsion angles [°] for btg105.

O(1)–C(1)–C(2)–C(3)	170.43(15)	O(1)–C(1)–C(2)–C(11)	–7.3(2)
O(2)–C(1)–C(2)–C(3)	–9.5(2)	O(2)–C(1)–C(2)–C(11)	172.75(14)
C(1)–C(2)–C(3)–C(4)	–178.52(14)	C(11)–C(2)–C(3)–C(4)	–0.9(2)
C(2)–C(3)–C(4)–C(5)	11.0(2)	C(3)–C(4)–C(5)–C(6)	–163.31(14)
C(3)–C(4)–C(5)–C(10)	–39.04(19)	C(4)–C(5)–C(6)–C(7)	70.45(18)
C(10)–C(5)–C(6)–C(7)	–54.45(17)	C(5)–C(6)–C(7)–C(8)	54.18(19)
C(6)–C(7)–C(8)–C(9)	–54.5(2)	C(7)–C(8)–C(9)–C(10)	55.85(19)
C(8)–C(9)–C(10)–C(5)	–56.42(17)	C(8)–C(9)–C(10)–C(11)	178.44(13)
C(4)–C(5)–C(10)–C(9)	–69.43(17)	C(4)–C(5)–C(10)–C(11)	57.30(17)
C(6)–C(5)–C(10)–C(9)	55.51(17)	C(6)–C(5)–C(10)–C(11)	–177.76(13)
C(1)–C(2)–C(11)–C(10)	–162.84(13)	C(3)–C(2)–C(11)–C(10)	19.5(2)
C(5)–C(10)–C(11)–C(2)	–46.83(18)	C(9)–C(10)–C(11)–C(2)	78.68(17)

Table 7. Hydrogen bonds for btg105 [\AA and $^\circ$].

D–H...A	d(D–H)	d(H...A)	d(D...A)	$\angle(\text{DHA})$
O(2)–H(2)...O(1A)	0.89(2)	1.76(2)	2.6464(16)	176(2)

Symmetry operations for equivalent atoms

A $-x, -y, -z+1$

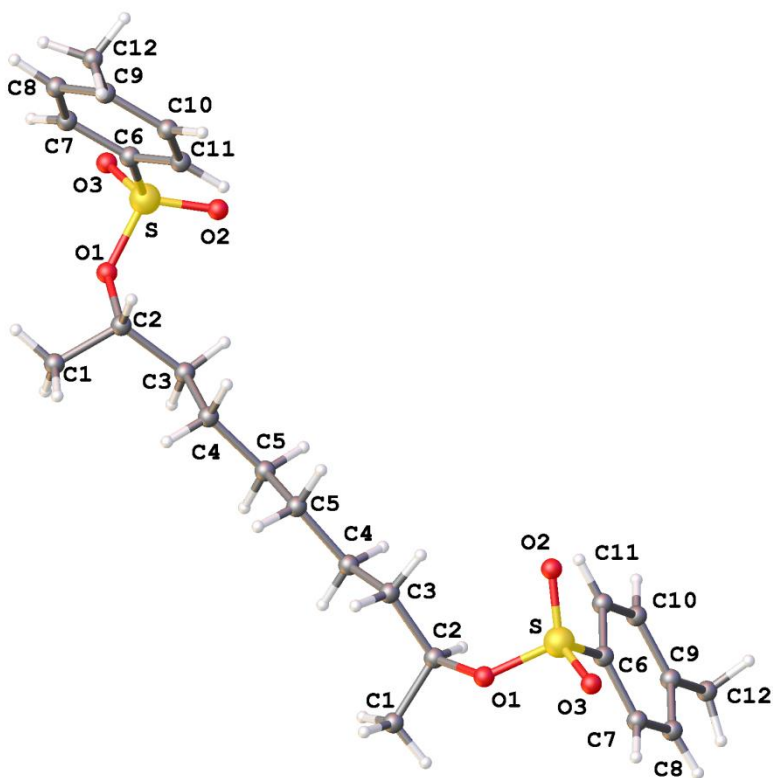


Table 1. Crystal data and structure refinement for ms2326.

Identification code	ms2326	
Chemical formula (moiety)	$C_{24}H_{34}O_6S_2$	
Chemical formula (total)	$C_{24}H_{34}O_6S_2$	
Formula weight	482.63	
Temperature	120(2) K	
Radiation, wavelength	synchrotron, 0.68890 Å	
Crystal system, space group	orthorhombic, Fdd2	
Unit cell parameters	a = 20.683(17) Å	□ = 90°
	b = 30.74(2) Å	□ = 90°
	c = 7.554(6) Å	□ = 90°
Cell volume	4803(6) Å ³	
Z	8	
Calculated density	1.335 g/cm ³	
Absorption coefficient μ	0.242 mm ⁻¹	
F(000)	2064	
Crystal colour and size	colourless, 0.02 × 0.02 × 0.00 mm ³	
Reflections for cell refinement	4052 (θ range 2.3 to 29.3°)	
Data collection method	Crystal Logic diffractometer and Rigaku	
Saturn 724+ CCD		
	thick-slice ω scans	
θ range for data collection	2.3 to 24.4°	
Index ranges	h -24 to 24, k -36 to 28, l -8 to 5	
Completeness to $\theta = 24.4^\circ$	97.7 %	
Reflections collected	7088	
Independent reflections	1895 ($R_{int} = 0.0723$)	
Reflections with $F^2 > 2\sigma$	1661	
Absorption correction	semi-empirical from equivalents	
Min. and max. transmission	0.9952 and 0.9998	
Structure solution	direct methods	
Refinement method	Full-matrix least-squares on F^2	
Weighting parameters a, b	0.1037, 2.5572	
Data / restraints / parameters	1895 / 1 / 148	
Final R indices [$F^2 > 2\sigma$]	R1 = 0.0576, wR2 = 0.1529	
R indices (all data)	R1 = 0.0669, wR2 = 0.1580	
Goodness-of-fit on F^2	1.084	
Absolute structure parameter	0.09(16)	
Extinction coefficient	0.0033(16)	
Largest and mean shift/su	0.000 and 0.000	
Largest diff. peak and hole	0.37 and -0.24 e Å ⁻³	

Table 2. Atomic coordinates and equivalent isotropic displacement parameters (\AA^2) for ms2326. U_{eq} is defined as one third of the trace of the orthogonalized U^{ij} tensor.

	x	y	z	U_{eq}
S	0.05203(5)	0.40090(3)	0.09696(17)	0.0455(4)
O(1)	0.06495(14)	0.38637(10)	0.2934(5)	0.0522(9)
O(2)	0.06162(16)	0.36521(10)	-0.0163(5)	0.0560(10)
O(3)	-0.01071(14)	0.42016(10)	0.1078(6)	0.0623(10)
C(1)	0.1314(3)	0.38294(17)	0.5420(9)	0.0602(15)
C(2)	0.1291(2)	0.37034(14)	0.3551(8)	0.0512(13)
C(3)	0.1366(2)	0.32112(15)	0.3228(8)	0.0551(13)
C(4)	0.2056(2)	0.30601(15)	0.3523(10)	0.0549(12)
C(5)	0.2146(2)	0.25710(14)	0.3443(9)	0.0553(13)
C(6)	0.10971(19)	0.44131(12)	0.0465(6)	0.0396(11)
C(7)	0.09865(18)	0.48426(12)	0.0976(8)	0.0458(11)
C(8)	0.1445(2)	0.51564(12)	0.0549(7)	0.0433(12)
C(9)	0.20158(18)	0.50436(13)	-0.0272(7)	0.0406(11)
C(10)	0.21132(19)	0.46134(13)	-0.0761(6)	0.0410(11)
C(11)	0.16546(19)	0.42931(12)	-0.0397(7)	0.0406(10)
C(12)	0.2524(2)	0.53840(14)	-0.0678(7)	0.0496(12)

Table 3. Bond lengths [Å] and angles [°] for ms2326.

S–O(1)	1.572(4)	S–O(2)	1.405(4)
S–O(3)	1.429(3)	S–C(6)	1.764(4)
O(1)–C(2)	1.491(5)	C(1)–H(1A)	0.980
C(1)–H(1B)	0.980	C(1)–H(1C)	0.980
C(1)–C(2)	1.465(8)	C(2)–H(2)	1.000
C(2)–C(3)	1.540(6)	C(3)–H(3A)	0.990
C(3)–H(3B)	0.990	C(3)–C(4)	1.517(6)
C(4)–H(4A)	0.990	C(4)–H(4B)	0.990
C(4)–C(5)	1.516(6)	C(5)–C(5A)	1.530(8)
C(5)–H(5A)	0.990	C(5)–H(5B)	0.990
C(6)–C(7)	1.395(6)	C(6)–C(11)	1.374(6)
C(7)–H(7)	0.950	C(7)–C(8)	1.390(6)
C(8)–H(8)	0.950	C(8)–C(9)	1.379(6)
C(9)–C(10)	1.388(6)	C(9)–C(12)	1.514(6)
C(10)–H(10)	0.950	C(10)–C(11)	1.394(6)
C(11)–H(11)	0.950	C(12)–H(12A)	0.980
C(12)–H(12B)	0.980	C(12)–H(12C)	0.980
O(1)–S–O(2)	109.2(2)	O(1)–S–O(3)	102.6(2)
O(1)–S–C(6)	106.81(19)	O(2)–S–O(3)	119.1(2)
O(2)–S–C(6)	108.8(2)	O(3)–S–C(6)	109.57(19)
S–O(1)–C(2)	122.7(3)	H(1A)–C(1)–H(1B)	109.5
H(1A)–C(1)–H(1C)	109.5	H(1A)–C(1)–C(2)	109.5
H(1B)–C(1)–H(1C)	109.5	H(1B)–C(1)–C(2)	109.5
H(1C)–C(1)–C(2)	109.5	O(1)–C(2)–C(1)	104.0(4)
O(1)–C(2)–H(2)	109.1	O(1)–C(2)–C(3)	111.3(4)
C(1)–C(2)–H(2)	109.1	C(1)–C(2)–C(3)	114.2(5)
H(2)–C(2)–C(3)	109.1	C(2)–C(3)–H(3A)	109.3
C(2)–C(3)–H(3B)	109.3	C(2)–C(3)–C(4)	111.8(4)
H(3A)–C(3)–H(3B)	107.9	H(3A)–C(3)–C(4)	109.3
H(3B)–C(3)–C(4)	109.3	C(3)–C(4)–H(4A)	108.7
C(3)–C(4)–H(4B)	108.7	C(3)–C(4)–C(5)	114.4(4)
H(4A)–C(4)–H(4B)	107.6	H(4A)–C(4)–C(5)	108.7
H(4B)–C(4)–C(5)	108.7	C(4)–C(5)–C(5A)	113.6(5)
C(4)–C(5)–H(5A)	108.8	C(4)–C(5)–H(5B)	108.8
C(5A)–C(5)–H(5A)	108.8	C(5A)–C(5)–H(5B)	108.8
H(5A)–C(5)–H(5B)	107.7	S–C(6)–C(7)	119.7(3)
S–C(6)–C(11)	118.7(3)	C(7)–C(6)–C(11)	121.5(4)
C(6)–C(7)–H(7)	120.6	C(6)–C(7)–C(8)	118.7(4)
H(7)–C(7)–C(8)	120.6	C(7)–C(8)–H(8)	119.5
C(7)–C(8)–C(9)	120.9(4)	H(8)–C(8)–C(9)	119.5
C(8)–C(9)–C(10)	118.9(4)	C(8)–C(9)–C(12)	120.8(4)
C(10)–C(9)–C(12)	120.3(4)	C(9)–C(10)–H(10)	119.3
C(9)–C(10)–C(11)	121.4(4)	H(10)–C(10)–C(11)	119.3
C(6)–C(11)–C(10)	118.3(4)	C(6)–C(11)–H(11)	120.8
C(10)–C(11)–H(11)	120.8	C(9)–C(12)–H(12A)	109.5
C(9)–C(12)–H(12B)	109.5	C(9)–C(12)–H(12C)	109.5
H(12A)–C(12)–H(12B)	109.5	H(12A)–C(12)–H(12C)	109.5
H(12B)–C(12)–H(12C)	109.5		

Symmetry operations for equivalent atoms

A $-x+1/2, -y+1/2, z$

Table 4. Anisotropic displacement parameters (\AA^2) for ms2326. The anisotropic displacement factor exponent takes the form: $-2\pi^2[h^2a^{*2}U^{11} + \dots + 2hka^*b^*U^{12}]$

	U^{11}	U^{22}	U^{33}	U^{23}	U^{13}	U^{12}
S	0.0415(5)	0.0362(5)	0.0589(9)	0.0028(5)	-0.0041(5)	
	-0.0041(4)					
O(1)	0.0436(15)	0.0554(18)	0.058(3)	0.0075(17)	-0.0040(14)	
	-0.0023(13)					
O(2)	0.0609(19)	0.0395(16)	0.068(3)	-0.0037(17)	-0.0021(17)	
	-0.0107(13)					
O(3)	0.0420(15)	0.0526(17)	0.092(3)	0.005(2)	0.0024(18)	
	-0.0067(13)					
C(1)	0.060(3)	0.050(2)	0.071(5)	-0.016(3)	-0.007(3)	0.000(2)
C(2)	0.044(2)	0.049(2)	0.060(4)	0.001(3)	0.002(2)	0.0015(17)
C(3)	0.051(2)	0.051(2)	0.064(4)	0.002(3)	-0.006(2)	0.0024(18)
C(4)	0.053(2)	0.054(2)	0.058(4)	0.000(3)	0.002(2)	0.0072(19)
C(5)	0.054(2)	0.047(2)	0.065(4)	-0.006(3)	-0.005(3)	0.0029(18)
C(6)	0.041(2)	0.0324(19)	0.046(3)	0.0015(17)	-0.0053(18)	
	-0.0016(14)					
C(7)	0.0375(19)	0.042(2)	0.057(3)	-0.003(2)	0.002(2)	0.0002(15)
C(8)	0.045(2)	0.0327(19)	0.052(4)	-0.0035(19)	0.002(2)	
	-0.0028(15)					
C(9)	0.0371(19)	0.040(2)	0.045(3)	0.002(2)	-0.0032(18)	
	-0.0004(15)					
C(10)	0.040(2)	0.040(2)	0.043(3)	-0.0025(18)	0.0033(17)	
	0.0022(16)					
C(11)	0.045(2)	0.0315(19)	0.045(3)	0.004(2)	-0.0020(19)	
	0.0026(15)					
C(12)	0.047(2)	0.044(2)	0.058(4)	-0.004(2)	0.010(2)	
	-0.0079(18)					

Table 5. Hydrogen coordinates and isotropic displacement parameters (\AA^2) for ms2326.

	x	y	z	U
H(1A)	0.1744	0.3767	0.5900	0.090
H(1B)	0.0989	0.3664	0.6082	0.090
H(1C)	0.1223	0.4141	0.5529	0.090
H(2)	0.1640	0.3861	0.2896	0.061
H(3A)	0.1074	0.3051	0.4039	0.066
H(3B)	0.1235	0.3143	0.1999	0.066
H(4A)	0.2336	0.3196	0.2616	0.066
H(4B)	0.2202	0.3165	0.4695	0.066
H(5A)	0.1935	0.2459	0.2358	0.066
H(5B)	0.1925	0.2438	0.4473	0.066
H(7)	0.0605	0.4919	0.1605	0.055
H(8)	0.1363	0.5453	0.0827	0.052
H(10)	0.2501	0.4535	-0.1357	0.049
H(11)	0.1726	0.3999	-0.0736	0.049
H(12A)	0.2946	0.5282	-0.0263	0.074
H(12B)	0.2413	0.5656	-0.0076	0.074
H(12C)	0.2541	0.5434	-0.1959	0.074

Table 6. Torsion angles [°] for ms2326.

O(2)–S–O(1)–C(2)	62.2(3)	O(3)–S–O(1)–C(2)	–170.5(3)
C(6)–S–O(1)–C(2)	–55.3(3)	S–O(1)–C(2)–C(1)	150.3(3)
S–O(1)–C(2)–C(3)	–86.3(5)	O(1)–C(2)–C(3)–C(4)	169.2(5)
C(1)–C(2)–C(3)–C(4)	–73.4(6)	C(2)–C(3)–C(4)–C(5)	173.0(5)
C(3)–C(4)–C(5)–C(5A)	170.7(4)	O(1)–S–C(6)–C(7)	–82.5(4)
O(1)–S–C(6)–C(11)	96.1(4)	O(2)–S–C(6)–C(7)	159.7(4)
O(2)–S–C(6)–C(11)	–21.7(4)	O(3)–S–C(6)–C(7)	27.9(5)
O(3)–S–C(6)–C(11)	–153.5(4)	S–C(6)–C(7)–C(8)	–179.4(4)
C(11)–C(6)–C(7)–C(8)	2.0(8)	C(6)–C(7)–C(8)–C(9)	–3.7(8)
C(7)–C(8)–C(9)–C(10)	3.6(8)	C(7)–C(8)–C(9)–C(12)	–177.9(5)
C(8)–C(9)–C(10)–C(11)	–1.7(7)	C(12)–C(9)–C(10)–C(11)	179.7(5)
S–C(6)–C(11)–C(10)	–178.8(4)	C(7)–C(6)–C(11)–C(10)	–0.2(7)
C(9)–C(10)–C(11)–C(6)	0.0(7)		

Symmetry operations for equivalent atoms

A $-x+1/2, -y+1/2, z$